Imperial College London

Iterative Synthesis for Precision Manufacture of High Value Polymers

Submitted by

Ruiyi Liu

Faculty of Engineering

Department of Chemical Engineering

A Thesis Submitted for the Degree of Doctor of Philosophy and the Diploma of Imperial College London

October 2018

Declaration of Originality

I hereby declare that this thesis and the work reported herein was composed by and originated entirely from me. Information derived from the published and unpublished work of others has been acknowledged in the text and the relevant references are included in this thesis.

Ruiyi Liu
Imperial College London
October 2018

Copyright Declaration

The copyright of this thesis rests with the author and is made available under a Creative Commons Attribution Non-Commercial No Derivatives license. Researchers are free to copy, distribute or transmit the thesis on the condition that they attribute it, that they do not use it for commercial purposes and that they do not alter, transform or build upon it. For any reuse or redistribution, researchers must make clear to others the license terms of this work.

Ruiyi Liu
Imperial College London
October 2018

Abstract

The precise chemical synthesis of monodisperse and sequence-defined polymers has been studied intensively by synthetic chemists. Monodisperse sequence-defined synthetic polymers have a wide range of applications in healthcare and nanotechnology, due to their unique structural complexity. In addition, controlling monomer sequence can also affect polymer functionality and properties. Currently, the industrial fabrication of synthetic macromolecules is generally poorly controlled and difficult to scale up. In this thesis, a universal strategy for iterative synthesis with organic solvent nanofiltration (ItSyN) is proposed for fabricating monodisperse and sequence-defined PEG polymers with different side chains. This technology combines iterative monomer couplings and selective membrane separations in a fully liquid environment. It offers advantages for optimising reaction kinetics, online monitoring and the potential to scale up. Polymers were assembled on a soluble three-armed support to triple the production and maximise efficiency during membrane purification.

For ItSyN, polybenzimidazole (PBI) organic solvent nanofiltration (OSN) membranes with surface modifications were fabricated and characterised. The surface modified membranes showed good tolerance towards different organic solvents and extreme pH conditions in chemical synthesis processes.

A series of chemical kinetic studies of building block coupling were undertaken. Optimisation of the reaction conditions guaranteed up to 99.6% three-arm completion and impurities were minimised. The excellent coupling efficiency aided membrane purification and the preparation of precise monodisperse PEG oligomers. Using the same strategy, two sequence-defined PEG polymers with different orders of the side-arms were synthesized with a purity of 99%. They were characterised with respect to the diversity of their polymer structures and physical properties using ultraviolet–visible spectroscopy (UV-VIS) and differential scanning calorimetry (DSC).

ItSyN offers a versatile platform to synthesize a wide diversity of sequence-defined polymers with good purities and yields. It also unlocks the potential of sequence-defined polymers for real-life applications in nanotechnology, healthcare and information storage.

Acknowledgements

It has been very meaningful four years for me, I have received so much guidance, help and support from many people to reach here. First of all, I would like to express my most sincere gratitude to my supervisor, Professor Andrew Livingston, for his guidance, patience and enthusiasm throughout the research project and my PhD studies. I would like to thank him for encouraging me to challenge myself and enjoy exploring in pursuit of my research.

Secondly, I would like to show my gratitude to Dr. Piers Gaffney, Dr. Patrizia Marchetti and Dr. Ruijiao Dong. They generously shared their knowledge and expertise in chemistry, membrane technology and polymer science. The scientific discussions with them always inspired and supported me in solving scientific problems and improving my research during my PhD work.

I am grateful to all my colleagues from Professor Livingston's group, past and present, who have given me help with many day-to-day matters. I would also like to thank all the analytical staff: Lisa Haigh for the mass spectrometry and Peter Hitchcock for NMR analysis. My thanks go to my office mates and lunch mates for their constant happiness and humour during our meals and social activities. Special thanks to my friend Alan Pawley for his precious advice, encouragement during my PhD, and his kind assistance in proof reading this thesis.

This work would not have been possible without the love and support of my family and friends. I am extremely grateful to my parents, who offered me the opportunity to study in the UK since Sixth Form. They always help in any way possible and support me in my life. I want to give my deepest thanks to my beloved husband Matt Scales. You have always stood by me over the past eight years. Your love and support continue to give me so much encouragement, and motivate me to pursue my dreams.

Table of Contents

List of Figures 10
List of Tables 13
Nomenclature 14
List of Abbreviations 14
1. Introduction 18
2. Literature review 20
2.1. Biopolymer definition, characterisations and applications 20
2.1.1. Natural macromolecules 20
2.1.2. Synthetic polymers (polyether, polyester) 21
2.1.3. Significance of monodisperse polyethylene glycol (PEG) polymers 21
2.1.4. Properties and promises of sequence-defined polymers 23
2.2. Precision polymer synthesis and separation methods 25
2.2.1. Sequence controlled biological polymerization processes 25
2.2.1.1. Template synthesis 26
2.2.1.2. Catalysis 28
2.2.1.3. Ribosomal machinery 29
2.2.2. Sequence controlled chemical polymerization processes 29
2.2.2.1. Chain-growth polymerization 30
2.2.2.2. Step-growth polymerisation 34
2.2.2.3. Reconstitution 35
2.2.2.4. Iterative synthesis 36
2.2.2.5. Synthesis of monodisperse polyethylene glycol (mPEG) 43
2.3. Organic solvent nanofiltration (OSN) membrane separation 48
2.3.1. Overview 48
2.3.2. Membrane separation processes 48
2.3.3. Membrane materials and compositions 49
2.3.4. OSN membrane fabrication and modification 50
2.3.4.1. Membrane crosslinking 51
2.3.4.2. Surface modification 52
2.3.4.3. Scale-up membrane modules 53
2.3.5. OSN membrane applications: purification and solvent recovery 54
2.3.5.1. Chemical synthesis with OSN 56

2.3.5.2. Diafiltration systems 58
2.3.5.3. Cascade system 60
2.4. Summary of the state of the art 64
3. Project objectives and tasks 67
3.1. Project overview 68
3.2. Objectives and tasks 70
4. PBI-based membranes for PEG organic synthesis 71
4.1. Abstract 71
4.2. Introduction 72
4.3. Methodology 75
4.3.1. Materials 75
4.3.2. Membrane preparation with batch casting 75
4.3.3. Membrane preparation with continuous casting 76
4.3.4. Membrane post-modification 78
4.3.5. Membrane characterisation and screening 78
4.3.5.1. Membrane cross-flow cell screening 78
4.3.5.2. Weight change 79
4.3.5.3. Brunauer, Emmett and Teller (BET) 80
4.3.5.4. Liquid-liquid porosimetry 80
4.4. Results and discussion 81
4.4.1. PBI membrane performance from bench casting 81
4.4.1.1. Non-woven backing choice was not significant 81
4.4.1.2. Dope concentration can control molecular weight cut off (MWCO) 83
4.4.1.3. Conditioning of the membrane 84
4.4.2. PBI membrane performance from continuous casting 85
4.4.2.1. Improvement of crosslinking by surface modification 85
4.4.2.2. Surface modifiers 86
4.4.2.3. Solvent effects on membrane performance 87
4.4.3. Membrane characterizations 92
4.4.3.1. Specific weight gain and membrane thickness 92
4.4.3.2. Pore size distribution and measurement 94
4.4.4. Case study: Membrane screening for PEG polyether iterative synthesis purification application in ItSyN conditions 99
4.5. Chapter conclusions 102
5. ItSyN for monodisperse linear PEGs 104

5.1. Abstract 104
5.2. Introduction 104
5.3. Methodology 107
5.3.1. Materials 107
5.3.2. General experimental procedures 108
5.3.3. Analytical techniques 109
5.3.3.1. Nuclear magnetic resonance spectroscopy (NMR) 109
5.3.3.2. Mass spectrometry (MS): ES-MS & MALDI-ToF-MS 109
5.3.3.3. Thin layer chromatography (TLC) 109
5.3.3.4. High-performance liquid chromatography (HPLC) 109
5.3.3.5. Ultra-performance liquid chromatography (UPLC) 110
5.3.3.6. Chain extension and deprotection 111
5.3.3.7. Membrane screening 111
5.3.3.8. Diafiltration set up 112
5.3.3.9. ItSyN procedure 113
5.4. Results and discussions 115
5.4.1. The design of the hub 115
5.4.2. Synthesis of heterobifunctional linear PEG using ItSyN 116
5.4.3. Membrane system selection 121
5.4.4. Membrane diafiltration and online monitoring 122
5.4.5. Online monitoring and product analysis of chain extension 126
5.4.6. Chemical kinetic study of chain extension 129
5.5. Chapter conclusions 137
6. ItSyN for sequence-defined branched PEGs 139
6.1. Abstract 139
6.2. Introduction 140
6.3. Methodology 142
6.3.1. Materials 142
6.3.2. General experimental procedures 142
6.3.3. Chain extension and deprotection 142
6.3.4. Diafiltration procedure 142
6.3.5. Analytical techniques 142
6.3.5.1. Building block synthesis, chain extension and deprotection 142
6.3.5.2. Membrane screening and diafiltration 144
6.3.5.3. Polymer properties characterisation 144

6.4. Results and discussion 145
6.4.1. Octyl branched PEG building block synthesis 145
6.4.1.1. Design of the building blocks 145
6.4.1.2. Choice of protecting groups for building block synthesis 146
6.4.1.3. Choice of side chain and chirality for building block synthesis 148
6.4.1.4. First building block synthesis approach 149
6.4.1.5. Sharpless' catalytic asymmetric dihydroxylation and crystallisation for chiral centre in building block 152
6.4.1.6. Synthesis scale up for the first building block (25) 158
6.4.1.7. Second building block synthesis approach 159
6.4.1.8. Alternative synthesis route with unsuccessful hydrogenolysis 165
6.4.2. Synthesis of sequence-defined octyl branched PEG using ItSyN 167
6.4.2.1. Membrane and solvent system selection 171
6.4.2.2. Chain extension and membrane diafiltration 174
6.4.2.3. The influences of side chain and its position in coupling reactivity 182
6.4.2.4. Polymer properties characterisation 184
6.5. Chapter conclusions 188
7. Conclusions and recommendations for future work 191
7.1. Conclusions 191
7.1.1. Preparation of OSN PBI membranes with enhanced chemical stability and selectivity for ItSyN and harsh chemical environments 192
7.1.2. The design of the soluble support and building block assembly 192
7.1.3. Kinetic studies of chain extension using long, linear building blocks 193
7.1.4. The development of the ItSyN process with product characterizations 194
7.2. Recommendations for future work 194
7.2.1. Investigate the cascade membrane system and its scale up 194
7.2.2. Prepare building blocks with more diversity 195
7.2.3. Synthesise monodisperse PEG (5000 Da) via ItSyN 195
7.2.4. Study site modification and characterise chiral sequence-defined polymers 195
8. Chemical synthesis experimental procedures 197
References 259
List of publications 276
Appendix 277

List of Figures

Figure 2.1 Synthesis of sequence-defined artificial macromolecules with evolutionarily optimized biological mechanisms [1]. Reprinted with permission from AAAS. 26
Figure 2.2 Chemical polymerization processes [44]. Reprinted with permission from the Royal Society of Chemistry.....31
Figure 2.3 Controlling sequences in a chain-growth polymerization[122, 125]. Reprinted with permission from WILEY‐VCH. 33
Figure 2.4 Chemical schemes of metal-catalyzed radical poly-addition (Left) [136] [137] and region-selective ROMP of asymmetric substituted cyclooctene (Right) [81]. Reprinted with permission from AAAS. 35
Figure 2.5 The concept of chemical iterative synthesis [1]. Reprinted with permission from AAAS.....37
Figure 2.6 Liquid phase synthesis of 2'-Me-RNA using multivalent hub, 1,3,5-tris(bromomethyl)benzene as a support [175]. Reprinted with permission from 2015 WILEY‐VCH. 40
Figure 2.7 Liquid-phase synthesis of sequence ordered block copolymers using a soluble polystyrene support [160]. Reprinted with permission from American Chemical Society. 42
Figure 2.8 Schematic of approaches for the synthesis of monodisperse PEG [199]. Reprinted with permission from the Royal Society of Chemistry. 45
Figure 2.9 ISA membrane formation process by phase inversion[217]. Reprinted with permission from American Chemical Society. 51
Figure 2.10 Iterative synthesis of peptide with membrane purification [251]. Reprinted with permission from American Chemical Society. 58
Figure 2.11 Case studies of purification via constant volume diafiltration in an ideal membrane separation system [217]. Reprinted with permission from American Chemical Society. 60
Figure 2.12 System diagrams of single-stage diafiltration and two-stage cascade diafiltration [256]. Reprinted with permission from the Royal Society of Chemistry. 61
Figure 2.13 Predicted yield improvement after 10 diavolumes for different product rejection [256]. Reprinted with permission from the Royal Society of Chemistry. 62
Figure 3.1 Schematic of ItSyN and project aims. 67
Figure 4.1 Photograph of a continuous membrane casting machine. 77
Figure 4.2 Schematically labelled 10L crosslinking tank for continuous casting membrane. 77
Figure 4.3 Schematics of membrane cross-flow cell screening.....78
Figure 4.4 PEG rejection data of bench casting PBI-DBX membranes in MeCN with different non-woven backings. 82
Figure 4.5 Membrane performance of bench casting PBI-DBX membranes with different PBI dope concentrations (17 wt%, 18 wt% and 19 wt%) in MeCN. 84
Figure 4.6 Schematic representation of the two-step crosslinking reaction between PBI and DBX. 86
Figure 4.7 Schematic of the membrane surface modification. 87
Figure 4.8 Solvent permeance of modified PBI membranes. 89
Figure 4.9 PS and PEG rejection data of modified PBI membranes shown above on panels (a) to (e). 92
Figure 4.10 Effect of surface modification on specific weight gain in (a) mg cm^{-2} and (b) mmol cm^{-2}. 93

Figure 4.11 SEM images and thickness of unmodified membrane and membranes modified with TPM and M-2005 (created by Dr. Patrizia Marchetti) 94
Figure 4.12 BJH adsorption and desorption for pore area of different surface modified membranes. 97
Figure 4.13 Pore size distributions of PEEK, 18% PBI-DBX-(RE1 2007) and 18% PBI- DBX-(M2005) asymmetric membranes determined by liquid-liquid porosimetry. 98
Figure 4.14 Case study Schematic of membrane separation of four pentagol building blocks and three armed tris(octagol) hub. 99
Figure 4.15 Case study of surface modified membranes; membrane permenace and rejections of building blocks and hub. 102
Figure 5.1 The Maldi-TOF spectrum of building block EG_{28} from Polypure, Norway. 108
Figure 5.2 Schematic of the two-stage diafiltration rig. 112
Figure 5.3 The ItSyN procedures of coupling, diafiltration and deprotection. 114
Figure 5.4 The ItSyN approach to monodisperse PEG synthesis. 118
Figure 5.5 MS spectrum of building block $ThpOEG_{28}OTs$ (a) and HPLC spectrums of building block $ThpOEG_{28}OTs$, $Hub(OEG_{28}ODmtr)_3$ and $Hub(OEG_{28}OH)_3$ (b). 120
Figure 5.6 P&ID of the two-stage membrane diafiltration rig. 124
Figure 5.7 Concentration profiles of building block and Hub product in two-stage membrane diafiltration rig. 125
Figure 5.8 HPLC traces of purified intermediates and products after each chain extension and deprotection. 127
Figure 5.9 The UPLC reaction progression of entry 10 using $Hub(OEG_{28}OH)_3$ and building block $TsOEG_{12}ODmtr$. 136
Figure 6.1 First approach of building block synthesis. 152
Figure 6.2 The reaction steps of the Sharpless dihydroxylation. 153
Figure 6.3 The use (1*R*)-(+)-camphanic chloride as the chiral auxiliary agent. 154
Figure 6.4 The ^1H NMR spectrum of camphanic derivative, d, for determining enantiomeric excess (ee) of (*R*)-1, 2-decanediol, 17. 155
Figure 6.5 The GC spectrum of the crude 1, 2-decanediol, 17, from asymmetric dihydroxylation. 157
Figure 6.6 The GC spectrum of the crude 1, 2-decanediol (17), purified (*S*)-1, 2-decanediol and purified (*R*)-1, 2-decanediol after crystallisation. 158
Figure 6.7 Second approach for building block synthesis. 161
Figure 6.8 HPLC spectrums of the final building blocks (25 and 33). 162
Figure 6.9 ^1H NMR spectrum of final building block 25. 164
Figure 6.10 ^1H NMR spectrum of final building block 33. 164
Figure 6.11 An alternative synthesis route if hydrogenolysis fails. 166
Figure 6.12 The ItSyN concept for sequence-defined PEG polymers. 168
Figure 6.13 The approach to sequence-defined PEG polymers synthesis. 170
Figure 6.14 Screening membrane performance of five different membranes with Octyl building block and Hub product in MeOH. 172
Figure 6.15 Screening membrane performance of 18 wt% PBI-DBX-M2005 with Octyl building block and Hub product in different organic solvents; on the right panel the MeOH was mixed with MeCN in the proportion indicated. 174
Figure 6.16 Concentration profiles of building block and Hub product in two-stage membrane diafiltration rig. 176

Figure 6.17 HPLC traces of purified sequence-defined intermediates and products after each chain extension and deprotection (a-d). 182
Figure 6.18 The HPLC reaction progression of the 1st and 2nd chain extensions using $Hub(OEG_8OH)_3$ and octyl building blocks A 25. 184
Figure 6.19 DSC temperature cooling profiles of hub-AAA, hub-AAABB and hub-ABABA. 187
Figure 6.20 UV- Vis spectrums of hub-AAA, hub-AAABB and hub-ABABA. 188
Figure 8.1 Concentration profiles of building block 4 and product 9 in two-stage membrane diafiltration rig. 204
Figure 8.2 Concentration profiles of building block 4 and product 11 in two-stage membrane diafiltration rig. 207
Figure 8.3 Synthesis of S2 and compound 43 from S1 236
Figure 8.4 Concentration profiles of building block 33 and product 44 in two-stage membrane diafiltration rig. 238
Figure 8.5 Concentration profiles of building block 33 and product 46 in two-stage membrane diafiltration rig. 241
Figure 8.6 Concentration profiles of building block 33 and product 48 in two-stage membrane diafiltration rig. 244
Figure 8.7 Concentration profiles of building block 42 and product 52 in two-stage membrane diafiltration rig. 249
Figure 8.8 Concentration profiles of building block 33 and product 54 in two-stage membrane diafiltration rig. 252
Figure 8.9 Concentration profiles of building block 42 and product 56 in two-stage membrane diafiltration rig. 254

List of Tables

Table 2.1 Comparison of current approaches for the monodisperse PEG synthesis. 47
Table 2.2 Details of pressure-driven separation processes and applications, as reported in references [208, 209]. 49
Table 5.1 Solvent gradients of monodisperse PEG HPLC method. 110
Table 5.2 Solvent gradients of monodisperse PEG UPLC method. 111
Table 5.3 Membrane screening results using different PBI membranes with building block 6 and Hub product 9 in MeCN and MeOH. 122
Table 5.4 Chemical kinetic study of chain extension of Hub($OEG_{28}OH)_3$ and building block $TsOEG_{28}ODmtr$ in different reaction conditions. 131
Table 5.5 Chemical kinetic study of chain extension of Hub($OEG_{28}OH)_3$ and building block $TsOEG_{12}ODmtr$ in different reaction conditions. 134
Table 6.1 Solvent gradients of PEG building block HPLC method. 143
Table 6.2 Scale-up results summary of building blocks synthesis in steps. 159
Table 6.3 Summary of the diafiltation of each of the homostar intermediates and products after each cycle with purities and yields. 178

Nomenclature

Symbol	Definition	Units
Å	A length unit equal to 10^{-10} m	m
r_A	Reactivity ratios of monomers A	-
r_B	Reactivity ratios of monomers B	-
B	Permeance	L m^{-2} h^{-1} bar^{-1}
R_i	Rejection of component i	-
V	Volume	m^3
A	Effective membrane area	m^2
t	Time of sample collection	s
Δp	Applied trans-membrane pressure	bar
$c_{P,i}$	Concentration of solute i in the permeate	mol
$c_{R,i}$	Concentration of solute i in the retentate	mol
k1	Mono-substituted imidazole crosslinking reaction rate	mol dm^{-3} s^{-1}
k2	Mono-substituted imidazole crosslinking reaction rate	mol dm^{-3} s^{-1}
D	Membrane pore diameter	m
$\beta_{A/B}$	Membrane separation factor	-
R	Fraction of (R)- enantiomer	-
S	Fraction of (S)- enantiomer	-
Q	Membrane flux	mL s^{-1}
V_f	Volume in the feed tank	m^3

List of Abbreviations

MeCN	Acetonitrile
API	Active pharmaceutical ingredient
A	Adenine
ATRP	Atom transfer radical polymerization
BJH	Barrett-Joyner-Halenda
Bn	Benzyl
BET	Brunauer, Emmett and Teller

BB	Building block
CM	Cross-metathesis
COSY	Correlation spectroscopy
C	Cytosine
DV	Diafiltration volume
DBB	Dibromobutane
DBX	Dibromoxylyne
DCM	Dichloromethane
DEO	Diepoxyoctane
DSC	Differential scanning calorimeter
DHP	Dihydropyran
Dmtr	Dimethoxytriphenylmethyl
DMSO	Dimethyl sulfoxide
DMAc	Dimethylacetamide
DMF	Dimethylformamide
DEPT	Distortionless enhancement by polarization transfer
ES-MS	Electrospray mass spectrometry
ee	Enantiomeric excess
EO	Ethylene oxide
ELSD	Evaporative light scattering detector
FID	Flame ionization detector
FDA	Food and drug administration
GC	Gas chromatography
GTI	Genotoxic impurity
Tg	Glass transition temperature
GA	Glutaraldehyde
G	Guanine
HSQC	Heteronuclear single quantum coherence
HPLC	High performance liquid chromatography
HWE	Horner−Wadsworth−Emmons
ISA	Integrally skinned asymmetric
IPA	Isopropanol
ItSyN	Iterative synthesis with organic solvent nanofiltration

LPOS	Liquid phase oligo synthesis
LPPS	Liquid phase peptide synthesis
MS	Mass spectrometry
MALDI-ToF-MS	Matrix assisted laser desorption ionization-time of flight mass spectrometry
MEPS	Membrane enhanced peptide synthesis
MsO	Methanesulfonyl
MeOH	Methanol
MWCO	Molecular weight cut off
MIS	Molecularly imprinted scavengers
mPEG	Monodisperse polyethylene glycol
Npm	Naphthylmethyl
NMR	Nuclear magnetic resonance spectroscopy
Mn	Number average molecular weight
Oligos	Oligonucleotides
OSN	Organic solvent nanofiltration
P-3CR	Passerini three-component reaction
PDA	Photo-diode array
P&ID	Piping and instrumentation diagram
PMB	P-methoxybenzyl
PEGs	Poly (ethylene glycols)
PGA	Poly(glycolic acid)
PAN	Polyacrylonitrile
PA	Polyamide
PANI	Polyaniline
PBI	Polybenzimidazole
PCL	Polycaprolactone
PDI	Polydispersity index
PEEK	Polyether ether ketone
PES	Polyethersulfone
PI	Polyimide
PLA	Polylactic acid
PCR	Polymerase chain reaction

PS	Polystyrene
PVDF	Polyvinylidene fluoride
PG	Protecting groups
QbD	Quality by design
ROMP	Regioselective ring-opening metathesis polymerizations
RNAi	RNA interference
SSD	Single stage diafiltration
NaH	Sodium hydride
SPOS	Solid phase oligo synthesis
SPPS	Solid phase peptide synthesis
TBDMS	Tert-butyldimethylsilyl
THF	Tetrahydrofuran
THP	Tetrahydropyranyl
TOABr	Tetraoctylammonium bromide
TPM	Tetraphenylmethane
TFC	Thin film composite
TLC	Thin layer chromatography
T	Thymine
TsO	Toluenesulfonyl
tRNAs	Transfer RNAs
TFA	Trifluoroacetic acid
Tr	Triphenylmethyl
UPLC	Ultra-performance liquid chromatography
UV-Vis	Ultraviolet–visible spectroscopy
M_W	Weight average molecular weight
XDA	Xylylenediamine

1. Introduction

In past years, scientists have given high attention to manipulating the architecture of synthetic polymer materials. Conventional approaches for common synthetic polymers generally offer poor control of the sequential arrangement of monomer units along polymer chains. This results in polydisperse homopolymers or random-monomer-distributed block copolymers with simple chain microstructures. Conventional polymers have been widely produced at an industrial scale, however they do not offer the structural and functional complexity required for medical and nanotechnology applications.

Unlike conventional synthetic polymers, natural bipolymers such as oligonucleotides (oligos), peptides, and oligosaccharides, normally consist of precisely defined sequences and monodisperse chain lengths. These natural biopolymers play an important role in pharmaceutical and nanotechnology applications. Due to limitations on natural resources, fabricating monodisperse and sequence-defined polymers has attracted great interest from polymer chemists. Sequence-controlled polymers are macromolecules in which monomer units of differing chemical nature are arranged in an ordered fashion. Like the natural biopolymers, monodisperse and sequence-defined synthetic polymers offer the great advantage of precise structural and functional definitions, with the broad chemical variability in polymer science. Monomer sequence regulation plays a key role in biology and is a prerequisite for crucial features of life, such as heredity, self-replication, complex self-assembly, and molecular recognition [1]. Iterative synthesis is inspired by nature; in order to ensure the accuracy and sequence purity, polymers are assembled iteratively using step-by-step monomer addition. Solid phase peptide and oligo iterative synthesis are commonly used in industry, but their purification and scale-up are challenging. Human engineered synthetic polymers such as poly (ethylene glycols) (PEGs), poly (ethylene imines) and poly (L-Lysine), are synthesized using conventional industrial approaches such as living/controlled polymerisation. These methods lead to polydisperse synthetic materials due to the statistical nature of polymerisation reactions.

A wide range of scientific and technological applications using synthetic macromolecules with controlled monomer sequences are anticipated. Protein- and DNA-based nanotechnologies demonstrate that information can be stored and transferred at the molecular level by synthetic polymer chains. Therefore data storage, by controlling the monomer sequence of a synthetic polymer, could become an interesting topic for polymer chemists to explore. Secondly, the

manipulation of the monomer sequences offers structural control of the macromolecules. The monomer sequence significantly influences macromolecular folding and self-assembly. Thirdly, it has been reported that monomer sequence control influences some macroscopic properties. Some physical properties of sequence-controlled polymers such as conductivity, rigidity, elasticity, or biodegradability vary with the order of the polymer sequence. For example, the conformation of the polymer in solution, like the self-assembly behaviour, was strongly affected by the monomer sequence [2]. Therefore, it is of great utility to achieve precise control of monomer sequence. It opens up opportunities for controlling the structural and macroscopic properties of the macromolecule materials, and ensures that they could be tuned by polymer construction.

In this thesis, an innovation new technology for the fabrication of monodisperse and precisely sequence controlled polymers, for use in healthcare and nanotechnology, is proposed and tested. The synthetic chemistry was implemented with an effective purification using organic solvent nanofiltration (OSN), and employing quality by design (QbD), with both integrated into one technology platform. This provides potential for a breakthrough in sequence designed polymer chemistry and manufacturing engineering. Synthetic polymers with different structures and functionalities might be designed and fabricated using this new technology at an industrial scale.

2. Literature review

2.1. Biopolymer definition, characterisations and applications

Biopolymers, synthetic polymers and their derivatives are commonly used in a variety of applications, especially in the pharmaceutical and medical fields. The rapid development in polymer chemistry and related technology in recent years has opened new and exciting prospects. The increasing interest of scientists has been focused on drug delivery systems, therapeutic systems and macromolecular prodrugs using natural and synthetic polymers, which are in high demand by the market and industry. In synthetic polymers, particular attention has recently been paid to polymerisation chemistry to synthesize precisely defined, monodisperse polymers. This is because they offer extraordinary advantages imparted by precise structural and functional characteristics, without restricting the broad chemical variability of synthetic polymers. Furthermore, biocompatible and biodegradable polymers have also been intensively investigated and reported in many papers. They have the advantage of being readily hydrolyzed into removable and non-toxic products, which can be subsequently eliminated by metabolic pathways[3]. Such biocompatible and biodegradable polymers show great potential to meet specific criteria required for macromolecular prodrugs for drug delivery systems and therapeutic systems [4].

2.1.1. Natural macromolecules

Oligonucleotides (oligos) play an important role in pharmaceutical use, due to their great potential for controlling protein expression mediated by RNA interference (RNAi) [5, 6]. Oligos show an advantage of safe and effective delivery in humans that makes them highly demanded in the pharmaceutical market. One of the major reasons for oligos being high cost is production scalability. So far most manufactured RNA is prepared using solid phase oligo synthesis (SPOS), since it has the advantage of ease of separating the solid support from any molecular species not covalently attached to it.

Natural macromolecules normally contain more than two monomers and if monomer sequence patterns are controlled at a complex level precise information can be coded at a molecular level along the polymer chains [5]. For example, the nucleic acids, such as DNA and RNA, contain

four-nucleotide monomer units and all of the molecules show an exact sequence order from the backbones. Proteins are even bigger macromolecules which are composed from 20 amino acids monomers [7]. The amino acids are arranged precisely in a regulated monomer sequence.

2.1.2. Synthetic polymers (polyether, polyester)

The development of synthetic polymers has been established for decades. A wide range of polymeric materials with different physical and chemical properties has been extensively studied, and tailored to meet the highly diversified demands of modern technologies such as coatings, adhesives, fibre, foams, and thermoplastic elastomers [8]. Inspired by natural biopolymers such as proteins and polysaccharides, some of the synthetic polymers also possess features of biocompatibility, such as bioabsorbability and mechanical resistance [9-11]. Synthetic polymers are widely employed in tissue engineering, biomedical and controlled drug delivery applications [4, 12, 13].

Polyethers and polyesters are useful candidates for medical use, and they have also been used as chemotherapeutic agents, local anaesthetics, anticoagulants, neuro-active drugs and anticancer agents [14]. Among polyurethanes, polyether-based polyurethanes are resistant to biodegradation, while polyester-based polyurethanes are readily biodegradable, such as polycaprolactone (PCL), polylactic acid (PLA) and poly(glycolic acid) (PGA) [15-17]. A large variety of monomers and various routes leading to the development of synthetic polyesters have recently been reviewed due to their important diversity and synthetic versatility [18]. The development of waterborne polymer formulations has been investigated [19, 20]; these synthetic polymers had the advantage of low viscosity at high molecular weight, non-toxicity, for medical applications [21].

2.1.3. Significance of monodisperse polyethylene glycol (PEG) polymers

PEGs are good, versatile, chemically stable polymers with applications across several fields including drug therapeutics [22], pharmacology [23], carbon nanotubes [24], material science [25, 26] and nanotechnology [27]. For example, a copolymer of ethylene and propylene glycols has been reported for applications in the therapies for constipation [28]. Non-ionic, water soluble PEG polymer has also played an important role in liposome development [29] and the delineation of the structural mechanisms of lipid-bilayer formation and fusion [30].

Heteromultifunctional PEGs with different reactive groups at either end of the chain or as side chains, have even wider applications than monodisperse PEGs. This is because they can be selectively modified and efficiently conjugated to molecules and surfaces without any risk of looping or homodimerisation [31].

Modification with appropriate reactive groups could make heteromultifunctional PEGs applicable for the PEGylation (the attachment of PEG to therapeutic molecules) of large biologically active species such as oligos, peptides and biopharmaceuticals for drug delivery purposes. PEGylation is a commonly used technology [32, 33]. It is effective in enhancing immunogenicity as well as increasing stability, pharmacokinetics and modes of action of pharmaceutical macromolecules. In addition, it has been used to dramatically extend serum half-life, and enhance the oral bioavailability of substrate molecules by increasing hydrophilicity in solution, and solubility [34]. A PEGylated macromolecular prodrug was formed by the conjugation of a therapeutic agent as a pendant group to polyethylene glycol as a substituent [35, 36].

The traditional polymerisation of ethylene oxide (EO) normally results in a size distribution, or polydispersity, of different chain lengths. The distribution of chain lengths for a given PEG size is Gaussian. The level of polydispersity is characterised by the polydispersity index (PDI=Mw/Mn), which is equal to the weight average molecular weight (M_W) divided by the number average molecular weight (Mn) [37]. Current commercial PEGs which are manufactured at industrial scale, which can form materials with a PDI as low as 1.03, are readily available [38, 39]. This corresponds to a wide half-height width of the Mw distribution. Due to the large variety of sequence compositions in polydisperse PEGs and the PEGylated conjugates, regulatory bodies considering polydisperse PEGs are inclined to demand further investigation for drug approval [40, 41].

Therefore it is desirable, particularly in nanotechnology and pharmaceutical applications, to fabricate polymers with a uniform chain length, i.e. monodisperse oligomers, which are completely defined, discrete structures, This is because the sharply defined structures give greater control of physical, chemical and pharmacokinetic properties of the PEGs. This is very important to eliminate disturbances and allow more accurate characterization. However, monodisperse PEGs are difficult to fabricate due to numerous purification processes and the resultant high cost. With the growth in molecular weight of PEG polymers, especially for the

highly valued heteromultifunctional PEGs, purification becomes even more difficult using column chromatography, and results in low yields.

Currently, there are a few challenges in PEG synthesis technology. Firstly in order to obtain pure PEGylated proteins, the monodisperse PEGs needs to achieve molecular weights which are greater than at least 5000 Da, as the enhancement of in vivo serum half-life is most significant at above 20 kDa [42]. Secondly, current commercial PEG sources are insufficiently pure, so scalable synthesis approaches for preparing monodisperse pure PEGs are required [31]. Lastly, the design of heteromultifunctional PEGs with different reactive groups for drug therapeutics is still under exploration. A versatile synthesis strategy for desirable heteromultifunctional PEGs, which could tolerate various reaction conditions, requires investigation.

2.1.4. Properties and promises of sequence-defined polymers

Most synthetic polymers are categorised as copolymers, which contain at least two monomers of different chemical nature in their side chains [43]. In conventional polymerisation approaches, the resulting polymer sequences vary from chain to chain. This is because the monomer distribution and the chain length of the polymers depends on the specific reaction mechanisms and are not well controlled. Ideally, in a sequence controlled polymer - such as alternating, periodic, or block copolymers - the monomers are arranged in precise order and length for all chains [44]. Synthesis becomes much more complex when the number of monomers increases and a precise sequence order is required for the copolymer composition along the chains. The synthesis of well-defined polymers with controlled primary structures and properties could be the next breakthrough in polymer design.

Sequence-defined polymers have opened up technological opportunities in material science regarding folding and self-assembly. Some features of proteins can be extended to chemically synthesised sequence-defined polymers [45]. In biology, the self-assembly behaviours of sequence-controlled oligomers, such as oligopeptides and oligonucleotides, have been studied [46, 47]. It was revealed that sequence-defined oligopeptides can self-organize into a variety of nanostructures, such as fibres, tapes, ribbons, vesicles, and tubes. The study of self-assembly behaviours has also been extended to other sequence-defined materials such as biocompatible polymers [48], conducting polymers [49], and inorganic matter [50]. For example, self-

assembly behaviour of triblock copolymers containing nucleobases is strongly influenced by the block sequences [51, 52]. Engineering of the nucleic acid sequence is an alternative to control and optimise the properties of macromolecules. For example monomer sequences of polymers have been engineered in order to obtain charged water-soluble middle blocks, flanked by two self-associating leucine zippers [53]. Such structure optimised polymers improved the pH and thermo-reversible gelling in an aqueous medium. In addition, the self-recognition of complementary DNA strands is currently an attractive feature for regulating and controlling building-blocks precisely and efficiently. Self-recognition technology has been developed for non-natural polymers based on biological mechanisms. Some protein-like globular materials can be prepared using different chemistries [54, 55], resulting in molecules exhibiting promising, enzyme-like behaviours. It has been reported that a monomer sequence of polymers could be regulated by the folding of individual polymer chains, driven by the helical assembly of non-natural side-chain molecular motifs [54, 55].

Moreover, sequence-regulation strongly influences the macroscopic properties of polymer materials. In recent publications, it has been shown that the solubility and phase transitions of fabricated polymers in water and organic solvents can be tuned by using precise monomer sequence modifications [56-58]. It has been discovered that the phase behaviour of polystyrene-based block copolymers can be influenced by sequence-controlled segments [59]. The mesophases and semicrystalline phases of the polymers could be altered by sequence rearrangement [59, 60]. More properties of polyelectrolytes, such as charge density [61] and persistence length [62], can also be precisely adjusted by sequence regulation. It has also been reported that the degradation kinetics of biodegradable aliphatic polyesters are strongly influenced by monomer sequences [63, 64]. The primary structures of sequence controlled non-natural polymers can also be tailored to optimise interactions with specific materials, i.e. DNA complexes. For example, monomer sequence was optimised in non-natural macromolecules for gene-delivery and the mineralization control of inorganic materials [65, 66].

Another great application for sequence-defined polymers using material science and nanotechnology is inspired by the non-biological use of DNA [47]. Similar to DNA molecules, different functional side chains from sequence-defined monomers can be regarded as codes and information that could be encoded and stored at the molecular level [67, 68]. In DNA polymers, heritable information is encoded with four nucleotide units arranged in the chain; the encoding storage capacity could be massive for polymer chains. In nanotechnology, the

information storage mechanism of DNA can be used in a non-biological context [69, 70]. A full textbook containing about 50,000 words has been written with DNA and read using next-generation sequencing technology, as reported by Church et al. [69]. In this research, nucleotides adenine (A) and cytosine (C) encoded a 0, whereas guanine (G) and thymine (T) encoded a 1, and short molecular barcodes were used for tracking in oligonucleotides chains. This breakthrough demonstrates the feasibility for data storage using sequence-defined polymers. Additionally, recent innovations in rewritable nucleic acid storage demonstrate that this technological field is progressing rapidly [71]. However DNA molecules have a limited variety of monomers and synthetic schemes for the manipulation of sequence order. Therefore, many alternatives for preparing sequence-defined macromolecules have been proposed to enable different structures and functionalities. Although the synthesis of sequence-defined polymers has been proposed, research in this area is still under exploration, and generally products are restricted to oligomers. However, the development of more efficient chemical kinetics and separation technologies holds great promise for the development of sequence-defined polymer fabrication.

In general, the development of synthetic, nonnatural sequence-regulated polymerization processes has permitted control over molecular arrangement, and could allow the design of polymer materials with desirable physicochemical properties. The discovery of nonnatural, sequence-defined synthesis has broadened the scope of available polymer structures, functionalities and applications. However the preparation of these sequence-defined polymers remains limited by economic and technical factors, chemical diversity, and scalability. In order to achieve a highly level of polymer sequence precision by chemical synthetic approaches, an efficient, scalable, and versatile technology platform needs to be designed by merging current biological knowledge and polymer chemistry techniques.

2.2. Precision polymer synthesis and separation methods

2.2.1. Sequence controlled biological polymerization processes

Various synthetic methods for controlling monomer sequences in polymers have been explored. Presently two main approaches are used to synthesize sequence-controlled polymers, which are based on biological and chemical mechanisms. The most prominent way to synthesize sequence-controlled polymers utilizes the biological principles of natural polymer sequences.

For instance, the DNA templates, enzymes, or even living organisms can be used to prepare sequence-defined polymers. In addition, sequence-controlled polymerization processes include replication, transcription, and translation of protein from a DNA sequence involving complex biological mechanisms. Sequence order in the macromolecules is highly controlled. Mimicking biological sequence regulation has been applied successfully in the preparation of some non-natural polymers. The biological approach highly relies on the specific biological mechanisms and can be very efficient for certain reactions. Using the biological concept, the polymerase chain reaction (PCR) [72] and protein engineering [73] have been developed to synthesize nonnatural biopolymers. Compared to traditional synthetic polymerization processes, biological approaches normally rely on very efficient mechanisms, permitting a greater rate of polymerisation in addition to a sequence that is precisely controlled. However the structure and functionality of the polymeric products is limited by the mechanisms.

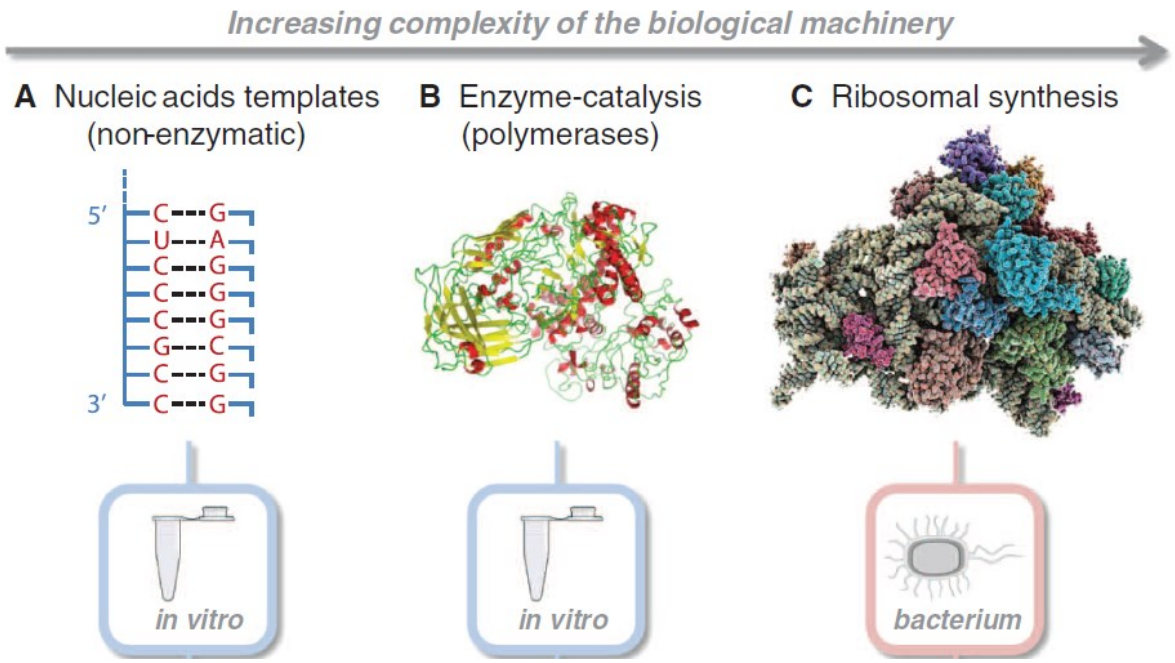


Figure 2.1 Synthesis of sequence-defined artificial macromolecules with evolutionarily optimized biological mechanisms [1]. Reprinted with permission from AAAS.

2.2.1.1. Template synthesis

For natural polymers, monomer sequences in polymers are controlled via template synthesis, for example in DNA, RNA and proteins. The processes of DNA replication, transcription and

translation all rely on template mechanisms [74]. The most widely used mechanism for non-natural biopolymers utilises DNA templates, shown in Figure 2.1 (A). In biology, sequence-defined biopolymers are synthesized by coupling of corresponding nucleotides via Watson-Crick base pairing on the oligonucleotide templates.

The DNA template concept has been pioneered and developed in many publications [74-76]. Methods using DNA templates have simple mechanisms; base pairing ensures the accuracy of the sequence and polymerization was formed via chemical bonds. In a synthetic process, a template mechanism denotes a polymerization performed in the presence of a complementary macromolecule [44, 77, 78]. Due to specific linkages with the template, this approach guarantees accurate sequence order in the biopolymers. The concept of template synthesis was extended to non-biological synthetic polymerizations in the late 1970s. Non-natural, or artificial, template backbones including non-natural peptide nucleic acids were used in synthesis [79-81]. Artificial backbones based on nonribose sugars and polyamide backbones based on peptide nucleic acids were efficiently used as templates for sequence-defined RNA synthesis [76, 82]. A further study was performed using macrocyclic peptide nucleic acids adapters, analogous to transfer RNAs [83]. They served as an intermediate layer between DNA templates and corresponding synthetic monomers to form long sequence-defined polymers with up to 40 units [83-85]. Unlike the DNA translation process, the template synthesis occurred in the absence of enzymatic replication of nucleic acids [86]. This work resulted in a wide range of chemical varieties incorporated in sequence-defined polymers using DNA templates. For example, β-peptides of up to 26 kD containing blocks comprising of 90 densely functionalized β-amino acid residues were synthesised from 16 consecutively couplings [85]. However without the assistance of enzymes, DNA template coupling suffers low efficiency and replication fidelity. This phenomenon may be caused by either low reaction activation without enzyme-catalyzed polymerizations or steric hindrance from two bulky coupled sequences for the consecutive monomers. Therefore the length and complexity of the obtainable sequence-defined polymers using DNA templates are limited.

Vinyl monomers with a set of nucleobases on the side chains can be used to synthesize sequence regulated polymers via free radical polymerization [77]. Successful synthesis of chemical polymers using these templates has been reported in a few studies, but the sequences were not precisely arranged [78, 87, 88]. DNA-templated synthesis has been also reported as a dissociative reaction scaffold between triphenylphosphonium and aldehyde to give a C=C bond

and phosphine oxide via the Wittig reaction. A sequence-regulated decamer was constructed by embedding building blocks from one DNA terminal to another [89, 90]. In order to encode information precisely in synthetic polymer chains, like DNA sequences, DNA strands were applied to synthesize sequence-defined linear and cyclic oligomers based on bis(2-thienyl) pyrrole and aniline [91]. However it has been found that the DNA strands limited the polymer chain lengths.

Controlling the direction of sequence synthesis is another key factor in improving the accuracy of polymer sequences. The design of the template significantly influences the control of the reaction selectivity in templates synthesis. It is reported that vinyl monomers with a radical initiator site and a recognition site have been used to prepare sequence-defined polymers with a good purity [92-94]. Again, this approach required a single monomer addition process and was limited to shorter oligomers. For longer polymers, multiple recognition sites needed to be arranged on a template, which caused reactivity to decrease. Combining template and chain growth polymerisation has been proposed; precisely defined periodic polymers were prepared using multi-vinyl monomers on a cleavable template; the immobilization of the vinyl groups on a template avoided both cross-linking reactions and unfavourable jumping propagation during the process of polymerization [94, 95].

In general, template systems have great utility for regulating monomer sequences in biopolymers. However they have disadvantages for synthetic polymers; they offer low overall polymer yields, with the correct sequence, and are difficult to scale up. Secondly, template synthesis restricts both coupling rate and achievable molecular weight. The structures of chemical polymers that can be prepared are also limited, depending on the mechanisms used to achieve sequence specificity.

2.2.1.2. Catalysis

In Figure 2.1 (B), another important biological mechanism is shown: the polymerase chain reaction (PCR) replicates sequence-encoded DNA strands using enzyme catalysts. The technique was initially studied with the Klenow fragment of DNA polymerase I [72]. Discovery of the thermostable Taq polymerase facilitated the use of PCR synthesis at commercial scale. However during strand dissociation, PCR requires high temperatures and the requirements of the enzyme catalysts limit the types of polymer that can be synthesized.

Applications of PCR were expanded to non-natural base pairs in enzyme-catalyzed conditions [96, 97]. However the coupling fidelity of non-natural nucleotides presents challenges. Reactions preparing artificial sequence-defined polymers using the noncanonical monomers were discussed by Malyshev et al. [98]. Leigh's group used an artificial rotaxane-based molecule as the catalytic machine for synthesising sequence specific peptides [99]. A molecular ring with a thiolate initiator moves on a molecular axle on which monomers are attached. The directional progression of the ring on the axle allows sequence-controlled polymerization to occur. Yttrium catalysts have been used to prepare alternating sequence polyesters from enantiomerically pure monomers [100]. This approach has the potential to form sequence-defined macromolecular structures, however the choice of the catalysts is still being explored, and they play important roles in controlling polymer sequences in this process.

2.2.1.3. Ribosomal machinery

The most complex biological mechanism for synthesizing sequence-defined polymers is the ribosomal machinery in a living organism, shown in Figure 2.1 (C). The synthesis of sequence-defined macromolecules such as therapeutic proteins, structural proteins, and enzymes has been developed and reported. For this, an artificial gene was incorporated into plasmid DNA and placed into a bacterial host. Expression occurred in the host to synthesize sequence-defined proteins [101, 102]. This technology has been utilized to synthesize non-natural proteins. In this case, the natural amino acids were removed from the bacterial host and nonnatural amino acids were placed into the proteins [103]. Improvements have been carried out to combine nonnatural monomers into the common 20-amino acid alphabet [104]. This protein engineering technology has been applied for better storage of the coded information within non-natural protein structures [73, 101]. The downside of combining the ribosomal machinery and nonnatural monomers to form sequence-defined polymers is a slower reaction rate, and the structural constraints imposed by the ribosome.

2.2.2. Sequence controlled chemical polymerization processes

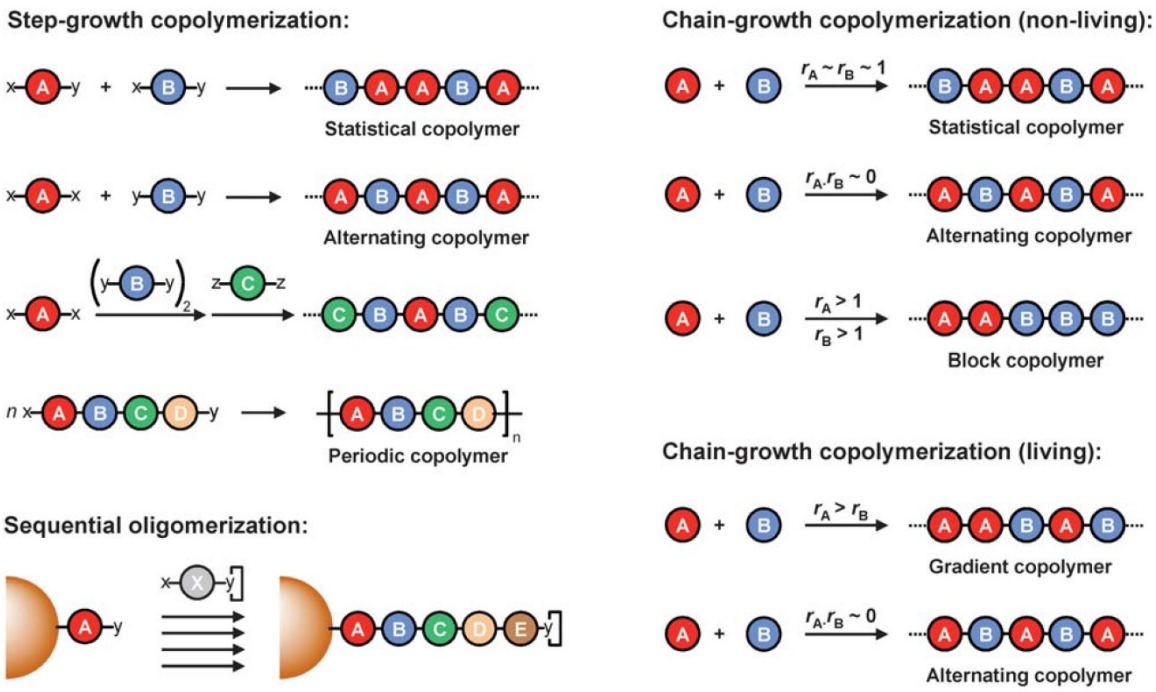
Although biological polymerization approaches give precise monomer control over the polymer chains, the structures and complexities of synthesized polymers are limited. Therefore the synthetic chemical processes are proposed to enrich the diversity of achievable polymers

using a variety of chemical mechanisms. In the past a few years, different chemical syntheses have been studied to widen the synthetic polymer categories. Chain-growth and step-growth polymerizations are two common methods to prepare simple sequence controlled materials on a large scale. However, such protocols cannot organise monomer sequences precisely. The chemical mechanisms required to form sequence-defined polymers are not well developed. The types and the lengths of synthetic polymers that are prepared in these processes are limited. Many factors such as specific kinetics, or the particular catalytic or template conditions, are not yet well investigated.

Different chemical mechanisms to control monomer sequence during polymerisation have been studied. The development of living polymerization methods such as ionic polymerizations [105], controlled radical polymerizations [106, 107], and ring opening metathesis polymerization [108], has opened up the opportunities to form multiblock copolymers with complex molecular structures via chemical reactions [109]. Macromolecular chemistry has successfully extended the synthetic sequence regulation to non-biological applications. The diversities of structures and functionalities of sequence-defined polymers have been broadened [110]. The development of molecularly encoded synthetic polymer chains may open up opportunities in materials science and nanotechnology.

2.2.2.1. Chain-growth polymerization

Sequence regulation can be achieved based on the reactivity between specific monomer pairs via chain-growth polymerizations, which consists of chain-initiation and chain propagation steps, as shown in Figure 2.2. During the chain-growth polymerizations, the propagation steps rely on highly reactive transient species, such as radicals or ions, which are difficult to control when preparing a sequence-defined polymer. For example, a distinct monomer pair does not always lead to the same polymer sequence in different polymerisation conditions [111-114]. A conventional free radical polymerization leads to a heterogeneous chain-to-chain composition, while a controlled or living radical polymerization process generates gradient copolymers with a homogeneous chain-to-chain composition [115-117].



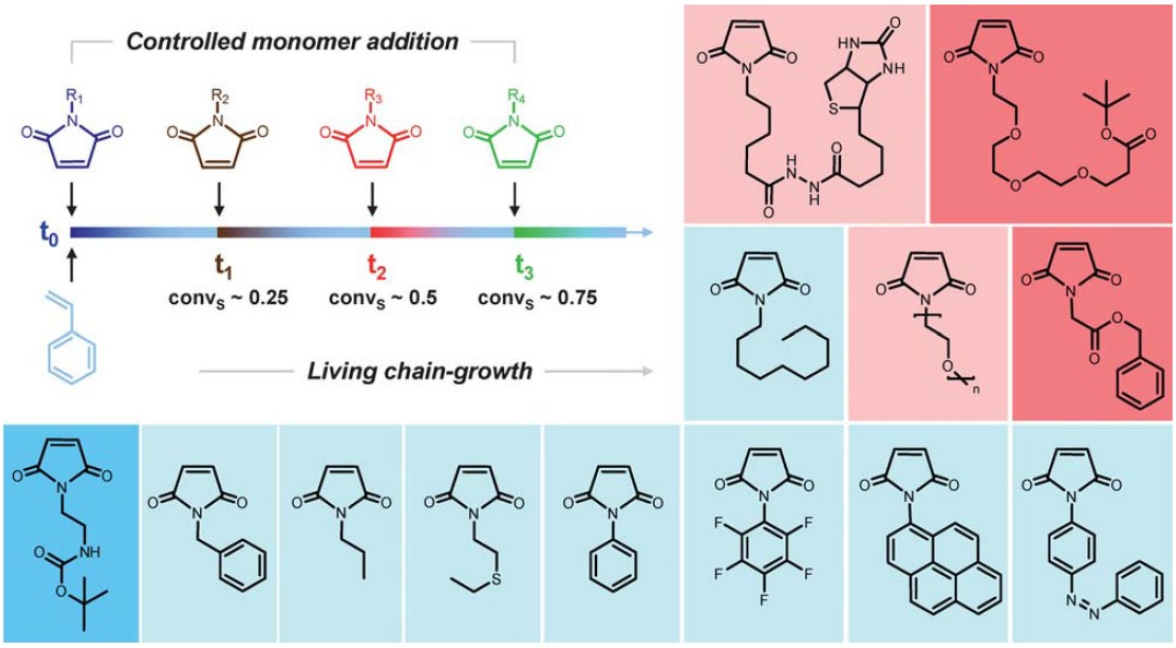
The capital letters A, B, C, D, E and X represent different monomer units. The letters x, y, and z represent different types of reactive functions. The letter y included in a square box represents a protected y function. The symbols rA and rB represent the reactivity ratios of monomers A and B, respectively.

Figure 2.2 Chemical polymerization processes [44]. Reprinted with permission from the Royal Society of Chemistry.

However, some publications demonstrated excellent control of primary polymers' structures with chain-growth processes, based on the intrinsic chemical reactivity of monomers [118-120]. Combinations of different monomers including one electron-donor monomers such as styrene and vinyl ether, and one electron-acceptor monomers such as maleic anhydride and maleimide, are shown in Figure 2.3. This copolymerization has two unique kinetic features: (i) all the polymer chains are growing simultaneously and (ii) the cross-propagation of the monomers is highly favoured as compared to homopolymerization. When the reactivity between the two monomers was much faster than the reactivity of the monomers themselves, a sequence-defined alternating polymer was obtained [121]. Other sequence orders, rather than alternating polymers between two monomers, can also be prepared with the specific reactivity of cross-propagation and homopropagation. In theory, the discrete amounts of one monomer can be

added and consumed extremely rapidly in the copolymerization process and they are therefore locally incorporated in narrow regions of the growing chains with the other monomer [122]. In the paper [123], the polymerisation of two monomers (A: maleimide as an acceptor, B: limonene as a donor) formed a sequence-defined polymer with repetitive AAB patterns. This unusual pattern was mainly explained in terms of the reaction solvent, fluoroalcohol; the interaction between the bulky fluoroalcohol and the carbonyl of the maleimide monomer (A) was more active, while the bulky limonene monomer (B) created strong steric hindrance for coupling monomer A. More precise control of monomer sequence was achieved by manually controlling the addition time of different monomers with monomer conjunction in living polymerization, by the Lutz group [124]. Sequence-defined polymers with side chains of different functionalities were prepared and reported. The concept was pioneered in controlled radical polymerization, e.g. atom transfer radical polymerization (ATRP), using the donor monomer, such as styrene in an excess amount and the functional acceptor monomers were controlled during the course of the reaction [124, 125]. Due to the favoured coupling of cross-propagation, by controlling the acceptor addition time, the acceptor monomers could be incorporated precisely in narrow regions of the growing polymer chains.

Lutz et al. continued their work to apply 20 functional N-substituted maleimides bearing various functional groups as acceptors. The functional N-substituted maleimides could be efficiently incorporated into the polystyrene chains, as shown in Figure 2.3. This concept was utilized for preparing macromolecules with programmed sequences of functional monomers. The sequence-controlled copolymerization of donor and acceptor monomers enables the preparation of PEGylated polymers with precisely controlled functional microstructures [122, 126]. Complex macromolecular structures and functionalities can also be obtained through post modification [127]. The disadvantage of this approach is that it was limited by its polymerization protocols, which yielded restricted polymer structures. These polymerization still showed some polymers' defects in length and sequence, the obtained polymers still exhibited a narrow sequence distribution [114, 128]. With this approach it is also difficult to create long sequences of functional monomers. For example, it is difficult to kinetically control the addition of five maleimides or more without automated assistance, such as online monitoring of monomer conversions and automated maleimide additions.



Apolar monomers (light blue); monomers bearing a hydrophilic moiety (pink); monomers with a protected basic function (dark blue); monomers with a protected acidic function (red).

Figure 2.3 Controlling sequences in a chain-growth polymerization[122, 125]. Reprinted with permission from WILEY-VCH.

In addition, selected monomers or catalysts with particular reactivity play important roles in regulating monomer sequences in chain growth polymerizations. For example, in highly controlled living polymerization mechanisms, some dormant species are used to prevent the inherent tendency of the monomers to react with themselves and form incorrect sequences. In order to avoid the inherent tendency of the monomers, the reactivity of the monomers during polymerization needs to be reduced. The reactivity of vinyl ethers as monomers for living cationic polymerization was studied with the catalyst of ZnI_2 [129].

Atom transfer radical polymerization (ATRP) is a common radical polymerization for controlled monomer sequence using single monomer addition [131]. However it requires that the monomer has an active terminal for radical generation and propagation, and sometimes metal catalysts for polymerisation are needed. For example non-conjugated vinyl monomers could undertake atom-transfer radical addition, then as the hydroxyl methyl side chain was subsequently oxidized into a carboxylic acid, the terminal site of the monomer became active

for radical propagation and the additions of allyl alcohol occurred iteratively. The side chains of the resulting sequence-defined polymer can be modified and functionalised via esterification [131]. Another popular monomer that is used in single-monomer addition is the vinyl monomer; the coupling of the monomers is achieved via the olefin cross-metathesis (CM) reaction. It is reported that 4-vinylbenzaldehyde was converted into a vinyl group via Wittig olefination and the monomer was then active for the sequential coupling CM reaction [132]. The sequence-defined conjugated oligo(phenylenevinylene)s were prepared with monomer addition via CM and olefination. This concept has been reported and a series of sequence-defined oligomers from dimer to hexamer were synthesized [133].

2.2.2.2. Step-growth polymerisation

Step-growth polymerisation is also studied for the synthesis of sequence-regulated macromolecules, relying on the reactivity of the functional monomers on the chain termini (x, y and z in Figure 2.2). This approach generally offers better control of polymer sequence than chain-growth process [124]. During step growth polymerisation, the distinct monomers of the xy-type normally lead to statistical polymerizations. Secondly, the ordered AB alternating sequence polymers are commonly prepared from this approach with selected reactivity using monomers of the xx and yy types [134]. Up to three monomers in ordered sequences can be achieved via step-growth polymerization with selected reactivity [96].

In order to iterate the chain extension, the building blocks were allowed to have a reactive site on the chain ends. The azide–alkyne cycloaddition polymerization used a 'click' reaction to form well-defined vinyl polymers [135]. Most of the radical polyadditions needed metal catalysts to generate a carbon radical species from the nonconjugated olefin, and a carbonchlorine bond to generate a vinyl chloride as the junction linkage, eventually giving vinyl polymers with periodic sequences, as shown in Figure 2.4. A wide range of metal catalysts have been considered, such as Ru, Fe and Cu, and their polymerisation efficiencies have been reported [136, 137]. Sequence-specific vinyl copolymers have been obtained from asymmetric substituted cyclooctenes through hydrogenation, via a process known as regioselective ring-opening metathesis polymerizations (ROMP), as shown in Figure 2.4 [81]. Using the same concept, sequence-defined vinyl polymers with a variety of alkyl chains as branches can be prepared from symmetric dienes via an acyclic diene metathesis

polymerization [79]. This versatile design also allows the introduction of amino acids and drugs at well-defined positions in polyethylene for biological applications [80].

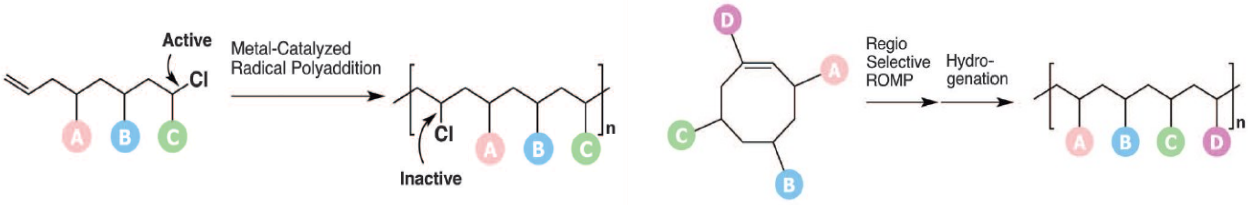


Figure 2.4 Chemical schemes of metal-catalyzed radical poly-addition (Left) [136] [137] and region-selective ROMP of asymmetric substituted cyclooctene (Right) [81]. Reprinted with permission from AAAS.

2.2.2.3. Reconstitution

Most present approaches for preparing sequence-defined polymers present challenges, in terms of optimising both chemistry kinetics and separation techniques, for directly synthesizing oligomers with relatively high molecular weight,. The molecular weights of monodisperse linear polymers that are synthesized using the traditional exponential-growth strategy rarely exceed 5000 Da [138, 139]. To combat this, the approach that is described as ‘‘reconstitution’’ involves linking short sequence-defined oligomers together to achieve longer polymer chains. The strategy has been applied to the synthesis of proteins entirely by chemical synthesis [140]. In order to assemble short oligopeptides into high molecular weight proteins with regulated sequence order, native chemical ligation and fragment condensation can be applied [141]. It is shown that ligation techniques are very efficient and reliable to synthesize sequence-ordered macromolecules of unprecedented high molecular weight [142-144]. In this way, short sequence-defined motifs have been prepared via ring opening polymerizations and step growth polymerizations achieving a good purity [145, 146]. Step growth ‘click’ polymerization has been applied to prepare short sequence-defined peptides [147]. The use of short oligopeptides that contained 3 to 10 ordered monomer units to form sequence-defined polypeptides has been published [148-150]. Shorter fragments of oligopeptides can be joined together to form longer sequences defined peptides via fragment condensation to overcome the arithmetic inefficiency of stepwise synthesis, but the long reaction time remains a disadvantage [151]. This strategy allowed the straightforward construction of high molecular weight macromolecules with

precisely controlled primary and secondary structures. A similar idea has also been developed for other synthetic polymers. The Lutz group has reported the synthesis of high molecular weight polymers with periodic functional motifs containing side chains of benzyl, FmocNH- and tert-butyl ester [126]. The allocation of these side chains indicated the accuracy of the sequence-defined oligomers. In this approach, the reactive precursors were ultimately polymerized by step-growth 'click' coupling to achieve reactive α-alkyne, ω-azido heterotelechelic polymers. This is to say, by controlling the sequence of the synthesized polymers, the structures and functionalities of the obtained polymers could be post modified and controlled by the sequence order.

2.2.2.4. Iterative synthesis

The strategies discussed above provide polymers with a narrow distribution of molecular weight, but did not achieve uniform chain lengths and precisely controlled sequences. In order to prepare truly uniform sequence-defined polymers chemically, the most obvious approach is to attach monomer units one by one in the desired sequence order, which is called iterative synthesis. During iterative synthesis, monomers are added stepwise according to the desired sequence. Each step involves a coupling reaction, known as a chain extension, after which unreacted monomer and reagents are removed from the product [1, 152]. The reactive site of the most recently added monomer, which was protected during coupling to prevent uncontrolled chain growth, is deprotected before the next chain extension. In theory, this strategy is very versatile and can be applied to any kind of monomers in any sequence, providing monomers can be created that both couple pairwise and permit the protection of one active site.

In iterative synthesis, reactive monomers of the xy-type can be sequentially polymerized if one of the monomer termini is temporarily deprotected. This approach is greatly simplified if the growing oligomer is attached to a support (i.e. crosslinked polymer beads or high molecular weight polymer chains) allowing straightforward and rapid purification steps.

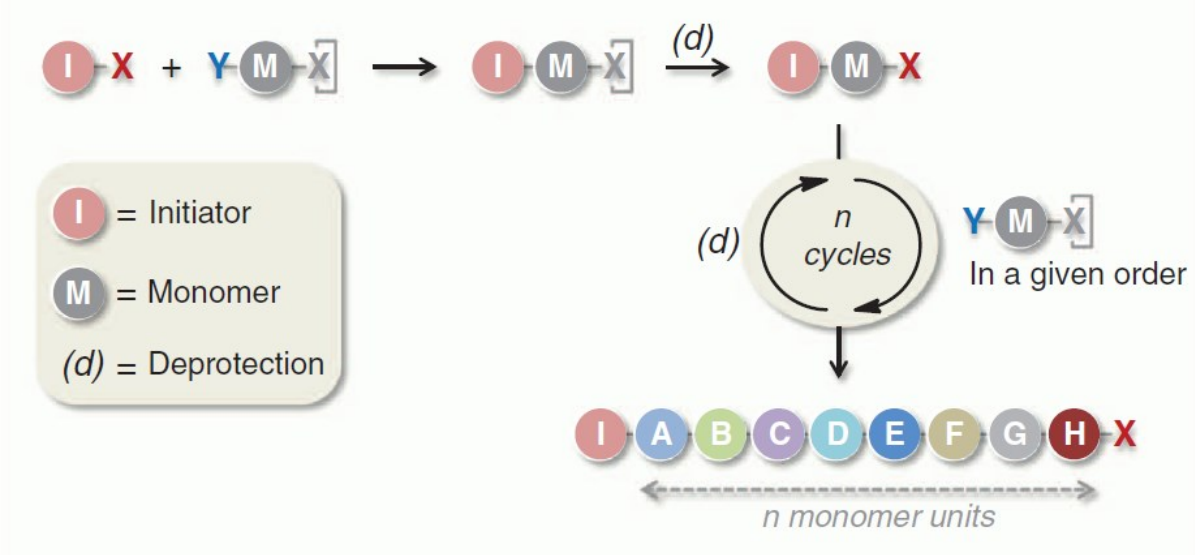


Figure 2.5 The concept of chemical iterative synthesis [1]. Reprinted with permission from AAAS.

The concept of iterative synthesis is shown in Figure 2.5, with the bulky support represented by circle 'I' and the sequentially added monomer units represented by 'M' and 'A' to 'H' on the figure. If first monomer A is attached on the support, then an excess of protected monomer B is coupled to the chain to form AB. After the coupling reaction, unreacted monomer B is removed by purifying the support molecules with solvents. The polymeric chain AB is then deprotected (i.e. unblocked) and the protecting group debris is removed by separation. This stage marks the completion of an iteration, with the product ready for the next coupling. The process is repeated until the desired sequence of monomers or chain length is achieved. Modifications of the chain terminus and side chains can be made after final cleavage from the support.

Solid phase iterative synthesis and separation methods

Solid supported-synthesis was first invented in the late 1940s by Merrifield and optimized for the sequence-ordered oligomerization of oligopeptides using amino acids as monomers [153]. In this iterative synthesis approach, a crosslinked poly (styrene-co-divinyl benzene) bead was designed as a polymer growing solid support to ease the purification. The C-terminus of an N-protected amino acid monomer is first linked to the support via a labile covalent linkage. After chain extension, the N-terminus of this amino acid is deprotected and reacted with the C-terminus of next N-protected amino acid, in the presence of an ester activator. However in

order to achieve high purity during the repetitive addition of the monomer, it required very high reaction conversions and tedious purification steps after each cycle.

In the past, solid-phase supported synthesis has been widely applied for the synthesis of sequence-defined biopolymers such as oligopeptides, oligonucleotides and oligosaccharides at an industrial scale [154]. Solid phase peptide synthesis (SPPS) was also used extensively for industrial applications. Polypeptides, limited in length to around 20-mers, were synthesized using PepTip [83]. Using similar solid phase supports, more types of chemical sequence-defined macromolecules were explored and constructed, such as oligoureas, oligocarbamates, oligoesters, polyamides and polyamidoamines [98, 102, 103]. The solid phase allows a simple process of purification through filtration and washing, thus it is also easy to automate [155]. However, the insoluble solid supports are normally expensive.

All solid phase syntheses suffer from the disadvantage of low efficiency of both coupling and deprotection reactions due to the insoluble resins. The solid support can cause steric hindrance due to the restricted accessibility of the reaction sites for the free monomers. The insoluble supports used exhibit a variety of physical properties, the substitution levels and distribution of the sites, which influence the solubility and reactivity of the entire polymer. Poor supports lead to a decline in coupling yields and the accumulation of deletion errors [156] and therefore this approach remains restricted to short oligomer synthesis. A second disadvantage is that all the monomers have to react and form the desired polymer and the support has to be removed before quality monitoring and quantitative analysis. This is not a practical process for fabricating high purity polymers [152, 157]. Moreover, solid phase synthesis is also difficult to scale up due to the insoluble support for separation. The largest production of RNAi therapies that is reported is about 1-2 kg per batch [108]. Product development greatly slows progress to production [84], precluding many industrial applications, particularly in materials science.

Liquid phase iterative synthesis and separation methods

In order to overcome the disadtanges of solid phase iterative synthesis, an alternative approach, liquid phase iterative synthesis, has been proposed in order to overcome the deficiency from solid phase synthesis [158]. In this approach, soluble polymer chains are applied as supports, which can be dissolved in a number of organic solvents for chemical synthesis and separation.

In 1966, a polystyrene soluble support was used to construct oligos via the phosphotriester approach [159]. Linear polystyrene soluble supports can be prepared by living polymerization techniques and the reactive site exposed to connect the polymeric backbone for iterative synthesis [160]. More soluble polymeric supports such as polyvinyl alcohol substituted by nucleotides and a cellulose acetate derivative were reported for the liquid phase oligo synthesis (LPOS) approach [161, 162]. In peptide synthesis, the exploration of soluble supports such as PEG [163], fluorous [164] or ionic liquid tags [165] has established the potential application of liquid phase peptide synthesis (LPPS). The discovery of PEG as a soluble, inert support with a high coupling yield of phosphorothioate oligonucleotides was discussed by Bonora et al. [166]. A pentaerythrityl-derived core was used as a soluble synthesis support with four growing oligo chains to synthesize homogeneous oligos [167]. In the current process, the soluble supports are cleavable in polymer synthesis. Some poor quality sequence-defined commercial polymers have been explained by inaccurate support cleavage [168-171]. Thus, there are some studies that have focused on the design of the macromolecular structures of the soluble supports for synthesizing sequence-defined polymers. It is important that the soluble supports are orthogonal to the chain coupling and deprotecting; however, they must be sensitive enough to be cleaved to avoid any damage to the polymers containing sequence-defined segments. Such tailored polymer supports have been synthesized by controlled radical polymerization techniques, which makes liquid phase iterative synthesis more feasible and versatile with different functionalities [160, 172]. In 2015, the Livingston Group demonstrated the utility of a symmetrical multivalent hub, 1,3,5- tris(bromomethyl)benzene, in the preparation of synthetic 2'-Me-RNA and PEG polymers, shown in Figure 2.6 [173, 174]. They also broadened the macromolecular architectures of the growing polymers. Different structures such as block, star and grafting topologies containing sequence-ordered motifs were investigated.

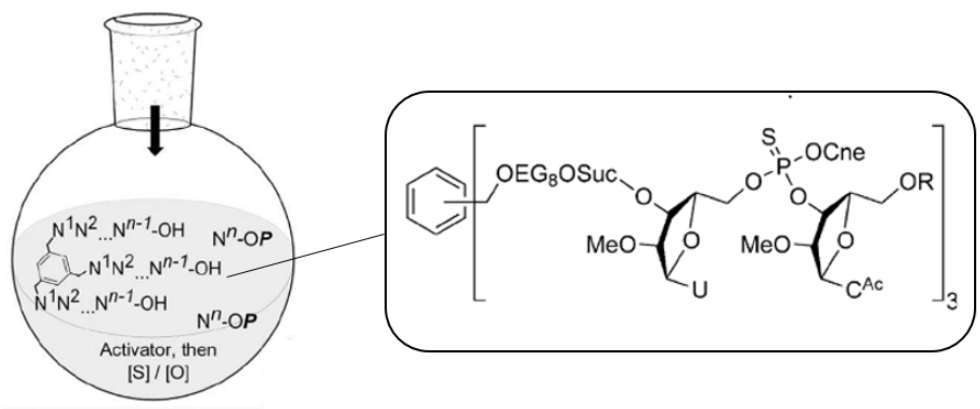


Figure 2.6 Liquid phase synthesis of 2'-Me-RNA using multivalent hub, 1,3,5-tris(bromomethyl)benzene as a support [175]. Reprinted with permission from 2015 WILEY-VCH.

Protecting group chemistry

Protecting group chemistry plays an important role in liquid phase synthesis; it prevents any excessive monomer attachments. The choice of the protecting groups for the coupling reaction conditions has limited applications due to the chemical compatibility. Barnes et al. applied epoxy-alkynes stereoisomeric building blocks with a t-butyldimethylsilyl (TBDMS) protecting group for the iterative exponential growth [176]. The acetyl (OAc) and benzyl (OBn) groups as functional side chains were inserted after the polymerisation by a 'click' reaction. The unimolecular polymers (>6 kDa) were produced with the overall yield of 19% (>99% purity) over 16 total steps. Another example using iterative synthesis was reported by Norris et al. [133], two acetal-protected monomers: unsubstituted p-phenylene unit and dialkoxy-substituted unit were designated. A series of oligomers up to hexamers were synthesized using Horner−Wadsworth−Emmons (HWE) chemistry, with the yield of 60%.

The synthesis of molecularly defined caprolactone oligomers and polymers up to the 64-mer via an exponential growth strategy was reported in 2008 [139]. The orthogonal protecting groups, TBDMS ether for the hydroxyl group and benzyl ester for the carboxylic acid group were employed. This synthetic strategy was highly efficient with a high cycle yield of 80-95% and the overall purity revealed to be greater than 95%.

Some nonnatural sequence-defined oligomers can be synthesized in the absence of main-chain protecting groups, relying on chemoselective backbone chemistry. Instead of monomers with one protected site, compatible pairs of successive building blocks are used [160, 178, 179]. For example the N-substituted glycines were used as building blocks for iterative synthesis of peptoids. However each N-substituted glycine unit is formed by successive coupling of two submonomer synthons during synthesis [180]. Monodisperse sequence-defined oligomers were also prepared iteratively without the aid of any protecting groups, using soluble tailor-made polystyrene supports synthesized by ATRP. The sequence order was arranged by the chemoselective 1, 3 dipolar cycloaddition of terminal alkynes and azides and the amidification of carboxylic acids with primary amines consecutively [160], shown in Figure 2.7.

In recent years, a number of liquid phase approaches have been exploited which allow access to a wider range of backbone chemistries, and more precise control over monomer sequence and side-chain functionality [1]. A few publications have reported sequence-defined polymers that have been uniformly built including polyamides, polyesters, thiol-ene click, azide-alkyne click, homologation of boronic esters [85, 177, 181-185]. High chain extension yields and sequence purities are assured, based on the fast coupling rates and specific kinetics.

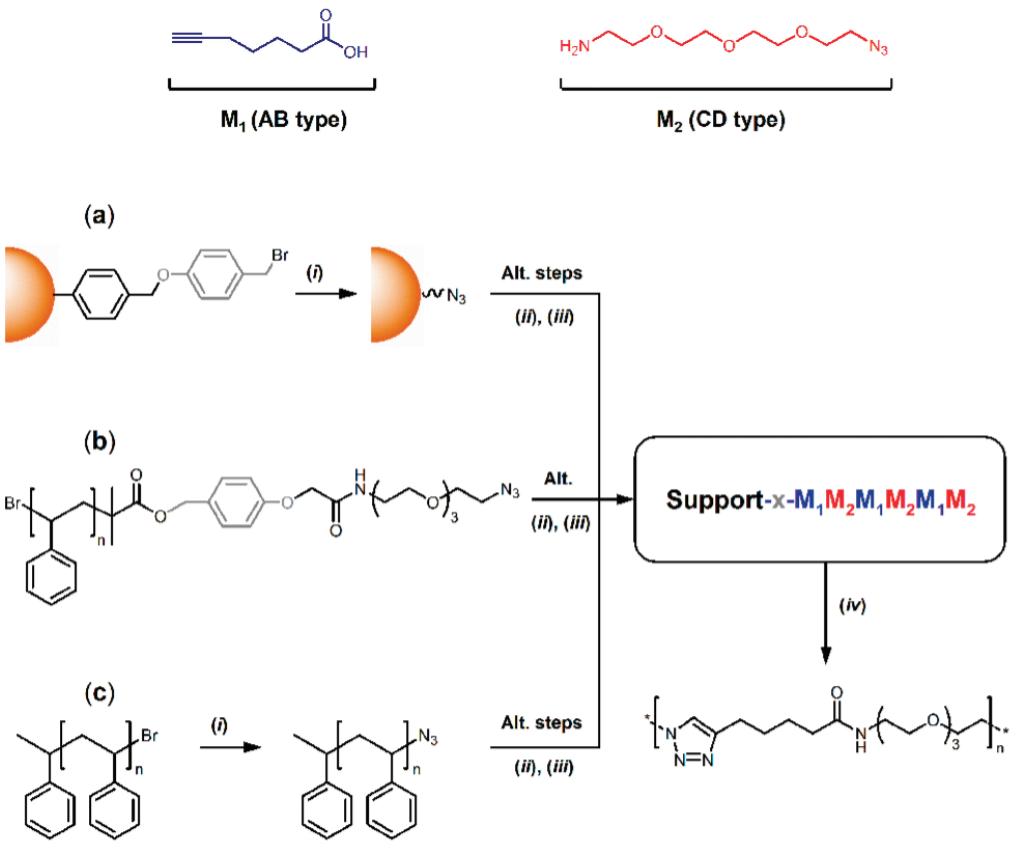


Figure 2.7 Liquid-phase synthesis of sequence ordered block copolymers using a soluble polystyrene support [160]. Reprinted with permission from American Chemical Society.

In general, liquid phase synthesis offers more efficient coupling compared to solid phase synthesis, benefiting from unrestricted liquid-phase kinetics and the potential to scale-up. It results in higher coupling yields of sequence-controlled polymers. Efficient online monitoring can also be used to ensure the completion of the chain extension, resulting in good sequence purity. However, the separation for liquid phase synthesis to purify the product from the excess reagents and byproducts at each stage is more challenging than in solid phase approaches. In previous studies, large growing polymers with soluble, efficient supports were isolated from excess monomers with low molecular weights via selective precipitation [186-188]. The current liquid phase iterative synthesis of oligonucleotide and oligopeptide [189-191] is heavily reliant on the facile precipitation processes. However, the yields of the final sequence-defined polymers from this separation technique are usually low and make this process undesirable. The conventional separation method of column chromatography to purify the soluble polymer after each coupling and deprotection cycle is time consuming and solvent intensive for

preparing complex macromolecular architectures. Successive column chromatography also decrease the overall yield of the products [7].

2.2.2.5. Synthesis of monodisperse polyethylene glycol (mPEG)

Conventional polymerisations of ethylene oxide normally result in a range of PEG chain lengths. Due to statistical chain growth in reactions, a Gaussian distribution of polymer molecular weights is often obtained [192]. Polymers with a polydispersion index (PDI) of exactly 1.0 are called monodisperse polymers. They have polymer chains with uniform length and are completely defined, discrete sequence orders and structures. In the current manufacturing process of mPEG2000 polymers, the lowest PDI achieved is 1.03 [31]. However this is not ideal for potential nanomaterials and pharmaceutical applications, as polydisperse polymers do not offer precise physical, chemical and pharmacokinetic properties. In addition, they also create difficulty for analytical interstation. In addtion, ethylene oxide is extremely flammable and explosive, which also limits its use in industial. The techniques of preparing highly monodisperse PEGs are laborious and the resultant high cost prohibits their scale up. Therefore, research into efficient synthesis strategies to fabricate monodisperse PEGs of high molecular weight has gained great interest.

Two main schemes to achieve the synthesis monodisperse PEG polymers are stated by Pulypure Technology [193]. Highly uniform monodisperse PEG oligomers can be obtained by 1) purifying polydisperse bulk PEG from polymerization process, or 2) using monodisperse PEG building blocks to eliminate the introduction of impurities to reactions.

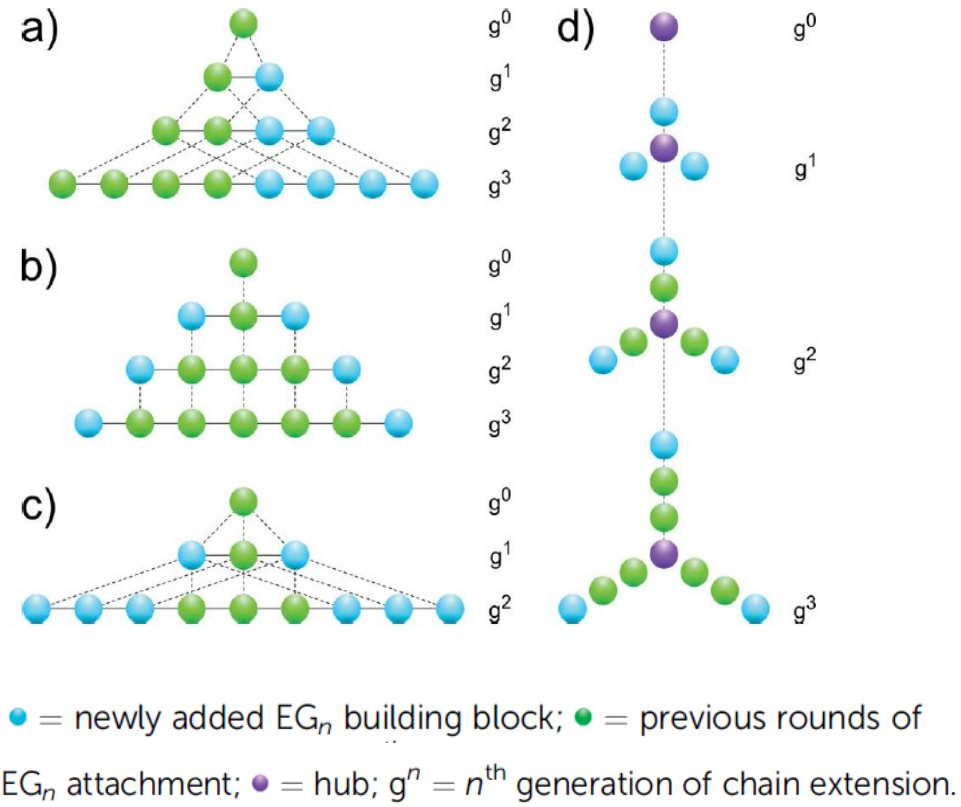
For monodisperse PEG purification, most of the current separation technologies cannot effectively locate specific oligomers for extraction with resolution approaching unity. Polypure uses sample displacement chromatography technology to purify $HOEG_8OH$ (370.4 Da) to high purity >95%. Unlike liquid chromatography based on solutes elution behaviours, the sample displacement chromatography process relies on species binding to sort samples by length. Therefore the process leverages the competition effects between sample components. It shows the advantage of retaining high sample resolution, without the high pressures and scaling complexities of HPLC. Production output at Polypure has increased to several hundred

kilograms annually. Using sample displacement chromatography, $HOEG_{28}OH$ with a purity >95% is the longest monodisperse PEG that has been prepared [193].

For monodisperse building blocks, the highly pure commercially affordable tetra (ethylene glycol) EG_4 is typically used to assemble longer building blocks such as EG_8 and EG_{16} with further coupling [194]. Minor impurities can be effectively separated at this stage, such as $-EG_1$ and $+EG_1$ in shorter oligomers, to guarantee the uniform PEG forming. However, a great number of chromatography purifications were required to secure the product purities, therefore more facile bulk operations such as extraction [195] and crystallization via macrocyclic sulfates [196] were developed to make processes more feasible. Although the preparation of the PEG building blocks is advanced, it still remains challenging to synthesize polymers with the molecular weights in the range of approximately 5,000-40,000 Da [197], which is the minimum requirement for PEGs to achieve the so-called stealth effect in biopharmaceuticals [198]. Many different approaches to synthesize monodisperse PEG polymers have been reported.

There are so far four conceptual ways to fabricate uniform monodisperse PEGs, which are shown schematically in Figure 2.8. The two most common approaches to synthesizing long PEG polymers are convergent chain doubling and bidirectional iterative coupling, shown in Figure 2.8 (a) and (b) [31, 199]. Chain doubling is the predominant strategy; a product with two different protecting groups from the last cycle is used as the building block for the next cycle, and the selective deprotection of one end of the building block chain is carried out. The doubled chain product can be de-symmetrised and converted into mono-activated, mono-protected building block, and mono-protected, mono-hydroxyl oligomer for the next coupling step. In 2004, a monobenzyl EG_{24} was assembled from hexaethylene glycol EG_6 through chain doubling in two steps [194]. French et al. conducted the synthesis of 16-, 32-, and 48-mers of ethylene glycol through chain doubling starting from tetraethylene glycol EG_4 [31]. In order to minimize contamination by other chain lengths, subsequent reverse phase flash chromatography was intensively applied at the shorter oligomer level. A remarkable purity and monodispersity was achieved for PEG_{16}, which gave PDI values between 1.000015 and 1.000002, and percentage purity between 99.6% and 99.9%. PEG_{32} was obtained from the next generation of chain doubling and PEG_{48} was obtained by the combination of one PEG_{32} and PEG_{16}, offering purities of 98.9% and 98.0% respectively. It is suggested that an end-group modified EG_{16} polymer can be crystallised and the structural packing inside the crystalline PEG

was simulated. In the approach, the highly pure PEG polymers have been produced on a scale of between 35 and 75 gram [196].



(a) Chain doubling, (b) bidirectional iterative coupling, (c) chain tripling and (d) iterative homostar growth. Blue: newly added EGn building block; green: previous rounds of EGn attachment and purple: hub

Figure 2.8 Schematic of approaches for the synthesis of monodisperse PEG [199]. Reprinted with permission from the Royal Society of Chemistry.

In bidirectional iterative coupling, the same building block is added repeatedly to both PEG chain termini. This approach offers higher coupling conversions to achieve longer PEG polymers. It is reported that EG_{44} diol was prepared from tetragol in five steps [200], affording an overall yield of around 17%, with 21% for coupling and 79% for deprotection. Niculescu-Duvaz et al. constructed EG_{29} using a central pentagol with additions of EG_6 building blocks via a two-step process, with an overall yield of around 58 %. However some contaminations of other chain lengths EG_{26} and EG_{25} are observed in the product mass spectrometry (MS) [200]. It was stated that bidirectional growth strategies are not suitable for

heterobifunctionalization [199]. In Figure 2.8 (c), the chain tripling approach is shown, which gives rapid expansion in terms of molecular weights. However the reaction efficiency decreased with the increasing chain length, especially in desymmetrizing PEGs of >12 units [194]. Loiseau et al. reported a failed chain tripling using EG_{16}, the reaction did not reach completion, resulting in a mixture of 31% EG_{32} and only 8% EG_{48}. Microanalysis was demonstrated as a purification tool to separate their compounds, but the accuracy and efficiency of the microanalysis are questionable. However, due to the limitations of chemical kinetics and purification, all of the approaches that are discussed above are almost impossible to scale up and cannot reach most pharmaceutically relevant chain lengths. In 2015, Zhang et al. developed the iterative nucleophilic ring-opening reactions of macrocyclic sulfates without performing group protection and activation and a series of M-PEGs, achieving an unprecedented 64-mer with a molecular weight of 2850 Da [196]. This offers the advantages of reducing half of the synthetic steps by removing group protection and activation. Also, the one-pot dual chain extension reaction minimized the synthetic steps by introducing two OEG fragments at a time.

A new approach to synthesize monodisperse PEGs by growing the chain from star polymer molecules ('PEG homostars') is reported by Livingston's group and illustrated in Figure 2.8 (d) [199]. The use of the hub, derived from 1, 3, 5-tris (bromomethyl) benzene, facilitates chromatographic purification or seeks other purification alternatives. The building block was added with one end protected, facilitating unidirectional growth from the hub centre with the chain terminus protected. This offers the opportunity to form straightforward monodispersity. With the robust three-arm structure, the molecular weight rose by three nucleotides per cycle and rapidly increased the reaction efficiency. To date, heterobifunctional linear PEG 56-mers are the longest discrete oligomer synthesized to date using the homostar approach, with a high purity of 92% [199]. The building block EG_{12} was used in iterative synthesis and it was prepared from the shorter oligomer EG_4 via desymmetrising protection of 3, 4- dihydropyran and tosylation on the unprotected end. This three-arm approach dramatically improves the retention of the complex and the viability of liquid phase polymer synthesis.

Table 2.1 Comparison of current approaches for the monodisperse PEG synthesis.

EG_n	$R^1 \neq R^2$	Overall Yield	Chain Purity	PDI	Source
48	no	15%	98%	1.00002	[31]
56	yes	12%	92%	1.0003	[199]
64	yes	15%	-	1.0003	[196]
28	no	-	>95%	-	Polypure AS (Norway)[193]
24	yes	-	96%	1.00006	Quanta BioDesign Ltd [201]

$R^1$and R^2 are the chain terminus functional groups; PDI is polydispersion index

The longest monodisperse PEG polymers that are prepared from the current published techniques were reviewed in Table 2.1 with their details. In general, PEG monofunctionalization remains challenging, because it requires a large excess amount of PEGs (up to 10 equiv.), expensive reagents, and tedious manipulation of protecting and activating groups. Moreover, during the synthesis of the monodisperse PEG polymers, the separations of the assembled building blocks and obtained PEG polymers get harder as the polymer chains grow longer. The longer PEGs chains interrupt the clean partition during extraction [195] and the compounds have strong affinity during chromatography column processes [31]. Given to the high effort for purification, iterative synthesis would be more effective if there were alternatives to the traditional separation methods such as precipitation and chromatography. Therefore, the development of efficient purification technology to address these issues for chemical synthesis is of great importance.

2.3. Organic solvent nanofiltration (OSN) membrane separation

2.3.1. Overview

Separation processes play an important role in the chemical and pharmaceutical industries. They account for up to 70% of the capital and operating costs of manufacturing [202]. Organic syntheses and purification in the chemical and pharmaceutical industry often involve organic solvents. There are many challenges to purifying high value products in organic solvents and reducing the usage and cost of processing these organic solvents for separation or solvent recovery. A new paradigm technology for membrane separation, organic solvent nanofiltration (OSN), was invented in 1960s. Compared to the traditional separation processes, such as distillation, evaporation, adsorption, extraction and chromatography, OSN membrane separation offers more efficient solvent operation in terms of process development, cost and environmental impact [203, 204]. In addition, membrane processes can be easily installed in a continuous process or combined with chemical synthesis processes into a hybrid configuration. Therefore it has more potential for scaling up in many industrial applications compared to other purification processes such as crystallisation or chromatography [205]. OSN membranes have been successfully implemented in different organic solvent processes, such as concentration, solvent exchange and purification.

2.3.2. Membrane separation processes

Membrane separation processes are driven by the different transport rate of chemical species through the membrane interface [206]**.** Therefore separation requires the membrane to have high selectivity to discriminate between solutes of different molecular size and their physico-chemical properties. The driving forces for solutes through membranes include hydrostatic pressure, concentration, and electrical potential differences [207]. There are four main types of pressure-driven membranes that are widely applied in industry due to their manageability and high performance, namely: microfiltration, ultrafiltration, nanofiltration, and reverse osmosis [208]. These separation processes are classified by membrane properties, application range and operation mechanisms. More details of pressure-driven membranes are listed in Table 2.2.

Table 2.2 Details of pressure-driven separation processes and applications, as reported in references [208, 209].

Separation Process	Operating Pressure	Membrane Pore Size(nm)	Separation Mechanism	Application Area
Microfiltration	0.1-1	100-10,000	Sieving mechanism due to pore radius and absorption	Steric filtration clarification
Ultrafiltration	0.5-5	2-100	Sieving mechanism	Separation of macromolecular solutions
Nanofiltration	3-20	0.5-2	Sieving mechanism	Liquid-phase separation removing dissolved fine solids
Reverse Osmosis	20-100	< 0.5	Solution diffusion mechanism	Separation of salts and macromolecules from solutions

2.3.3. Membrane materials and compositions

Based on materials used, membranes can be classified as polymeric membranes or ceramic membranes. Polymeric membranes act as semi-permeable barriers to separate distinct sizes of solutes. Typically, the size range of polymeric membranes has led to their use in microfiltration and ultrafiltration applications. Polymeric membranes that are made from polyamide (PA), polyethersulfone (PES), polyimide (PI) and polyvinylidene fluoride (PVDF), are commonly used membranes in many industries. The two main types of polymeric membranes are the Integrally Skinned Asymmetric (ISA) membrane and the Thin Film Composite (TFC) membrane. ISA membranes consist of a skin layer on top of a more porous sublayer with the same composition. The thin top layer affects the final membrane performance (selectivity and permeance). TFC membranes consist of an ultra-thin “separating layer” cast on top of a chemically distinct porous support. TFC membranes are very flexible and are characterised by some freedom in their design for a specific application. In general, TFC membranes are difficult to scale up due to complex fabrication, and are more expensive than ISA membranes [210]. But TFC OSN membranes have the potential to achieve higher fluxes than ISA OSN membranes, without compromising selectivity [211].

Polymeric membranes generally show good film properties, being robust and stable to operate. Polymeric membranes have shown significant advantages over conventional separation approaches in industrial processes such as distillation and flocculation. For example, they inherently require low energy costs and have lower thermal resistances. In addition, the fabrication process of polymeric membranes is well established, the pore size distribution and thickness are well controlled, and the cost of production is relatively low. However, polymeric membranes suffer a few drawbacks; for example, the membrane surface may be fouled by capturing colloids, chemicals or microbes [212]. Membrane fouling restricts membrane permeations and creates concentration polarisation of solute selectivity. Therefore polymeric membranes can suffer from high cleaning and maintenance costs, and/or low efficiency in flux [213]. Moreover, membrane selectivity is limited by the inability to tailor pore microstructure in fabricated membranes [212].

Ceramic membranes are fabricated using the materials of alumina, zirconia, titania and ceria in metal oxides. Due to the ceramic properties, they often offer good stability in extreme chemical and thermal environments. The ceramic membranes also give good mechanical strength and long, reliable life without breakage if they are prepared with a careful sintering procedure. However, for commercial purposes, ceramic membranes have high fabrication cost, low packing density, and cracks and fractures can be caused by their intrinsic brittleness, especially for high temperature industrial applications [208]. The fabrication technique and characteristics of the ceramic membranes needs further investigation for large-scale applications.

2.3.4. OSN membrane fabrication and modification

Based on the membrane types, different membrane fabrications are applied: phase inversion for ISA polymeric membranes and interfacial polymerisation and dip-coating for TFC polymeric membranes. In addition, different cross-linking techniques and post-treatment procedures after fabrication have also been developed [205]. Polymeric membranes have solvent stability and preserve their separation characteristics in organic solvents. ISA membranes are most suitable to be scaled up in industrial use, due to their straightforward methods of fabrication and post modification. ISA membranes are prepared by the phase inversion technique, developed by Loeb and Sourirajan [214]. In most cases, non-woven

backing materials were used in phase inversion techniques, being solvent stable and improving membrane mechanical stability. During this technique, the polymer dopes were precipitated from a casting solution by immersion in a non-solvent bath, shown in Figure 2.9. The residual solvent left in the membrane forms the membrane pores [214]. The surface film was first contacted with a non-solvent and formed the dense, selective layer on the top membrane, which has a significant effect on membrane rejection and permeance [215]. The non-solvent penetrated the bottom layer slowly and forms a more porous substrate. Many studies of membrane preparation via phase inversion to improve membrane performance have been published [204, 216].

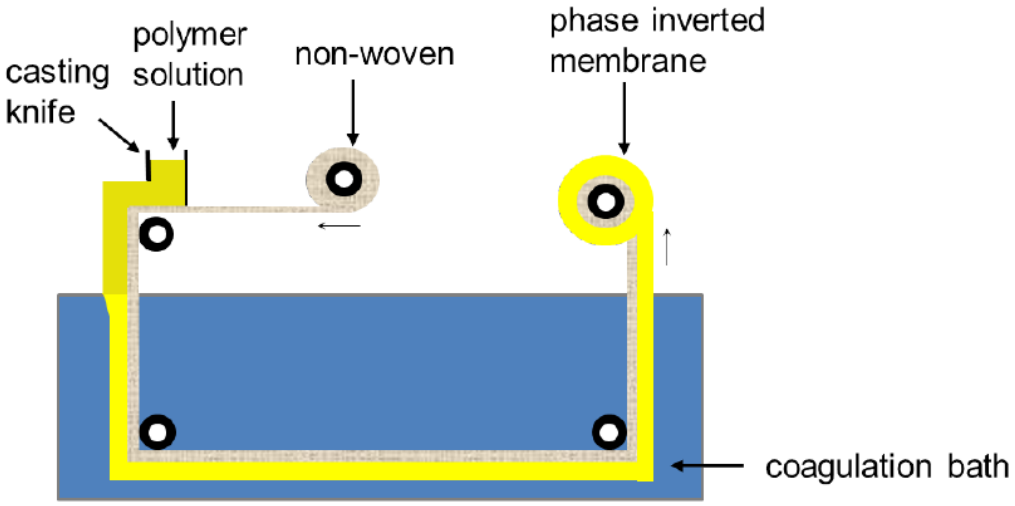


Figure 2.9 ISA membrane formation process by phase inversion[217]. Reprinted with permission from American Chemical Society.

2.3.4.1. Membrane crosslinking

Various approaches to post modifications after membrane fabrication have also been investigated to enhance membrane performance in terms of separation selectivity, solvent and mechanical stability and withstanding harsh environments in organic solvents. Common approaches include crosslinking, wet or dry annealing, drying by solvent exchange, and conditioning agents [216]. Crosslinking is used to enhance the structures within the polymeric membrane and improve the chemical stability and physical properties of the membranes. The methods include thermal, UV, and chemical crosslinking for different applications [218, 219].

In order to make the process efficient and less hazardous, Vanherck et al. have combined the phase inversion process and the crosslinking step into one simple step [220]. The polyimide membranes were chemically crosslinked with p-xylylenediamine and xylylenediamine (XDA) to achieve high performance and stability in a range of solvents [218, 219]. Dutczak et al. have crosslinked membranes using di-isocyanates. The membranes were dried and crosslinked at high temperature for a long time. The crosslinked polyamide-imide membranes possess good stability in high temperature processes. It was also suggested that the membrane molecular weight cut off (MWCO) could be varied with crosslinking time [221]. Polybenzimidazole (PBI) membranes were crosslinked with dibromoxylyne (DBX) or dibromobutane (DBB) as crosslinkers by Valtcheva et al.; the PBI OSN membrane showed good tolerance towards extreme pH conditions and various solvents [222, 223]. Other crosslinkers such as glutaraldehyde (GA) and 1, 2, 7, 8-diepoxyoctane (DEO) have also been investigated by the same research group.

The work of SeeToh et al. also verified the effects from thermal crosslinking; high temperatures improved the rejection of PI OSN membranes, but decreased the membrane permeance, due to the reorganisation of the polymer chains at elevated temperatures [224]. More polymeric materials such as polyacrylonitrile (PAN) and polyaniline (PANI), have also demonstrated that crosslinking at 70 °C gives excellent chemical and thermal stability [224]. UV crosslinking with proper photo-initiators has been also studied to enhance the solvent stability of polymeric membranes. The UV crosslinked membranes were affected by the photo-initiator type and crosslinker functionality, but they showed good stability and performance. For example, the combinations of acyl phosphine oxide-based photoinitiators with a pentaacrylate crosslinker gives a polysulfone UV-crosslinked membrane, which could be operated in various solvents [225]. Pore preservation is also a common post treatment to avoid pore collapse or aging of the membrane after drying [226]. Siddique et al. have combined crosslinking and pore preservation in one step [226]. The membrane was crosslinked and the pores preserved using Jeffamine® 400 as one agent; the membrane appeared stable in harsh solvents and showed flexibility and strong mechanical strength.

2.3.4.2. Surface modification

Surface modification is another approach to post modification after membrane fabrication. One of the main purposes of surface modification is to control the membrane pore size and the

surface chemistry [227]. In particular, surface modification has been widely used in ceramic membranes to improve membrane performance and passivate the membrane surface from potential surface reactions or adsorption. Tsuru et al. demonstrated this by grafting the top layer with hydrophobic groups via silanation on the ceramic membrane surface to achieve higher fluxes [228]. It was found that water can adsorb to the inner surface of unmodified silica-zirconia membranes and block the permeation of other solvents [229]. Additionally, separation performance of alcohol and alkane solutes in alcohol solvents were investigated. The effect of silanation treatment on membrane performance has also been reported for TiO_2 multilayer membranes, with the surface modifications of hydrophilic γ-Al_2O_3, in terms of hexane and water permeability and their MWCOs [230]. By coating the porous membrane surface with methylated SiO_2 colloidal sol solutions, organic/inorganic hybrid membranes achieved an excellent and consistent performance in the nanofiltration of polyolefin oligomers in n-hexane solutions [231].

Surface modification can also be used to functionalise ceramic nanofiltration membranes for different applications. Membranes can be grafted via Grignard chemistry, permitting the covalent bonding of the desired functional group to the metal, such as Al, Zr and Ti, of the metal oxide matrix. For example, TiO_2 membranes have been differently functionalised with a series of alkyl groups (methyl, pentyl, octyl, dodecyl). This occurred via partial replacement of the OH-groups on the membrane surface and resulted in an amphiphilic character of the modified membrane surface. These surface modified hydrophobic ceramic membranes were able to permeate both polar and non-polar solvents with high fluxes. The retention of polystyrene in acetone was significantly enhanced after modification. A similar technique has been applied to OSN polymeric support membranes. It aims to improve the membrane resistance to biofouling by modifying the hydrophilic polymers [232]. Surface modifiers such as Jeffamine® M-2070 and poly (ethyleneimine) have been discovered and applied to treat poly (ether imide) membranes and polyether ether ketone (PEEK) membranes.

2.3.4.3. Scale-up membrane modules

Based on the approaches of membrane fabrications and post modifications, membranes could be prepared in modules for large-scale separation. In membrane modules, the membranes are packed in an efficient way, resulting in a high surface area to volume ratio, which enhances

membrane performance. High chemical stability membranes and flexible mechanical strengths are two main requirements for the design of the membrane modules [214]. The most common design for flat sheet OSN membranes is the spiral-wound module. The pressurised feed flows parallel to the permeation channel, while the permeate flows radially through the spiral-wound permeate spacer towards the central collection pipe. A permeate spacer is applied between the internal sides of the leaves to avoid collapse due to pressure and rapid permeance.

A spiral-wound module of the ISA PANI membrane was prepared for solvent exchange application [233]. The modules showed good chemical stability with solvents and the performance is consistent over time. The spiral-wound membrane module also has been studied for large-scale pharmaceutical purification. Commercially available Duramem® 200 membrane was rolled into modules and a case-study on active pharmaceutical ingredient (API) from its oligomeric impurities in tetrahydrofuran (THF) is reported [234]. The aging and consistent performance of a spiral-wound membrane module with commercial Starmem® 122 membranes were studied with 0-20 wt% solutions of tetraoctylammonium bromide (TOABr) in toluene [235]. Janssen Pharmaceutica NV has reported an application using spiral-wound membrane modules with Duramem® membranes. An oligomeric intermediate was successfully fractionated from impurities to achieve 99.7% final purity and 90% API recovery. These spiral-wound membrane modules operated in dimethylformamide (DMF) and THF with a stable performance over a long period of time.

However, the diversity of the membrane modules heavily relies on the long-term material stability of the membrane and the adhesives in the organic solvents. Challenges are the discovery appropriate adhesives, which do not degrade in harsh chemical environments, and high temperatures and pressures.

2.3.5. OSN membrane applications: purification and solvent recovery

It is reported that purification accounts for more than 50% of the total manufacturing costs in chemical and pharmaceutical processes [203]. Purification performance can be assessed by product yield and purity, purification time and solvent consumption. OSN membrane offers significantly efficient solvent operations because it has an excellent separation performance, low cost and is more environmentally friendly. In order to achieve high performance in

chemical and pharmaceutical purification, OSN membranes should effectively discriminate between the product and impurities. The larger the differences in rejection of product and impurities, the better the separation performances; this difference is also called membrane selectivity. In addition, membrane permenace is key to determining separation time efficiency and solvent consumption.

For example, most active pharmaceutical ingredient (API) synthesis in the pharmaceutical industries is normally performed in organic solvents, which requires subsequent isolation of products with high added value from the impurities and the solvents. In pharmaceutical purification, it is strictly required to lower the limits of genotoxic impurities (GTI) in APIs, calling for GTI-specific purification steps [236-238]. OSN membrane processes show strong potential to replace the conventional API purification methodologies, such as chromatography and recrystallization. This is because the OSN membrane offers a high separation yield and purity to achieve ultra-low impurity levels, less solvent intensity and energy consumption. Membranes also prevent APIs from high temperature separation, and especially the degradation of the heat sensitive products. The OSN membrane process has great potential to scale up and to be automated. It has been reported that a single pass nanofiltration system has 200 times lower energy consumption than a conventional distillation unit [203]. Székely et al. has published an environmental and economic analysis to quantitatively compare current separation techniques, which outlines the benefits of OSN [239]. Currently, apart from impurity removal, OSN membranes have been developed for a wide range of applications such as OSN-assisted chemical synthesis and catalytic processes [217].

OSN membranes could also be used to recover and reuse organic solvents to reduce the overall solvent consumption. In addition, compared to distillations OSN-based solvent recovery offers energy savings, and low safety and environmental risks due to mild operating conditions. Commercial membranes such as Starmem® 122 and Duramem® 150 membranes have been applied to recover a wide range of solvents, such as methanol, ethanol, isopropyl alcohol and ethyl acetate after synthesizing API products and improving the sustainability of API production [240]. The comparison of solvent recovery using OSN membranes, distillation and crystallisation was quantitatively analysed [241]. It has been reported that OSN uses 25 times less energy per litre of recovered solvent compared to distillation [241]. By taking advantages of different separation methods, a hybrid approach combining OSN and other purification methods could achieve better performance with less energy. For example, a combination of

distillation and an OSN membrane, with a slightly increased temperature has been investigated; it prevented impurity precipitation during the filtration process and the energy consumption was lower than when distillation alone was used [242]. Another hybrid approach was reported by Nimmig et al.; the process combined single-column chromatography, racemisation and solvent recovery by membrane filtration to produce single enantiomers at high yields [243]. Szekely et al. purified some small genotoxic impurity through the membrane from the API product. The API was further purified by impurity specific molecularly imprinted scavengers (MIS) featuring methacrylic acid binding sites. Molecular imprinting is a recent development to effectively recover the solvent with adsorption and decrease the impurity levels in active pharmaceutical ingredients [244, 245]. Therefore, the MIS approach can be developed to remove any trace impurities from the solvent recycle during the filtration process. It requires less energy and solvent, and it has the potential for large-scale solvent recovery. A case study of MIS application has been reported as the three way separation of ternary systems comprising an API, a potentially genotoxic building block and a catalyst [204].

In general, the publications on OSN membrane applications show that OSN membranes have excellent chemical and thermal stability and good selectivity in the liquid phase [246]. It is also cost effective and viable to scale-up to the kilogram scale for a commercial process. OSN membranes also have more potential for improved performance, through membrane modifications at all stages of membrane manufacture, including: dope preparation, membrane crosslinking and casting. Also, OSN membranes could be implemented with other techniques, such as grafting or coating. Therefore numerous studies about membrane modification to improve purification performance are still undertaken [247]. Another attractive advantage that makes OSN membrane more viable for industrial application is that suitable OSN membrane modules can be provided and a large scale manufacturing process can be optimized for proprietary separation purposes, integrated with synthesis processes.

2.3.5.1. Chemical synthesis with OSN

Purification plays an important role to secure high product purity in iterative synthesis. In between the iterative addition of monomer building blocks in the liquid phase chemical synthesis, purification at each stage is continued in the liquid phase, by a process of organic solvent nanofiltration (OSN) [248]. In this process, purification processes can be applied using

a pressure difference across the OSN membrane; the selective barrier allows the excess of smaller building blocks to flush through the membrane, whilst the bulkier synthetic polymer intermediate is retained on the feed side of the membrane. A key advantage of the OSN process in iterative synthesis is that only one solvent or solvent mixture needs to be used throughout the process to carry out all the coupling, deprotection and purification steps. Purification is the most solvent consuming step. Unlike other conventional purifications such as chromatography and precipitation, membrane nanofiltration does not change the solvent gradient. This advantage facilitates easier scale up of the viable process and in-situ solvent recycling. In order to select the right membrane for separation performance, solute rejection and solvent permeability in terms of permeate flux can be screened and monitored before installing in membrane rigs.

Many previous studies have reported the use of OSN membranes for various chemical synthesis environments, but OSN membranes have rarely been studied in combination with iterative synthesis purification. It has been proven that OSN membranes show a great potential to be used in some complex synthesis processes and improve delivery to a commercial scale [217, 249]. The first liquid-phase synthesis of a biopolymer using membrane separation was reported in 1977 [250]. A sequenced peptide was formed with PEG-10,000 support and purified with ultrafiltration in water after each chain extension cycle. Building on this, OSN was applied by So et al. to improve peptide solubility during the separation process, in a process termed membrane enhanced peptide synthesis (MEPS) [246]. The model peptide H-Tyr-Ala-Tyr-Ala-Tyr-OH with a soluble polymeric support, methoxy–amino–PEG, was assembled through four steps in each iterative cycle: amide coupling, excess reagents removal, deprotection and deprotected reagents removal, shown in Figure 2.10. Constant volume diafiltration was applied during both reagent removal steps, which does not require solvent exchange. The process challenges of LPPS using OSN membranes were discussed, with an example of synthesizing a 5-mer peptide from a linear support [251]. The invention of the bulky soluble support [173, 174] from the Livingston group could assist the rapidly growing MW of the PEG products, which would allow purification by size exclusion, based on the rapidly emerging membrane technology platform of organic solvent nanofiltration.

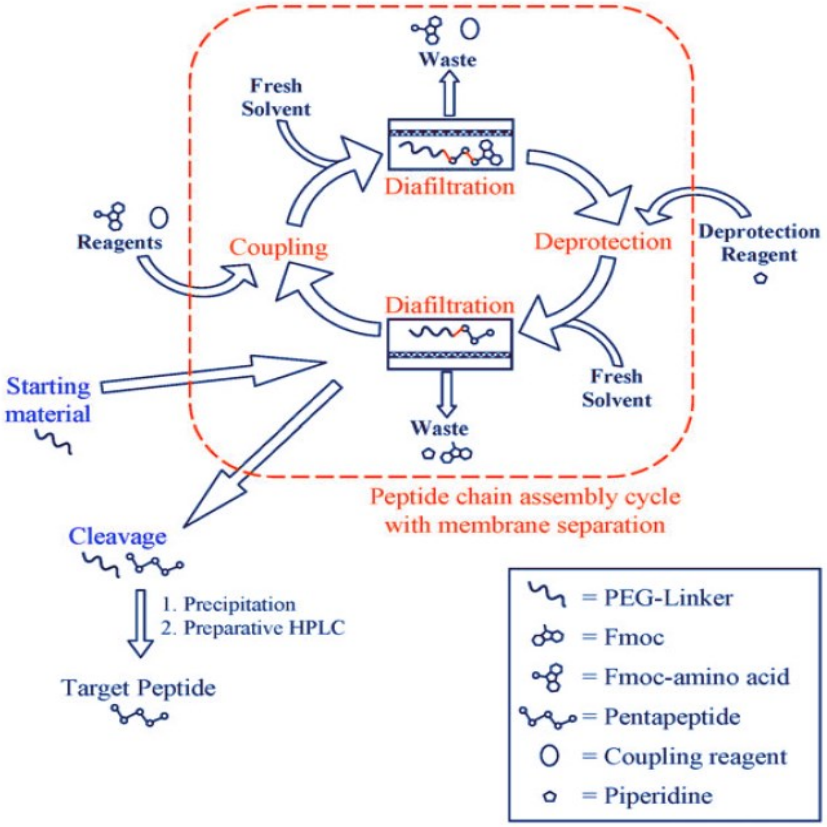


Figure 2.10 Iterative synthesis of peptide with membrane purification [251]. Reprinted with permission from American Chemical Society.

2.3.5.2. Diafiltration systems

The membrane separation of molecules in a system works continuously by using constant volume diafiltration. Chemical molecular species, such as proteins, peptides or nucleic acids are washed out through the porous membrane with buffered solvents. Selective filtration for certain molecular sizes occurs. Pressure is applied to drive the flow through the membrane. The minimum pressure necessary to complete one diafiltration volume is that which forces at least half of the volume through the membrane. Diafiltration also prevents the accumulation of impurities in the circulation of solvent cross flow. Székely et al. have utilised the OSN process in a diafiltration mode. With a flow force, the relatively small impurities were pushed through the membrane by the continuous addition of fresh solvent to the retentate. The diafiltration mode improves the separation performance based on membrane selectivity and the polarity of the impurity [239].

In order to maintain a constant retentate volume, a fresh solution is added to the retentate at a constant rate. Therefore the concentration of smaller solutes and solvent are lowered gradually with the washing feed, while the molecules that are larger than the membrane pores are retained and accumulated. The amount of removed molecules depends on the diafiltration volume (DV). For a continuous process, one round of diafiltration indicates that a diafiltration volume of solvent has been passed through the membrane system. Membrane filtration processes are dynamic systems with variable concentrations and flowrates. Therefore membrane performance criteria like solute rejection and permeance are variable quantities over time. For example, the concentration of both smaller solutes and product in both retentate and permeate change with the solvent feed addition. Figure 2.11 showed a case study of an ideal separation in a single stage membrane diafiltration. The concentration profiles of both product and impurities were plotted, based on mass balance equation of single stage membrane process, shown below [217].

$$\frac{dc_i}{dt} = \frac{Q}{V_f}[c_i{}^{in} - (1 - Rej_i)c_i] \qquad \textbf{Equation 1}$$

where $c_i{}^{in}$ Is the concentration of solute *i* entering the retentate loop; *t* is diafiltration time; Q is the membrane flux; V_f is the volume in the feed tank and Rej_i is the membrane rejection of solute *i*.

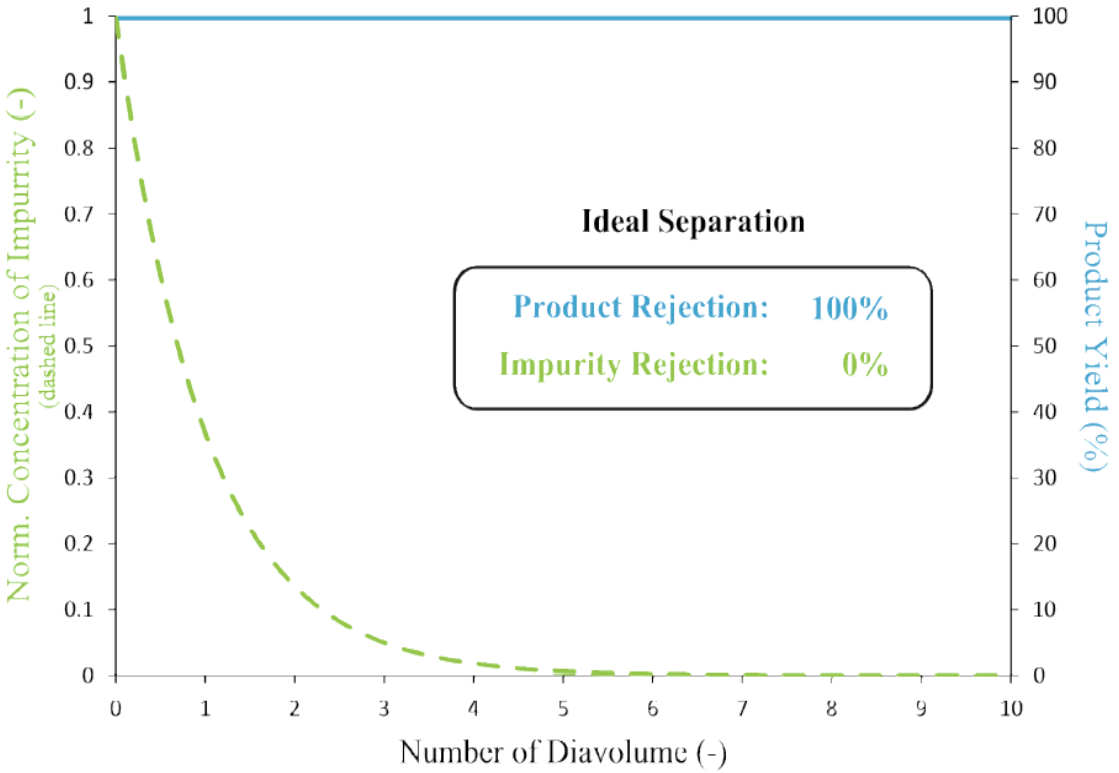


Figure 2.11 Case studies of purification via constant volume diafiltration in an ideal membrane separation system [217]. Reprinted with permission from American Chemical Society.

It has been published that using constant volume diafiltration will purify active pharmaceutical ingredients (APIs) and remove trace genotoxic impurities from the class of aminopyridines and sulfonates [239]. It has been found that some OSN operating conditions could influence the effects of impurities on API recovery in constant volume diafiltration, such as pH adjustment and addition of water in the membrane rig [253, 254].

2.3.5.3. Cascade system

Figure 2.11 illustrates that the concentration of impurities decreases as an exponential decay during diafiltration. Therefore the first few volumes of diafiltration solvent will be heavily contaminated, but in order to achieve high product purity, more solvent needs to be flushed through. There is a trade-off in OSN membranes to remove impurity and secure product yield. If a large amount of solvent was required to obtain sufficient purity of the product, it may cause significant product loss with low purification efficiency. In distillation column, multi-stage counter-current cascades are used to obtain a better separation performance, and cascade

nanofiltration can be designed based on this concept [255]. The membrane cascade system is to regard the permeate stream from one filtration unit as the feed for another filtration unit, while the retentate is recycled.

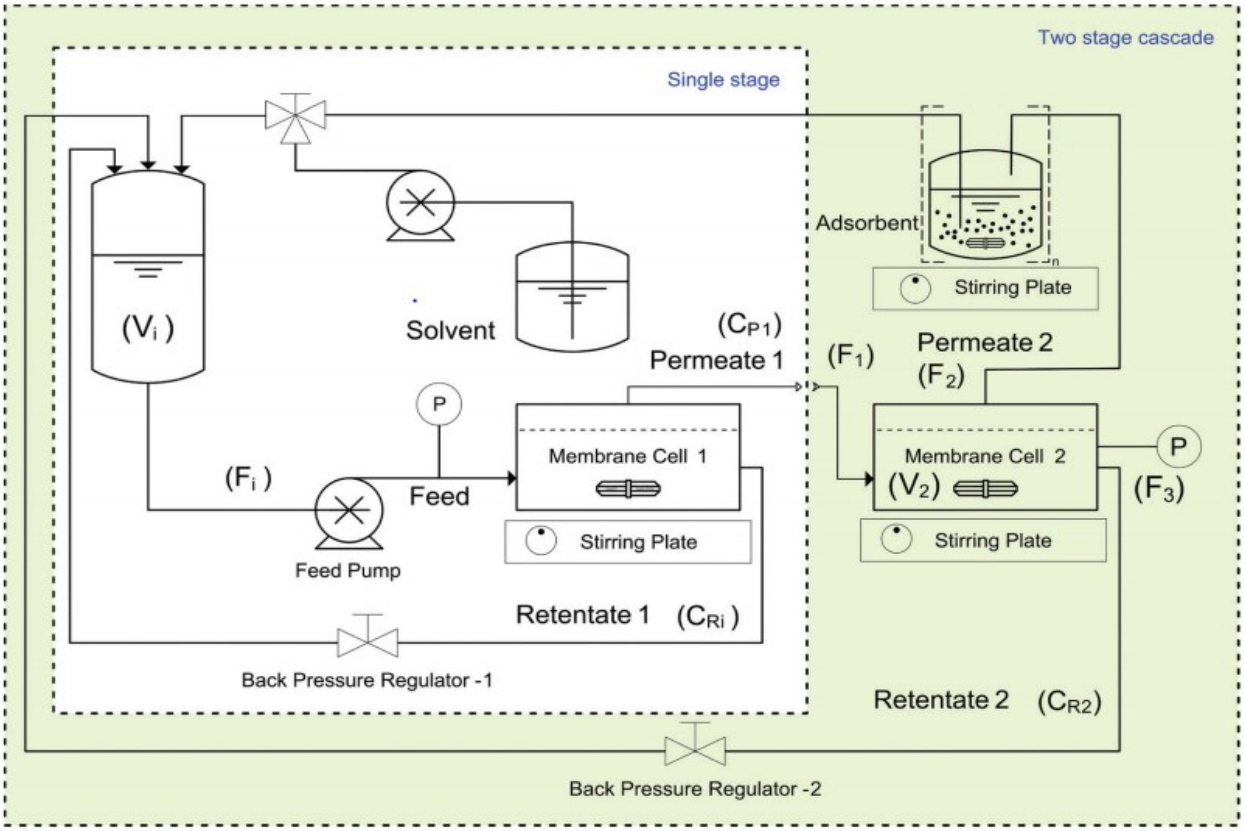


Figure 2.12 System diagrams of single-stage diafiltration and two-stage cascade diafiltration [256]. Reprinted with permission from the Royal Society of Chemistry.

Figure 2.12 shows continuous single stage and cascade stage diafiltration systems. The configuration normally works in a semi-batch manner. Free solvent is withdrawn by a high performance liquid chromatography (HPLC) pump from the solvent reservoir. The flow rate is the same as the permeate outflow rate, in order to keep the volume of the feed tank constant. The membrane module is fed from a feed tank with a pressurised N_2 stream, and the pressure can be controlled by using the three-way valve for venting the excess gas to the atmosphere. The fluid retained in the retentate can also be recirculated to the feed tank by the circulating pump. However, the efficiency of the single stage diafiltration (SSD) may be restricted by membrane performance. The yield and purity of the product depends on the membrane selectivity. Moreover SSD only offers a limited contact time between solution and the membranes, which is insufficient for membrane permeation and screening. Therefore, a two-

stage membrane cascade approach has been trialled to repeat the subsequent diafiltration to maximize the product yield and improve the membrane performance [256]. This process is repeated until the unwanted salts, solvents, or smaller molecules are removed. Each subsequent diafiltration removes more of the small molecules. The use of the dialfiltration system makes the system more versatile and efficient.

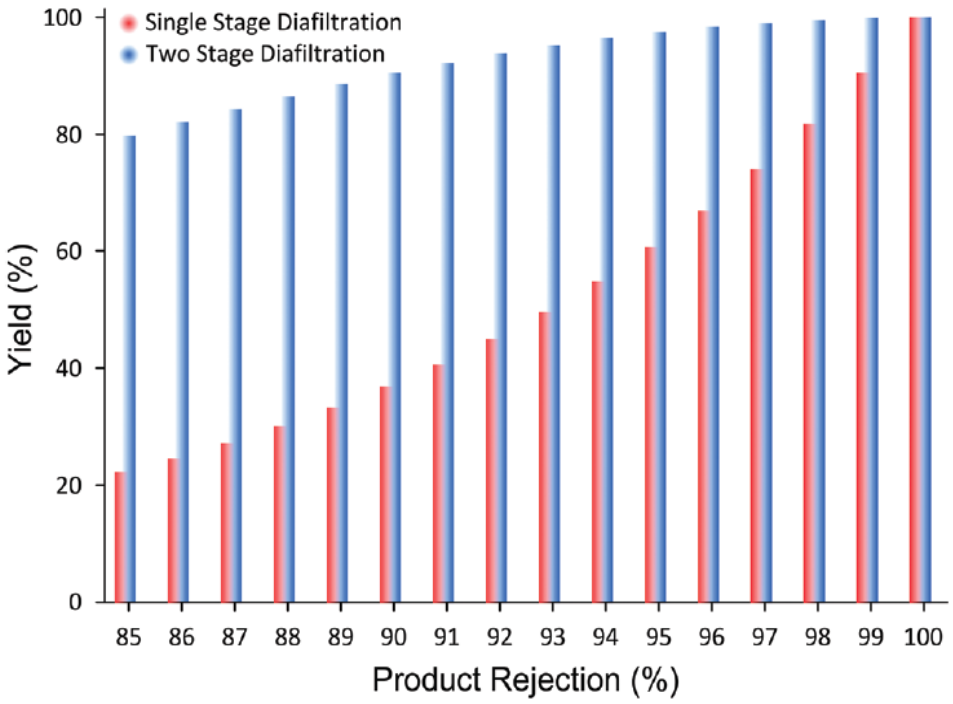


Figure 2.13 Predicted yield improvement after 10 diavolumes for different product rejection [256]. Reprinted with permission from the Royal Society of Chemistry.

Jeong at al. illustrate the significant yield improvement achieved after 10 DVs by implementing the two-stage diafiltration system proposed in Figure 2.13. The system offers great improvements when the membrane rejection below 90% in single stage. For example, the yield of purification improved 4 times from 22% in single-stage diafiltration to 80% in two-stage diafiltration when the membrane rejection of the product is only 85%. Conversely, the rejections of the impurities are required to be less than 50% in two-stage system, so that the final product purity can also be satisfied [204]. In conclusion, two-stage diafiltration transforms the membrane process from "unfeasible" status to an economically sustainable and viable process, and makes it highly competitive to other conventional processes.

The two-stage OSN system has been developed and practically applied in a few different areas. A cascade membrane rig has recovered up to 99% of a drug product, reported by Martinez et al. [257]. Another cascade membrane configuration of Duramem® 150 and 200 membranes were installed to separate API product from impurities with a small molecular weight difference of only 33 g mol^{-1} [258]. Peeva et al. demonstrated continuous purification of an API from a potentially genotoxic impurity in a two-stagemembrane cascade: high purity of the API >99% could be achieved from the feed stream purity of 78% [259]. More cascade models have been proposed [260-262], however they are not versatile, being difficult to implement for different applications.

Kim et al. showed that the two cascade membrane configuration increases the final product yield significantly from 58% to 95%, without compromising the final product purity [256]. The second stage of diafiltration with a recycle ratio of 0.5 was implemented to prevent the loss of the product. The cascade configuration also allowed a higher separation performance, so it can be used to achieve high yields and membrane performance in a reduced purification time. The cascade membrane rig avoids the use of buffer tanks in-between membrane units and pressure pumps, reducing capital expenditure and simplifying the process control. The versatility of this membrane process can enhance the sustainability and efficiency of the industry. Even more, solute fractionation was also recently performed by employing a 3-stage cascade for a mixture of an API and an excess reagent. The separated API-rich product stream could be further improved by crystallisation, which is not feasible with the original feed solution [263, 264].

2.4. Summary of the state of the art

The proof of concept and development of iterative synthesis with organic solvent nanofiltration (ItSyN), reported in this thesis, is based on current cutting edge sequence-controlled synthesis and membrane technology. The goal of ItSyN is to achieve world-leading synthesis of monodisperse, sequence-defined PEG polymers. To contextualise this, the current state of the art methods for polymer synthesis are described below. ItSyN is a novel approach for PEG synthesis, but the Livingston group has previously used similar methods for oligo- and peptide-synthesis [175], [246]. Those efforts are described for comparison.

ItSyN-like approaches for sequence controlled oligo- and peptide-synthesis

First of all, the most up to date developments and applications of OSN membranes for iterative synthesis are stated here. OSN membranes have rarely been studied in combination with iterative synthesis purification. The purifications in chemical synthesis require membranes to offer a good selectivity to discriminate between the product and impurities. In addition, membrane should have excellent reproducibility and good stability in harsh solvents or acid/base environments, with a reliable lifetime.

A ceramic OSN Inopor® ZrO_2 coated membrane with hydrophobic surface modification was applied to synthesize sequence-defined peptide Thymopentin (H-Arg-LysAsp-Val-Tyr-OH) [246]. The OSN Inopor® ZrO_2 had a pore size of 3 nm and it aimed to permeate amino acid which has the molecular weight of 597 g mol^{-1}. The peptide, which needs to be retained by the membrane, was assembled on a soluble polymeric support, methoxy–amino–PEG with molecular weight (MW) 5000 g mol^{-1}. The membrane was operated in DMF in a single-stage rig. 0.6 g of 5-mer peptide was obtained with the purity of 94% and overall yield was estimated to be 92%, which gave better performance than SPPS.

2'-Me RNA phosphorothioate 9-mer was also synthesized iteratively using an OSN membrane with 17wt% PBI [175]. The phosphorothioate product was extended on a three arm soluble support 1, 3, 5- tris(bromomethyl)benzene to create size discrimination for membrane separation. A two-stagesystem of 17wt% polybenzimidazole PBI membrane was operated in MeCN to separate the chain extended phosphorothioate product (from 4465Da) from the protected phosphoramidite building block of 800Da. 9 mg of 9-mer oligo was obtained with purity of 94% and overall yield of 76%.

Monodisperse PEG synthesis

Secondly, the latest technologies for monodisperse PEG synthesis with purification are discussed here. The longest monodisperse PEG oligomers that have been synthesized to date are EG_{64} [196] and EG_{56} [173], both with PDI of 1.00003. They are asymmetric and have different chain termini on each end, which results in heterobifunctional polymer chains. However, there is no technology so far that could synthesis PEGs with molecular weight (MW) greater than 4000 Da to achieve the stealth effect in biopharmaceuticals [198]. The coupling rate, affinity strength and low resolutions during chromatography are the main challenges to prepare high MW monodisperse PEGs. Therefore, new synthetic and purification strategies to address these issues are of great importance.

The monodisperse EG_{56} (PEG2500) was synthesized via unidirectional, iterative chain extension of a 3-arm PEG homostar [173]. Highly pure EG_8 with a Dmtr protecting group were used as building blocks. The heterobifunctional linear EG_{56} chains had a hydroxyl at one end, and either a toluene sulfonate, or a tert-butyl carboxylate ester at the other end. The sequence purity of the final EG_{56} chain was a modest 92% and total yield of 12% after 7 cycles of chain extension. The production scale was milligrams and synthesis was assisted by chromatography columns. The longest monodisperse EG_{64} (PEG2850) was prepared from an innovative macrocyclic sulfate-based approach [196]; building blocks were added iteratively to a one-pot dual chain extension reaction after nucleophilic ring-opening. The longest monomethoxy PEG with 64-mer (PDI=1.00003) was prepared in eight steps with an overall yield of 15%. The synthesis scale of this approach was in the range of 1-5 g and all the intermediates were intensively purified by flash chromatography.

Sequence-controlled polymer synthesis with a variety of backbones

Thirdly, the cutting edge for sequence-defined polymer synthesis with purification is discussed here. A number of liquid phase methodologies have been exploited with a wide range of backbone chemistries, and more precise control over monomer sequence and side-chain functionality. Previous studies focused more on the chemistry variance of the coupling efficiencies and product purities. To the best of our knowledge, precise sequence-defined PEGs with tunable side-arm functionalities have never been synthesized to date Optimization of inherent properties by manipulating polymer sequence order have barely been studied.

A sequence-defined 20-mer (with 7046.40 g mol^{-1}) with 10 different side chains including aliphatic, aromatic, and olefinic moieties, was synthesized by iterative Passerini three-component reaction (P3CR) and subsequent deprotection [265]. The sequence-defined 20-mer was obtained over 20 reaction steps with an overall yield of 21 % and high purity. The reactions were carried out on 2.4 g 10-mer and 0.81g final 20-mer product; most reactions were purified by column chromatography. A sequence-specific 16-mer polymer (with 2198.02 g mol^{-1}) incorporating nine different side chains was synthesized using allyl acrylamide building blocks. Side chain functionalities could be added with photoinitiated thiol−ene 'click' addition [177] . Fluorous tags as a soluble support were employed and the overall yields was 68% with a high purity. A stars-like polymer structure containing 12-block sequence-defined polymer (with 50000 g mol^{-1} and PDI =1.01) was made by iterative exponential growth (IEG). Four different macromers with high MW from 2490 to 5690 Da were employed as building blocks: polystyrene, poly (t-butyl acrylate), poly (ethylene glycol) and poly (methyl acrylate). The final sequence-defined polymers represented an overall yield of 35% at the scale of 14 mg; the purification at each cycle was carried out by preparative size exclusion chromatography (SEC) and column chromatography [22].

3. Project objectives and tasks

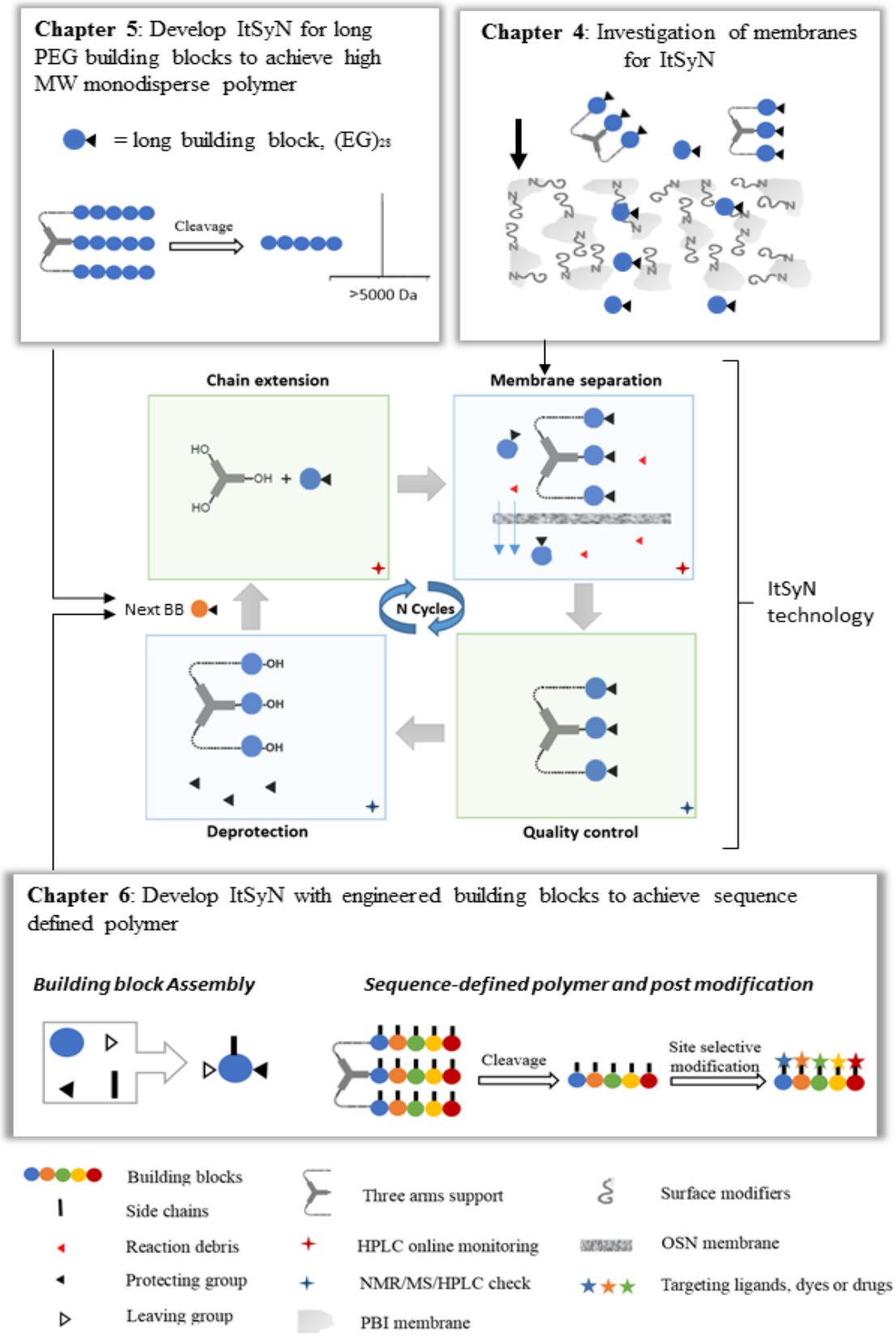


Figure 3.1 Schematic of ItSyN and project aims.

3.1. Project overview

In past years, the primary structure in a polymer chain has been generally poorly controlled in synthetic macromolecules. Traditionally, the routes to monodisperse and sequence- controlled oligomers have been heavily reliant upon extensive and time-consuming chromatography. Synthesis and purification strategies discovered so far are effective for the synthesis of oligomers, but the procedures are difficult to scale up for to synthesis polymers at good yields and purities.

In this project, like the bifunctional polymer fabrication described in the introduction, iterative synthesis in the liquid phase was developed. Sequential addition of monomers ensures the accurate construction of targeted chain lengths and sequences. An effective purification with OSN is applied at each stage in the liquid after synthesis. This scalable iterative synthesis with organic solvent nanofiltration (ItSyN) approach, entirely in the liquid phase, can provide significant control of the sequence purity. The project firstly aimed to use a fully liquid iterative synthesis paradigm to synthesize polymers, and to overcome the limitations of difficult coupling and purification scale up currently experienced in solid phase synthesis. Secondly, it aimed to make iterative synthesis viable for a variety of synthetic polymers, including oligo and peptide biopolymers and other chemical synthetic polymers such as PEGs, with different structures and functionalities. The introduction of the reactive functional groups on the side-arms allows the potential of precise site-selective multifunctionalisation at a later stage [266, 267].

The procedure of ItSyN is shown in Figure 3.1. A soluble support molecule with three arms is used and the first monomer, is tethered to the support; the covalent bond is cleavable, but it is orthogonal to the coupling and deprotection reaction. The second monomer, with one end protected, is added to form sequence chain. Excess monomer is then removed by OSN membrane diafiltration. In accordance with the size exclusion idea, the unreacted building block passes through an OSN membrane, whilst the growing polymer with the support, which is bulkier, is retained by the membrane. After coupling, the protecting group is removed from the chain terminal; the protecting group debris from this deprotection reaction is removed using further diafiltration. After *n* synthesis cycles, sequence-defined polymer-star is obtained. Cleavage of the polymer-star from the hub, unblocking of any side-arm protecting groups and

further site-selective side-arm modification can be also undertaken to generate a multifunctional sequence-defined polymer.

The ItSyN liquid phase process offers the opportunity for precise manipulation of the sequence orders and chain lengths of the synthetic polymers; it also generates the defined structure and programmable functionalities. The ItSyN concept represents an exciting advance with high potential for unlocking the availability of peptide, oligos and other synthetic polymers at a commercial scale.

This project investigated the feasibility of synthetic PEG construction with ItSyN, aiming for monodisperse polymers with pharmaceutically desired chain lengths (molecular weight ≥ 5000 Da), and heteromultifunctional PEGs with different side chains. Such monodisperse and sequence-defined PEG polymers are in high demand in medical applications, as they can be conjugated with biologically active molecules for drug delivery, tissue repair scaffolds and use as drugs, along with non-biological applications such as nanotechnology [178]. To the best of our knowledge, this project is the first work to combine the physical and biological advantages of PEGs with the structural and information-bearing complexity of sequence-defined functional heteropolymers. In future work, the established technology could be automated to provide synthetic polymers with specified monomer orders and precise molecular weights. This technology platform could also be used for different polymeric backbones and more functionality could viably be incorporated. This would open up myriad applications for healthcare, nanotechnology and other fields.

The hypotheses of the projects were: (1) Liquid phase synthesis gives a more efficient coupling reaction, due to the good solubility and the monitoring ensures good reaction completion. (2) Iterative synthesis also constructs more precise sequence structures. Compared to the conventional convergent or chain doubling approaches, it overcomes their kinetic limitations by precise monomer additions. (3) By recycling the excess monomers and solvents, the monodisperse and sequence-controlled synthetic polymers can be fabricated more efficiently and at lower cost.

3.2. Objectives and tasks

The project aimed to establish a versatile ItSyN process as a new manufacturing paradigm for sequence-defined, monodisperse synthetic heteromultifunctional PEGs. Specific and measurable objectives for the project were as follows.

Objective 1. Develop an OSN membrane with good performance for ItSyN (Chapter 4)

Task 1.1. Investigate the reproducibility of OSN PBI membrane fabrication.
Task 1.2. Improve the membrane performance and stability by surface modification in different solvents.
Task 1.3. Discover a membrane system that can separate reaction mixture with high selectivity to achieve purity > 99% and yield > 95%.

Objective 2. Investigate ItSyN feasibility for high MW monodisperse PEG (Chapter 5)

Task 2.1. Chemical kinetic study of chain extension using highly pure long PEG building blocks and a soluble three-arm support.
Task 2.2. Study ItSyN diafiltration system and online monitoring for building blocks and polymer products.
Task 2.3. Complete four chain extension cycles to produce monodisperse PEG polymers with MW of 5000 Da.

Objective 3. Investigate feasibility of ItSyN for sequence-defined PEG (Chapter 6)

Task 3.1. Design a versatile synthetic scheme of branched PEG building blocks including the chirality and protecting group chemistry.
Task 3.2. Develop ItSyN diafiltration system and online monitoring to prepare two sequence-defined PEG polymers (4-5 extension cycles) with yield > 95%.
Task 3.3. Deliver optimal operating conditions for iterative synthesis of sequence-defined polymers using a Quality by Design approach.
Task 3.4. Characterise polymer properties for PEG polymers with different sequence orders.

4. PBI-based membranes for PEG organic synthesis

4.1. Abstract

This chapter reports the development of a new class of organic solvent nanofiltration (OSN) membrane, for application in ItSyN, fabricated from polybenzimidazole (PBI) with surface modification; it was developed for membrane purification for scalable chemical synthesis. Crosslinked PBI membranes with α, α′-dibromo-p-xylene (DBX) exhibit superior long-term chemical stability in harsh environments compared to other well-known polymeric membranes such as polyimide. However the performance of PBI-DBX membranes cannot be tuned and is not consistent over time. Therefore studies of PBI membrane fabrication and modification to control membrane pore size and improve membrane performance were carried out, as reported in this chapter.

The effects of basic membrane fabrication conditions such as dope concentration, non-woven types and crosslinking were studied first. In order to enhance the membrane performance and life expectancy, a new approach to surface modification on organic solvent nanofiltration (OSN) membranes fabricated from polybenzimidazole (PBI) is reported. Surface membrane modification was carried out with four different types of surface modifiers, such as Jeffamine® (M-600 and M-2005), Elastamine® (RE1-2007) and mono-amino tetraphenylmethane (TPM). Improvements of membrane performance and physico-chemical properties after modification were assessed for the different modifiers, with a variety of polymer lengths and degrees of hydrophobicity. The surface modified membrane exhibited superior chemical stability and excellent reproducibility compared to the unmodified membrane and other well-known commercial polymeric membranes. Also, the modified membranes showed good tolerance towards a wide range of organic solvents and extreme pH conditions, which offers a great potential for applications in the chemically harsh conditions of chemical synthesis processes.

In order to critically assess membrane performance in realistic chemical conditions, a case study of PEG polymers iterative synthesis purification was implemented with different modified membranes. 18 wt% PBI-DBX-M2005 membrane in methanol (MeOH) to acetonitrile (MeCN) (1:1) gained the highest separation factor (7.25) between the bulky hub product and building blocks. Furthermore, 18 wt% PBI-DBX-M2005 membrane showed an excellent permeance of 5.3 L m^{-2} h^{-1} bar^{-1} and enabled the removal of all the impurities in a reasonable diafiltration volume.

4.2. Introduction

Purification processes are critical in the chemical and pharmaceutical industries; the yield and purity of the high value products are significantly affected by separation methodologies. Organic synthesis of chemicals or high value APIs are normally carried out in organic solvents, therefore the removal of the impurities has to be conducted in organic solvents [249]. These requirements raise concerns of the operational costs, manufacturing scalability and energy consumption. OSN is a new technology that has been applied to separate chemical species based on molecular size discrimination. Many previous studies have reported the use of OSN membranes for various separation purposes and environments. It has been proven that OSN membranes show a great potential for use in complex manufacturing processes and to achieve improved delivery to a commercial scale [217].

There are a few major challenges for developing OSN purification as a viable process. Firstly, membranes must have good solvent and pH resistance; also, they should have chemical and physical stability within chemical synthesis operating conditions. Secondly, membranes should have a high selectivity between product and impurities to secure high purity and permanence to lower the solvent consumption. Finally, the membrane fabrication process should be relatively easy to operate, highly reproducible and have the potential to scale up to industrial production standards [268]. In order to increase the membrane stability in harsh solvents or acid/base environments typically required for OSN membranes and chemical synthesis, several fabricating materials, including both inorganic and polymeric, have been investigated [217]. A variety of post-treatments were also studied to improve the long term stability of the OSN membrane, including crosslinking, drying and conditioning agents [269]. Crosslinking has been studied extensively to enhance the chemical stability of integrally skinned asymmetric (ISA) membranes after phase inversion. Numerous crosslinking methods have been studied for polymeric membranes, including thermal, UV, and chemical crosslinking [270]. The crosslinking conditions such as the type of crosslinker, crosslinking time and temperature usually play important roles in membrane properties and performance [271]. Crosslinked membranes possess good mechanical properties and thermal stability at high temperatures and pressures in a wide range of organic solvents.

The separation performance of the ISA membrane is critically determined by the top selective porous layer. The pore sizes are normally non-uniform across the membrane surface and

controlling the pore size is difficult during phase inversion; but chemical post modification of OSN membranes gives a great opportunity to tailor the pore structure and achieve high selectivity and permeability. Post modification also controls the surface functionalization of the membrane for specific separation purposes [272], [273].

Thin-film formation via polymerization, polyelectrolyte modifications, incorporation of nanoparticles and grafting are well-established modification methods of dense skin layers for OSN applications [204],[274]. Thin-film formation via polymerization and polyelectrolyte modifications are generally used for a multilayer ultra-thin film upon an asymmetric, porous support-layer. However due to technical limitations, these methods can easily result in membrane defects and are difficult to scale up. Incorporation of nanoparticles involves the use of inorganic materials in the membrane. The key problem with this is the severe aggregation of the nanoparticles due to their high surface area and their weak compatibility with polymer materials [275]. Covalent grafting with functional groups is widely applied in OSN membranes. Pore structure has been decorated with grafted polymers to reduce the pore size to nanometre scales and the membrane surface hydrophilicity could be tuned by the nature of the modifiers [276]. This approach gives the potential of membrane scale-up and versatility by tuning membrane properties to the separation type of interest.

Several facile modifications via surface grafting were reported to improve the permeation property and pore size. Tailored functional polymers such as polyetheramine and PEG-based materials of various molecular weights have been used as surface modifiers due to the structural flexibility and chemical stability. Polysulfone membranes were grafted by amphiphilic PEG copolymers, which can form a dense hydrophilic brush of side chains on the hydrophobic backbone with the membrane base. This offered excellent resistance to protein adsorption and inherent biocompatibility [277]. OSN ceramic membranes are normally grafted by hydrophobic functional groups as the original surface hydroxyl group OH discourages the applications of non-aqueous separations due to their hydrophilic nature. Membranes such as γ-Al_2O_3, SiO_2/ZrO_2 and γ-Al_2O_3/TiO_2 have been grafted with hydrophobic groups by silane treatment to improve membrane performance in organic solvents [278], [279]. Rezaei Hosseinabadi et al. reported that functionalized tubular TiO_2 ceramic nanofiltration membranes were grafted with a series of n-alkyl groups and organometallic Grignard reagents in order to change membrane affinity [280]. In this case, the presence of both grafted organic groups and remaining OH groups at the membrane surface increases the permeation flux of both polar and non-polar solvents, while remaining an excellent molecular weight cut off (MWCO).

A recent study on crosslinked polybenzimidazole (PBI) membranes in OSN applications showed the great potential for the implementation of PBI membranes in pharmaceutical separations [281]. The α, α′-dibromo-p-xylene (DBX) crosslinked PBI membrane showed superior chemical and mechanical stability in a wide range of solvents and high concentrations of acids and bases. It is stated that the MWCO of this PBI-DBX membrane is approximately 2000 Da, which indicates that any impurities with a molecular weight of hundreds of Daltons could be removed. A further detailed study on achieving higher degrees of crosslinking and long membrane lifetime was carried out by optimising crosslinking reaction parameters based on Design of Experiments [271]. In order to convert this membrane into an industrial separation process, PBI membranes have been studied in a cascade OSN membrane rig for pharmaceutical API purification [256]. PBI membranes have also been fabricated at large scale using continuous phase inversion casting machines. Spiral-wound membrane modules may also be of use in industrial applications [282].

However, it has been found that the performance of PBI-DBX membranes is not stable in separation processes, but changes over time. A PBI-DBX membrane needs to be conditioned to achieve the desired performance. It has been observed that the separation yield of the solutes is unexpectedly lower than the theoretical rejection, due to the chemically active membrane surface. Reactive bromomethyl groups could remain on the PBI-DBX membrane surface after crosslinking, which may cause undesirable adsorptions or reactions [282].

In order to resolve this problem, surface modification was investigated to improve the permeation pathways of the OSN membrane. The primary goal was to hamper the reactive site of the membrane (i.e. surface passivation) and make the membrane an inert environment for separation species. An additional aim was to tune the hydrophobicity-hydrophilicity balance of a membrane in a controllable fashion and constrict the pore size for better performance.

In this chapter, four different types of surface modifiers were investigated for the purpose of performance improvement and surface passivation. A small rigid coating group called 4-amino tetraphenyl methane (TPM) was proposed as a hydrophobic modifier. A class of Jeffamines® and Elastamine®, as flexible linear brushes with different lengths and degrees of hydrophobicity, were also used to investigate the hydrophobicity-hydrophilicity effects on

membranes. The different performance of modified membranes, as well as the physico-chemical characterisation of the newly developed membranes, are reported.

4.3. Methodology

4.3.1. Materials

Commercial 26 wt% polybenzimidazole (PBI) solution dissolved in dimethylacetamide (DMAc) (Celazole® S26 PBI, MW = 27,000 g mol^{-1}, with 1.5 wt% stabiliser lithium chloride) was purchased from PBI Performance Products Inc., USA. All solvents used in this study, such as DMAc, MeOH, IPA, MeCN, DMF, toluene and n-heptane were HPLC grade and were used as received from VWR, UK. Deionized water was produced by passing tap water through a reverse osmosis filtration unit. The chemical for crosslinking was α, α‘- dibromo-p-xylene (DBX) from VWR, UK. Jeffamine® (M-600 and M-2005) and Elastamine® (RE1-2007) were kindly donated by Huntsman, USA. Mono-amino tetraphenylmethane (TPM) was synthesized by our research group. Polyethyleneglycol (PEG) of molecular weights of 400, 2000 and 8000 g mol^{-1} were purchased from VWR, UK and Sigma Aldrich, UK. Polystyrene (PS) of nominal molecular weight of 580, 1000 and 1300 g mol^{-1} were purchased from Agilent, USA.

4.3.2. Membrane preparation with batch casting

Integrally skinned asymmetric PBI membranes were prepared by phase inversion. 17 wt%, 18 wt% and 19 wt% PBI stock dope were diluted from a commercial 26 wt% PBI solution in a DMAc solution. To homogenize the PBI solution after dilution, the mixtures were stirred continuously at 21 ± 0.5 °C for at least 6 hours. The solutions were then left still to degas for several hours. PBI membranes were cast on two types of polypropylene nonwovens, Novatex 2471 and Evonick. The bench casting machine with an adjustable knife was set at 250 μm and cast at 4 cm s^{-1} (Elcometer, UK). After the membrane precursors formed, they were immediately immersed into a DI water bath for phase inversion at 21 ± 1°C. The water bath was replaced every hour and repeated three times. Subsequently, membranes were rolled and immersed in measuring cylinders with IPA and stirred for one hour to remove residual solvent and water. The IPA was replaced every hour, with two changes conducted.

Membranes were crosslinked with 3 wt% DBX in MeCN solution. The crosslinking reaction was operated in an oil bath at 80°C for 24 h under constant stirring. After crosslinking, the

membranes were rinsed with IPA to remove the excess crosslinking solution. Then the membranes were rolled and immersed in measuring cylinders with 500ml IPA and stirred for two hours to remove residual solvent, which was repeated three times in total. In order to store the dry membranes for a longer time, the membranes were impregnated with PEG400 to preserve the pore structure. The membranes were immersed in a 500 ml PEG400/IPA (1:1) solution and continuously stirred for four hours. The membranes were then hung in the fume hood until they dried.

4.3.3. Membrane preparation with continuous casting

18 wt% and 19 wt% PBI dope solution were prepared as described in Section 4.3.2. The membrane was cast using a continuous casting machine (SepraTek, Korea) with the casting knife set at 200 μm and the casting speed set at 2.2 cm s^{-1}, shown in Figure 4.1. The water bath temperature for the phase inversion was set at 20°C. Subsequently, the membranes were rolled up and immersed in IPA or MeCN in large measuring cylinders, then the solution was stirred to leach out residual solvent and water. The washing solvent was also replaced three times before crosslinking.

The crosslinking procedure for continuous casting was in anhydrous conditions under N_2 protection. The reaction solvent MeCN was dried over baked 4Å molecular sieves to improve the extent of crosslinking and ensure better reproducibility. The rest of the crosslinking procedure remained the same as in Section 4.3.2. Now the crosslinking procedure was still carried out in lab scale, however the setup of a 10L crosslinking tank for modifying continuous casting membrane in several metres is shown in Figure 4.2.

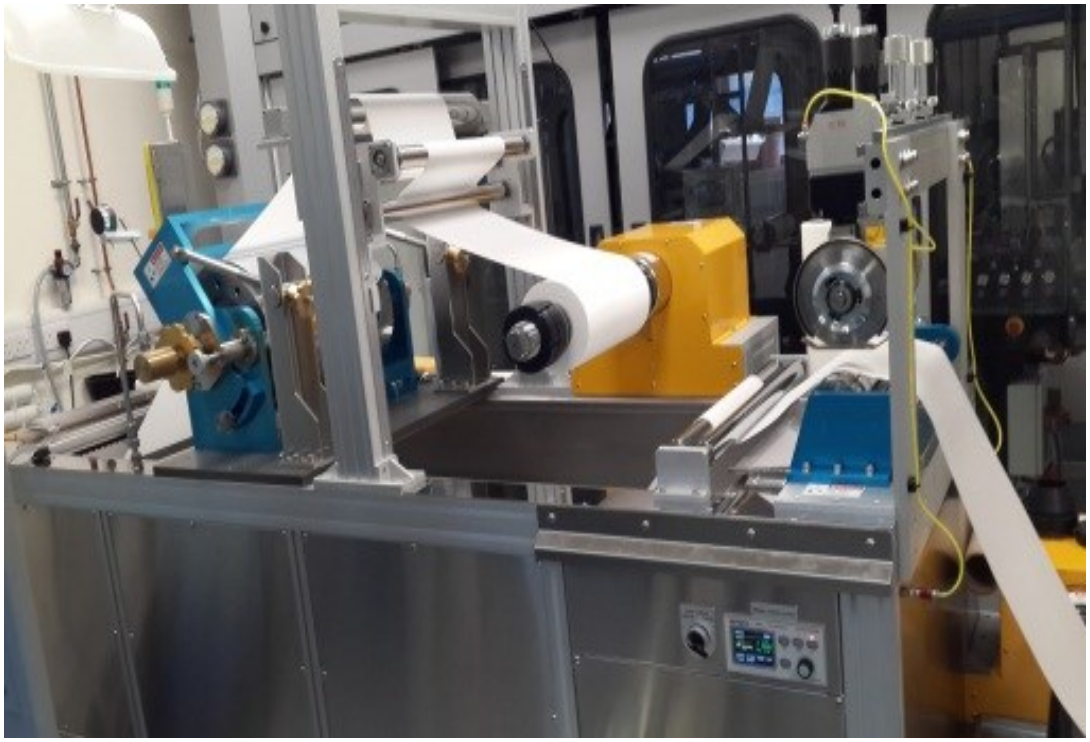


Figure 4.1 Photograph of a continuous membrane casting machine.

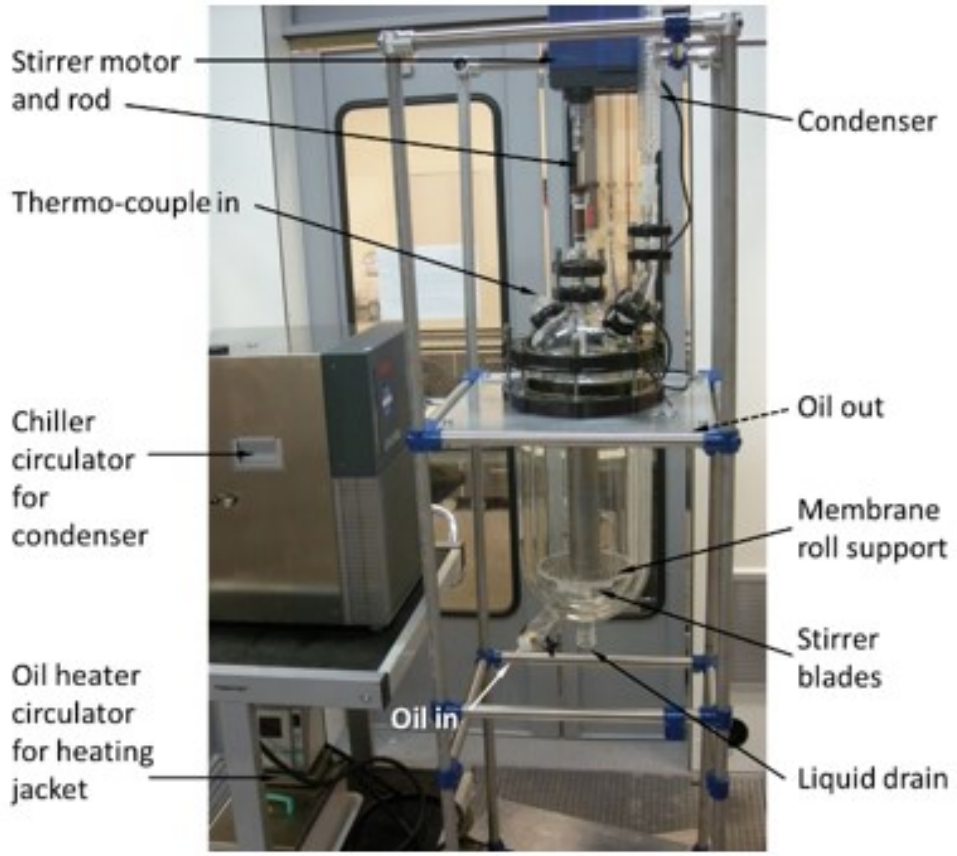


Figure 4.2 Schematically labelled 10L crosslinking tank for continuous casting membrane.

4.3.4. Membrane post-modification

Membrane surface modification was carried out right after membrane crosslinking and before PEG impregnation. The PBI-DBX membranes were rinsed with anhydrous MeCN to remove the excess crosslinking solution before re-immersing in MeCN (83 mL). 50 mL of surface modifier, mono-amine Jeffamine® (M-600 or M-2005) or Elastamine® (RE1-2007), were added to the mixture with Hunig's base (17 mL). The mixture was then heated at 80°C and continuously stirred for another 24 hrs. A similar reaction was also performed with mono-amino tetraphenylmethane and the amount of MeCN was increased to 150 mL.

4.3.5. Membrane characterisation and screening

4.3.5.1. Membrane cross-flow cell screening

The membrane performance was determined by filtration experiments. A multi-cell cross-flow rig was used and operated at 10 bar and at room temperature. A 305 Series HPLC pump (Gilson, UK) with a 100SC pump head, was used as a feed pump. The system was steadily circulated at a flow rate of 100-150 L h^{-1} with the assistance of a Micropump (Michael Smith Engineers Ltd., UK). Each membrane disc had an effective area of 14 cm^2. Two or more discs were used for each membrane type, to check the membrane reproducibility.

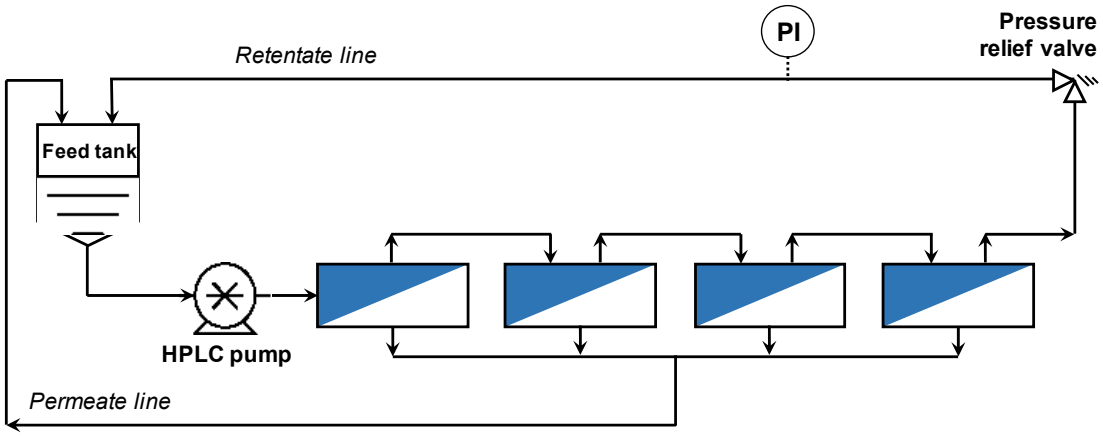


Figure 4.3 Schematics of membrane cross-flow cell screening.

Permeance, B [L m^{-2} h^{-1} bar^{-1}], is defined as the liquid volume flowing through the membrane per unit membrane area, per unit time and per unit applied pressure. Rejection of component i, R_i, is defined as a function of the solute concentration in the permeate, $c_{P,i}$ and the solute

concentration in the retentate side, $c_{R,i}$. These were calculated using Equation 1 and 2 respectively:

$$B = \frac{V}{A \cdot t \cdot \Delta p} \qquad \textbf{Equation 2}$$

V is the volume collected, A is the effective membrane area, t is the time over which the sample is collected, Δp is the applied trans-membrane pressure.

$$R_i = 1 - \frac{c_{P,i}}{c_{R,i}} \qquad \textbf{Equation 3}$$

$c_{P,i}$ and $c_{R,i}$ represent the concentration of solute i in the permeate and the retentate, respectively.

Membrane screening was initially tested with two types of standard markers of PEG and PS. They both had a wide range of molecular weights which could be soluble in a variety of solvents with different polarities. 1 g L^{-1} PEG of each three different molecular weights (400, 2000 and 8000 g mol^{-1}) and 0.5 g L^{-1} PS of different nominal molecular weights (from 580 to 1300 g mol^{-1}) were used for membrane cross-flow cell screening.

Samples were collected from both retentate and permeance streams. An Agilent HPLC coupled to an evaporative light scattering detector (ELSD, Varian-385) was used to analyse PEG and PS samples. The ELSD evaporator was set at 40°C and the nebulizer at 55°C. Nitrogen gas was supplied to the detector at a flow rate of 1.5 standard L m^{-1}. A reverse phase column (C18-300, 250mm×4.6mm, ACE Hichrom) was used. The mobile phases were MeOH-MeCN (1:4) and the DI water buffered with 0.1 M ammonium acetate. The HPLC pump flow rate was set at 1ml min^{-1} and the column temperature was set at 30°C.

4.3.5.2. Weight change

Samples of membranes with an area of 2.5 cm^2 were washed three times with MeCN, dried under vacuum overnight and then weighted using an analytical balance. Three samples of each membrane type were weighed; the standard deviation was used to calculate error bars. The unmodified membrane was used as an internal standard. Three samples of polypropylene non-

woven support were also weighed and their average specific weights [mg cm^{-2}] were subtracted from the total weights of the PBI membranes to get the specific weights of the membrane layer.

4.3.5.3. Brunauer, Emmett and Teller (BET)

Membrane pore size was determined using Brunauer, Emmett and Teller (BET) theory using Micromeritics TriStar Surface Area and Porosity Analyser and TriStar3000 V6.07 software (Micromeritics UK Ltd, UK) with oxygen-free nitrogen (99.998 vol %, BOC, UK). Prior to a measurement, the samples were degassed in nitrogen for at least 4 hrs at 80°C, the isotherms can be found in the Section 4.4.

4.3.5.4. Liquid-liquid porosimetry

Liquid-liquid porometry is a pore size measurement in a fully liquid medium. The membrane samples were soaked in isobutanol-saturated water to fill the pores, then water-saturated isobutanol was pressurized through the membrane pores to displace the initial liquid. The pressure was increased from 100 bar to 400 bar with an increment of 5 bar min^{-1}. The flux rate of water-saturated isobutanol from the membrane permeate was recorded. The pore size of the membrane was then calculated by measuring differential pressures and the flux of membrane permeate.

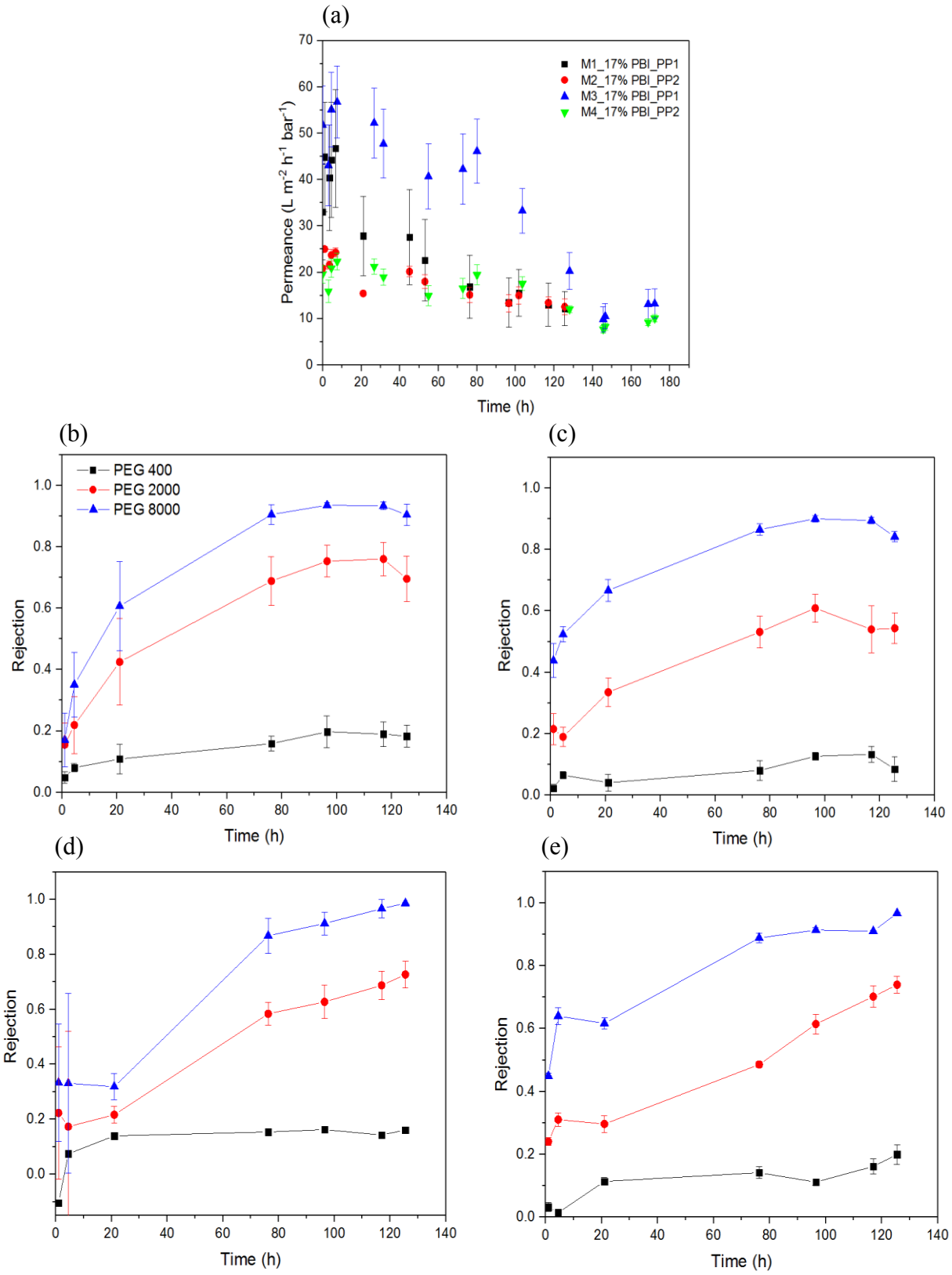
4.4. Results and discussion

4.4.1. PBI membrane performance from bench casting

4.4.1.1. Non-woven backing choice was not significant

In order to scale up PBI membranes to the spiral-wound module and widen the diversity of PBI membrane configurations, different non-woven backing layers for the membrane to cast on were studied in this work. The backing layer material is important for spiral-wound membrane assemblies such as rolling and gluing, and membrane solvent capability [283] [284]. Ideally, a non-woven fabric should give a sufficient pore size to allow solvent passage of the permeate, but restricted enough to interfere with the formation of the membrane layer. Two commercial polypropylene non-woven backings Novatex 2471 (PP1) and Evonick (PP2) were used to fabricate 17 wt% PBI membranes following the procedure reported by Valtcheva et al. [281]. The effect of different non-woven backings on membrane performance in MeCN is shown in Figure 4.4 below.

Membrane M1 and M3 were fabricated on Novatex 2471 (PP1) and showed slightly more open performance at the beginning of screening, which resulted in higher permeance of around 50 L h^{-1} m^{-2} bar^{-1} with larger variances which eventually stabilised after 120 hours to about 10 L h^{-1} m^{-2} bar^{-1} at a more realistic separation performance. Membrane M2 and M4 were fabricated on Evonick (PP2); they gave a much more stable performance, the permeance only fluctuated from 20 L h^{-1} m^{-2} bar^{-1} initially. The final steady permeance of membranes on both supports had minimal difference and the same conclusion was reached on membrane rejections. Membranes on both non-woven backings gave a similar rejection profile with time; again, the rejections of membranes with Novatex 2471 (PP1) had higher variances in the first few hours. This gradually decreased to a more consistent performance. Based on the rejection trends, the higher the solute molecular weight, the greater the rejection difference was between the initial time point and a steady state. The increase rate of PEG8000 rejection was steep; the value grew three times higher from 30% at t=0 to 90% at t=125h. The rejection of PEG400 levelled off more quickly. All membranes require at least 80 hours to reach the stable rejections of 90% for PEG8000, 70% for PEG2000 and 10% for PEG400. In conclusion, although the performance of membranes varied from batch to batch, especially with the initial screening results, different non-woven backings did not affect the final membrane performance after conditioning for several hours.



(a) Permeance; (b) Rejection of M1_17 wt%_PP1; (c) Rejection of M2_17 wt%_PP2; (d) Rejection of M3_17 wt%_PP1; (e) Rejection of M4_17 wt%_PP2.

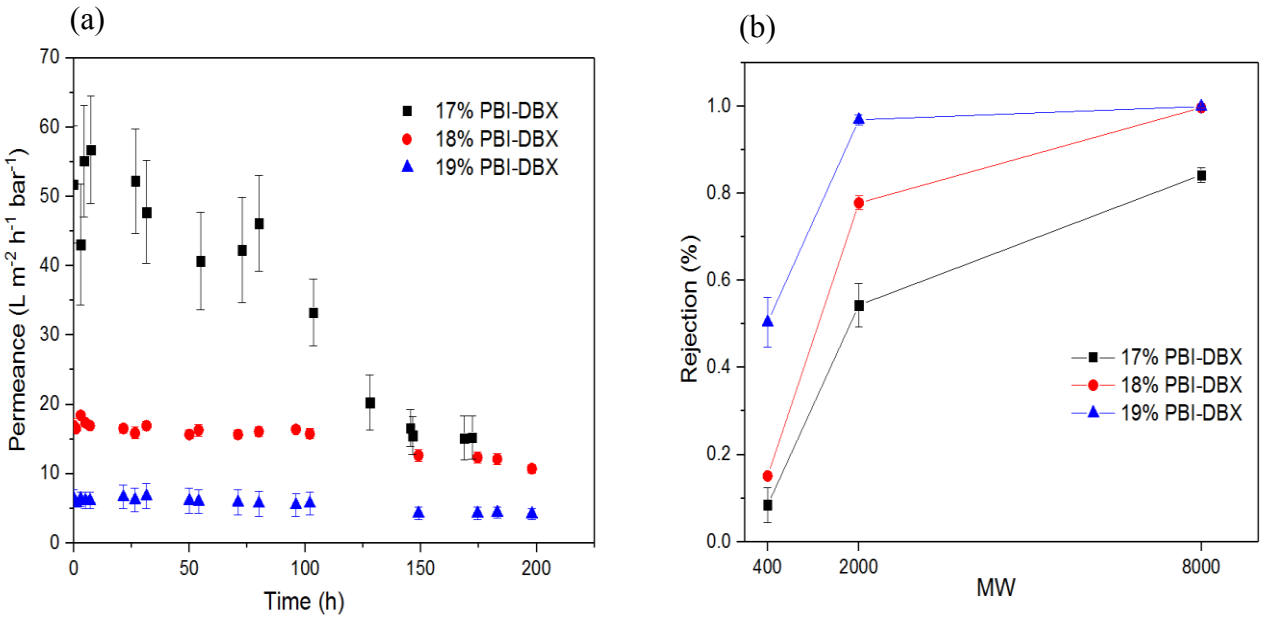
Figure 4.4 PEG rejection data of bench casting PBI-DBX membranes in MeCN with different non-woven backings.

4.4.1.2. Dope concentration can control molecular weight cut off (MWCO)

In this project, a simple method is reported for controlling the MWCOs of PBI-DBX membranes prepared via phase inversion. Different PBI polymer concentrations in the dope solution were explored, namely 17 wt%, 18 wt% and 19 wt%. The results showed that it is possible to vary the MWCO with the solutes' molecular weights ranging from 2000 g mol^{-1} to 8000 g mol^{-1} by adjusting the dope concentrations. Two replications for each membrane were performed to ensure reproducibility.

Figure 4.5 shows the general trends of the PBI dope concentration with membrane performance. Higher dope concentrations gave a tighter membrane structure, which led to lower permenace and higher rejections. Moreover, the permenace of 17 wt% PBI-DBX membrane dropped significantly over 200 hours. It started from approximately 55 L h^{-1} m^{-2} bar^{-1} and stabilised at 20 L h^{-1} m^{-2} bar^{-1} in a steady state, which was slightly higher than the 18wt % membrane. This phenomenon may have been caused by membrane compaction due to the loose membrane structure. Conversely, 18 wt% and 19 wt% PBI-DBX membranes gave a much more stable permenace; there was always about 10 L h^{-1} m^{-2} bar^{-1} difference between 18 wt% and 19 wt% PBI-DBX membranes, despite the compaction effect with time.

In the low PEG molecular weight region of 400 Da, the 17 wt% and 18 wt% PBI-DBX membranes had much lower rejections than the 19 wt% membrane. However the rejection of the 18 wt% membrane got closer to the 19 wt% membrane as the molecular weight of solute increased. The 19 wt% membrane showed the tightest performance, 50% of PEG400 was rejected; PEG2000 and PEG8000 were almost fully rejected. The 18 wt% membrane rejection ranged from 15% to 98% depending on the molecular weights, indicating that the 18 wt% membrane had the best selectivity to separate molecules from 400 Da to 8000 Da. In conclusion, PBI dope concentrations were shown to have a significant effect on the membrane performance; the membrane selectivity could be tuned by changing the dope concentrations. However for fabricating PBI membranes, the choice of polymer concentration is limited[271], if the dope solution is too dilute, it may affect its mechanical strength or form a poor polymeric network during membrane formation. On the other hand, if the dope solution is too concentrated, the physical properties of the membranes may be affected adversely, which could cause more problems in membrane performance.



(a) Permeance over a period of 200 h for membranes with different dope concentrations; (b) Final PEG rejection of membranes at 200 h

Figure 4.5 Membrane performance of bench casting PBI-DBX membranes with different PBI dope concentrations (17 wt%, 18 wt% and 19 wt%) in MeCN.

4.4.1.3. Conditioning of the membrane

In last two sections, reproducing the bench PBI-DBX membrane to achieve good membrane performance was attempted. However the reported rejections of PEG400, PEG2000 and PEG8000 in MeCN could not reach a steady state after several hours. At the beginning of the screening, PEG rejections were low and permeance was significantly high. After pressurized circulation for over 80 hours, the rejection increased, permeance decreased and the membrane was conditioned and stabilized for further use.

Another problem was the membrane reproducibility; the membrane performance varied from batch to batch using a bench-casting machine. Occasionally, variance from the batch produced in the same dope solution could be greater than the changes in other fabrication parameters. This interfered with the membrane performance and influenced the reproduction consistency. Membrane performance was affected by more than the common compaction issue, here because the permeance of pure solvent kept constant when the membrane was pressurized for circulation. This suggested the hypothesis of the reactive adsorption between the solute and the membrane surface causing the change of membrane performance. It was observed that the

amount of solute decreased from the beginning of the solution circulation and the conditioning was irreversible, therefore the adsorbed solutes were not leached out during subsequent separation.

4.4.2. PBI membrane performance from continuous casting

4.4.2.1. Improvement of crosslinking by surface modification

Controlling the degree of crosslinking is critical for membrane performance and reproducibility. Therefore it is important to understand the crosslinking reaction kinetics and reaction parameters. An electrophilic alkylation reaction occurs during crosslinking leading one DBX molecule to connect two PBI polymer chains to enhance the membrane network. In the crosslinking reaction, the bromide group from DBX attacks the multiple bonded nitrogen as an electrophile to protonate N-alkyl-imidazole on PBI. The resulting charged species is not stable and the other free bromide group then reacted with another PBI polymer chain through electrophilic alkylation. Therefore the PBI network is formed via DBX linkages, using two ends from DBX molecules connecting PBI polymer chains. Although crosslinking never goes to completion, the degree of crosslinking is affected significantly by crosslinker hindered diffusion through membrane and crosslinking reaction rate. Therefore, both mono-substituted (k1) and di-substituted imidazole (k2) moieties are formed in the membrane structure, shown in Figure 4.6. The di-substituted imidazole, for a tighter network, could be obtained by reacting both bromide groups at the same time. It is kinetically preferred when the alkylating agent is in an excess amount. During crosslinking, the membrane surface is in contact with a higher concentration of DBX in the reaction medium. The mono-substituted imidazole is most likely to be formed on the membrane surface, which gives some pedant DBX chains, which gives $k1 > k2$. The DBX molecules are harder to diffuse into the deeper membrane structure. The concentration of the DBX gradually decreases through the membrane while the high concentration of PBI is maintained. Therefore the di-substituted imidazole is favoured to form and enhance the connectivity inside of the membrane structure, i.e. $k2 > k1$.

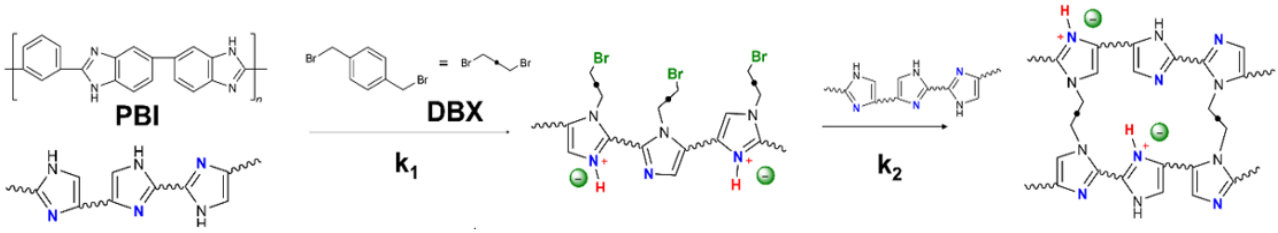
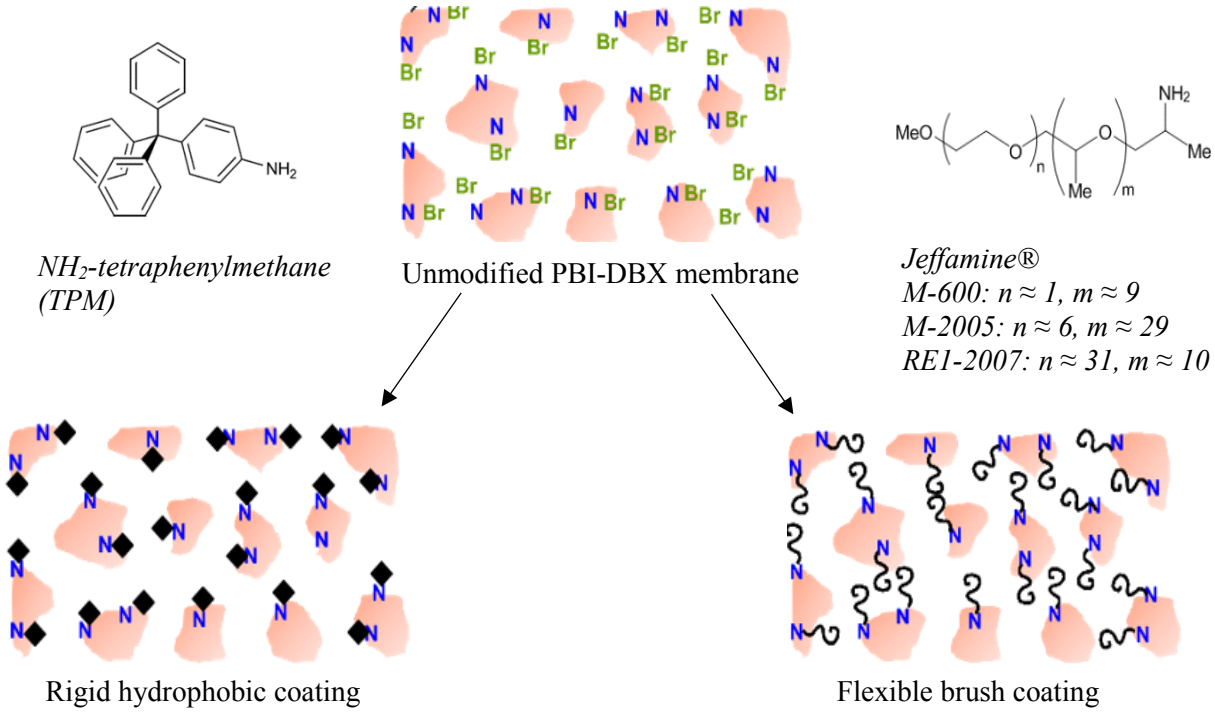


Figure 4.6 Schematic representation of the two-step crosslinking reaction between PBI and DBX.

The final crosslinked PBI-DBX structure is reactive and charged. The mono-substituted imidazole can be protonated by any acidic solvents or solutes, which makes the membrane charged and slight acidic with the presence of H^+. Hence, the membrane was soaked in Hunig's base for 24 h at 80°C during modification; the base was able to react the pendent DBX group to the OH group on the terminal of the crosslinking chain. Surface modification is required for the PBI-DBX membrane, because the process neutralized the membrane charge and chemically stabilized the membrane.

4.4.2.2. Surface modifiers

Surface modifiers with different chain lengths and hydrophobicity were applied to tune the membrane performance, which affects the separating of solvents and solutes. The schematic of the membrane surface modification is shown in Figure 4.7. TPM is a small, rigid and hydrophobic molecule. The membrane which was modified with TPM showed less steric hindrance inside the pore structure; higher permeance and lower rejection were obtained from the TPM modified membrane. The effect of the modification of the polymer lengths on the membrane structure was explored with Jeffamine® M-2005 and RE-1 2007. These gave different hydrophobicities on the membrane surface, which showed a significantly different membrane performance for the same separation environment. Both modifiers gave long flexible brush chains and offered great resistance inside the pore channels which resulted in tighter membrane structures. By contrast, the shorter modifier M-600, with only 10 monomers, had a more open membrane. Some material physico-chemical characterizations were completed on both the unmodified and modified membranes. The results are shown in the following Section 4.4.3, and they give a better understanding of the effects of the surface modification on membrane performance.



Membrane surface modification using 4-amino tetraphenyl methane (TPM), giving a rigid and hydrophobic coating. Jeffamines® with different lengths and degrees of hydrophobicity, produce a flexible brush coating.

Figure 4.7 Schematic of the membrane surface modification.

4.4.2.3. Solvent effects on membrane performance

Membrane performance in an OSN application was tested with standard PEGs and PS markers. A wide range of solvents from polar (such as water, MeCN) to apolar (such as toluene and heptane) were examined. The aim was to study the solvent effect on different surface modified membranes for controlling membrane pore size and hydrophilic-hydrophobic balance. After modification, the performance of the membrane had become much more stable compared to the unmodified PBI-DBX membrane. Permeance and PEG rejection were constant from the beginning over a period of 100 hours. In addition, the membrane performance became easier to reproduce and control. The PS and PEG rejection data of modified PBI membranes is shown below in Figure 4.8 and Figure 4.9.

Membranes that are modified with Jeffamines® M-600 and TPM generally gave higher peamenace due to the small molecular size of M-600 and TPM. The modifiers did not cause significant steric hindrance on the permeation pathways. Conversely, the membranes with

RE1-2007 and M-2005 gave a relatively lower permenace, due to their longer brush chains. The unmodified PBI-DBX membrane did not always show the highest permeance despite the unrestricted pathway compared to the modified ones. This is because some surface modifiers may assist the permenace when they favour the solvent in terms of hydrophobicity. For example, although the polymer brush M-2005 is long and bulky, the membrane coated with hydrophobic M-2005 still gave a higher permenace in hydrophobic toluene and THF compared to the unmodified one. Conversely the hydrophilic brush RE1-2007 restricted the permeance with the dissimilar solvent; toluene, THF and MeCN to less than 5 L m^{-2} $h^{-1}bar^{-1}$.

The membranes were tested by hydrophobic solute PS of nominal molecular weight of 580, 1000 and 1300 $g \cdot mol^{-1}$. In THF, the PS rejections were on average higher than with other solvents. When the PS molecular weight increased, membranes with the shorter modifiers gave lower rejections, whereas longer modifiers provided higher rejections due to the steric effect. In MeCN, the membrane with the longest hydrophilic modifier, RE1-2007, had the highest PS rejection; it was almost twice as high as M-2005, which was attributed to the nature of the membrane hydrophobicity. In the more hydrophobic solvent toluene, the M-2005 modified membrane showed advantages to retain solutes with the molecular weight less than 1000 g mol^{-1} while the RE1-2007 modified membrane had much lower rejections. In n-heptane, all the membranes suffered low rejections (10% to 20%) and may lose the selectivity between different sizes of the PS solutes. There were two negative rejection values with Jeffamine® modified membranes in n-heptane. This could be attributed to a collapse of the Jeffamine® modifiers against the pore walls, with a consequent effect on the hydrophilicity of the pore walls.

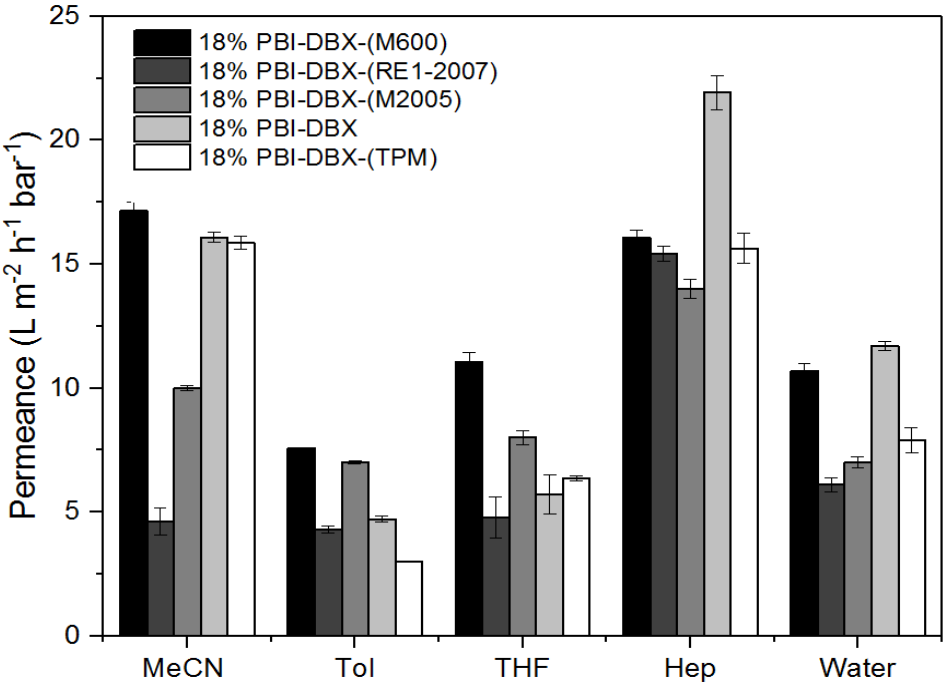
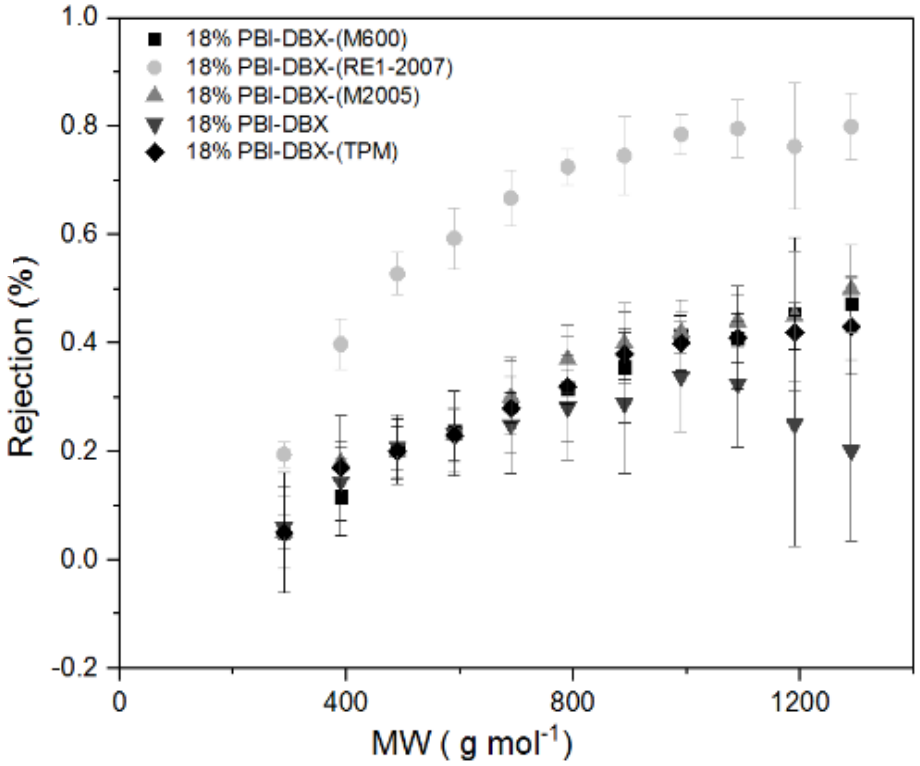


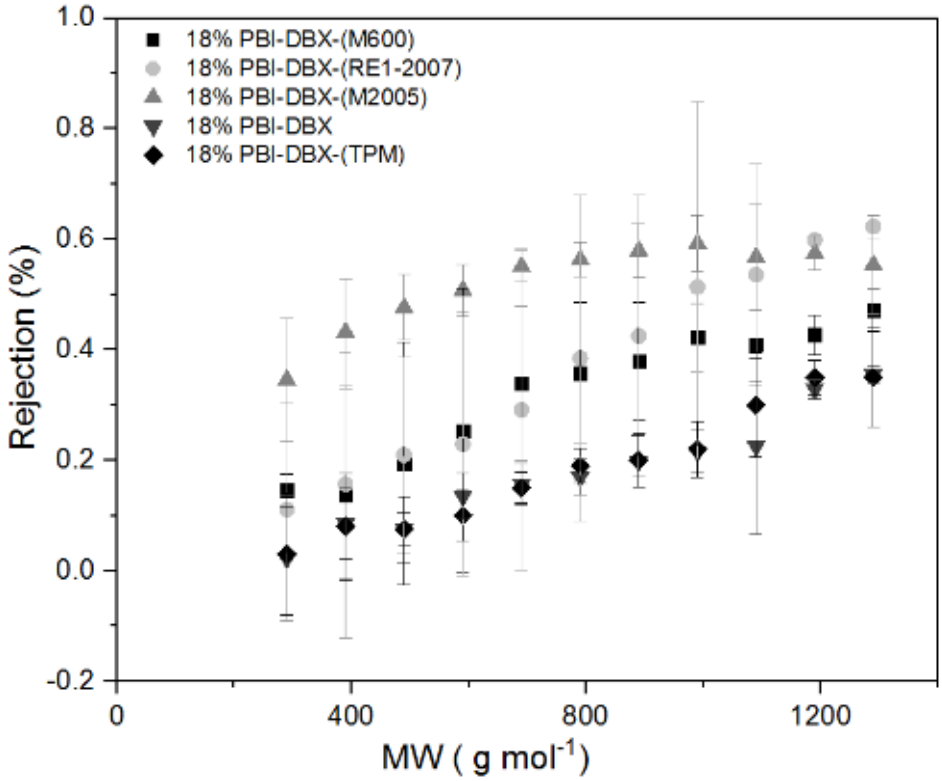
Figure 4.8 Solvent permeance of modified PBI membranes.

In Figure 4.9 (e), the PEG rejections in water of the modified membranes are shown. The large modifiers gave much higher rejections compared to the unmodified one. In addition, the unmodified membrane did not have a good separation selectivity between PEG400 and PEG8000. From the rejection gradient, it is suggested that RE1-2007 gave the best selectivity to separate PEG400 (20%) from PEG 2000 (90%) among all the membranes, while the rejection selectivity decreased in the higher PEG MW region. After modification of RE1-2007, PEG8000 rejection of the membrane significantly increased; roughly five times from 20% to 99%. Even though the modifier TPM is small, the PEG8000 rejection increased to 62%. However the rejection differences between the types of Jeffamine® modifiers such as Jeffamines® M-600, M2005 and RE1-2007 were small. This could be attributed to the nature of linear PEG solutes and their tendency to align to the pore walls with the grafted brush chains, perhaps overcoming the steric hindrance during permeation. Different surface modifiers could be used to tune membrane MWCO, even if the membranes were fabricated from the same dope concentration.

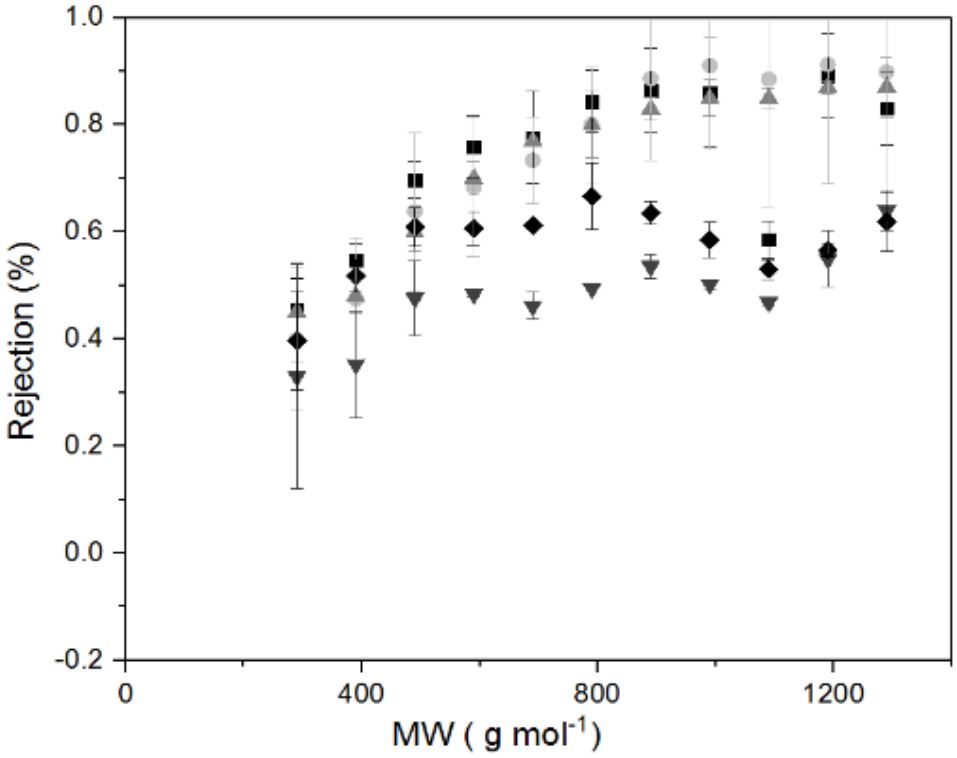
(a) Rejection of PS in MeCN



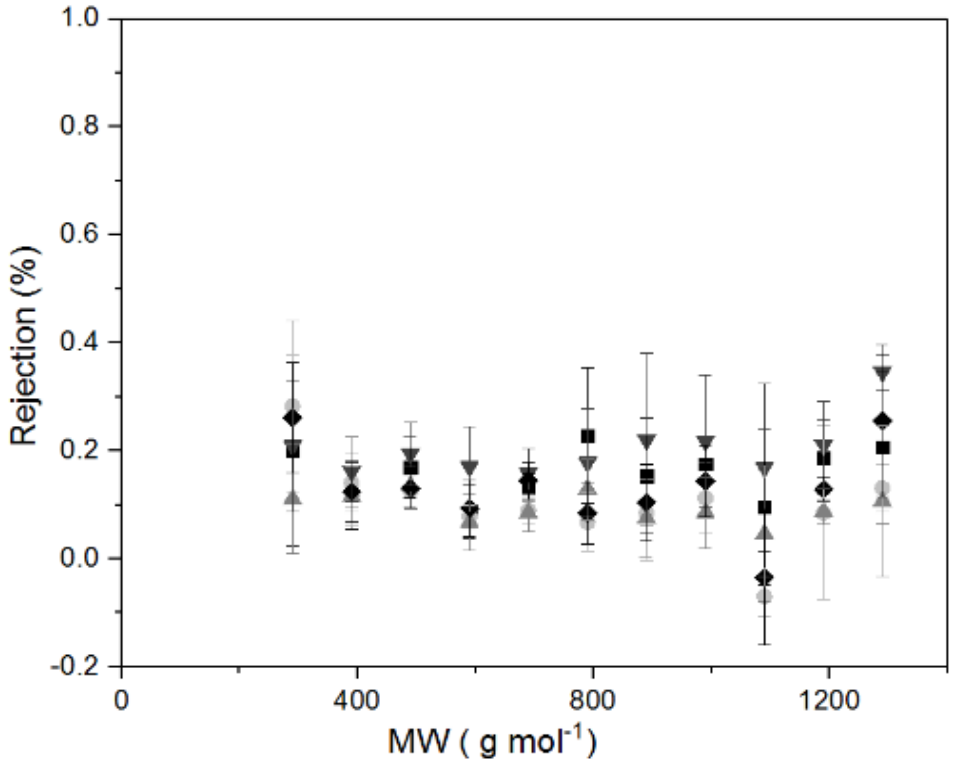
(b) **Rejection of PS in toluene**



(c) Rejection of PS in THF



(d) Rejection of PS in n-heptane



(e) Rejection of PEG in water

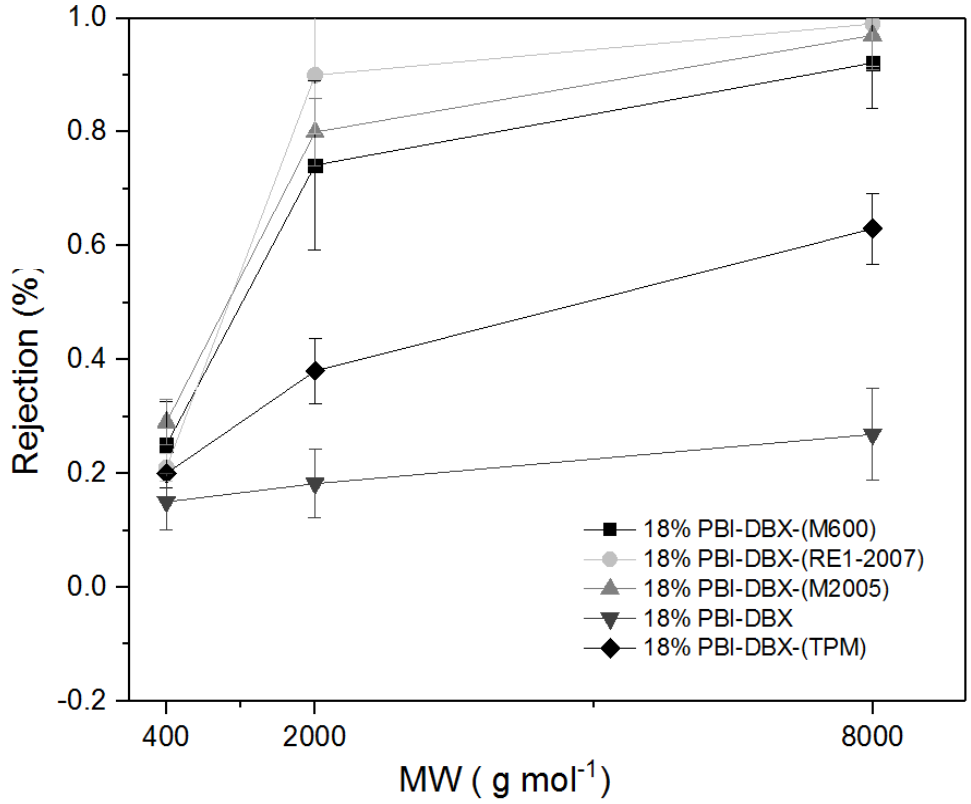


Figure 4.9 PS and PEG rejection data of modified PBI membranes shown above on panels (a) to (e).

4.4.3. Membrane characterizations

4.4.3.1. Specific weight gain and membrane thickness

Controlling the extent of the modification reaction is the key to controlling the pore size and the membrane performance. Specific weight gain is the most direct way to demonstrate the extent of the modification reaction; it indicates the mass of modifiers attached per unit area [mg cm^{-2}]. After the dried membrane had been PEG400 implemented, the cut samples were washed with MeCN to remove excess PEG400. Then the samples were dried under vacuum overnight to remove the infiltrated MeCN. The result of the specific weight gain of each membrane is shown in Figure 4.10. Due to the small molecular weight of TPM, the mass weight gain of the TPM was small compared to the longer chain of Jeffamine®. Alternatively, by converting the mass weight gain to molar weight gain [mmol cm^{-2}], it showed the actual degree

of molar modification. One possible explanation for results is shorter modifiers M-600 diffused faster inside the membrane and therefore reacted more equivalent with the dangling DBX on the interior of the membrane channel. On the other hand, longer modifiers (such as M-2005 and RE1-2007) may have reacted less, because their bulky structures made the modifiers more difficult to make contact with the inner membrane structure.

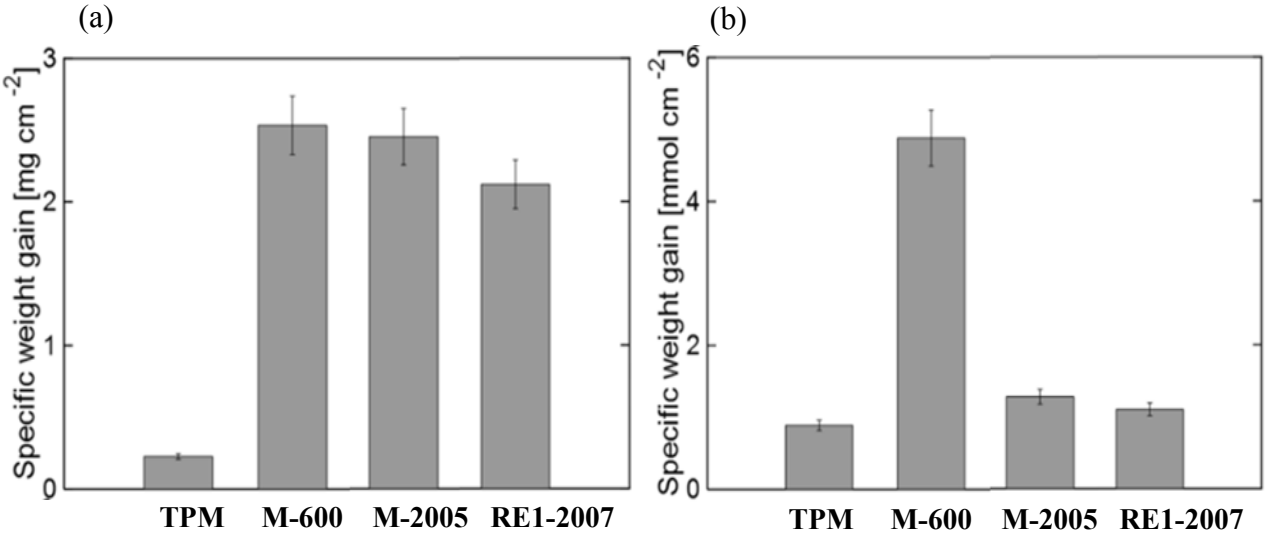


Figure 4.10 Effect of surface modification on specific weight gain in (a) mg cm^{-2} and (b) mmol cm^{-2}.

The change of membrane thickness with modification was also investigated in this study. Figure 4.11 shows SEM images of membrane porous cross-sections and measured thickness. In a previous study [271], an effect of crosslinking reaction time was observed on the membrane thickness. The membrane thickness increased during crosslinking time with the PBI polymer chain arrangement. However, here there was no observed difference in membrane thickness with membrane modification. This could be because the surface modification may have only decorated the membrane surface and pore structure and therefore there is no change of membrane thickness.

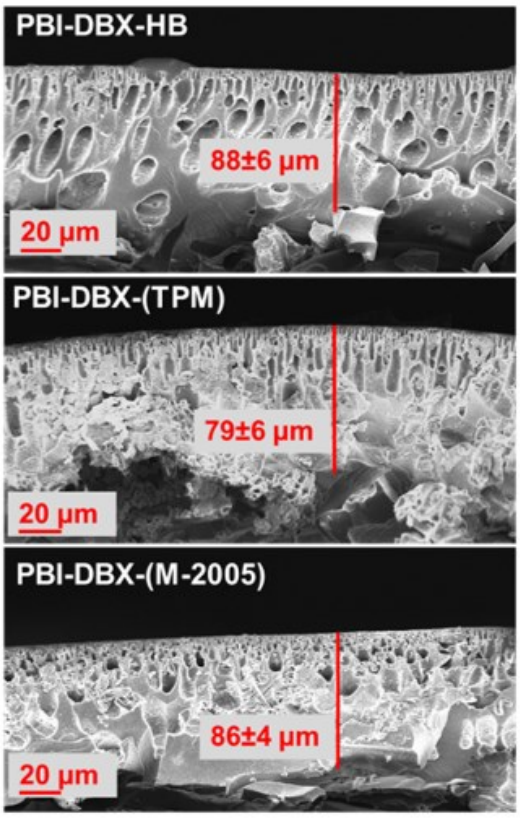


Figure 4.11 SEM images and thickness of unmodified membrane and membranes modified with TPM and M-2005 (created by Dr. Patrizia Marchetti).

4.4.3.2. Pore size distribution and measurement

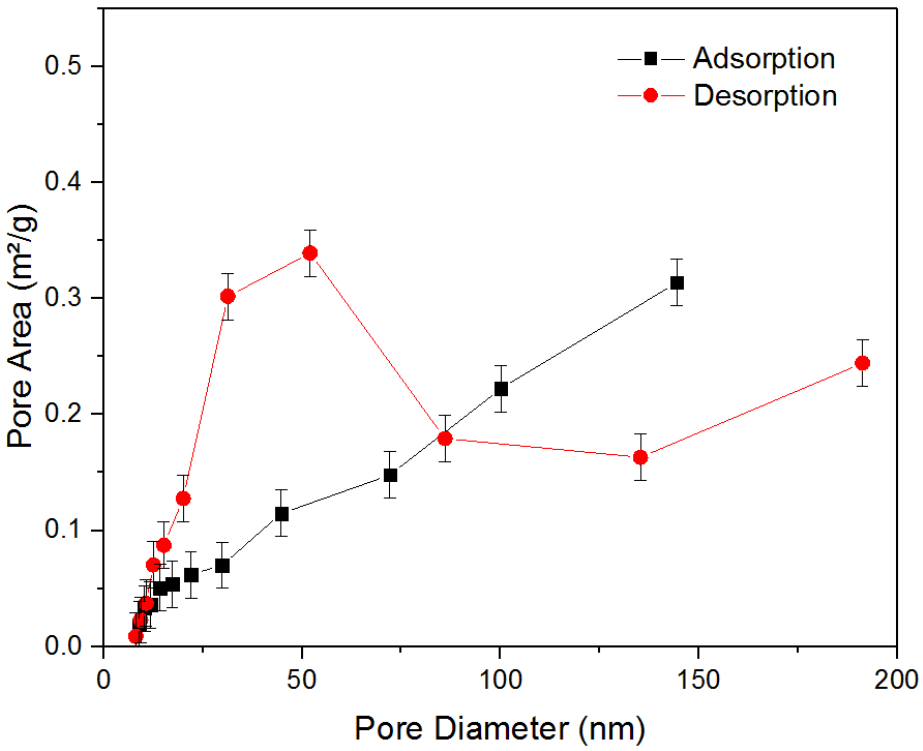
Barrett-Joyner-Halenda (*BJH*) analysis

Brunauer–Emmett–Teller (BET) analysis provides precise specific surface area evaluation of a PBI membrane by nitrogen multilayer adsorption, measured as a function of relative pressure. Barrett-Joyner-Halenda (BJH) analysis can also be employed to determine pore area and specific pore volume using nitrogen adsorption and desorption techniques. The gas is allowed to condense in the pores with the small dimensions. This measurement of pore size distribution is independent of the external area, due to particle size of the sample. Three types of continuous cast membrane were chosen for this analysis: unmodified 18 wt% PBI-DBX membrane with Hunig's base treatment, 18 wt% PBI-DBX-M2005 membrane and 18 wt% PBI-DBX-RE1-2007 membrane were tested.

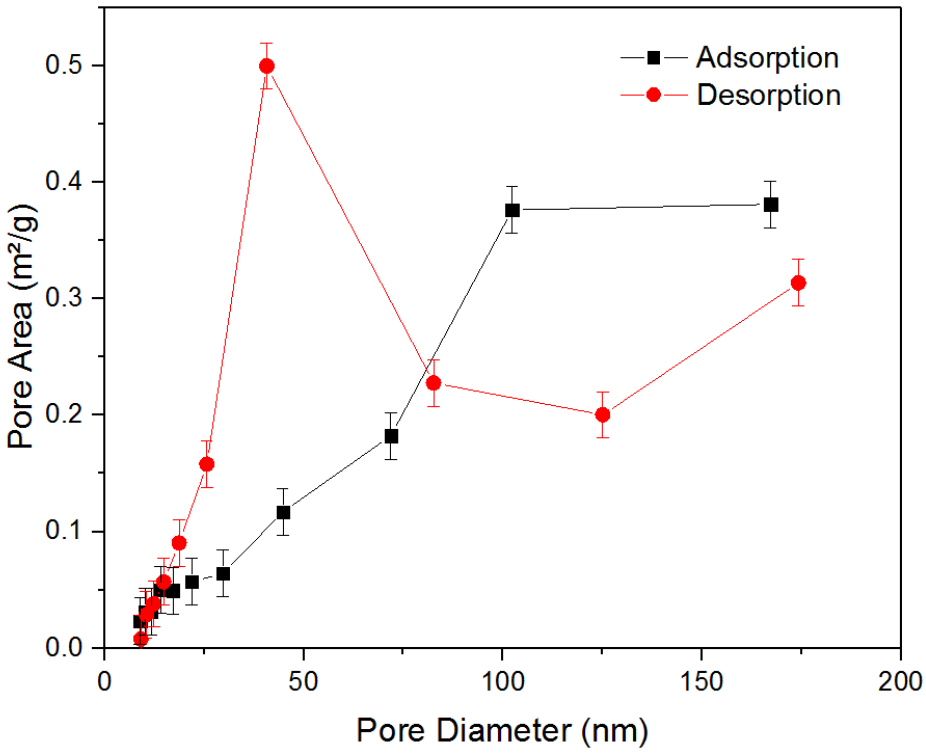
The average pore diameter (4V/A) was determined by BJH adsorption and desorption. The pore size distributions only showed in the desorption process, while the pores were filled with nitrogen in the adsorption process, so that the adsorption curve can be neglected. A limitation

was that the smallest pore size of the membrane that can be detected using this analysis was approximately 5 nm. Larger pore sizes through membrane channels are shown in Figure 4.12 (a) for the unmodified 18 wt% PBI-DBX membrane with Hunig's base treatment; it has an average pore size of 55 nm, which probably was the pore size from the membrane's porous sublayer. After modification, the pore size distribution of the 18% PBI-DBX-TPM membrane has been slight shifted to the left. Average pore size was less than 50 nm; however the pore area per unit mass increased from 0.35 m^2 g^{-1} in the unmodified membrane to 0.5 m^2 g^{-1}. The sublayer pore size of the 18% PBI-DBX-M2005 membrane was the smallest at about 30 nm, probably due to the long polymer chains. Also it has the greatest pore area per unit mass of 0.65 m^2 g^{-1}.

(a) 18% PBI-DBX membrane with Hunig's base treatment



(b) 18% PBI-DBX-(TPM) membrane



(c) 18% PBI-DBX-(M2005) membrane

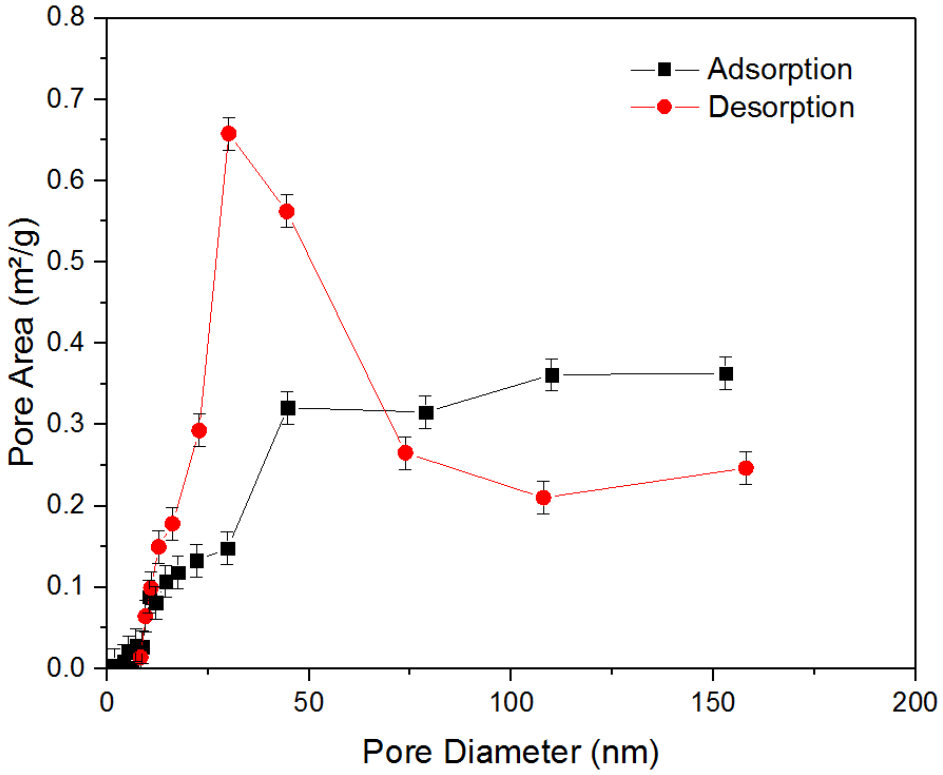


Figure 4.12 BJH adsorption and desorption for pore area of different surface modified membranes.

LLP Liquid-liquid displacement porosimetry

Liquid-liquid displacement porosimetry is also used to probe information through membrane pores. This method is operated in liquid medium under pressure and gives more precision to the measurement of the smallest sized channels compared to BJH analysis. It mimics the membrane separation process in the liquid phase and pushes the liquid through the whole membrane structure to achieve a sensitive measurement of the smallest membrane pore size. It is realistic and useful for ISA membranes, because it determines the pore size of the top selective layer which is the layer that determines rejection performance.

In order to determine the membrane with the smallest pore sizes on the selective layers, which influence rejection, three dense robust asymmetric membranes were investigated. Out of the

membranes fabricated expressly for this work, as discussed above, the two most promising were considered, namely: 18 wt% continuous casting PBI membrane cross-linked with DBX and modified with Jeffamine® (M-2005) and Elastamine® (RE1-2007). Additionally one 12 wt% PEEK membrane, fabricated in the Livingston group, was also considered at this stage [285].

The membranes' pore size distributions were determined by liquid-liquid porometry and the results are shown in Figure 4.13. The average pore size of 18 wt% PBI-DBX-M2005 was around 5.0 nm and the pore size distribution on the top dense layer was well distributed between 4.2 nm and 5.8 nm, which was significantly larger than those of the PEEK membrane (≈ 3.5 nm). The pore size of the PEEK membrane was the smallest, ranging down to 2 nm. The majority of the pores were evenly spread in the region from 3.2 nm to 4.2 nm, which fits with PEEK's low-permenace and high-rejection performance that was reported by Burgal et al. [284]. The average pore size of 18 wt% PBI-DBX-RE1 2007 was about 4.0 nm. There were two pore size distribution peaks, one peak was close to the pore size of 12 wt% PEEK and the other peak was slightly smaller than 18 wt% PBI-DBX-M2005, which in turn was unimodally distributed with a mean of 4.8 nm.

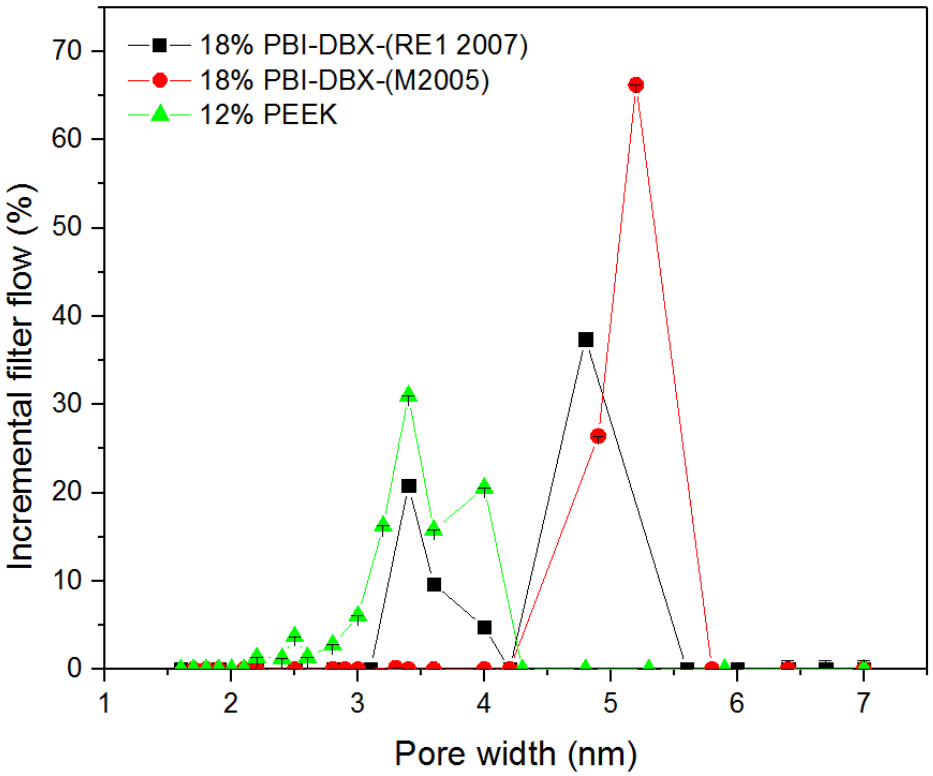


Figure 4.13 Pore size distributions of PEEK, 18% PBI-DBX-(RE1 2007) and 18% PBI- DBX-(M2005) asymmetric membranes determined by liquid-liquid porosimetry.

4.4.4. Case study: Membrane screening for PEG polyether iterative synthesis purification application in ItSyN conditions

In order to implement organic solvent nanofiltration in liquid-phase polyether synthesis, three modified 18 wt% PBI membranes and one 12 wt% PEEK membrane were screened for chemical synthesis purification peformance. Membrane technology offers a chromatography-free approach to separate the reaction debris from the growing polymer. It gives the advantage of operating iterative synthesis under fully liquid conditions to optimise reaction kinetics. Its fundamental simplicity and the high efficiency for the separation process are also commendable. This is a case study to apply our fabricated PBI membrane to a real synthesis application. The crude mixture, used to make multi-functionalisation sequence-defined polyethers with excess building blocks, was used to investigate the membrane separation application, shown in Figure 4.14.

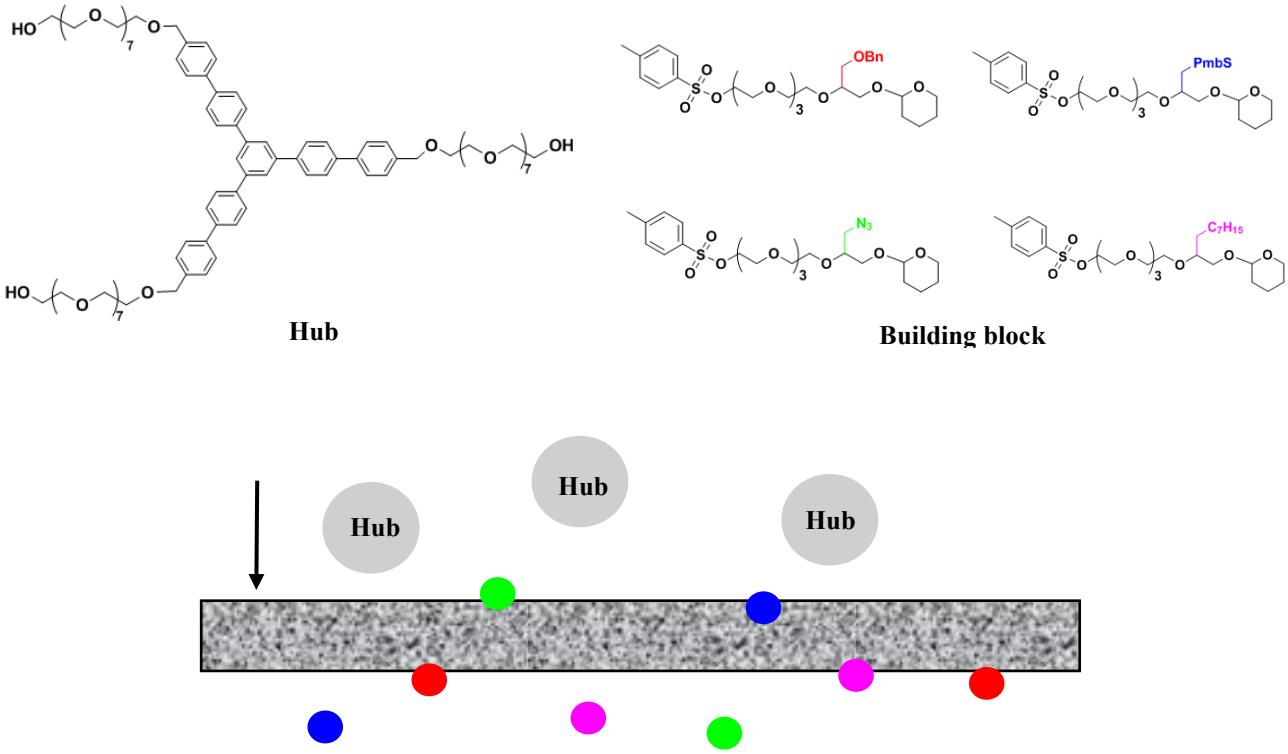


Figure 4.14 Case study Schematic of membrane separation of four pentagol building blocks and three armed tris(octagol) hub.

Building blocks, hubs and chemistry are as used in the ItSyN process described in this thesis. Their properties and preparation are discussed in more detail in Chapter 6. Briefly, a bulky

three-armed star Hub(OEG_8-OH)$_3$ was employed as a soluble support for growing polyether, shown in Figure 4.14. It had a large diameter of the rigid central unit with the growing arms in three directions. The size of the large polyether-star minimised permeation through the membrane compared to the relatively small building blocks, and separation efficiency was maximized. Three types of building blocks (BBs) with chemically reactive side-arms BnO-BB, N3-BB, PmbS-BB, and an inert building block Octyl-BB with a hydrophobic side-arm were studied. The different side arms exhibited different chemical and physical properties and gave slight size differences to the building blocks. Different chemical species and the reaction residues created diverse environments for the membrane to contact with and membrane stability was reviewed in this real application.

Membrane efficiency in separating two compounds based on their different sizes can be described by the separation factor $\beta_{A/B}$. Here the results show the membrane selectivity between solutes A (Hub(OEG_8-OH)$_3$) and B (building blocks). The equation for membrane separation factor is shown in Equation 3 below.

$$\beta_{A/B} = \frac{C_B^P / C_A^P}{C_B^R / C_A^R} = \frac{1-\mathrm{rej}_B}{1-\mathrm{rej}_A} \qquad \textbf{Equation 4}$$

where C_A^P and C_B^P are the concentration values of A and B in the permeate, respectively and C_A^R and C_B^R are the concentration values of A and B in the retentate, respectively. The separation factor can also be calculated from the membrane rejection of solutes A and B.

The molecular weights of the building blocks ranged from 531 to 642 Da, while the molecular weight of the hub was 1,682 Da and the size of hub polymer gradually increased with the chain growth. Therefore, the best membrane to perform for this separation was that a bulkier hub can be retained and smaller building blocks can be permeated. According to the results from liquid-liquid displacement porosimetry in Section 4.4.3.2, 12 wt% PEEK membrane and 18 wt% PBI-DBX membranes modified with both Jeffamine®(M-2005) and Elastamine® (RE1-2007) met the pore size requirements. Another, 18 wt% PBI-DBX membranes modified with Jeffamine®(M-600) was also investigated in this case study.

Different solvents including MeCN, MeOH, toluene, ethyl acetate and THF, were studied in membrane screening to determine the best separation performance. For 12 wt% PEEK membrane, THF-MeOH (4:1) was used, because the PEEK membrane had to be operated in

the presence of THF and MeOH, which improved the permenace of the PEEK membrane. In this study, PEEK still showed the lowest permenace and the tightest performance. The PBI membranes also showed variable performance, depending on the solvents. For 18 wt% PBI-DBX-M2005 membranes, the rejections of the building blocks in MeCN, toluene and ethyl acetate were higher than 70% and the rejections of the hub were all above 97%. This causes difficulty in removing building blocks completely while achieving a good yield. In MeOH, the membrane seemed to become more open and the rejection of the building blocks went down to only 24%, whilst the rejection of hub also decreased to 82%. This is not feasible for the purification process, because of significant hub product loss. Therefore MeOH-MeCN (1:1) was used for PBI membrane screening to reduce the rejection of building blocks while maintaining a high rejection of the Hub, of at least 90% for first chain extension cycle.

It was confirmed that the building block rejections were not affected by the presence of the Hub compound. The bulky hub and mild concentration did not cause any steric effect to prevent building blocks passing through the membrane. Although we screened each building block and hub separately, the results here represent the rejection of the crude mixture after chemical synthesis. In addition, all purification for different building blocks was operated in one separation rig with the same membrane. Therefore, the performance of the chosen membrane depended on the selectivity between hub and the particular building block that was the hardest to remove, i.e. highest rejection, assuming any building block had a rejection lower than that which could be purified with lower diafiltration volumes.

The membrane screening results are shown in Figure 4.15. Of the four membranes, 18 wt% PBI-DBX-M600 showed the highest solvent permeance of 10.8 L m^{-2} h^{-1} bar^{-1}; but the small rejection differences between hub and building blocks resulted in a small separation factor and 18 wt% PBI-DBX-M600 had the lowest separation factor of 0.26, while the rejection of hub was only 84%. The low hub rejection made the membrane less favourable due to the loss of expensive Hub products. The 18 wt% PBI-DBX-RE1-2007 membrane had a similar hub rejection as the 18 wt% PBI-DBX-M2005 membrane, observed at 92% and 94% respectively. However the 18 wt% PBI-DBX-RE1-2007 membrane gave the low permeance and high building block rejection of 70%, which was insufficient to give a good separation performance. The 12 wt% PEEK membrane showed the tightest performance in permeance of 1.2 L m^{-2} h^{-1} bar^{-1}, the separation factor also remained high due to the hub rejection which was close to 100%. The highest separation factor (7.25) between the hub and building blocks was obtained by the 18 wt% PBI-DBX-M2005 membrane in MeOH:MeCN (1:1). When compared to the PEEK

separation factor (4.5) in THF-MeOH (4:1), the target polyether-stars could be rapidly and efficiently isolated from the various reaction debris by the 18 wt% PBI-DBX-M2005 membrane. This was because of its higher permenace of 5.3 L m^{-2} h^{-1} bar^{-1} and excellent selectivity with hub rejection of 92% and building block of 42%. This suggests higher interconnectivity and microporosity of the PBI intermolecular networks after modification with appropriate chemicals and solvents. 18 wt% PBI-DBX-M2005 membrane makes the membrane separation process feasible, enabling the removal of all impurities after chemical synthesis in a reasonable diafiltration volume.

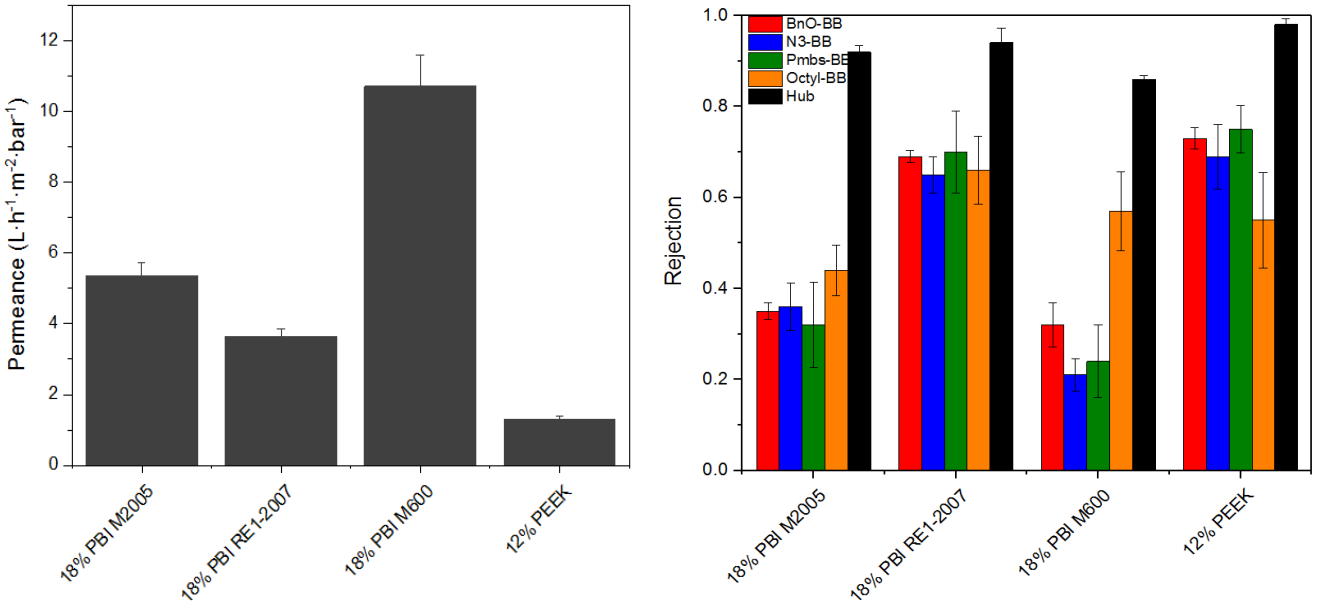


Figure 4.15 Case study of surface modified membranes; membrane permenace and rejections of building blocks and hub.

4.5. Chapter conclusions

Chemically stable ISA PBI nanofiltration membranes were successfully prepared via DBX crosslinking and surface modification. The membranes showed consistent and reliable separation performance in MeOH, MeCN, DMF, toluene and n-heptane using a wide molecular weight range of PEGs and PS solutes as nanofiltration markers. It was also found that continuous casting membranes exhibited better reproducibility and superior performance to those of the bench casting ones in all tested solvents. Furthermore, the effects of membrane fabrication conditions such as dope concentration, non-woven types and crosslinking have been studied in this chapter. Subsequently, the effect of using different modifiers on PBI membranes

has been investigated in organic solvent environments. Higher permeance and lower rejection were obtained from the post modified membrane using a shorter modifier. The structures and the hydrophobicities of the modifiers gave significantly different membrane performance in the same separation environment. Specific interactions between membrane, solvent and solutes improve the separation efficiency in terms of permeance and rejections. In addition, the membranes showed good chemical tolerance towards these extreme conditions for long periods of time, and the properties of the membrane did not need to be restored. The extent of post modification from different modifiers was verified by specific weight gain after modification. Modified membranes were much more stable, and could withstand harsh chemical environments, facilitating successful use in the case study of a PEG iterative synthesis purification without degradation. The modified PBI membranes showed great advantages for the implementation of membrane technology in separation processes in chemical synthesis environments. The properties and behaviours of the modified PBI membranes were well studied in this chapter, culminating in an application specific case study. Ultimately 18 wt% PBI-DBX-M2005 was the most suitable membrane for PEG iterative synthesis purification with these building blocks; it was investigated in this role using a batch membrane rig, as described in Chapter 5 and Chapter 6.

5. ItSyN for monodisperse linear PEGs

5.1. Abstract

A new technology platform combined with an iterative synthesis approach with membrane purification was explored to prepare uniform, monodisperse poly(ethylene glycol) $HOEG_{112}OH$ with an excellent quality. In order to improve the synthesis efficiency, two long building blocks were prepared: $TsOEG_{12}OThp$ and $TsOEG_{28}ODmtr$. In addition, a trivalent hub was designed by the Livingston group and applied to grow three PEG oligomers synchronously, via four rounds of Williamson etherification and diafiltration using 18% PBI-DBX-M2005 membrane. However, slow coupling between building blocks and the inevitable formation of the large dimer caused the accumulation of inaccurate or incomplete sequence lengths. Therefore a shorter building block $TsOEG_{12}ODmtr$ was used as an alternative. A series of chemical kinetic studies of chain extension and some improvements to chain extension conditions were investigated. The effects of reaction conditions on the reaction coupling, such as reaction concentrations, temperatures, solvents and base equivalent, were studied. Passivating the surface of the reaction flask improved the reaction completion to 99.6% of the 3-arm with fewer impurities in 12 hours. This study confirmed the feasibility of using $TsOEG_{12}ODmtr$ to synthesize good purity PEG polymer. The excellent coupling efficiency eased the membrane purification, and the use of membranes with iterative synthesis was shown to provide a general strategy for the preparation of precise, monodisperse PEG oligomers.

5.2. Introduction

Poly(ethylene glycols) (PEGs) are a class of biocompatible polymers that have been widely used in pharmaceutical applications. They are hydrophilic and have a flexible structure. For pharmaceutical applications, the use of PEGs in therapeutic molecules showed great advantages of excellent water solubility, non-toxicity and biocompatibility [286]. It is desirable to use polyethylene glycol with a minimum dispersity, ideally uniform in the chain length and precise in the sequence order. This allows for a better prediction of the polymer behaviour in vivo. Incorporating PEGs into complex functional molecules such as peptides, proteins, and biopolymers, is a well-developed approach to influence their physical properties and biological activities. Previous studies indicated that by the covalent attachment of PEG, the PEGylated molecules have prolonged serum half-life [287], improved drug stability and solubility [32],

and reduced immunogenicity[288]. Gabizon et al. also suggested PEGs played key roles in lipid self-assembly, including liposome development and the delineation of the structural mechanisms of lipid-bilayer formation and fusion [29].

Various PEGylated therapeutics have been approved by the US Food and Drug administration (FDA), meeting clinical value and safety criteria. With the growth of PEG applications and research, improving the purity of PEGs has received significant attention[173]. Monodisperse PEGs with well-defined chain lengths are ideal quality for any potential applications, as the uniform structure offers unique and tightly controlled physical, chemical and pharmacokinetic properties. For research and pharmaceutical use, a uniform compound also makes analytical interstation easier, such as MS spectra and X-ray diffraction (XRD); it permits a clearer understanding. Although monodispersity offers significant advantages, the synthesis of uniform PEGs remains challenging. Synthesis time and costs are far more extravagant compared to conventional polymerization, especially for longer uniform PEGs with molecular weight over 2500 Da [31].

However in order to achieve the stealth effect in drug delivery, PEGs with greater molecular weight are highly desirable, i.e. $\geq$ 4000 Da in biopharmaceuticals [42]. Therefore new synthesis strategies to fabricate monodisperse PEGs of high molecular weight at an affordable price are of great interest. Accordingly, many have reported new synthetic methods to reduce the dispersity of PEG, while pushing up the molecular weight range [31, 199, 289]. Initial study focused on synthesizing simple, symmetric PEGs [192, 200, 290-292]. However, unmodified PEG chains have limited applications, with asymmetric derivatives having drawn more interest in pharmaceutical and biomedical purposes [195, 293]. In the 1930s, the first discrete EG oligomer with 42 units was prepared using the concept of chain terminus desymmetrization to control the polymer coupling [294]. The Thp protecting group, monotosylation and benzylation was introduce to desymmetrize and furnish monofunctionalization of poly(ethylene glycol) diols in good yields and high purities [295]. However the efficient and selective monosubstitution of long symmetric PEGs still face challenges to achieve a good yield[194, 296]. Therefore shorter and commercially available PEG oligomers are preferred to use in polymer chain extension after desymmetrizing.

A few papers published routes to achieve long uniform PEG polymers. In general, four conceptual ways to elongate the PEG chain have been utilised, namely

unidirectional/bidirectional iterative coupling, chain doubling and chain tripling. Chain tripling results very fast in polymer growth, however it is limited by difficulties in desymmetrizing PEGs of >12 units [194]. Chain doubling is a more practical model to exponentially elongate the PEG chain [292]. Iterative strategies have been applied in a bidirectional extension of PEG diols with benzylated PEG tosylates as building blocks, with the chain length up to 44 units [200]. The longest uniform PEG oligomers synthesized to date are EG_{56} using an iterative strategy and EG_{64} using chain doubling with the molecular weights in the range of 2000 - 3000 Da [31, 173].

In order to ensure coupling completion and reduce the synthesis cost, cheap and commercially available tetra(ethylene glycol) $HOEG_4OH$ is typically pre-assembled into targeted longer building blocks. Common building blocks EG_8 or EG_{12} are normally prepared from symmetric EG_4 without chromatographic steps but more facile separation, which is extraction due to the high water solubility of EG_4. The monodisperse PEG EG_{56} polymer was synthesized from EG_8 building blocks after six rounds of chain extension [199]. Although significant progress has been made in the synthetic chemistry of monodisperse PEGs, in order to minimize contamination by other chain lengths, chromatographic purifications were intensively used which resulted in relatively low yields [195].

For synthesizing monodisperse PEG via iterative synthesis, a variety of protecting groups and leaving groups have been studied to achieve a high yielding process at a multigram scale [194]. The introduction of a THP protecting group gave linear PEG diol only in low yields of 55% due to its fragility during subsequent ether synthesis. However, monofunctionalized tosylate, benzyl-protected and *p*-methoxybenzyl (PMB)-protected PEGs showed excellent yields and high purities during desymmetrizing. The study of removing protecting groups selectively indicated that selective monodeprotection of these bifunctional molecules has to be performed in the following order: THP > PMB > Bn [194]. The bulky trityl protecting group was also used to protect PEG diol with a fairly good yield. The introduction of chloride as a leaving group to the monobenzyl-protected PEG using thionyl chloride was unsucessful and the tosylate group has been shown to be a good precursor for PEG chain extensions.

Apart from the coupling kinetic problem, shorter building blocks and tedious cycles of chromatographic purifications caused difficulties in accessing pharmaceutically relevant PEG polymer lengths with the molecular weight range of approximately 5,000- 40,000 Da [197]. In

addition, it is reported that the high molecular weight of the PEGs polymer from chain doubling strategies showed strong affinity to chromatographic media, which caused problems in product separation [31]. In 2015, the Livingston Group demonstrated the utility of using a small, symmetrical multivalent hub, 1,3,5- tris(bromomethyl)benzene, in the preparation of synthetic 2'-Me-RNA and PEG polymers [173, 175]. The use of this bulky soluble support could assist the rapidly growing MW of the PEG products, which would allow purification by size-exclusion, based on the rapidly emerging membrane technology platform of organic solvent nanofiltration (OSN).

For the work reported in this chapter, the aim was to prepare EG_{112} (Mw=4952 Da) with an excellent purity, using membrane filtration to separate the excess building blocks and reagents after each chain extension on the growing polymer. Monodisperse building blocks EG_{12} and EG_{28} were purchased commercially and used in the PEG polymer iterative synthesis. They reduce the number of required chain extension cycles to achieve high molecular weight polymers. The highly pure EG_{12} and EG_{28} as the building blocks simplify the procedures and the reduced number of chain extension cycles increases the final product yield and purity. This reduces the chances of impurity formation and accumulation through multiple reactions and prevents product loss from multiple purifications. Once the desired target length is attained, the oligomer can be functionalized and cleaved from the hub via hydrogenolysis to yield the linear, uniform, heterobifunctional PEG polymers. The membrane-based separation avoids the yield loss of PEG products with high molecular weights, which comparably are often lost due to a strong affinity to the media in chromatographic processes. In addition, the membrane process provides an opportunity for scalable manufacturing of this high value polymer with monodisperse purity.

5.3. Methodology

5.3.1. Materials

The monodisperse building blocks, octacosaethylene glycol EG_{28} and dodecaethylene glycol EG_{12}, were purchased from Polypure, Norway. Both oligomer purities averaged at greater than 95%. However the purity of EG_{28} used in the ItSyN chain extension was re-examined in Maldi-

TOF and the result showed a high purity of >99% in Figure 5.1. Therefore, EG_{12} and EG_{28} were used without further purifications.

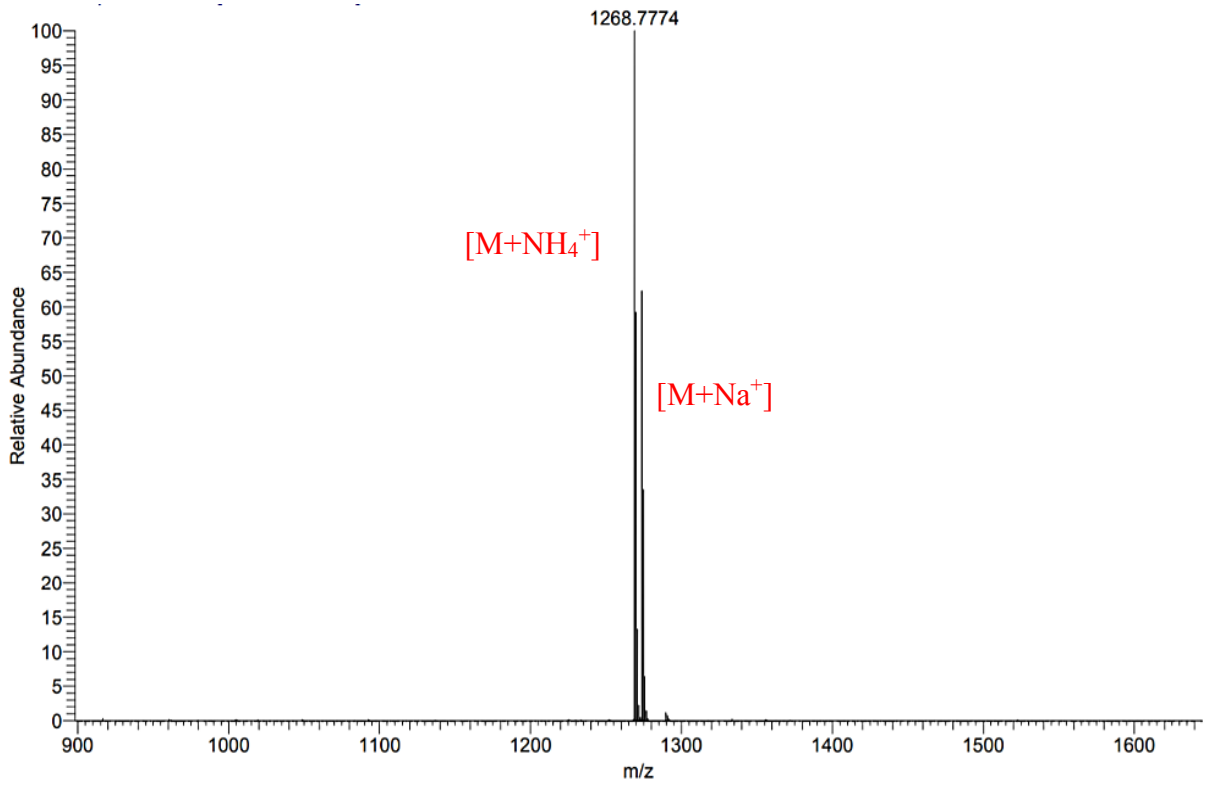


Figure 5.1 The Maldi-TOF spectrum of building block EG_{28} from Polypure, Norway.

5.3.2. General experimental procedures

Reactions were carried out under anhydrous conditions and in an atmosphere of argon or nitrogen. Reaction solvents dichloromethane (DCM), MeCN, THF and DMF were dried and stored over baked 4Å molecular sieves. All other reagents were purchased from commercial sources and were used as provided. Flash column chromatography was performed using Geduran (Si 60) from Merck for normal phase columns or Merck silanised silica for reverse phase columns in a 9 cm diameter, porosity 3, glass sinter funnel.

5.3.3. Analytical techniques

5.3.3.1. Nuclear magnetic resonance spectroscopy (NMR)

^{1}H NMR, ^{13}C NMR, distortionless enhancement by polarization transfer (DEPT)-135, heteronuclear single quantum coherence (HSQC) and homonuclear correlation spectroscopy (COSY) spectra were acquired using a Brüker AVANCE III-400 spectrometer, with working frequencies of 400 (^{1}H) and 101 (^{13}C) MHz, at 293 K. All samples were dissolved in $CDCl_3$ or [D_6] DMSO, which were purchased from VWR, UK.

5.3.3.2. Mass spectrometry (MS): ES-MS & MALDI-ToF-MS

The electrospray mass spectrometry (ES-MS) were recorded on a Waters LCT Premier (ES-ToF)/Acquity *i*-Class mass spectrometer. The matrix assisted laser desorption ionization-time of flight mass spectrometry (MALDI-ToF-MS) were conducted on a Brüker ultrafleXtreme MALDI-ToF/ToF mass spectrometer (with an Nd:YAG laser, λ = 355nm) using 1,8-dihydroxy-9(10H)-anthracenone (Dithranol) as the matrix. A typical sample preparation protocol was as follows: the samples and the matrix (Dithranol) were dissolved in MeCN or THF at 10 mg/mL and 20 mg/mL, respectively, then mixed together in typically a 1:49 ratio to ensure an excess of matrix. 0.5 μL of the MeOH solution containing 10 mg/mL NaOAc was also added to promote Na adducts. Once mixed, 0.5 μL of the mixtures was spotted onto the MALDI plate. The samples were air-dried, then run in reflection or linear mode.

5.3.3.3. Thin layer chromatography (TLC)

Reactions were monitored by thin layer chromatography using a Merck aluminium plate of 60 F_{254} silica gel. Compounds were visualised using UV light with either $KMnO_4$ stain or for Dmtr-ethers, trifluoroacetic acid (TFA) vapour stain.

5.3.3.4. High-performance liquid chromatography (HPLC)

HPLC analysis was performed on a 1100 Series Agilent HPLC system equipped with a UV diode array detector and a 1100 Infinity analytical scale fraction collector, using a reverse-phase C18-300 column (250 mm × 4.6 mm, ACE Hichrom). The mobile phases for HPLC were

deionized water buffered with 5 mM ammonium acetate (solvent A) and 20% MeOH in MeCN (solvent B). The samples were injected using an Agilent 1100 Series (G1367A) autosampler with a capacity for 100 samples, and the injected volume was 30 µL. The samples were eluted with the method shown in Table 5.1. The HPLC pump flow rate was set at 1 mL min^{-1} and the column temperature was kept at 30 °C. The detector was an Agilent 1100 Series (G1314A) variable wavelength detector and the eluent was monitored at 260, 280, 290 and 300 nm.

Table 5.1 Solvent gradients of monodisperse PEG HPLC method.

Time (min)	20% methanol in MeCN (%)	Water (%)	Flowrate (mL/min)
0.00	40	60	1.00
2.00	40	60	1.00
22.00	90	10	1.00
25.00	40	60	1.00
35.00	40	60	1.00

5.3.3.5. Ultra-performance liquid chromatography (UPLC)

UPLC analysis was performed on a Waters Acquity UPLC system which consists of a binary solvent manager, a sample manager and a high temperature column heater. The system was equipped with a photo-diode array (PDA) detector, an evaporative light scattering (ELS) detector and a mass spectrometer. A reverse-phase C18 column (1.7µm, 2.1 × 100 mm, ACQUITY UPLC) was used here. The mobile phases for the UPLC analysis were deionized water buffered with 5 mM ammonium acetate (solvent A) and 20% MeOH in MeCN (solvent B). The 7.5 µL samples were injected using the sample manager. The eluting gradient of the mobile phase is shown in Table 5.2. The UPLC binary solvent manager provided a flow rate of 0.3 mL min^{-1} and the column temperature was kept at 60 °C. The PDA detector was operated with variable wavelengths between 200 to 500 nm.

Table 5.2 Solvent gradients of monodisperse PEG UPLC method.

Time (min)	20% methanol in MeCN (%)	Water (%)	Flowrate (mL/min)
0.00	70	30	0.30
0.28	70	30	0.30
3.00	95	5	0.30
5.00	95	5	0.30
5.10	70	30	0.30
6.00	70	30	0.30

5.3.3.6. Chain extension and deprotection

After evaporation from anhydrous MeCN, hydroxyl-terminated polyether-homostar and BB tosylate (6-12 equiv.) were re-dissolved in DMF. To this solution was added NaH (6 equiv.). The resulting mixture was stirred for 12-24 h at 60 °C until complete, confirmed by HPLC. Saturated NH_4Cl (aq.) was added, and solvent evaporated in vacuo. The residue was re-dissolved in CH_2Cl_2 and partitioned with half-saturated brine, back-extracting the aqueous layer. The combined CH_2Cl_2 layers were dried (Na_2SO_4), and the solvent stripped off. The crude material purified by diafiltration, the retentate was washed from the apparatus and evaporated to provide the Thp-terminated polyether-star.

To Thp-terminated polyether-homostar in CH_2Cl_2-MeOH (1:1) was added MsOH (0.05 M). After 30 min, the reaction was quenched with saturated $NaHCO_3$ (aq.) and the solvent evaporated. The residue was dissolved in $CHCl_3$, partitioned with half-saturated $NaHCO_3$ (aq.), and back-extracted with further $CHCl_3$. The combined organic phase was dried with Na_2SO_4 and concentrated at reduced pressure to afford the hydroxyl-terminated polyether-star.

5.3.3.7. Membrane screening

The membrane cross-flow screening was carried out using the same method as in Chapter 4. The membranes were screened with the initial chain extension crude before diafiltration. The product concentration was between 0.8 g L^{-1} and 2 g L^{-1}.

5.3.3.8. Diafiltration set up

The diafiltration systems were run in a two-stage rig; the schematic is shown in Figure 5.2 below. Four membrane cells were installed and connected in series in the first stage of the membrane rig. In the second membrane stage, only two membrane cells were used to secure the loss of the product from the first stage. Each membrane disc had an effective area of 52 cm^2. The transmembrane pressure at each stage was about 20 bar. Therefore the diafiltration rig was operated at 40 bar in the first stage and 20 bar in the second stage and at room temperature. As a constant volume diafiltration, a 1 L measuring cylinder was used to collect the diafiltration permeance from the system. In order to replenish the system diafiltration volume, a 3 L dropping funnel was used as a fresh solvent tank and operated at a flow rate equalling the membrane flux from the membrane second stage. A 100 mL bottle was used as a feed tank and a stirring plate was installed to help with mixing of fresh solvent and membrane retentate. A 305 Series HPLC pump (Gilson, UK) with a 100SC pump head, was used as a feed pump. The system was steadily circulated at a flow rate of 100-150 L h^{-1}, with the assistance of one Micropump (Michael Smith Engineers Ltd., UK) in each membrane stage.

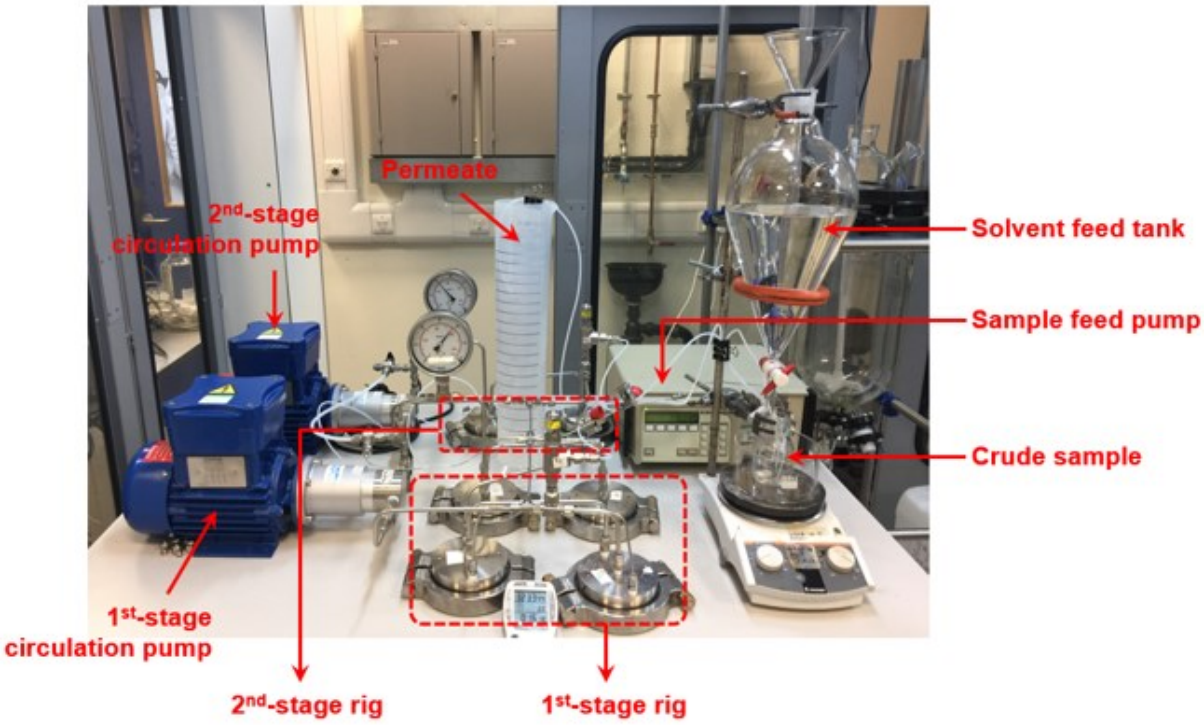


Figure 5.2 Schematic of the two-stage diafiltration rig.

5.3.3.9. ItSyN procedure

This scalable iterative synthesis with an organic solvent nanofiltration (ItSyN) approach is entirely in the liquid phase. In each cycle, there are three steps: coupling, diafiltration and deprotection. As it is shown in Figure 5.3, the chain extension was carried out in round flasks after diluting with diafiltration solvent in the feed tank. The diafiltration was operated for roughly 20 diafiltration volumes to separate impurities in permeance and were then collected in measuring cylinders. The retentates from both stages were drained and washed from the rig at the end of diafiltration. The solvent from both retentate and permeance can be stripped off under reduced pressure. The concentrated permeance can be purified and the unconsumed building blocks can be recycled for future use. A quality control was carried out with the concentrated product from the retentate, as stated in analytical techniques Section 5.3.3. The purified product was then diluted in a round flask for the deprotection reaction and a simple extraction was then accomplished to remove the protecting group debris. Another quality control was needed to ensure that the deprotection was completed before the next cycle of coupling reactions.

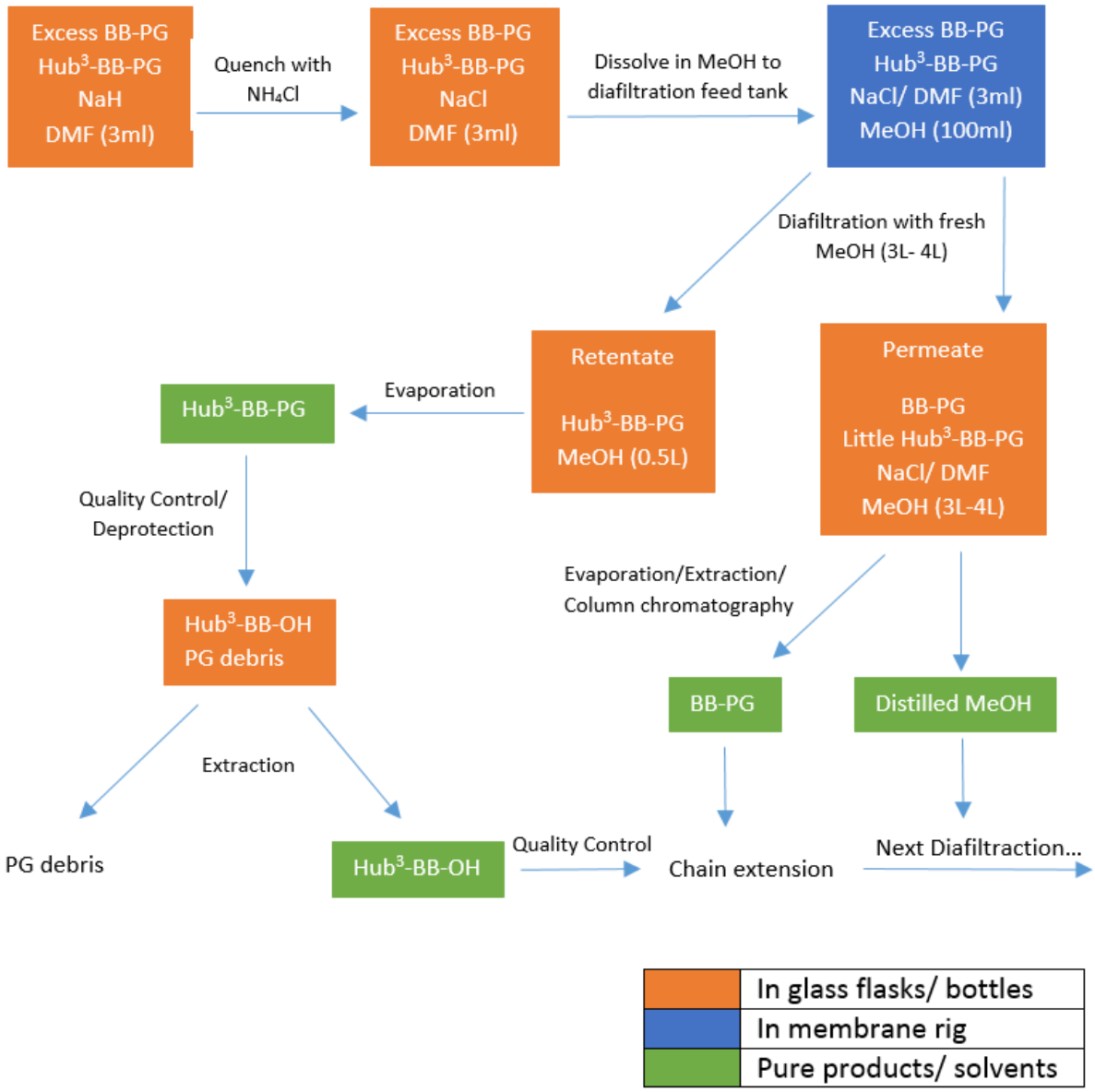


Figure 5.3 The ItSyN procedures of coupling, diafiltration and deprotection.

5.4. Results and discussions

5.4.1. The design of the hub

For the iterative synthesis, the use of a bulky soluble support increases the size difference between the chain extended product and the small building blocks; especially for membrane separation. The distinguishing size difference assists the membrane performance, increasing the yield and the efficiency of the purification. A three-armed hub designed by the Livingston Group was used here. The hub product with three growing chains exhibited a branched star-like geometry, while the building blocks were linear. A desirable membrane is characterized by a high selectivity to retain the growing product and an efficient permeate to allow the excess building block to pass through after each chain extension. In addition, a trivalent hub leads to three unidirectional chains growing simultaneously, thus speeding up the chain extension efficiency and tripling the growth in size of the large molecule ('homostar') to be retained in the membrane. The polyether chains were attached on a support via benzylic ether linkages, as the soluble support normally acts a protecting group for one end of the polyether. Moreover a benzylic ether linkage is stable in etherification conditions, while it can be cleaved by hydrogenolysis or Lewis acids. In order to avoid the loss of the protecting groups during the cleavage of the benzylic support and during hydrogenolysis, the final protecting group of the building block also has to be chemically stable during hub cleavage, such as a methoxy group.

In 2005, the Livingston research group demonstrated the use of a small trivalent hub, 1, 3, 5-tris(bromomethyl)benzene (Hub^1–CH_2Br), in the preparation of synthetic 2'-Me-RNA [175]. However due to the structural difference between oligonucleotides and PEG building blocks, despite the hub's branched nature and significant size contribution, it did not show a good rejection on membrane purification. In other words, the product yield would have significantly reduced whilst permeating the building block impurities away. Therefore, it was decided that the size hub should be increased to enhance the membrane's performance. The branched star-like geometry with three arms and the benzylic ether linkages were kept for the new hub, with their advantages as discussed above. A larger analogue Hub^3-Br (Figure 5.4, **9**) with similar benzyl bromide terminal functionality was synthesized from commercially available 1, 3, 5-Tris (4'-carboxy [1, 1'-biphenyl]-4- yl) benzene (Hub^3-COOH) by our group. With the extra aromatic rings, the support became more rigid with a large diameter. It improved the support's molecular architecture and the product was sufficiently distinguishable from other components

in the crude product mixture. The results of rejections of the first Hub^3 generation, $Hub(OEG_{28}ODmtr)_3$ in different membranes are shown in Section 5.4.3.

During the reaction and diafiltration, the growing polyether was supported on a bulky three-armed star, bearing flexible PEG chains around it. All Hub^3 derivatives were easily soluble in both reaction and diafiltration solvents. The Hub^3 structure also acted as a label for monitoring reactions and diafiltration because of its high UV extinction coefficient.

5.4.2. Synthesis of heterobifunctional linear PEG using ItSyN

The aim was to prepare $HOEG_{112}OH$ (Mw=4952 Da) with an excellent purity, using membrane filtration to separate the excess building blocks ($HOEG_{28}OH$) and reagents after each chain extension on the growing polymer. This was a new and efficient approach to achieve monodisperse PEG5000. Due to the availability of the highly pure long building blocks, only four cycles of chain extensions were required for iterative synthesis, reducing the chance for impurity formation and accumulation. The membrane separation makes this approach of using long PEG building blocks possible. By contrast in chromatography, with increasing chain length the longer PEGs chains dominate the main chemical and physical properties of the polymers, and the chromatography elution reduces resolution between the compounds [31]. Furthermore, the longer polyether chain has a stronger affinity to the chromatographic media, which enables it to bind onto the flush silica and causes a loss of product yield [195]. Therefore column chromatography becomes infeasible with higher MW PEG separation. In addition, the membrane also simplifies and makes the separation scalable at each synthesis cycle and improves the separation yield. Here the new strategy, the synthesis scheme of monodisperse linear $HOEG_{112}OH$ is shown in Figure 5.4, including the building blocks synthesis, hub loading and coupling and deprotection for each ItSyN step.

For the preparation of the PEG building blocks, due their linear flexible structures, the size of the protecting group and the leaving group at both ends significantly influences the bulkiness of the building block. Therefore the design of the building blocks was considered for the separation performance based on its membrane rejection. The choice of a relatively small tetrahydropyranyl acetal as the protecting group enhances the membrane permeance. The toluenesulfonyl group was chosen as the leaving group, as it showed a good coupling efficiency

and offers a reasonable size for membrane diafiltration. The strong UV indication is also convenient for online monitoring during both synthesis and diafiltration.

Using a similar methodology as employed for the fabrication of uniform PEG2500 [297], the building block EG_{28} was asymmetrically protected with DmtrCl, using $HOEG_{28}OH$ with 1 equiv. DmtrCl, followed by tosylation, detritylation and Thp protection to $ThpOEG_{28}OTs$ **6**. Due to the high unit price, it is not ideal to use a large excess of $HOEG_{28}OH$ to reduce the amount of bis-protected product. Using Dmtr gave a higher yield than direct desymmetry with 3, 4-Dihydro-2H-pyran. This is because DmtrCl gives an efficient chemoselective attachment on a single side of the PEG building blocks. The Dmtr group also assists the building block to achieve higher yields in column purification for building block synthesis.

The first modified building block, $DmtrOEG_{28}OTs$ **4,** was used for initial hub loading, which required three equivalent of $DmtrOEG_{28}OTs$ to be connected to a three-arm anchor (hub) via a benzyl linkage, as shown in Figure 5.4 (i). With the same advantages of the Dmtr group mentioned above, the Dmtr group used in hub loading, instead of the Thp group, offered a distinguishable elution to give a good separation of the Hub product as a starting material in a reverse phase column with a high yield of 98%.

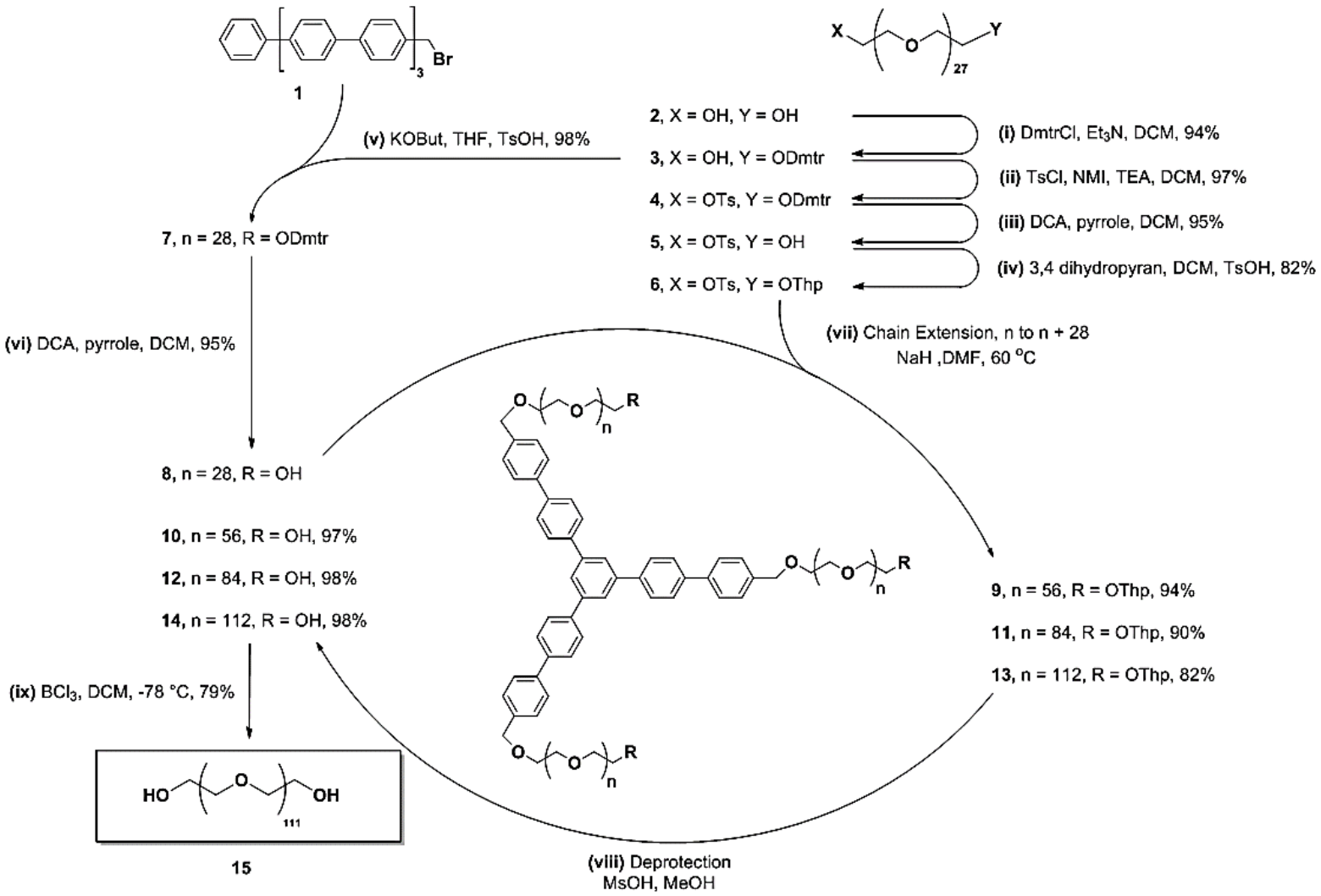
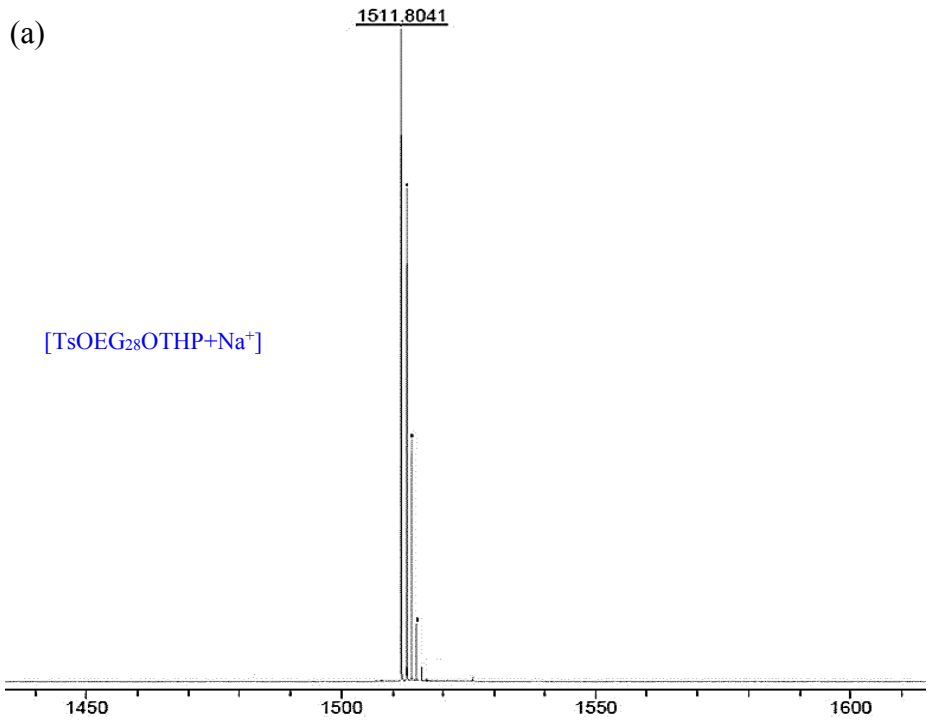


Figure 5.4 The ItSyN approach to monodisperse PEG synthesis.

In order to secure the high purity of the extended polymer, the purities of the starting materials and building blocks were examined carefully. Achieving high quality for the building block decreases the risk of introducing impurities, such as [M – EG_1] as well as [M + EG_1] from each cycle. The mass spectrum of the final modified building block 6 is shown in Figure 5.5. The quality of hub loading is also important for the polymer purity; incomplete hub loading leads to the lack of homostar arms and gives impurities such as [M- EG_{28}] and [M- EG_{56}]. The HPLC spectrum of the final building block of ThpOEG_{28}OTs **6**, hub loading of the first generation homostar Hub(OEG_{28}ODmtr)$_3$ **7** and the deprotected compound Hub(OEG_{28}OH)$_3$ **8** are shown in Figure 5.5. All the peaks looked sharp and clean. The retention times of both the building block and the starting material were recorded as the references for chain extension online monitoring. The building blocks were eluted at 13 mins, which was much earlier than Hub products. The retention time of the protected Hub(OEG_{28}ODmtr)$_3$ **7** was one minute later than the deprotected Hub(OEG_{28}OH)$_3$ **8**, due to the hydrophobicity change caused by the loss of three Dmtr groups.



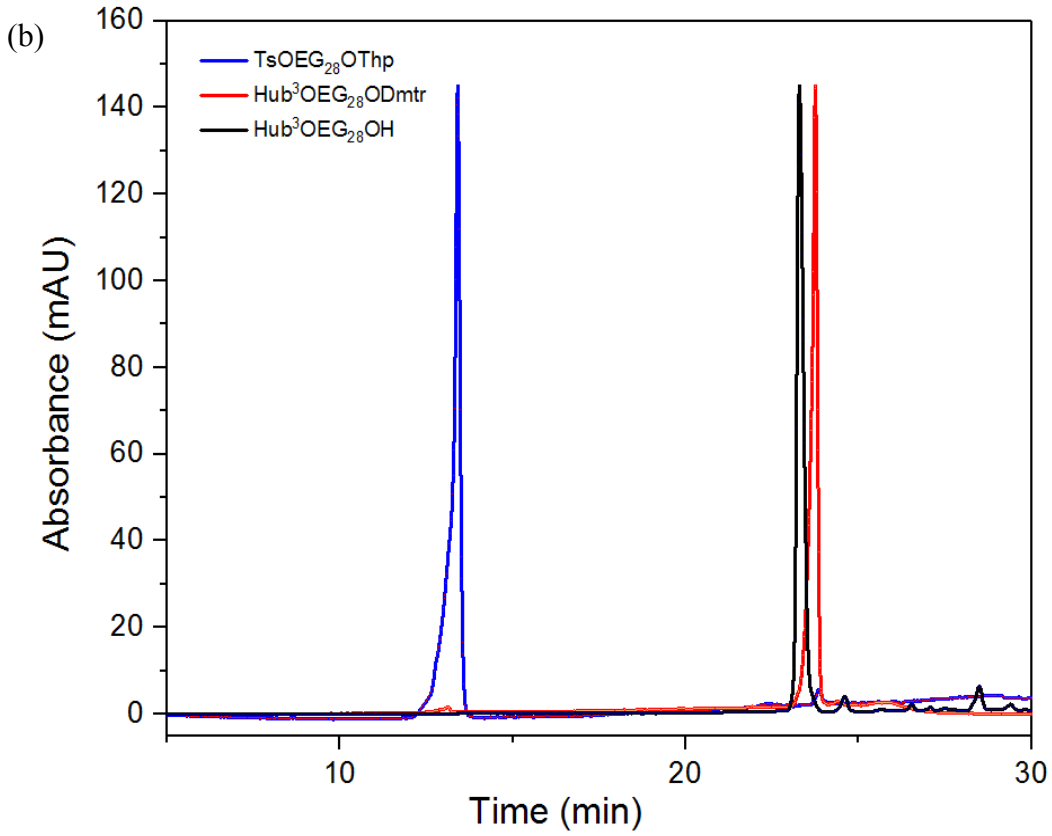


Figure 5.5 MS spectrum of building block ThpOEG$_{28}$OTs (a) and HPLC spectrums of building block ThpOEG$_{28}$OTs, Hub(OEG$_{28}$ODmtr)$_3$ and Hub(OEG$_{28}$OH)$_3$ (b).

During iterative synthesis, 10 equiv. (3.3 equiv. per arm) activated building blocks, ThpOEG$_{28}$OTs **6,** were used in each chain extension cycle. In fact, only 3 equiv. of building blocks was needed for the deprotected trivalent starting material via Williamson etherification. However, high concentration of the building blocks increased the chain extension rate and ensured reaction completion. The chain extension via Williamson etherification with NaH, DMF at 60 °C for 12 -24 h was used to yield the successive generation of the longer homostar. The extent of the reaction was monitored by HPLC, and the reaction was quenched when all the hub related peaks converted to the completed the three-arm product. Dimer ThpOEG$_{56}$OThp and derivatives from the excess building blocks are the major impurities that formed during esterification. After quenching, the product mixture would be diluted and loaded for diafiltration. For the next cycle of chain extension, the purified homostar needed to be deprotected with 50 mM MsOH in MeOH for 1 hr. The quality of each deprotected product was also examined by both HPLC and NMR before the next chain extension. Four cycles of

chain extension and purification were used to achieve Hub($OEg_{112}OH)_3$ **14**. The final monodisperse polymer could be functionalized and cleaved from the hub via BCl_3 treatment [298], [299] to release the linear, uniform, heterobifunctional PEG polymer (Figure 5.4, **ix**).

5.4.3. Membrane system selection

Based on the concept of the ItSyN approach, the membrane purification after each chain extension cycle is accomplished by washing reaction debris through with a suitable organic solvent while the product is retained. Therefore, after each coupling reaction, membrane separation was employed to purify crude products. The reaction mixture was dissolved into a desired solvent and loaded into a membrane diafiltration rig. The membrane purification process attains sufficient purity and can be potentially scaled up, compared to other purifications that are unfeasible for this synthesis e.g. chromatography and extraction.

Five types of PBI membrane with different combinations of different dope concentrations (18% and 19%) and surface modifiers (Jeffamine® M2005, M600, M1000 and RE-1 2007) were considered. As discussed in Chapter 4, clearly the dope concentrations would affect the membrane pore size; moreover the different surface modifiers with different chain lengths and hydrophobicity change the separation performance. Thus, a wide range of membranes with different physical properties were considered. The best selective membrane was chosen to separate the $TsOEG_{28}OThp$ **6** building blocks and homostar with a hydrophobic centre and three long hydrophilic arms. The product of the hub loading Hub($OEG_{28}OH)_3$ **8** was purified using column chromatography. The first generation of the homostar for membrane separation was Hub($OEG_{56}OThp)_3$ **9** with the excess building blocks **6** from reaction **vii**. Therefore the crude mixture from reaction **vii** was used for membrane screening; the ratio of all the solutes simulated the real separating environment. Rejection of the homostar should increase with the growing chains due to the increase in size. Two diafiltration solvents MeCN and MeOH were tested, which are commonly used in industry and give good solubilisation for all the compounds in Figure 5.4. All the membrane performances from different PBI membranes were recorded in Table 5.3.

Table 5.3 Membrane screening results using different PBI membranes with building block **6** and Hub product **9** in MeCN and MeOH.

Membrane	MeCN			MeOH		
	Permeance ($L\ m^{-2}\ h^{-1}\ bar^{-1}$)	Rejection (±0.02)		Permeance ($L\ m^{-2}\ h^{-1}\ bar^{-1}$)	Rejection (±0.02)	
		6	**9**		**6**	**9**
18% PBI-M600	29.6±0.4	0.63	0.65	-	-	-
18% PBI-M1000	27.0±0.1	0.57	0.74	-	-	-
18% PBI-M2005	25.7±0.3	0.58	0.75	**18.4±0.2**	**0.27**	**0.91**
19% PBI-M2005	8.6±0.3	0.85	0.95	4.4±0.2	0.44	0.95
19% PBI-RE1-2007	-	-	-	5.8±0.6	0.46	0.89

Based on the screening results, membrane performances were assessed by membrane selectivity to retain hub and remove building block; a relatively high permeance was also required, so that for the same diafiltration volume, there would be less diafiltration time for each cycle. In Table 5.3, 18% PBI-DBX-M2005 membrane performance in MeOH met the requirements for synthesis purification; $Hub(OEG_{56}OThp)_3$ rejection of 91% and building block rejection of 27% with a reasonably high solvent permeance. The 19% PBI-DBX-M2005 membrane in MeOH gave slightly higher rejection for both the building block and homostar, at 44% and 95% respectively, implying good membrane selectivity for the separating process; however, its permeance was four times lower than the 18% PBI-DBX-M2005, which made the process slow and inefficient. In MeCN, the 19% PBI-DBX-M2005 membrane offered the same homostar rejection; however the rejection of the building block was 85%, which was too high for the process to completely remove impurities in a reasonable diafiltration time. In general, membranes in MeCN gave lower homostar rejection and higher building block rejection compared to being in MeOH. All the other types of membranes tested did not provide good membrane selectivity and they were not viable for high performance diafiltration.

5.4.4. Membrane diafiltration and online monitoring

This ItSyN technology offers an efficient process to grow monodisperse PEG polymers to a pharmaceutically relevant size in realistic cycle times. The membrane demonstrates a promising separation to purify high molecular weight polymer products from relevant

impurities with a good yield, which is not feasible by column chromatography. In addition, the membrane showed a great potential to convert to large scale processes, which another challenge for current monodisperse PEG synthesis. For the diafiltration system, the pressure gradient between the two sides of the membrane creates a driving force to push impurities through the membrane with the solvent, with the hub product retained. The solvent acts as solute carrier and the solvent flow is unidirectional based on the pressure gradient to form a constant volume diafiltration. In order to replenish the solvent that has washed away, fresh solvent from the feed tank was fed simultaneously into the membrane rig at the same rate as permeate. The fresh solvent keeps flushing through the membrane until all the impurities are washed away. The diafiltration extent is described as the diafiltration volume, which is the ratio of the total wash volume to the rig volume.

The 18% PBI-DBX-M2005 membrane with MeOH was chosen for use in diafiltration. In order to improve separation performance with the original 91% homostar rejection, a two-stagemembrane process was applied. Compared to the single stage diafiltration, the two-stagediafiltration minimizes the product loss and maximizes the purity; therefore a higher yield could be achieved in a two-stage membrane rig. In addition, the solvent-consumption/productivity ratio is reduced. The piping and instrumentation diagram (P&ID) is shown in Figure 5.6 below. The permenace from the first membrane stage, which consists four membrane cells, is connected as a feed to the second membrane stage, which consists of two membrane cells for further purification and also secures product loss from the permeate.

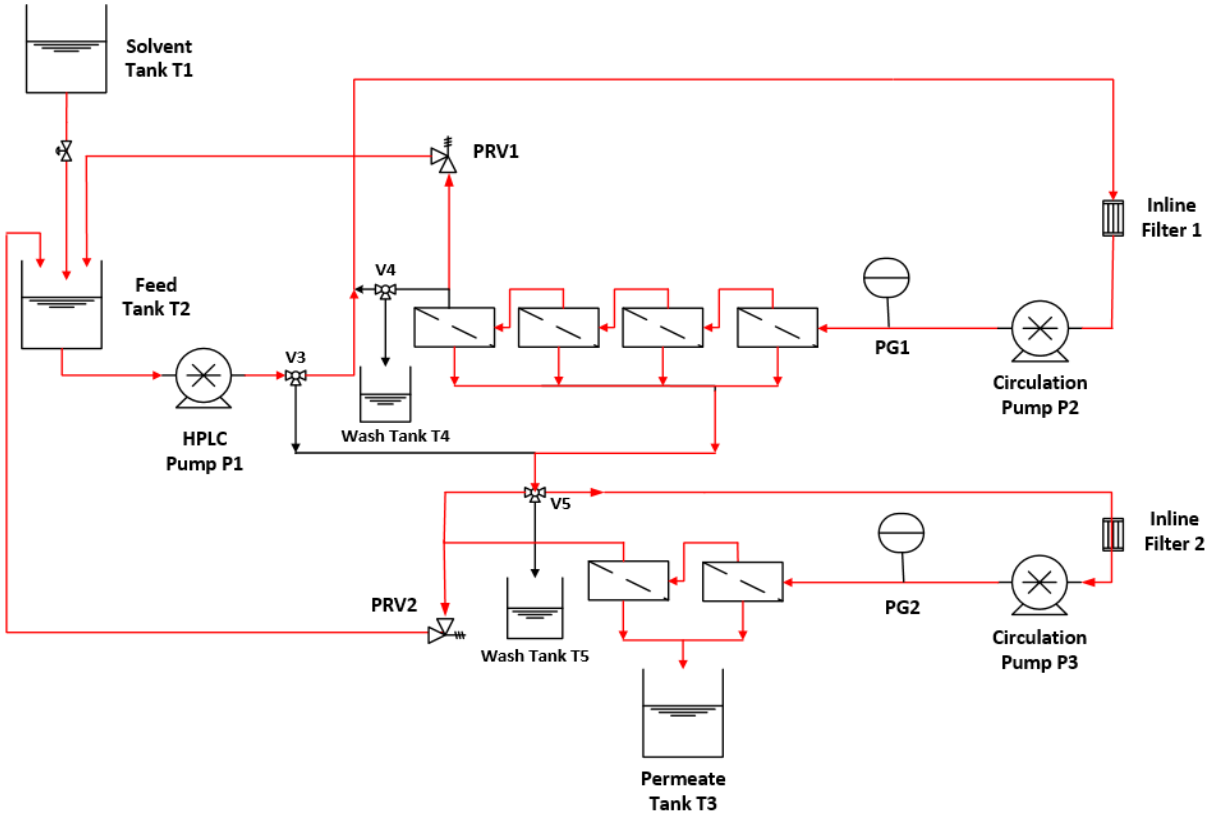


Figure 5.6 P&ID of the two-stage membrane diafiltration rig.

During diafiltration, Figure 5.7 shows that half of the building blocks were removed by the PBI membrane in three diafiltration volumes. However with the decrease of the building block concentration, it took much longer to remove the other half of the building blocks. In total, the purification was completed in 16 diafiltration volumes. The membrane rejection of the building block during diafiltration seemed slightly lower than the screening results, at 23%, presumably due to the constant driving force from the diafitration flow. The rejection of the hub stayed at 91%, as in the screening results. With the assistance of the two-stage rig, it can be seen that the majority of the homostar remained in the first stage and that there was little hub product being flushed out. 4L of diafiltration volume were washed through the system. The overall yield of each diafiltration cycle was about 90%. The product recovery showed significant advantages to the conventional chromatographic purification, especially with the growing size of the monodisperse PEG product. The membrane can retain more products with the increasing membrane rejection of larger Hub products, whereas the larger product becomes more adhesive for the chromatography column due to the increasing polarity. At the end of the diafiltration,

the retentate containing hub products was drained and thoroughly washed from the rig. The membrane permeate, containing building blocks and other impurities, was collected and purified using column chromatography for future chain extension.

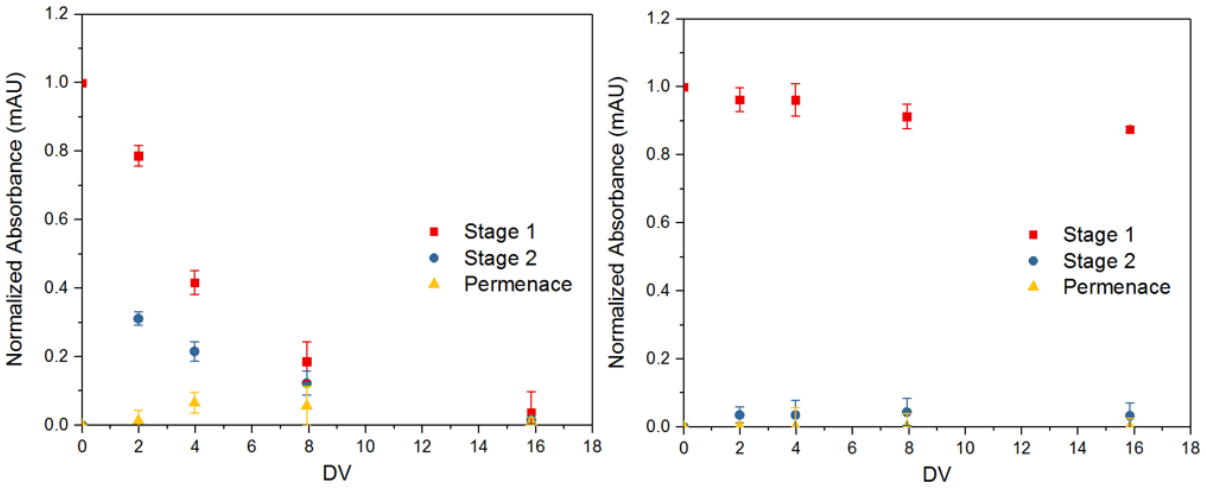


Figure 5.7 Concentration profiles of building block and Hub product in two-stage membrane diafiltration rig.

Feasibility of combining deprotection and diafiltration

Deprotection was carried out after each diafiltration using 50 mM MsOH in MeOH for 1 hr to restore the OH group in the chain terminus. The deprotection reaction was quenched with saturated aqueous $NaHCO_3$; all the Thp debris was removed by simple extraction.

In an attempt to streamline the ItSyN process, the deprotection step was trialled in the membrane rig. Operated in the membrane rig allows deprotection debris to be removed with the help of diafiltration. The deprotection was trialled during the end of the diafiltration; MsOH was added in both the first and second stages. The continuous removal of the deprotection debris from the diafiltration also shifted the deprotection equilibrium and assists the deprotection to completion. A small amount of building block and other impurities were also deprotected in the rig; the reduction of the impurities' size sped up their permeation from the membrane. The last deprotected permeate of building blocks was neglected and discarded. Deprotection in the rig eliminates the extraction step to remove the debris and also makes this process more versatile for other protecting groups, especially for the debris that cannot be removed from the aqueous phase by extraction.

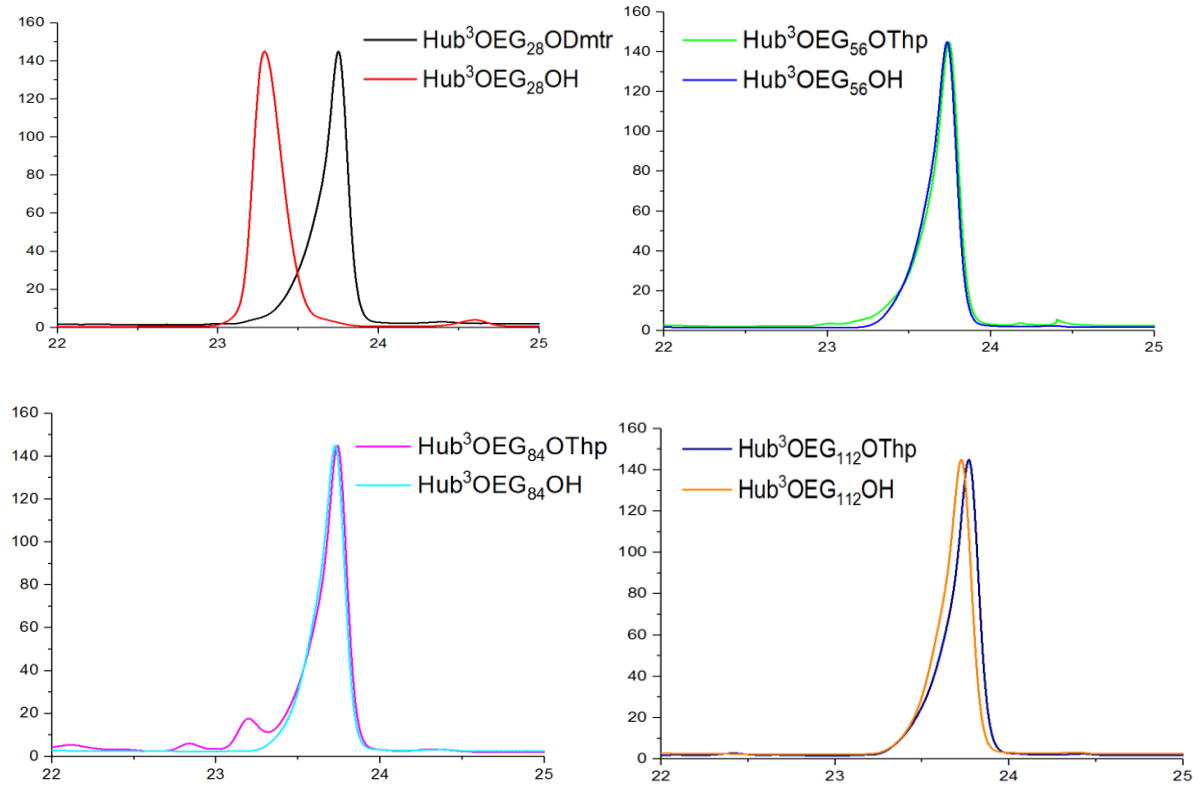
However, there are still some limitations to the deprotection in the membrane rig. The diafiltration solvent must have a fraction of MeOH, because it is indispensable for deprotection. Secondly, although the membrane can withstand a harsh acidic environment, the membrane performance was not consistent during this diafiltration protocol, probably as it was irritated by the change of pH. Due to the acid protonation, a small amount of base was added to neutralize and restore the membrane to initial performance. However the complex treatment of the membrane disturbs the natural properties of the membrane and makes the membrane performance inconstant during diafiltration. Last but not least, acid addition to a stainless steel rig and the acid contact with other equipment such as pumps causes enormous corrosion in the long term; which is not practical for a large scale industrial process. The blurred NMR spectrum and inconsistent yields of the deprotected products from the rig were observed, which presumably was due to chelation of the leached ions. Therefore it was decided to separate diafiltration and deprotection steps in the preliminary study. However it shows the possibility of having an integrated process of diafiltration and deprotection steps with other protecting groups and membrane rigs made of other materials, such as polytetrafluoroethylene (PTFE) or titanium.

5.4.5. Online monitoring and product analysis of chain extension

Four cycles of chain extensions and membrane diafiltration were carried out with HPLC online monitoring at each stage. The HPLC spectrums of protected and deprotected compounds at each cycle are shown in Figure 5.8. All the peaks look sharp and clean. The peak of homostar Hub($OEG_{84}OThp$)$_3$ had two small lumps on the left hand side of the main peak at the retention time of 23.7 min, but after the deprotection, homostar Hub($OEG_{84}OH$)$_3$ once again became a single sharp peak.

The MALDI-ToF was not applied for the online monitoring process due to the high requirement of the equipment and the difficult analysis of the high MW PEG polymers. The MALDI-ToF spectrum of all the intermediates and products were obtained after all syntheses. All the deprotected homostars were submitted as samples for MALDI-ToF spectrum, thus avoiding the analytical disturbance from any protecting group fragments. However the MALDI-ToF spectrums showed that the purities of all the intermediates were poor. The chain extensions were not completed from the first cycle.

The percentages of hub related products, in MALDI-ToF spectrum for Hub(OEG$_{56}$OH)$_3$ were 5% of 1-arm incompletion, 5% of 2-arm incompletion and 90% of 3-arm full completion products. In the MALDI-ToF spectrum of Hub(OEG$_{84}$OH)$_3$, the impurities from incomplete reactions accumulated were even higher, there was 15% of starting material, 5% of 1-arm incompletion, 20% of 2-arm incompletion and 60% of 3-arm full completion products. The molecular weight of Hub(OEG$_{112}$OH)$_3$ was not shown in MALDI-ToF spectrum; the polymeric ions may not be accelerated and therefore did not travel to the detector due to the heavy molecular weight.



x-axis represents time (Minutes); y-axis represents absorbance (mAU)

Figure 5.8 HPLC traces of purified intermediates and products after each chain extension and deprotection.

Overall the results revealed a major impurity of [M – EG$_{28}$] from each cycle, which accumulated with each chain extension. The lack of arms was caused by either the incomplete chain extension during Williamson etherification or previous incomplete deprotection prior to chain extension. NMR analysis showed successful deprotection during each step, as the

spectrum of the deprotected compounds did not show any trace of residual Thp acetal. However with the chain growth, the increasing peaks of accumulated impurities; [M – EG_{56}] and [M – EG_{84}] also confirmed the incompletion of the sequential chain extension. Insufficient washing of the membrane rig from the previous diafiltration could also contaminate the hub product with [M – EG_{28}]. Extra chain extensions may also have contributed impurity [M + EG_{28}] due to the undesired deprotection. The deprotection of the building blocks during storage or handling could result in uncontrolled chain extension. The hydrolysis of the TsO group of the building blocks can cause self-coupling between building blocks during chain extension. This dimer was another major reaction impurity. Due to the larger size of dimer, it takes much longer to remove the dimer from the hub product even when the concentration of the dimer is much less than the building blocks.

After diafiltration, inevitability, some building blocks or its dimer that is contained in the product will also be deprotected to become $HOEG_{28}OTs$ or $HOEG_{56}OH$. This is undesirable for this process, as the impurities will suffer double coupling during chain extension and grow larger. It leads to a variety of impurities that are more difficult to permeate from the membrane due to their size. It was almost impossible to remove impurities with the size larger than the dimer $HOEG_{56}OH$ without losing a significant amount of the hub product. Therefore, increasing the chain extension efficiency and controlling dimer formation would greatly improve the purity of the final PEG polymer product.

From the analysis, using the long commercial EG_{28} as the building blocks avoided the most abundant impurities in polymerisation, namely [M – EG_1] as well as [M + EG_1]. This type of impurity came from the original building blocks; however it was difficult to purify using chromatography, which could not prevent an increase in the number of impurities with each building block addition. For monodisperse PEG, depolymerisation by losing one or more EG units during reactions is reported. However they were not detected in the Maldi-ToF, and it is shown that the polyether bond is robust enough for all the reaction conditions that were used.

Due to the unsuccessful chain extension, BCl_3 treatment was not used for impure $Hub(OEG_{112}OH)_3$ cleavage. This was because the multiple by-products from uncompleted reactions would have disturbed the analysis of hub cleavage performance. Instead, in order to study the BCl_3 treatment, the reaction was done with pure $Hub(OEG_{28}OH)_3$. The cleavage was finished in three hours, and the crude product was flushed through a thin layer of silica, with a

yield of 73%. The obtained product was pure $HOEG_{28}OH$, and there was no sign of other smaller EG fragments. Therefore, the polyether bond was robust enough for BCl_3 treatment conditions that were used.

5.4.6. Chemical kinetic study of chain extension

In order to achieve a high purity PEG polymer in the iterative synthesis, approximate full completion of chain extension at each cycle is required. From the previous failed attempt, it was decided to study the kinetics of Williamson etherification to increase the reaction rate and understand the formation of the by-product. Two initial modifications were made before the chemical reaction study, in response to the results of the previous attempt.

Firstly, the online monitoring of the reaction did not work well, as there were no obvious peak shifts in the HPLC spectrum, see in Figure 5.8, with building block additions on each arm. This was because the polarity of the homostar product was dominated by a long hydrophilic PEG backbone and the hydrophobic central hub support. The addition of more building blocks did not significantly change the polarities of the homostar. Therefore the Thp protecting group was replaced by the Dmtr protecting group to ease online monitoring. With the strong UV signal and the hydrophobic property, Dmtr protecting group on each building block made the HPLC detection more sensitive and ensured each intermediate with chain extended arms had separated peaks. One disadvantage of using the Dmtr group is its bulky structure. In order to avoid the difficult membrane separation, deprotection was carried out before the diafiltration to reduce the size of the building blocks. In this case, the quality of online monitoring was critical for the process, as the quality control to check the reaction completion needed to be done before the deprotection and diafiltration.

The second improvement for the chain extension process was to replace the traditional HPLC system to an UPLC system for online monitoring. The two systems share the same concept of analysis, but the UPLC system was more than five times quicker than HPLC and it took only six minutes to obtain the full spectrum of the crude mixture and conduct the online monitoring simultaneously. Moreover, the UPLC was operated with a variable wavelength of between 200 to 500 nm. In the UV wavelength of 310nm, it was found that only the hub-related species would be visible, which made the chain extension analysis more straightforward without any disturbance.

During the first chain extension between Hub($OEG_{28}OH)_3$ and building block $HOEG_{28}ODmtr$, slow etherification reactions between homostar chain terminal alcohols and PEG EG_{28} toluene sulfonates (3.3 eq. each arm) were observed. From the analysis, 6 equivalent NaH was consumed or deactivated before the end of the reaction. The main by products were building block, which lost its tosylate leaving group $HOEG_{28}ODmtr$ and dimer $DmtrOEG_{56}ODmtr$. This may be because water existed or was generated in the reaction and consumed NaH. Water and NaH formed NaOH also destroyed the tosylate group of the building block. The low concentration of the building blocks slowed the reaction rate, or even worse, the resultant OH group from the building block would react with another building block to form the dimer $DmtrOEG_{56}ODmtr$. The fast consumption of the building block in the dimer formation may have left insufficient equivalent for three arms chain extension. The dimer was the unfavourable impurity for membrane removal, because the size of the dimer was twice that of the building block and the difficulty of diafiltration increased significantly.

This section reports work that aimed to increase the esterification rate and minimise the formation of the by-product, especially the dimer. The same chain extension was run between starting material Hub($OEG_{28}OH)_3$ and building block $TsOEG_{28}ODmtr$. Different parameters of reaction conditions to improve the reaction rate and prevent the water flow were varied. The reaction conditions and results are summarized in Table 5.4.

Table 5.4 Chemical kinetic study of chain extension of Hub($OEG_{28}OH)_3$ and building block $TsOEG_{28}O$Dmtr in different reaction conditions.

Entry	Reaction concentration (mol/L) (±0.01)	Drying method	Flask	Reaction T (±1)	Solvent	NaH Equiv. (±1)	Left BB (±0.5%)	Product Completion (±0.5%)		
								1arm	2arm	3arm
1	0.10 (Low)	molecular sieve (4Å)	joint neck	60°C	DMF	6	0.8%	0	0	100%
2	0.11 (Low)	MeCN/DMF azeotrope	Sealed neck	60°C	DMF	6	21.6%	26.2%	38.4%	35.4%
3	0.36	MeCN/DMF azeotrope	Sealed neck	60°C	DMF	10	2.3%	3.6%	23.8%	72.6%
4	0.35	MeCN/DMF azeotrope	Sealed neck	80°C	DMF	6	7.4%	1.2%	20.4%	78.4%
5	0.35	MeCN/DMF azeotrope	Sealed neck	60°C	THF	6	9.6%	2.4%	16.5%	81.1%

One possible source of water is insufficient MeCN azeotrope drying of the mixture of the starting material homostar and building blocks, due to the highly viscous, oily texture of the mixture. In reaction **entry 1**, a 4Å molecular sieve was used for drying the starting material and 10 equiv. building blocks in MeCN for 12 hours before doing azeotrope. A crystalline composition with small uniform pores in the molecular sieve could capture the H_2O molecule from the MeCN solution. Samples of this mixture solution were taken before and after the molecular sieve treatment using the HPLC system. The reaction went to completion within 24 hours, and there was little original building block left in the crude mixture. However the sample after molecular sieve treatment showed that some of the homostar seemed to be adsorbed onto the 4Å molecular sieve, because the HPLC spectrum showed that concentration of the homostar had approximately halved while the concentration of the building blocks remained the same. Therefore the actual equivalent ratio of building block to homostar was 20 instead of 10; the high concentration of the building blocks accelerated the completion of the chain extension. Although the reaction went to completion, using 20 equiv. building block for each chain extension was shown to be impractical and wasteful, as it was inefficient to remove the excess 17 equiv. building block with the membrane. More importantly, this molecular sieve treatment significantly decreased the yield of valuable homostar, which was not an improvement to the reaction.

In order to confirm the assumption about the homostar adsorption, the reaction was run in the same reaction concentrations without the molecular sieve treatment in **entry 2**. This time, the reaction only formed 35% of 3-arm homostar product in the same reaction time. In the azeotrope drying, a few millilitre of DMF was added in MeCN to ensure the homostar was well dissolved and remove any moisture inside the mixture. The two-piece, joint-neck round flask was also replaced by a sealed neck on the round flask, with the aim to of preventing any moisture from the atmosphere entering the reaction during sampling or from the refluxing DMF vapour. Due to the slow conversion rate in the low reaction concentration, **entry 3**, **4** and **5** all tripled the reaction concentration. The formation of the 3-arm homostar increased to 73%-81%, however it was still not fully completed. Increasing the amount of NaH kept the reaction activated, however it also increase the rate of by-product formation; in the end of the reaction, there was little building block left to finish the chain extension. In **entry 5**, the reaction solvent DMF was replace by THF. It was suspected that the homostar product might have a better solubility to open the homostar arms more widely to expose the reactive site of the PEG chain.

These conditions did improve the reaction rate of the coupling, however the moisture resources were not verified and the chain extension did not complete with 10 equiv. of building blocks.

From **entry 6** to **10**, the shorter building block $TsOEG_{12}ODmtr$ was prepared and used for the chain extension study, based on the unsatisfactory results from the long flexible building blocks. The shorter building blocks gave the advantages of a simpler structure and also made it harder to entangle and embrace the reactive sites. The short building blocks offered a fast reaction rate with less steric hindrance, while the chain length grew with more steps to achieve the same size as the homostar. In addition, the resulting shorter reaction time limits the side reactions of building blocks such as electrophile elimination and hydroxy-terminal depolymerisation. Therefore, a shorter building block with more chain extension cycles may ultimately become the only choice for preparing the PEG polymer with a molecular weight of over 5000 Da. In Table 5.5, the reaction conditions and chain extension results of using EG_{12} building block are summarized.

In **entry 6**, the same original reaction conditions were used, with the shorter $TsOEG_{12}ODmtr$ building block. The reaction was roughly 98% completed within 12 hours and a minimal amount of the 2-arm was not converted into the product. However there was little building block left; the moisture consumption of the building block was much faster than the chain extension rate. The sealed flask was also investigated, as it has a large contact area for the reaction mixture during the reaction and it is one of the most likely ingress sources of moisture. The flask underwent flame drying at 150°C to remove any water molecules in **entry 7**. Interestingly, the reaction rate decreased and only 91% of 3-arm homostar was formed within 12 hours. It seemed that flaming increased the reactivity of the surface of the flask. The NaH reacts directly with the surface silanol (Si-OH) units and the rate of reaction of sodium hydride with the glass competed with that of the chain extension. In **entry 8** and **9**, more equivalent of base NaH and higher temperatures were tested, and the results were almost same as in the original conditions. The key problem was always the disappearance of the building blocks and a slowdown in the coupling reaction rate.

Table 5.5 Chemical kinetic study of chain extension of $Hub(OEG_{28}OH)_3$ and building block $TsOEG_{12}ODmtr$ in different reaction conditions.

Entry	Reaction concentration (mol/L) (±0.01)	Drying method	Flask	Reaction T (±1)	Solvent	NaH Equiv. (±1)	Left BB (±0.5%)	Reaction Completion (±0.5%)		
								1arm	2arm	3arm
6	0.39	MeCN/DMF azeotrope	Sealed neck	60°C	DMF	6	0.3%	0	1.7%	98.3%
7	0.36	MeCN/DMF azeotrope	Sealed neck Flame dry	60°C	DMF	6	2.7%	0	9%	91%
8	0.35	MeCN/DMF azeotrope	Sealed neck	60°C	DMF	12	0	0	1%	99%
9	0.38	MeCN/DMF azeotrope	Sealed neck	80°C	DMF	6	2.3%	0	1.4%	98.6%
10*	0.35	Confidential methodology					9.6%	0	0.4%	99.6%

In **entry 10**, a study was carried out to passivate the surface of the reaction flask. In this case, there seemed to be very little water related dimerisation of the tosylate electrophile were formed and 9.6% of the building blocks were left compared to the previous entries. NaH would react with the only alkoxide available in the reaction which is the homostar in the solution. As such, the building block tosylate would be consumed for the chain extension instead of other side reactions. Since the results are not published yet, the details for the reaction improvement are not disclosed in this thesis. 99.6% of the 3-arm was prepared in 12 hours, which is high enough for the iterative synthesis. The reaction progression is shown in Figure 5.9. This method confirmed the feasibility of using $TsOEG_{12}ODmtr$ to synthesize good purity PEG polymer. In addition, less building block was converted into other impurities, which eased the membrane purification.

Moreover, a new chain extension of $Hub(OEG_{28}OH)_3$ and $TsOEG_{28}ODmtr$ was carried out under the same conditions as **entry 10**. As expected, the reaction was slower than using the shorter building blocks. The reaction was 95% completion within 24 hours and with plenty of BB remaining and eached completion in 36 hours. The improvement seems due to preventing the water moisture into the reaction mixture; but the flexible long PEG chain of the building block reduced the reactivity of the chain extension. For subsequent chain extensions, the coupling would become more difficult. Therefore the long PEG building block $TsOEG_{28}ODmtr$ was abandoned to synthesize the target polymer of over 5000 Da.

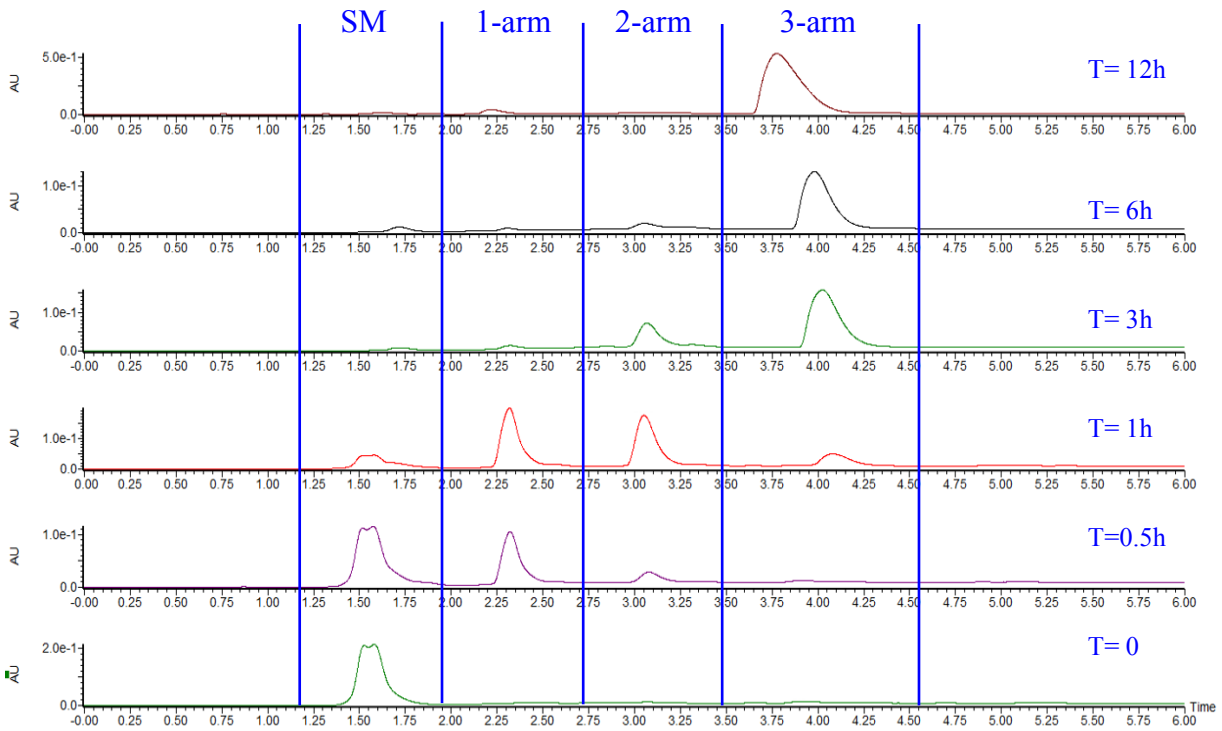


Figure 5.9 The UPLC reaction progression of **entry 10** using $Hub(OEG_{28}OH)_3$ and building block $TsOEG_{12}ODmtr$.

Further work could be undertaken to minimise other impurities created in the reaction. Based on previous studies, the combination of sodium hydride in DMF can lead to the formation of an amine side product [300]. With regard to the esterification with PEG building blocks, the possible side reactions are shown below. The combination of NaH and DMF could act as a masked equivalent of water. So for this side reaction, it is suggested that these problems can be avoided by changing the solvent from DMF to THF. Therefore, the impurities related to building block need to be identified in the NMR and MS and research is needed to discover some likely reasons for the impurity formation. Some possibilities are as follows:

$Me_2NCH{=}O + NaH \rightarrow Me_2NCH_2O^-Na^+$

$Me_2NCH_2O^-Na^+ + TsOEG_{12}ODmtr \rightarrow Me_2NCH_2OEG_{12}ODmtr + TsO^-Na^+$

$Me_2NCH_2OEG_{12}ODmtr \leftrightarrow Me_2N^+{=}CH_2 + {}^-OEG_{12}ODmtr$

$Me_2N^+{=}CH_2 + {}^-OEG_{12}ODmtr + NaH \rightarrow Me_3N + Na^+{}^-OEG_{12}ODmtr$

On changing the solvent to THF, the change of the trace of dimer and other impurities related to building block should be monitored to see the improvements. If THF prevents building block derivations, it would help the couplings force to completion over a long reaction time. Building block would be efficiently recovered, and incomplete 2-arm intermediate would no longer be obscured by a dimer.

Although Dmtr is a relatively bulky protecting group, it would be ideal to discover a membrane which can permeate the Dmtr group, so that the diafiltration and online monitoring can be conducted before the final deprotection. In this procedure, the Dmtr would offer a good detection of both homostar and building block during diafiltration. It is also a good idea to assure a good purity of the product after diafiltration, as more chain extension and diafiltration could be carried out before deprotection to make up for any imperfection. However, the deprotected Dmtr debris cannot presently be removed by extraction, so other purifications need to be investigated in future work, such as those for deprotection debris Dmtr-Pyrrole ion exchange and precipitation.

5.5. Chapter conclusions

In this chapter, the aim was to synthesize high purity uniform PEGs with a molecular weight greater than 5000 Da, which is widely used in drug delivery applications. The commercially available building block $HOEG_{28}OH$ was modified as $ThpOEG_{28}OTs$ and used for chain extension on a three-arm hub support iteratively, using efficient liquid phase membrane purification. The long monodisperse PEG building block was used to shorten the chain extension cycles. Traditional chromatography-based approaches face major challenges to be able to have a clear resolution between products and impurities, due to the strong domination of PEG hydrophilic chains; however, iterative synthesis with membrane-based separation can be driven to greater oligomer lengths and is readily scalable to manufacturing operations, both of which are key advantages.

The membrane separation system was established and the 18 wt% PBI-DBX-M2005 membrane was used in the diafiltration with MeOH. It gave excellent permenace of 18.4 $L\ m^{-2}\ h^{-1}\ bar^{-1}$ and good selectivity with a rejections hub of 91% and a building block of 27%. The quality control from the MS spectra indicated that although the building blocks were removed

after 16 DV from the diafiltration, the bulky dimer ThpOEG$_{56}$OThp was extremely difficult to remove from the membrane system. The misinterpretation of the online HPLC monitoring during coupling, and the accumulation of the impurity dimer, revealed the existence of inaccurate or incomplete polymer sequences.

Therefore, two types of building block DmtrOEG$_{28}$OTs and DmtrOEG$_{12}$OTs were experimented to study the kinetics of Williamson etherification, in order to increase the reaction rate and understand the formation of the dimers. As was expected, increasing reaction concentrations, temperatures and base equivalent, increased the coupling efficiency. But the reaction did not reach completion, and the formation of the dimer impurity also increased. Other parameters could also influence the reaction rate such as reaction solvents, drying methods and the reaction kit, so these were also investigated. It was found that a new approach, using the surface passivated flask and the shorter building block TsOEG$_{12}$ODmtr, improved the reaction completion to 99.6% of the 3-arm in 12 hours. The formation of the dimer was reduced to a minor amount. Further work is necessary to be able to continue the chain extension to the targeted molecular weight. This study confirmed the feasibility of using a long monodisperse building block to synthesize good purity PEG polymer. The excellent coupling efficiency eased the membrane purification and the process represents the first purification technique realistically capable of accomplishing extensions of monodisperse PEG polymer to pharmaceutically relevant lengths.

6. ItSyN for sequence-defined branched PEGs

6.1. Abstract

The precise synthesis of sequenced defined polymers with specific functions has been studied intensively by synthetic chemists. However, precision control technologies involving synthesis and separation over monomer sequence are not efficient, and still face challenges for a large-scale processes. In this chapter, a universal strategy for fabricating sequence-defined synthetic polymers with different side chains is investigated. This ItSyN technology combines iterative building block couplings and selective membrane separation in a fully liquid environment. The liquid phase iterative synthesis offers the advantages of optimising reaction kinetics, online monitoring and scaling up.

In order to test this concept, a general and versatile approach of preparing various building blocks with different side-arm functionalities for iterative synthesis was studied. The choice of protecting groups and leaving groups were studied in building blocks based on the coupling and purification efficiency. The tetrahydropyran-1-yl (Thp) acetal group was selected for temporary protection of the building block termini and the toluenesulfonyl (TsO) group was chosen as the leaving group of the final building blocks. Two *α, ω*-functionalised terminal PEG building blocks with different locations of the octyl chain were prepared. In addition, a chiral centre was incorporated with the side chain using Sharpless dihydroxylation and crystallisation. The optically pure building blocks with functionalised side chain were prepared with the purity of 99% and on multi-gram scales. Polymers were assembled on a soluble three-armed star-shaped support to triple the production and maximise efficiency during membrane purification. This strategy allowed the construction of two sequence-defined PEG polymers at high yield and purity, with different side-arm order. Mass spectra and NMR were used to prove the numbers of monomers with different side-arms, and their precisely defined locations. The two obtained sequence-defined PEG polymers were characterised for the diversity of the polymer structures and functionalities.

This building block synthesis approach with the ItSyN strategy offer opportunities to introduce structural versatility and physicochemical diversity into sequence-defined synthetic polymers. The functional side chains also give opportunity for manifold site-selective modifications for healthcare and biotechnology synthesized polymer application.

6.2. Introduction

Nature produces macromolecules including oligonucleotides (oligos), peptides, and oligosaccharides, which are sequence controlled and monodisperse polymers [301]. Sequence-defined polymers have exactly uniform chain length, and monomers with different chemical natures are organised in a specific order along the backbone. These biopolymers show a wide range of applications for living organisms in healthcare and nanotechnology, due to their unique structural and functional complexity and variability [302]. Moreover, controlling monomer sequence not only affects polymers' primary structures, but also plays a critical role in polymer folding, self-assembly, molecular recognition and a number of polymer physical properties. The present technologies for industrial fabrication of synthetic macromolecules do not in general permit good control of the polymer sequence. In the last few decades, synthetic polymer chemistry towards making non-natural sequence-controlled polymers for pharmaceutical use, such as poly (ethylene glycols) (PEGs), poly (ethylene imines) and poly (L-Lysine) has been widely studied.

Some synthetic approaches to controlling monomer sequences such as chain-growth and step-growth polymerizations [176, 303], specific kinetics control [125] and particular template conditions [88, 304], and monomer addition [305], result in regulating polymer sequence and narrowing down polydispersity. However, these sequence controlled methods are not as precise as natural polymers. In order to mimic the natural synthetic approach of a precise, sequence-defined polymer, iterative synthesis was applied here, which is sequentially adding one specific building block at a time to one end of the growing chain for manipulating the polymer architectures. Purification to remove excess monomers from the chain extended polymer at each stage before the next polymer chain extension has to be undertaken [1, 265]. Traditionally, solid phase iterative synthesis [153] is widely used for a sequence-defined polymer chain growth on an insoluble support. It is a well-developed industrial process for some biopolymers such as peptides [306, 307], due to its ease of filtration separation, the quick reaction and automation potential [155]. However product purity and yield from solid phase synthesis is limited, because the quality of the intermediates during synthesis cannot be readily monitored due to the insoluble supports [265]. The bulky solid support restricts the accessibility of the reaction sites and limits the diffusion rate to the solid support, which decreases the coupling efficiency and accuracy of the polymer sequence [308]. In addition, the high cost of the solid

supports and the handling of the solid production make solid phase synthesis impracticable for large scale industrial applications [176, 265].

Therefore, an alternative to resolve these challenges, using a soluble support for liquid-phase iterative synthesis has been investigated. The fully liquid environment overcomes the problems of reaction kinetics and online monitoring of each intermediate, for more precise sequence coupling. In recent years, a wide range of liquid-phase methodologies have been reported for sequence-defined polymers. They aimed to discover different backbone chemistries, control of polymer sequence and the side-chain functionality/ modification. The soluble supports are also studied; the choice of which depends on their robustness during coupling conditions, solubility in solvents and the sensitivity to support cleavage. A few publications on synthesizing sequence-defined polymers at rapid coupling rates, including polyamides [177], polyesters [181] [139], thiol-ene click[265], azide-alkyne click[160], and homologation of boronic esters [309] have been reported. Common liquid phase iterative synthesis is challenging in the purification process after each cycle. The conventional approach of chromatography is often time consuming and solvent intensive. Alternatively, precipitation has been widely explored in liquid phase oligo synthesis [310], but multiple cycles of inefficient separation in iterative synthesis does not offer an attractive yield and a versatile process, which limited the potential to scale up.

In this study, sequence-defined synthetic PEG polymers with different structures and functionalities were chosen due to their wide pharmaceutical applications [286]. The study of the complex architecture, construction and chemistry built upon previous discoveries around the synthesis of monodisperse PEGs, as reported in Chapter 5. Two different synthesized sequence-defined pentagol PEG polymers contained the same numbers of monomer, but the sequence order of monomers are different. The influences of the monomer sequence on physical and structural characteristics of two sequence-defined polymers were investigated. Furthermore, this strategy offers opportunities to introduce structural versatility and physicochemical diversity into sequence-defined synthetic polyethers, by incorporating different reactive functional groups on the side-arms; also further site-selective multifunctionalisation could be studied after polymerisation [266]. Therefore the technology has the potential to unlock the utility of sequence-defined polymers for widespread applications ranging from healthcare and nanotechnology to information storage.

6.3. Methodology

6.3.1. Materials

All building blocks with side chains were assembled from either monodisperse linear PEG monomer ethylene glycol or tetragol from Sigma Aldrich, UK. Ethylene glycol is available in high purity (ca. 99.9% EG_2, with <0.003% water) and tetragol has a purity of (ca. 99.2% EG_4, with 0.5% EG_3 and 0.2% EG_5) and they were used without further purification.

6.3.2. General experimental procedures

The general experimental procedures were the same as in Chapter 5.

6.3.3. Chain extension and deprotection

The chain extension and deprotection procedures were the same as in Chapter 5.

6.3.4. Diafiltration procedure

The diafiltration procedure was the same as in Chapter 5.

6.3.5. Analytical techniques

6.3.5.1. Building block synthesis, chain extension and deprotection

NMR, MS and TLC

Several Analytical techniques, such as NMR, MS and TLC, were operated using the same procedures as described in Chapter 5.

High-performance liquid chromatography (HPLC)

The HPLC analysis was performed using the same HPLC system and operating conditions as in Chapter 5. For PEG building block synthesis, HPLC column was a reverse-phase C4-300 column (250 mm × 4.6 mm, ACE Hichrom). The mobile phases for HPLC were deionized water buffered with 5 mM ammonium acetate (solvent A) and methanol (solvent B). The samples were eluted with the method shown in Table 6.1.

Table 6.1 Solvent gradients of PEG building block HPLC method.

Time (min)	MeOH (%)	Water (%)	Flowrate (mL/min)
0.00	70	30	1.00
2.00	70	30	1.00
12.50	95	5	1.00
30.00	95	5	1.00
32.00	70	30	1.00
35.00	70	30	1.00

For the chain extension of sequence-defined PEG polymer, the HPLC column was a reverse-phase C4-300 column (250 mm × 4.6 mm, ACE Hichrom). The mobile organic phase was MeOH; the eluting gradient of the mobile phase is shown in Chapter 5.

Chiral gas chromatography (GC)

GC chromatographs were recorded on a Shimadzu 2010plus gas chromatograph fitted with an autosampler and a flame ionization detector (FID). All samples were separated on a Supelco Beta Dex 120 capillary column. The GC analysis was carried out in the following conditions: injection 1 μL split ratio of 100:1; injection port temperature 250 °C; column isothermal at 140 °C for 80 min, ramped at 10 °C min^{-1} to 170 °C holding for 8 min, FID at 210 °C, carrier gas of helium 20 cm s^{-1}.

The enantiomeric purity was evaluated by calculating enantiomeric excess (ee, %) value, comparing peak areas of each enantiomer according to corresponding concentrations, where *S* is the fraction of S isomer and *R* is the fraction of R isomer. When it was applied to gas chromatography, the peak area of each isomer was used. The enantiomeric excess was determined by Equation 5 below.

$$\boldsymbol{ee}\ (\%) = \left(\frac{\boldsymbol{R-S}}{\boldsymbol{R+S}}\right) \times \mathbf{100}\% \qquad \textbf{Equation 5}$$

6.3.5.2. Membrane screening and diafiltration

The membrane cross-flow screening was carried out using the same method as in Chapter 5. The membranes were screened with the initial crude chain extension. The product concentration was between 0.8 g L^{-1} and 2 g L^{-1}. The membrane diafiltration was operated in the same two-stage rig reported in Chapter 5, the chosen membrane and diafiltration solvent were re-loaded. The diafiltration was also operated in the same conditions as in Chapter 5.

6.3.5.3. Polymer properties characterisation

Differential scanning calorimeters (DSC)

The glass transition temperatures of synthetic polymers are tested on the DSC Q2000 V24 from TA Instruments. The analysis was carried out in the presence of Nitrogen and Helium at the flowrate of 50 ml min^{-1}. Five temperature ramps were operated between -160 °C and +50 °C at the rate of 40.00 °C min^{-1}.

Ultraviolet–visible spectroscopy (UV-Vis)

The UV-Vis absorption spectra of the samples were recorded on a Thermo Electron-EV300 UV-Vis spectrophotometer at room temperature. The slit width was set as 1 nm, and the scan speed was set at 480 nm min^{-1}. The wavelength of the spectra ranged from 200 nm to 700 nm.

6.4. Results and discussion

This section is organised in two parts, first reporting work conducted to synthesis appropriate building blocks for Ocytl branched PEG synthesis (Section 6.4.1), before reporting the synthesis itself (Section 6.4.2).

6.4.1. Octyl branched PEG building block synthesis

6.4.1.1. Design of the building blocks

In order to synthesize sequence controlled heteromultifunctional PEG polymers, the iterative strategy was proposed, to increase the yield and purity through etherification. It requires fewer building blocks at each cycle compared to a chain-doubling or -tripling strategy. It also reduces the chance for excessive impurity accumulating by statistical chain growth. Shorter EG building blocks are normally used for chain extension, because they give the advantage of a simple structure and are not entangled to embrace the reactive sites. Thus, the short building blocks offer a fast reaction rate with less steric hindrance, while the chain length grows [200]. In addition, the resulting shorter reaction times, from shorter building blocks reduces the chance for the side reaction of building blocks, such as electrophile elimination and hydroxy-terminal depolymerisation.

In this building block synthesis, the functional side chain was inserted into the PEG building block by connecting one single unit of ethylene glycol (1, 2-diol) with a designed side chain and monodisperse linear ethylene glycol oligomers (EG_2 or EG_4). The length of build blocks could be adjusted by the length of the linear ethylene glycol oligomers. The position of the side-arms could be shifted along the PEG building blocks depending on the length of ethylene glycol oligomers that connected on the each side of 1, 2-diol. Moreover, a chiral centre was formed with the insertion of the side chain. Chirality of both enantiomers could be obtained by Sharpless asymmetric dihydroxylation with the 1, 2 diol double bond. This chiral design provided another distinguishable property to study that could potentially influence the polymer physical structure.

This approach facilitated sequence-defined PEG polymers with side-arms on a continuous PEG backbone to be constructed. It also widened the variety of PEG building blocks available for

synthesis, which allows structural and functional diversity for sequence-defined PEG polymers. After polymerisation, the functional side chain could undergo site-selective modification for potential applications in nanotechnology, healthcare and information storage.

6.4.1.2. Choice of protecting groups for building block synthesis

This section explains the rationale for the protecting groups chosen for use in building block synthesis.The protecting groups (PG) play important roles in iterative synthesis. During chain extension, the building blocks are added in excess to increase the reaction rate and ensure reaction completion. One end of the building blocks is protected by a temporary protecting group, so that the growing polymer extends in a controlled order. After the completion of chain extension and purification of each cycle, the protecting groups needed to be removed to restore OH groups at the chain terminals for the next chain extension. Therefore, protecting groups prevent undesirable chain growth and ensure the precision of polymer sequence and chain length. Loss of the protecting groups normally leads to doubled coupling and decreases the sequence precision and polymer monodispersity.

There are a few criteria for the choice of protecting groups that must be addressed for iterative synthesis. (1) All chosen protecting groups need to be robust enough for Williamson etherification, building block synthesis conditions and separation processes, (2) The temporary protecting group must also be orthogonal to the polymer product, as they must be sensitive enough to be cleaved during deprotection without damaging polymer product/building block. (3) For iterative synthesis, a bulky three-arm hub star was applied as a soluble support; polyether chains are unidirectional, growing with one end attached on support via benzylic ether linkages. Therefore, the protecting group of the building block has to be chemically stable during hub cleavage to obtain the final polymer. There were a wide range of acid-labile temporary protecting groups available to satisfy these requirements and they have been reported in previous studies [31]. The protecting groups chosen for this work are presented below with the theoretical considerations that were taken into account in their choice.

4, 4'-dimethoxytriphenylmethyl (Dmtr)

In a previous study of PEG iterative synthesis, a few acid-labile protecting groups such as triphenylmethyl (Tr) and 2-tetrahydropyranyl (Thp) were proposed, in the presence of benzyl

ethers [31]. The 4, 4'-dimethoxytriphenylmethyl (Dmtr) group was another possible option for a temporary protecting group. It is twice as acid-labile as the Tr-ether protecting group, which means that deprotection is much more straightforward while avoiding any hub cleavage [311]. The Dmtr protecting group also has a strong UV signal on TLC to detect the related products; it is also sensitive to TFA vapour stain giving it a more acute and unique detection. Using such an acid sensitive protecting group, synthesis handling and storage need to have extra attention to avoid undesirable loss of the protecting group during building block synthesis and chain extension. A small amount of mild base, such as Et_3N, was added to all the storage and analytical products to prevent any deprotection. The Dmtr group also increased the size of the products due to its bulky structure; this posed difficulties during the membrane separation process using size exclusion to remove excess building blocks that were protected by the Dmtr group. The high molecular weight of dimethoxytrityl group increased the mass/molar ratio of the related products. To achieve the same amount of final product, the Dmtr intermediates/products, which have a heavy mass load, made their synthesis and purification procedures more difficult.

Tert-butyldimethylsilyl (TBDMS)

The T*ert*-butyldimethylsilyl (TBDMS) protecting group is hydrolytically stable and is used for different applications. Effective protection on various alcohols has been reported using mild reaction conditions and *tert*-butyldimethylsilyl chloride (TBDMS-Cl) as a silylation agent [312]. The TBDMS protecting group is very robust and has a good size for membrane application, with a fast chemoselective cleavage in high yield which is compatible with other function groups, has been studied [313].

2-naphthylmethyl (Npm)

The 2-naphthylmethyl (Npm) and benzyl (Bn) protecting groups were proposed to be used for PEG building block assembly, because 2-naphthylmethyl (Npm) and benzyl (Bn) offers relatively good stability during etherification and the strong UV signal from aromatic rings gives it a good TLC detection during the reaction. The Benzyl group (Bn) is stable towards both acids and bases and is a general protecting group. It is a good candidate as a temporary protecting group; however it was not chosen for use as the final protecting group because its linkage is benzylic ether, which is the same as the support hub linkage. Deprotection of both Npm and Bn is normally performed as palladium-catalysed hydrogenolysis. The Bn group is slightly easier to cleave off than Npm during hydrogenolysis. However, 2-naphthylmethyl

(Npm) can be cleaved by a selective unblocking procedure in the presence of simple benzyl ethers [314]. Another advantage of using the Npm group is that the protection group debris after deprotection is inert for the following reactions and it could be purified using a thin layer of charcoal.

Thp acetal (Thp)

The final selected protecting group of the PEG building block was Thp acetal for temporary protection of the chain termini. The Thp group was reported as being a useful protecting group for alcohols and phenols in organic synthesis[173]. It has several advantages: low cost of dihydropyran (DHP), ease of introduction and good solubility. The Thp group also offers good chemical stability during etherification and purification. The size of the Thp acetal is relatively small, which aids membrane purification when removing excess protected building blocks.

6.4.1.3. Choice of side chain and chirality for building block synthesis

This section explains the rationale for the side chains selected for synthesis, in terms of their utility in validating the iterative synthesis with nanofiltration (ItSyN) technique. A Thp-protected building block with a chiral (+) (R) octyl side chain was designed to prove the concept of PEG sequence control iterative synthesis. The octyl chain is not reactive and it's compatible with chain extension, deprotection and purifications. The inactive octyl chain helped establish the ItSyN methodology without any side effects from the side chain. Although the octyl side chain cannot be site modified, it offers a hydrophobic property to the building block, which gives the sequence controlled polymer specific physical functionality. In the pharmaceutical industry, enantiomerically pure molecules are always highly desirable for drug candidates. In this project, constructing an enantiomeric building bock from achiral starting materials was investigated. French et.al reported that highly pure linear PEGs gave X-ray crystal structures like the closely-packed 3_{10}-helix dominated by a gauche arrangement of individual EG units and every EG_5 per turn [31]. Therefore pantagol with a chiral side chain was chosen for the building block. The polymerisation of chiral (+) (R) PEG building blocks enhanced the chirality of the synthetic polymer. If the structure is similar to that of French et al. the side chains on the helical PEG backbones would point in the same direction due to the multiple chiral centres, forming a brush structure with the pendant long octyl chains. As such, the chiral

side chains may also have an effect on the intermolecular packing of the PEG backbone, which could give novel polymer structures.

By attempting this versatile strategy with the stable (+) (R) octyl side chain, the ultimate idea is to control the polymer properties by tuning the position and the amount of octyl side chains along the sequence-defined PEG polymer. Potentially the choice of side chain and chirality could be broadened, so different functionalities and complexities of the sequence-defined polymer could be introduced and studied.

6.4.1.4. First building block synthesis approach

To simplify the incorporation of octyl chains, the first attempted PEG pentagols were assembled from ethylene glycols with a chiral octyl chain and desymmetrised tetragols. This approach reduced the overall synthetic steps, as it only required one esterification to form pentagols, which is the step that has the biggest influence on the yield of the building block.

The (*R*)-2-Octyl-α-tetrahydropyranyl-ω-toluenesulfonate pentagol **25** was synthesized in 8 steps starting from 1-decene **16** and highly pure tetragol **19.** The schematic synthesis of 2-Octyl PEG pentagol is shown in Figure 6.1. The synthesis was begun by making the chiral octyl chain using Sharpless' catalytic asymmetric dihydroxylation. A mixture of reagents that acts as an asymmetric catalyst was added, including K_2CO_3, the chiral ligand $(DHQD)_2PHAL$, a catalytic amount of osmium tetroxide and a stoichiometric amount of potassium ferricyanide, which lowers the amount of toxic and expensive osmium tetroxide that is necessary. The optical purity of Sharpless' catalytic asymmetric dihydroxylation was approximately 100% ee and the reaction yield was about 93%. The 4, 4'-Dimethoxytriphenyl chloride (DmtrCl) was then reacted with (*R*)-1, 2-decanediol **17**, to selectively give (*R*)-1-Dmtr-ethers **18.** By the slow addition of DmtrCl, the primary hydroxyl group of 1, 2 diol can be selectively protected over secondary alcohols. The secondary alcohol was left for later tetragol attachment. The protection reaction was almost instant with mild conditions and 72% yield.

The insertion of the octyl chain into the PEG backbone was achieved by reacting the hydroxyl group of **18** with desymmetrised tetragols **20** via the etherification reaction. 2-naphthylmethyl (Npm) was chosen to protect one hydroxyl group of tetragol selectively to form desymmetrised

tetragols **19a**; the tetragol was provided in a large excess amount. The 2-naphthylmethyl (Npm) group is orthogonal to etherification and the following manipulations of protecting groups, such as Dmtr deprotection and Thp protection. On the other end of the protected tetragol, the hydroxyl group was a very poor leaving group in S_N2 reactions; therefore it was converted into the methanesulfonyl (MsO) leaving group. The mesylates tetragol gave a higher reaction yield of 85% in coupling reaction **(iv)** compared to the yield of 70% with the toluenesulfonyl (TsO) leaving group. The conversion of the OH group to mesylate is shown in reaction **(iiib)**; with the addition of mesyl chloride, the lone pair of the alcohol oxygen attacked the sulfur of the chloride, and better leaving groups were formed with the release of HCl. The mesylation can be purified with simple extraction instead of time-consuming column chromatography, due to the good water solubility of the excess mesyl debris. The smaller size of the leaving group has advantages in scaled up synthesis. Although the methanesulfonyl (MsO) leaving group did not offer a strong UV chromophore for synthetic analysis, the protecting group of 2-naphthylmethyl (Npm) from desymmetrised tetragols **20** contributed to the UV detection for reaction monitoring.

The pentagol was formed in reaction (**iv**) by Williamson etherification, which is the key reaction to grow the continuous PEG backbone. In a previous study, THF and DMF had been used as the reaction solvent for Williamson etherifications of PEGs. It has been shown that DMF gave a better PEG solubility and a higher coupling rate [194] [173]. Sodium hydride (NaH) as a base was used for building block coupling; the ratio between NaH and (*R*)-1-(4, 4'-Dimethoxytriphenylmethyl) decan-2-ol **18** was 2:1 with 2 equiv. excess of tetragol methanesulfonate **20**. Utilising an accurate amount of sodium hydride ensured the completion of the coupling reaction and avoided the formation of by-products such as vinyl ether. Before coupling **(iv)**, azeotropic drying with MeCN was carried out to remove the water in the starting materials. Any water residue could hydrolyse NaH to NaOH. The NaOH base could attack the leaving group such as MsO, TsO and convert it into hydroxide, which would reduce the concentration of the reagents and cause self-coupling of the dimer. By adding NaH, the alkoxy ion (RO^-) was given from the OH side as a nucleophile, it attacked the carbon with the good leaving group (MsO), formed a C- O bond and broke the C- OMs bond. The rate of S_N2 reaction was dependant on the concentration of coupling units and the reaction temperature. This reaction was operated at a reasonably high temperature of 60 °C for 6 hours and 85% of coupling yield was obtained.

In reaction (**vii)**, a simple, highly reproducible protocol for the hydrogenolysis was used. The catalyst was prepared in situ from palladium (II) acetate and charcoal. This active catalyst allowed a low catalyst loading (0.025 mol %) and mild reaction conditions, at room temperature [315]. The reaction solvent played a key role in the cleavage rate for hydrogenolysis. The reactions with 10% MeOH in THF, ethyl acetate and MeCN were studied; however, all the reactions were slow and incomplete even at a high temperature and pressurized conditions. The rate of the reaction was significantly improved using MeOH, It gave a higher conversion and the reaction was completed within 6 hours. In addition the reaction was carried out under room temperature and pressure; it reduced the risk of solvent ignition and reagents flammability during reaction.

In previous work, chlorination or sulfonation as leaving groups for the PEG building block terminal have been reported; however PEG chlorides have been reported to be unstable during etherification [194]. The toluenesulfonyl group was chosen as the leaving group of our final building block **25**. This is because it is a great leaving group under basic conditions and it has a UV chromophore for reaction and purification online monitoring. Compared to methane sulfonates, toluene sulfonates shows greater lipophilicity, which has an advantage in extraction or reverse phase adsorption to secure a high yield of building blocks. Additionally, the toluenesulfonyl group has a reasonable size for membrane separation. During the tosylation (**viii**), excess trimethylamine needed to be added to stabilise the acid-labile Thp protecting groups. The basic conditions in the presence of triethylamine and catalytic 1-methylimidazole, also prevented the hydrolysis of the excess TsCl and the building block terminus. Overall, with the final manipulation of functional and protecting groups, the process afforded pentagol toluene sulfonate building blocks with octyl side-arms on multi-gram scales and with a good overall yield of 96%.

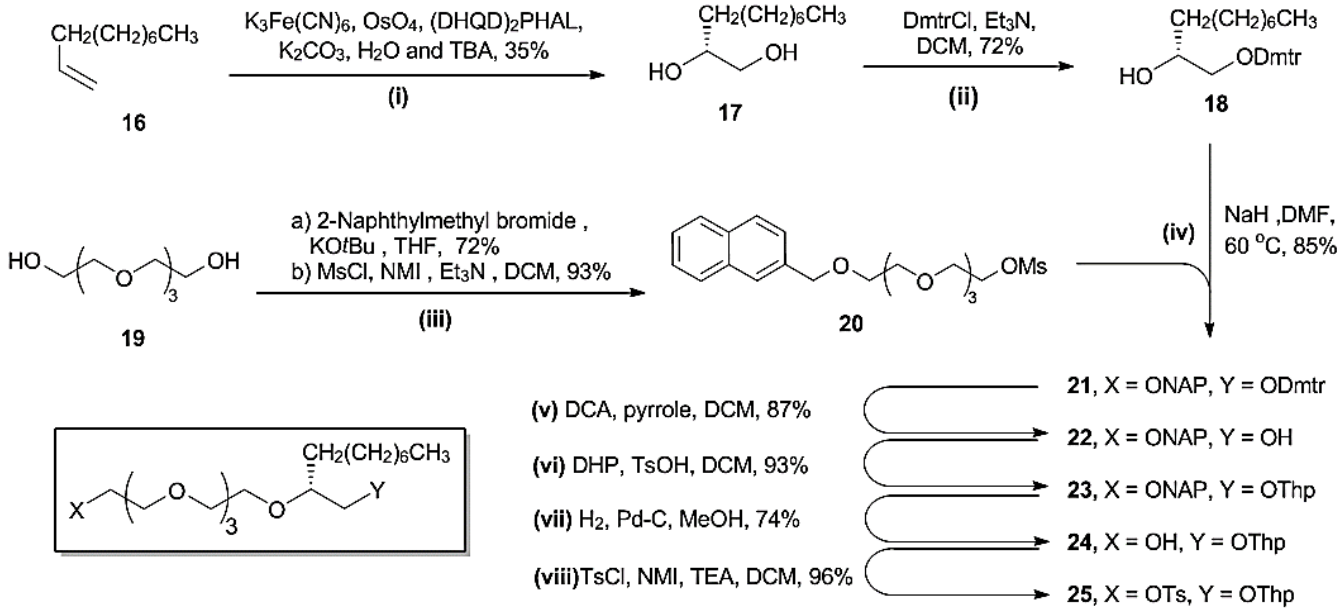


Figure 6.1 First approach of building block synthesis.

6.4.1.5. Sharpless' catalytic asymmetric dihydroxylation and crystallisation for chiral centre in building block

This section explains the chiral synthesis and its mechanism for branched building blocks. There is a significant demand for enantiomerically pure compounds for pharmaceutical drugs, and building blocks with chiral centres have been designed to construct chiral macromolecules. Sharpless' catalytic asymmetric dihydroxylation provides optically pure vicinal diols and the side chain could be formed from achiral starting materials with alkenyl functional groups. OsO_4 gives an efficient and reliable reaction for many applications [316], and OsO_4 has a great binding ability to alkaloid and mediated dihydroxylation. In a past study, it was suggested that the enantiomeric excess of the product can be improved by increasing the concentration of the alkaloid ligands [317]. However with OsO_4, the process requires a relatively small amount of chiral catalyst to produce a large amount of enantiomerically enriched product. During the reaction, the alkaloid ligands and OsO_4 form a complex in equilibrium, and the binding constant of ligands is extremely sensitive to the steric hindrance near the reacting centre. Quinuclidine derivatives were chosen to be the chiral ligands as they have intrinsically higher affinity for OsO_4. However, there are limitations in carrying out this catalytic reaction at a large scale due to the toxicity of OsO_4 and the high cost of the cinchona alkaloid ligands.

To achieve enantiomerically-enriched (R) - 1, 2-diol **17**, the same chiral ligand $(DHQD)_2$ PHAL was used, as shown in Figure 6.1. The ligand accelerates the reaction and transfers the chiral information to the targeted achiral olefins. Apart from OsO_4, $K_3Fe(CN)_6$ were added as stoichiometric oxidants in the catalytic cycle and a buffered solution of K_2CO_3 in water and tert butanol was made to ensure a stable pH, since the slight basic environment accelerates the reaction rate. For small-scale synthesis, commercially available pre-packaged mixtures of AD-mix β were purchased for enantiomerically-enriched (R) - 1, 2-diol. Solid $K_2OsO_2(OH)_4$ as the source of OsO_4 was used in AD-mix β, as it is safer to handle as it is non-volatile. In order to reduce the cost in scaling up the reaction, compounds were bought separately and mixed during the reaction in the standard equivalent ratio as in the AD-mix β. So 1mol of OsO_4 required 2.3 equiv. of $(DHQD)_2$ PHAL, 712.6 equiv. of both $K_3Fe(CN)_6$ and K_2CO_3 each. Overall, the standard AD procedure calls for 1.4 g of this AD-mix per millimole of olefin.

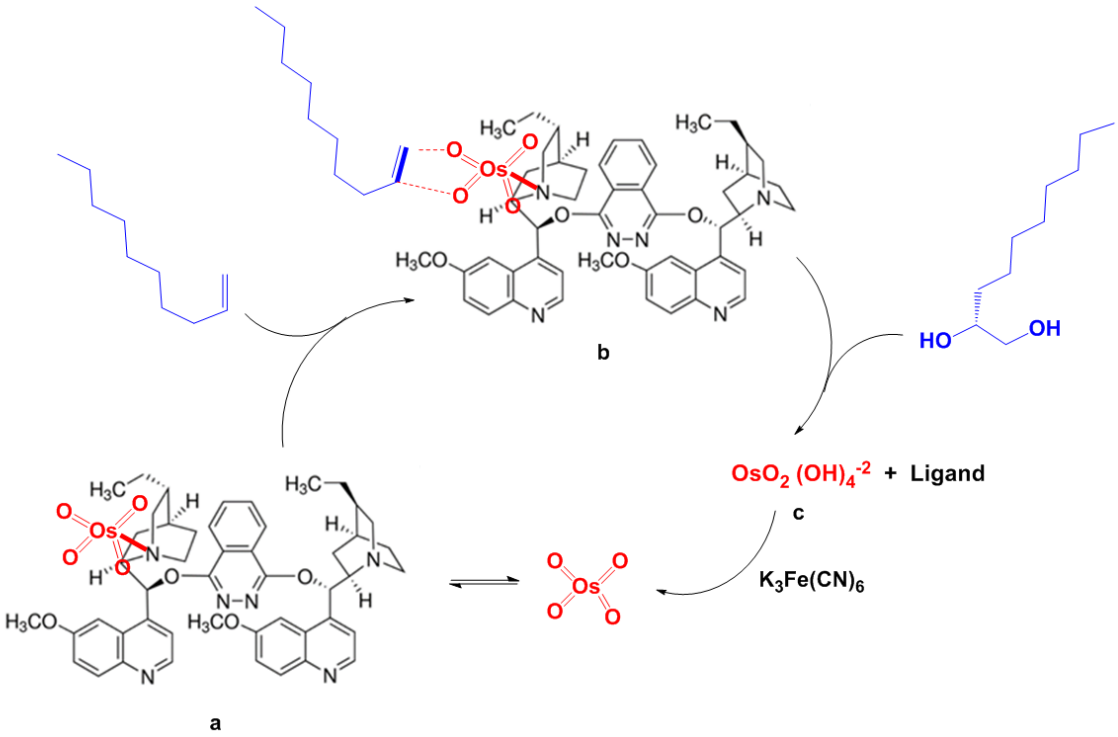


Figure 6.2 The reaction steps of the Sharpless dihydroxylation.

The reaction steps of the Sharpless dihydroxylation are shown in Figure 6.2. The osmium tetroxide and ligand firstly formed a complex, **a**. The two free oxygen atoms from the complex and the double bond from the 1-decene underwent [3+2]-cycloaddition with a cyclic

intermediate, **b**. 2 equivalents of water participated in the basic hydrolysis to release high enantioselectivities of (*R*)-1, 2-decanediol, **17,** and the reduced $OsO_2(OH)_4^{-2}$. Using oxidant $K_3Fe(CN)_6$, the catalyst osmium tetroxide – ligand complex was regenerated.

To calculate the enantiomeric excess of the chiral building blocks, it is important to identify and quantify each enantiomer of product mixture from Sharpless' catalytic asymmetric dihydroxylation. The enantiomers are mirror-image isomers, and are able to be distinguished chemically using a derivatization reagent to create stereoisomeric recognition. A homochiral form derivatization reagent can interact with the chiral pair of each enantiomer to produce diastereomeric pairs, they show different properties that can be distinguished from one another [318].

Camphanic acid chloride (Figure 6.3, **e**) has proven to be an efficient chiral derivatization reagent for the determination of stereoisomers [319]. In order to ensure that the camphanic acid chloride is attached on the chiral C centre of the (*R*)-1, 2-decanediol, the analytical reaction with camphanic acid chloride was carried out after Dmtr protection **ii** of the primary OH of (*R*)-1, 2-decanediol, so that only secondary OH was exposed for the reaction. The (1*R*)-(+)-camphanic chloride, as a chiral derivatization reagent, was chosen for the reaction; the camphanic derivative (Figure 6.3, **d**) contained two chiral centres. Because the (+) (R) octyl building block is the major targeted product from asymmetric dihydroxylation, the major stereoisomeric product (R, R) was expected to be obtained, together with a minor amount of (S,R). Distinct ^{1}H NMR signals were observed from two diasereomers with different chemical shifts on the chiral C position. The procedure that uses (1*R*)-(+)-camphanic chloride as the chiral auxiliary agent is cost-effective and no extra analytical equipment is required.

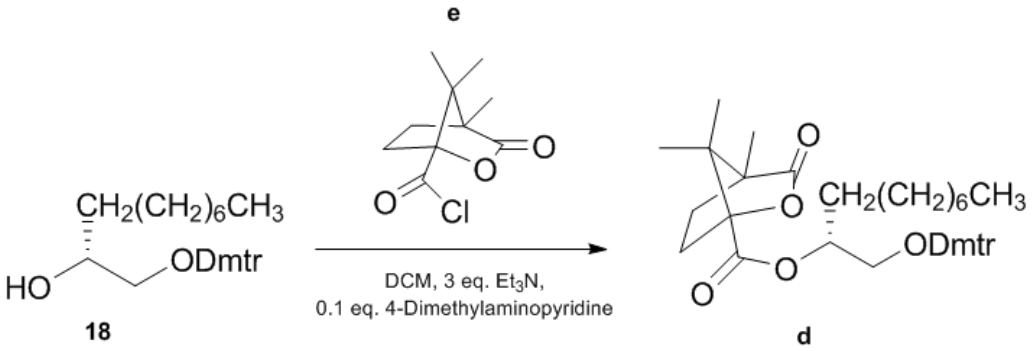


Figure 6.3 The use (1*R*)-(+)-camphanic chloride as the chiral auxiliary agent.

To determine the optical purity of the product from asymmetric dihydroxylation, Dmtr protected compound **d** was dissolved in $CDCl_3$ for NMR analysis. The ^1H NMR spectrum is shown in Figure 6.4. There are two split peaks representing one H atom from the same chiral centre of the different enantiomers. The chemical shift of the H atom in (*R*-) enantiomer was about 0.98 ppm, while the (*S*+) enantiomer was 1.01 ppm and the peak is much smaller. The integration of the peak areas represented the equivalent of the H atom in each enantiomer. The enantiomeric excess (ee) was calculated based on peak integration, and 80% optical purity was obtained. This chiral analysis with camphanic acid chloride can only be carried out after Dmtr protection, which meant the immediate purity check could not be performed after asymmetric dihydroxylation. It was time consuming to discover the enantiomeric excess of the product and it was impossible to improve the stereoisomeric purity in the (*R*)-1, 2-decanediol (**17**) step once the tritylation was finished. Thus it would have been more efficient if the purity check could be operated straight after asymmetric dihydroxylation. In this way, the optical purity could be confirmed before tritylation, thus avoiding wasteful procedures. Furthermore, the NMR spectrum does not provide an accurate measurement for the enantiomeric excess due to the noisy baseline.

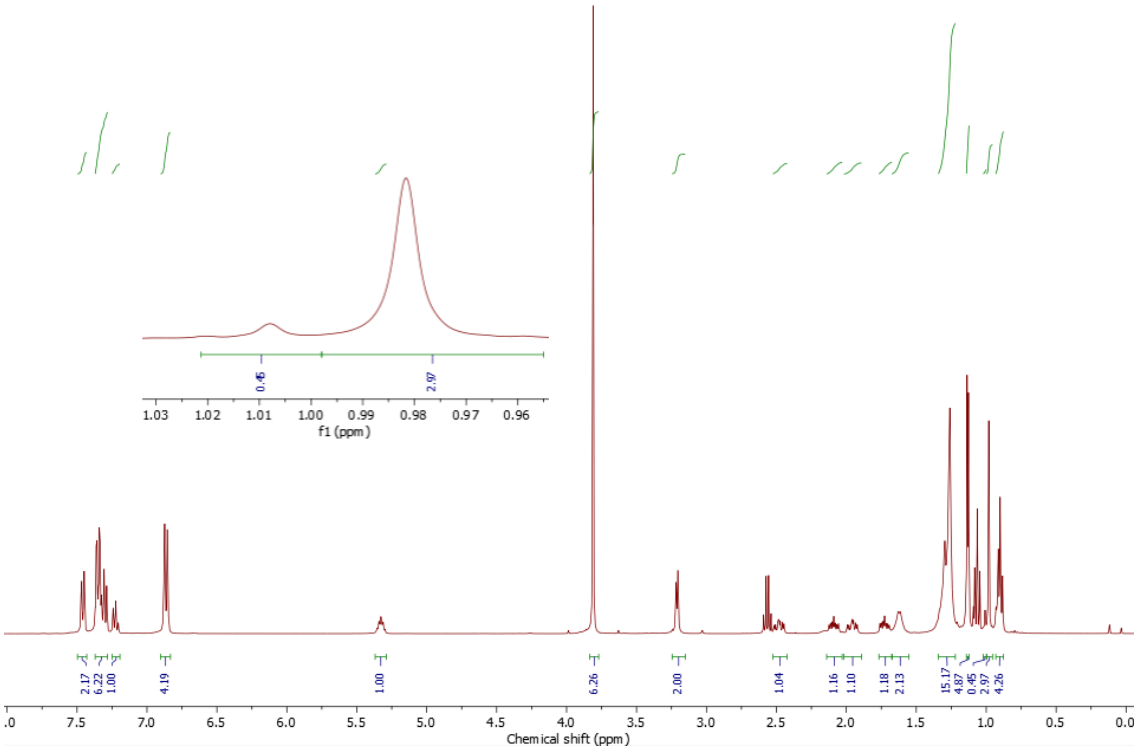


Figure 6.4 The ^1H NMR spectrum of camphanic derivative, **d**, for determining enantiomeric excess (ee) of (*R*)-1, 2-decanediol, **17**.

This optical purity of building block was only 80%, which is not suitable for synthesizing sequence-defined polymers, because the impure building block would be the main source of impurities for each synthesis cycle. Further purification was required to improve the enantioselectivities of product to achieve a higher optical purity of the desired enantiomer i.e. 100% ee. It was decided to use direct crystallization to conglomerate the (*R*) - enantiomer and increase the enantiomeric purity [320]. All the crude material was dissolved in a small amount of MeCN. The mixture was heated to about 80 °C; near the boiling point of MeCN, ensuring all enantiomers were well dissolved. The solution was then filtered through a filter paper and the filtrate was left still for 4 hours. The crystallization occurred slowly as the solution cooled naturally to the room temperature of 30°C. The crystal was separated from the mother liquor using a sinter funnel. The crystallisation was repeated using the same procedure one more time. The final (*R*)-1, 2-decanediol appeared as white flaky crystals. The optical purity from the crystallisation was examined by an alternative approach: chiral gas chromatography rather than camphanic acid chloride analysis.

Chiral gas chromatography was applied to achieve quantitative and qualitative analysis of the products from asymmetric dihydroxylation and crystallisation. The improvement after crystallisation can be observed from the GC spectrum. As in the NMR analysis, the integrated peak areas represented the concentration of each enantiomer in the product mixture and the enantiomeric purity can be calculated from there. This GC spectrum is quick and accurate.

The GC spectrum of the crude diol product from asymmetric dihydroxylation is shown in Figure 6.5. This GC method offered a good resolution to separate both enantiomers. In Figure 6.5 there are two clear peaks in the GC spectrum; a main peak appeared at a retention time of 77 mins for (*R*)-1,2-decanediol **17** and a small peak with a slightly earlier retention time of 75.5 mins was suspected to be (*S*)-1, 2-decanediol. Based on the integrated area shown in Figure 6.5 the purity of the desired (*R*)-1, 2-decanediol was calculated to be about 68.7%, which roughly matched the NMR analysis of 80% optical purity that was discussed above.

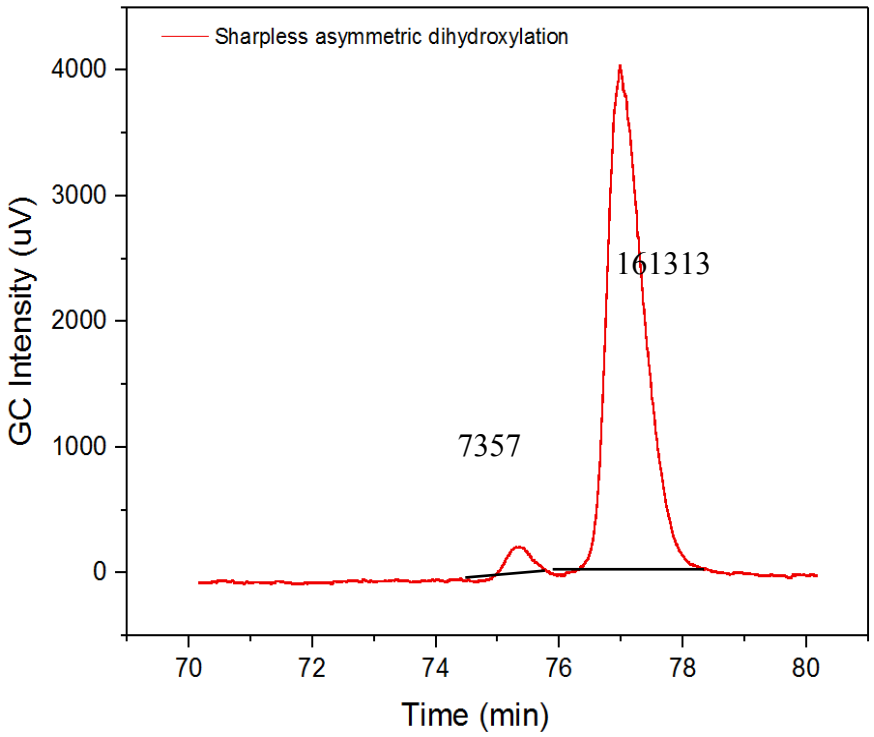


Figure 6.5 The GC spectrum of the crude 1, 2-decanediol, **17**, from asymmetric dihydroxylation.

The enantiomeric purity of the enantiomer diol product after two crystallisations was also assessed using chiral GC gas chromatography. The enantiomeric excess (ee) of the purified product increased dramatically to approximately 100%. The single blue peak from the purified product in Figure 6.6 confirmed that compound **17** after crystallisation was enantiomerically pure with a retention time of 77 mins. In conclusion, crystallisation is an important method to increase the enantiomeric purity, especially to enable the compound, whose composition was already partial to one enantiomer, to effectively achieve a higher purity. However due to the double crystallisation, the overall yield was only 35%. Potential improvements to optimise crystallisation performance include better crystallisation solvent choices, cooling profile, seeding etc. which could be studied in future work.

To identify the small impurity peak in the original crude product, as shown in Figure 6.5, the other enantiomer (*S*)-1,2-decanediol was synthesized using the (S-) chiral ligand $(DHQ)_2PHAL$ and purified using the same crystallisation method. Again, high enantiomeric excess (ee) of approximately 100% of the (*S*)-1, 2-decanediol was obtained. The GC spectrum of this compound is shown as the yellow peak in Figure 6.6, which overlapped the small impurity red

peak from the crude product. The same retention time of 75.5 mins confirmed that (*S*)-1, 2-decanediol is the major impurity from Sharpless catalytic asymmetric dihydroxylation.

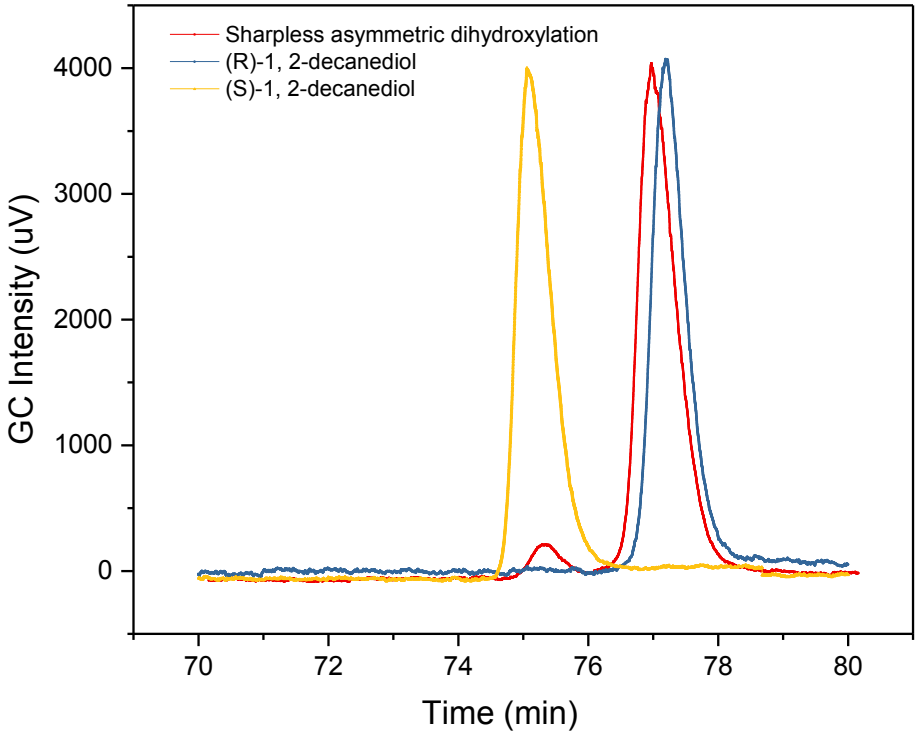


Figure 6.6 The GC spectrum of the crude 1, 2-decanediol (**17**), purified (*S*)-1, 2-decanediol and purified (*R*)-1, 2-decanediol after crystallisation.

6.4.1.6. Synthesis scale up for the first building block (25)

In addition to the aim of establishling a general chemical synthesis route for making high yield and purity PEG building block, production scale up to the level of grams was also desired. Three syntheses for building blocks were attempted. The production scale of compound **25** was increase from less than one gram in the first synthesis to several grams in the third, as shown in Table 6.2. The 2-3 L reaction flask, 5L dropping funnel for exaction and a large glass sinter funnel with a diameter of 15 cm for 50 g mass load column chromatography were used for the large scale production. The crystallisation for 1, 2 diol was also a great improvement for building block purity. Despite the low crystallisation yield, the asymmetric dihydroxylation must be operated in an excessive scale to ensure the final building block production. The

replacement of individual compounds for the AD-mix β reduced the cost of the reaction and allowed for a large-scale synthesis from the first intermediate 1, 2 diol. The performance and production scales of other reactions were also improved by optimising the reaction conditions based on the understanding of the reaction and the experimental proficiency.

Table 6.2 Scale-up results summary of building blocks synthesis in steps.

Compound	**First synthesis** (±0.01ml or ±0.001g)		**Second synthesis** (±0.01ml or ±0.001g)		**Third synthesis** (±0.01ml or ±0.001g)	
	Scale	Yield	Scale	Yield	Scale	Yield
15	0.57ml	-	0.79 ml	-	19.18ml	-
AD mix	4.210 g	-	5.860 g	-	140.490 g	-
17	0.416 g	79.7 %	0.622 g	80.5 %	16.560 g, 6.180 g (c)	94%, 35% (c)
18	0.547 g	76.6 %	1.742 g	93.8 %	9.130 g	72%
19	50.000 g	-	59.500 g	-	110.000 g	-
19a	2.570 g	30.2%	7.370 g	72%	27.200 g	72%
20	2.617 g	69.7%	2.919 g	92%	31.100 g	93%
21	0.282 g	65%	1.693 g	61.2%	14.280 g	85%
22	0.060 g	60 %	0.505 g	80%	6.760 g	87.3%
23	-	-	0.483 g	92.7%	5.980 g	93%
24	-	-	0.264 g	77.8%	3.320 g	73.8%
25	-	-	0.150 g	80.4%	4.050 g	96.4%
c means crystallization						

6.4.1.7. Second building block synthesis approach

This section reports work aiming to incorporate octyl chains into a different position in the PEG pentagols; the synthetic procedure was shown in Figure 6.7. The new synthetic approach for such building blocks showed a great potential for more structural diversity using the proposed methodology. The position of the long hydrophobic side chain along the PEG backbone could be shifted. The length of the building block and the position of the side chain can be determined by the assembly units and the method used to structure it. Such changes in

the chiral position and the functional side chain could influence the chemical and physical properties of the final sequence-defined polymers described in Section 6.4.2.3.

In the first synthesis approach, the octyl chain was located in the β-position adjacent to the protecting group. The pentagols were assembled from ethylene glycol (EG) with chiral octyl chains and desymmetrised tetragols (EG_4). In the second approach, the chiral octyl chains were shifted from the β-position to the 8-position in the middle of the PEG backbone. Therefore two desymmetrised diethylene glycols (EG_2) were connected to both sides of ethylene glycol (EG) with chiral octyl chains. Three assembly units were required to be modified for etherification, so a few more steps were needed compared to the first approach.

During the second synthesis approach, a benzyl (Bn) group replaced the 2-naphthylmethyl (Npm) group as temporary protecting groups to desymmetrise diethylene glycols. Based on the previous experience in the first approach, 2-naphthylmethyl (Npm) was very robust to cleave resulting in a low conversion in hydrogenolysis and was at risk of undesired deprotection. Therefore, the benzyl group (Bn) was chosen for its good stability in coupling conditions and ease of cleavage. The Thp group was applied in the same way as in the first approach, which protected one end of the diethylene glycols due to its good selectivity and stability.

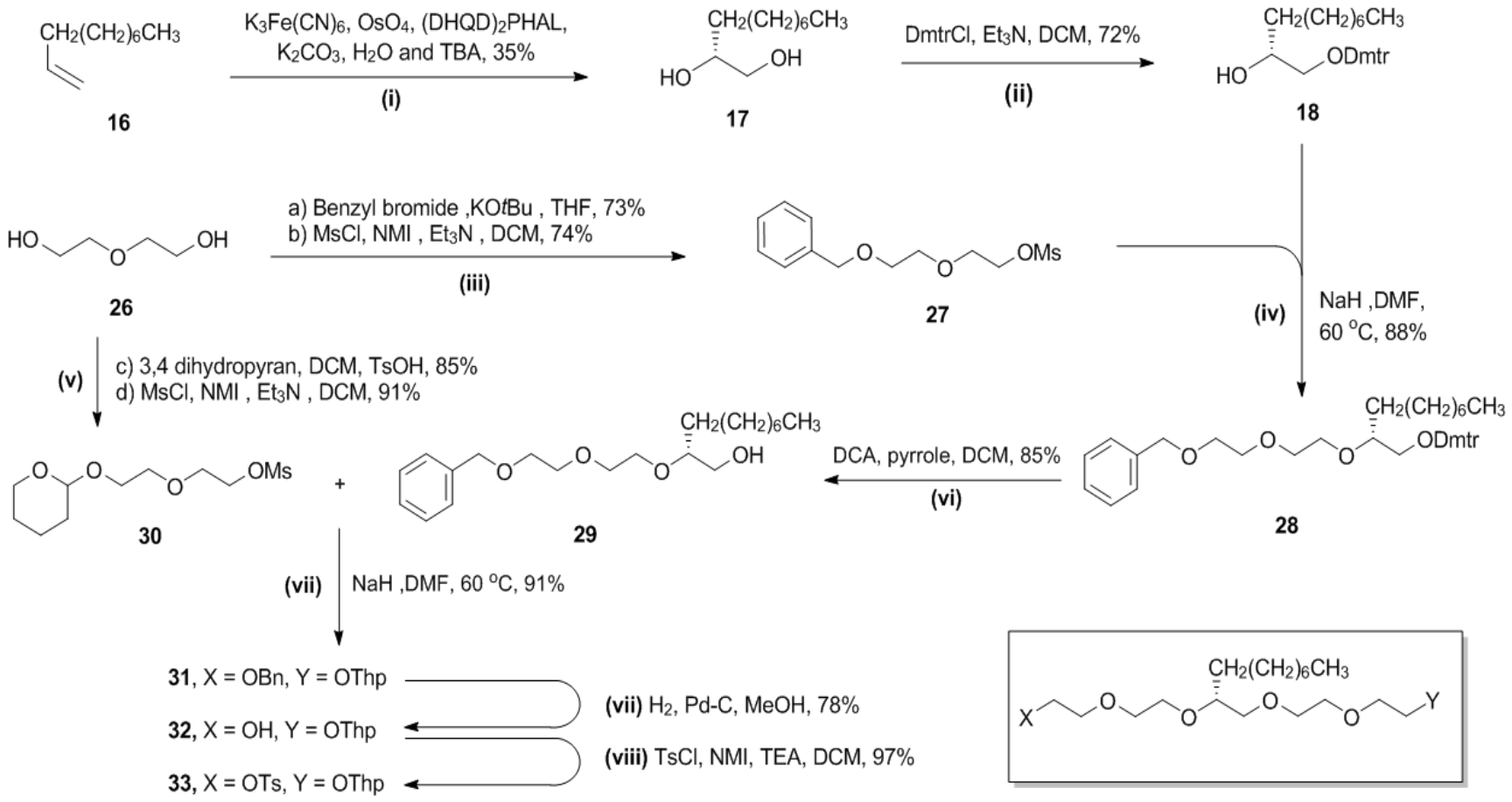


Figure 6.7 Second approach for building block synthesis.

(*R*)-8-Octyl-α- tetrahydropyranyl-ω- toluenesulfonyl pentagol, **33**, was prepared in multi-gram scales with high reaction yields. Although the octyl chain was shifted along the PEG backbone, the corresponding results from compound **33** were similar to (*R*)-β-Octyl-α-tetrahydropyranyl-ω- toluenesulfonyl pentagol, **25**. Both synthesized isomers possessed the same functional groups and the polarities were almost the same. The same mass spectrum and R_f from the TLC were obtained from both isomers. Because of the same principles, two isomers also had the same retention time of 9.8 mins in the HPLC spectrums eluting with the same mobile phase. As shown in Figure 6.8, the HPLC spectrum also revealed the purity of the final building blocks; both isomers showed sharp single peaks. Apart from the peak at a retention time of 2.5 mins, which was caused by a solvent effect, there were small lumps which were next to the main peaks. Poor solubility of the octyl chain in the organic phase was suspected to be the reason for the slightly unsmooth sharp peaks.

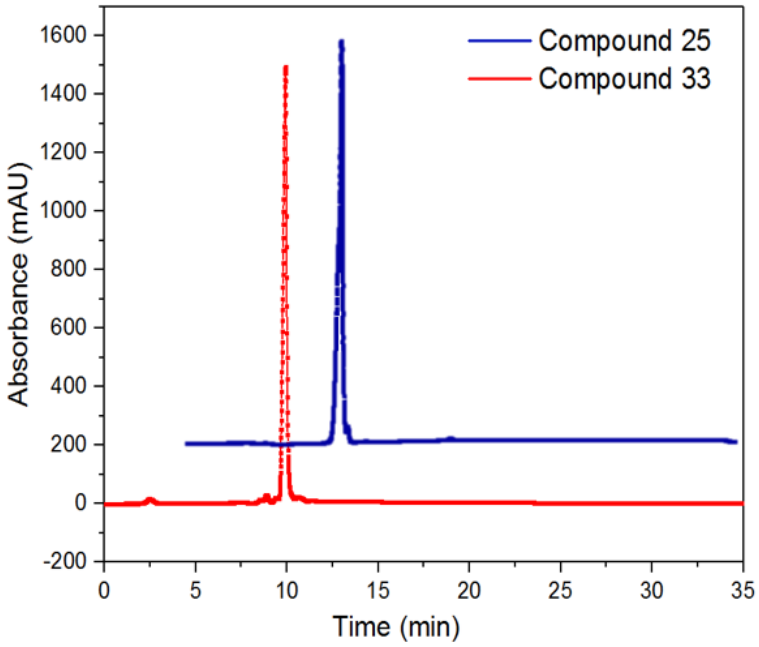


Figure 6.8 HPLC spectrums of the final building blocks (**25** and **33**).

NMR analysis was the only effective way to confirm the change of the octyl chain position of the building blocks. Distinct ^{1}H and ^{13}C NMR signals can be observed from two diasereomers with different chemical shifts. The ^{1}H NMR spectrums of both building blocks **25** and **33** are shown in Figure 6.9 and Figure 6.10 respectively. Most of the protons in both isomers experienced the same neighbouring environment. However different peak splits appeared on

one hydrogen from the CH of the Thp group, due to coupling with different neighbouring protons. This unique H atom from the CH Thp group gave a chemical shift of approximately 4.5 ppm. The H atom was strongly influenced by the adjacent octyl chain in compound **25**. Therefore the multiplets peak indicated that the CH of the Thp group was surrounded by different hydrogen environments from the octyl side chains, whereas in compound **33** a triplet peak appeared in the ^{1}H NMR. The H atom for the CH Thp group lost the proton interaction with the octyl side chain, because the side chain moved further along. The peak split was only affected by the two H atoms on the saturated six-membered ring which was adjacent to the CH Thp.

In addition, since all the functional groups were located near the end of the building block backbone in compound **25**, the H atoms of the PEG backbone experienced similar environments; therefore more peaks from the H atoms were overlapping than the ones in compound **33**.

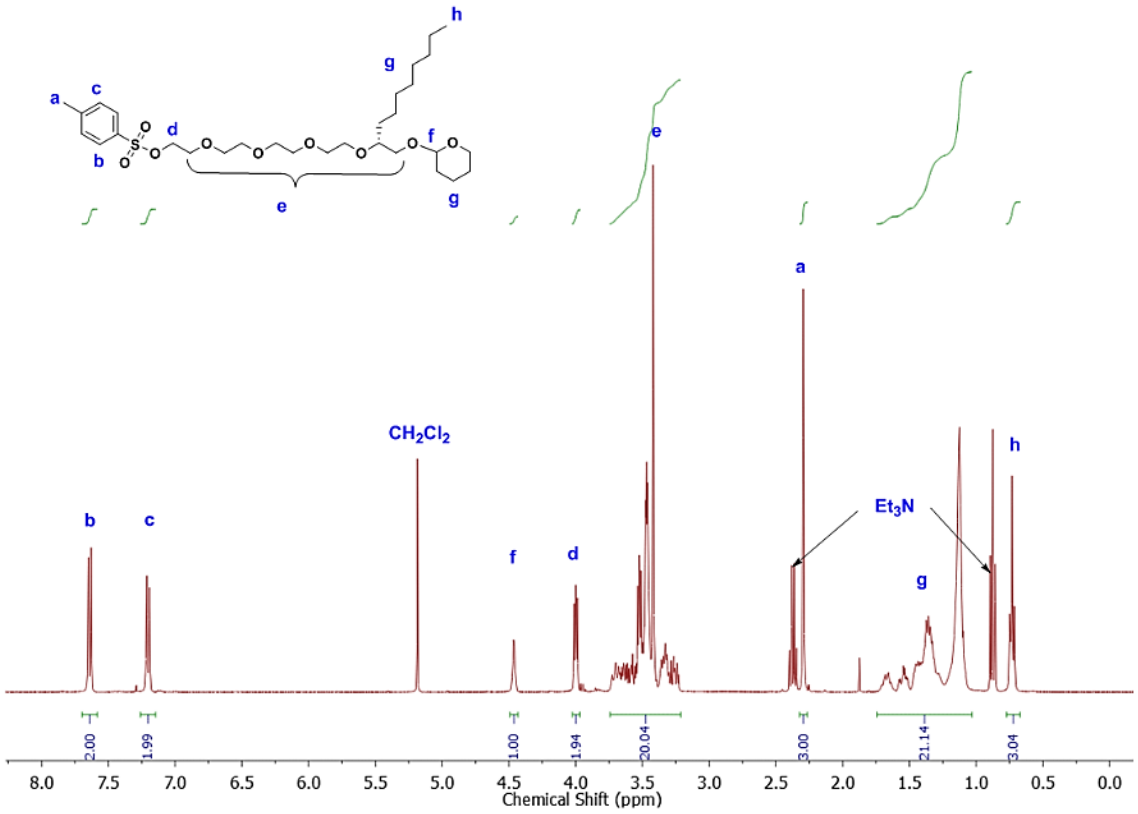


Figure 6.9 [1]H NMR spectrum of final building block **25**.

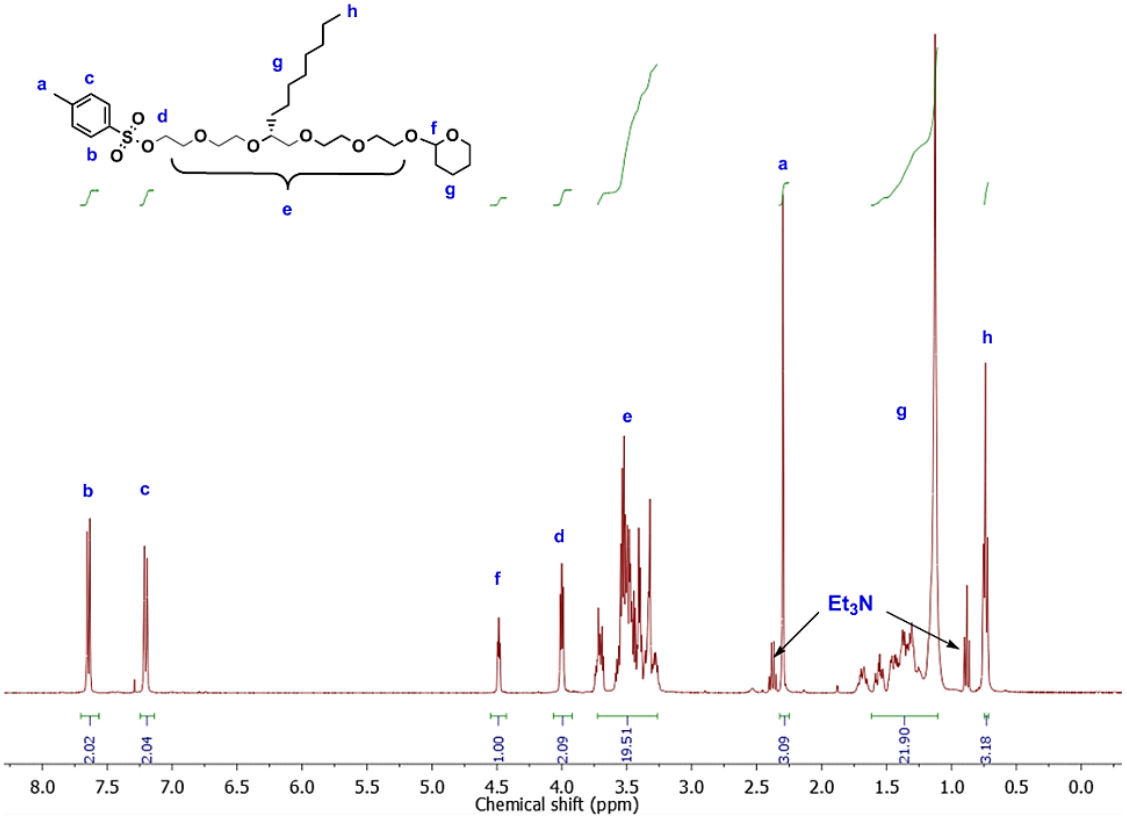


Figure 6.10 [1]H NMR spectrum of final building block 33**.**

6.4.1.8. Alternative synthesis route with unsuccessful hydrogenolysis

During reaction **vii** in Figure 6.1, there was a risk of Thp group cleavage, which could occur if the reaction conditions were severe, such as running hydrogenolysis over 6 hours or operating the reaction in a concentrated condition. The reaction solvent, MeOH, significantly improved the reaction conversion and also provided a good environment for Thp deprotection. The catalyst $Pd(OAc)_2$ could act as a Lewis acid and potentially attack the Thp group in the MeOH, which causes deprotection while running hydrogenolysis [321]. Excessive cleavage gave undesired (*R*)- β -Octyl pentagol **34** with two hydroxyl groups on both sides. The NMR analysis showed no H peak in the Thp six-membered ring or any protecting linkage. This is another good example proving that benzyl ether is safer to use as a temporary protecting group. The second approach of building block synthesis showed the advantages of benzyl ether, such as the ease of cleavage and a shorter reaction time. In the protecting reaction, the normal requirement was 5-10 equivalent excess of cheap PEG oligomers, such as diethylene glycols and tetragols. Therefore, the selective protection normally occurred at the beginning of all the syntheses. However at this stage, it was challenging to protect a specific end of an OH group on building blocks selectively without wasting valuable starting materials.

Here the t*ert*-butyldimethylsilyl (Tbdms) protecting group was chosen to selectively protect (*R*) - β -Octyl pentagol **34**. The reactive silyl group would protect the *ω*- position of the PEG building block, while leaving the *α*- position, a free hydroxyl, due to the steric hindrance from the octyl chain. The protection of the Tbdms group at the PEG *ω*- position secured the stereochemical integrity of the final building block. In order to make the selective protection, only one equivalent of TbdmsCl was used to control the double side protection or the *α*-position protection. The crude residue from the TbdmsCl reaction was fractionated using chromatography. The major product (*R*)-2-Octyl-*ω*-*tert*-Butyldimethylsilyl pentagol **35** and the side product (*R*)-2-Octyl-*α*- *tert*-Butyldimethylsilyl pentagol **36** were successfully separated. There are two routes to convert (*R*)-2-Octyl pentagol **34** to the final building block **25**, depending on the Tbdms protecting positions. The full synthetic plan is shown in Figure 6.11. In order to convert all the intermediates into the same building blocks, the order with which to attach TsO and Thp groups was reversed. Tbdms showed a good stability in acid and base conditions in the presence of TsOH and Et_3N. The efficient chemoselective cleavage was also carried out successfully without damage to the Thp and TsO groups. The overall yield was

lower than in the original synthetic plan, because there were a few more steps to modify the terminal groups and there was some yield loss with the double protection in reaction **ii**. However this is a possible alternative synthesis, which secures the valuable intermediates from unexpected deprotection and achieves the same purity of building blocks as the original approach.

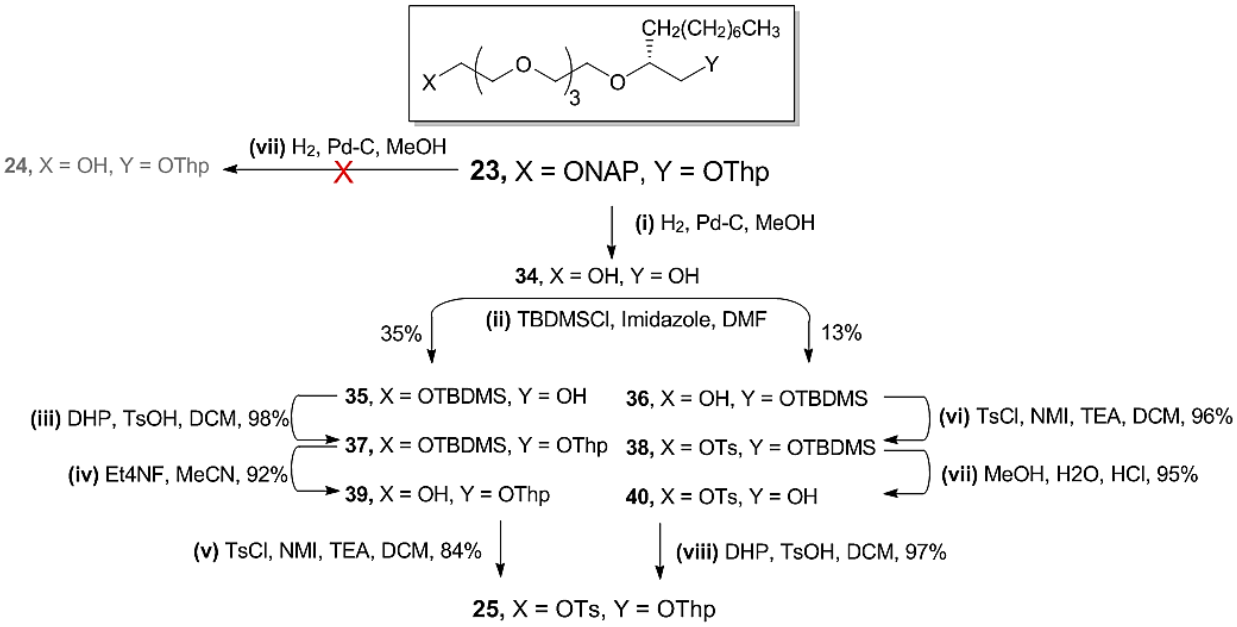


Figure 6.11 An alternative synthesis route if hydrogenolysis fails.

6.4.2. Synthesis of sequence-defined octyl branched PEG using ItSyN

This section reports work undertaken to synthesise sequence-defined PEG polymers using the iterative synthesis by organic solvent nanofiltration (ItSyN) technique. The monomer building blocks reported in the previous Section 6.4.1 were utilised.

The ItSyN procedure followed the same methodology as in Chapter 5, including iterative synthesis and membrane diafiltration in a fully liquid environment, as shown in Figure 6.12. In order to achieve the desired sequence length, during the polymeric synthesis, building blocks with one end protected were added to the exposed end of the growing polymer. After the completion of the chain extension and purification, the temporary protecting group was removed for the next chain extension. Building blocks with different side chains were added in an ordered fashion and the sequence-defined multifunctional PEG polymer was synthesized in a controlled approach. The concerns for fabricating the sequence-defined polymer were to ensure all the functionalities of the growing PEG polymer were orthogonal to the coupling conditions, via Williamson etherification, and diafiltration. In addition, during deprotection to remove the protecting groups, it was desired that all the other functional groups were orthogonal to the acidic conditions. Due to the same requirements, a benzylic ether linkage was selected as hub linkage and a tetrahydropyran-1-yl acetal (Thp) acetal was chosen as the temporary protection of the chain termini.

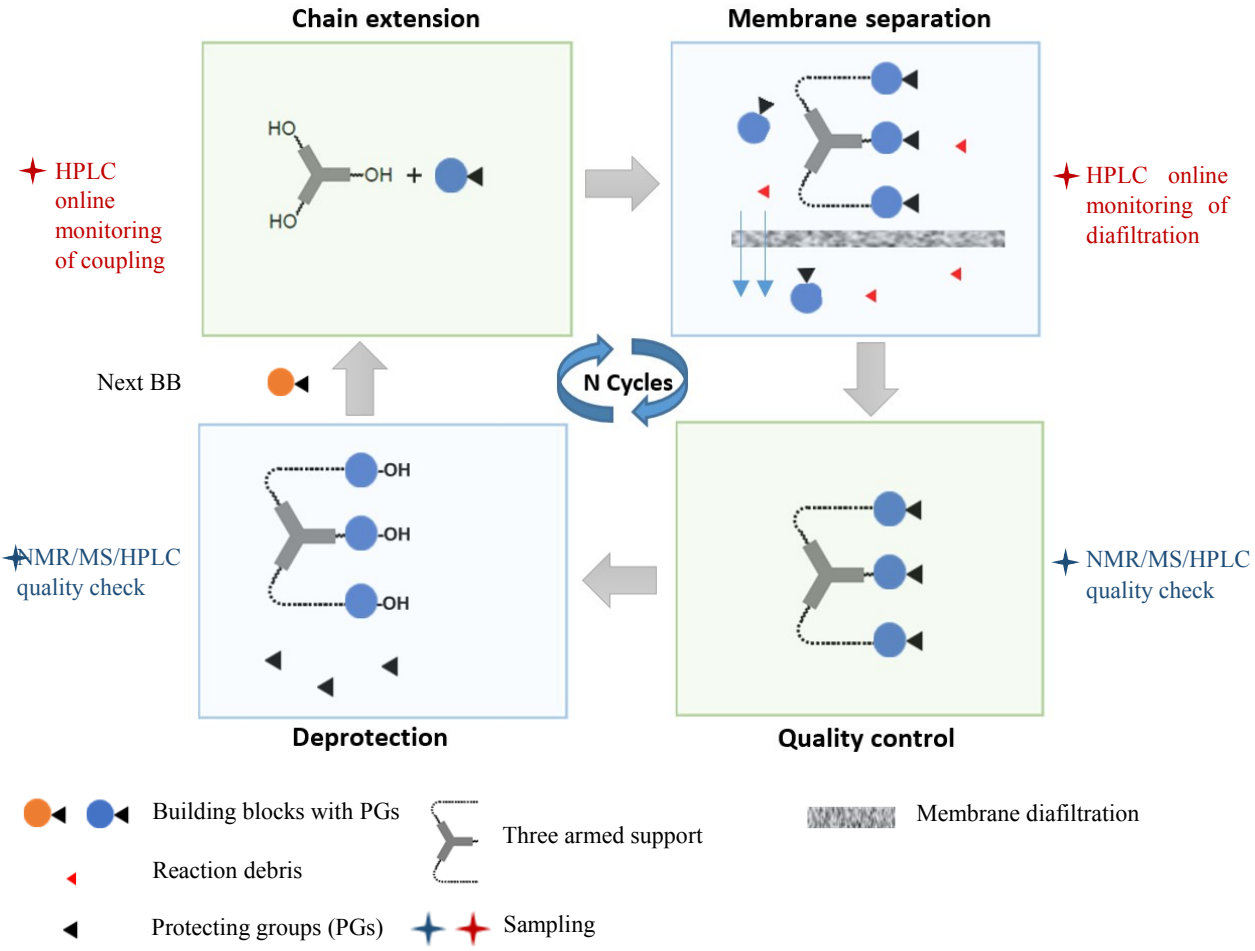


Figure 6.12 The ItSyN concept for sequence-defined PEG polymers.

The strategy of the chiral pentagol building block with an octyl side chain synthesis **33** is reported in detail in Section 6.4.1. The overall chemical scheme of preparing the linear building block and both sequence-defined polymers are shown in Figure 6.13 below. To make modified linear building blocks, 3, 4 dihydropyran was reacted with 10 equiv. of commercial tetragols to give ThpOEG$_4$OH **41**. The desymmetrised tetragols were then reacted with TsCl to afford pentagol toluene sulfonate building blocks with Thp protecting groups TsOEG$_4$OThp **42** on multi-gram scales in a good purity. The building block **33** and **42** were assigned the coding letters **A** and **B** respectively. Two different synthesized sequence-defined pentagol PEG polymers hub-**AAABB** and hub-**ABABA** were synthesized in 4 and 5 cycles respectively. As after chain extension of hub-**AAA**OH **49**, a longer building block TsOEG$_8$ODmtr was used as **BB** to extend the linear sequence in one reaction. One time column chromatography needed to be carried out to remove any contamination from the membrane rig when the final polymers hub-**AAABB** and hub-**ABABA** were obtained. Therefore the Dmtr protecting group was used

in **BB** to achieve **50**; it gave a good elution and resolution in chromatography to secure a good yield and purity.

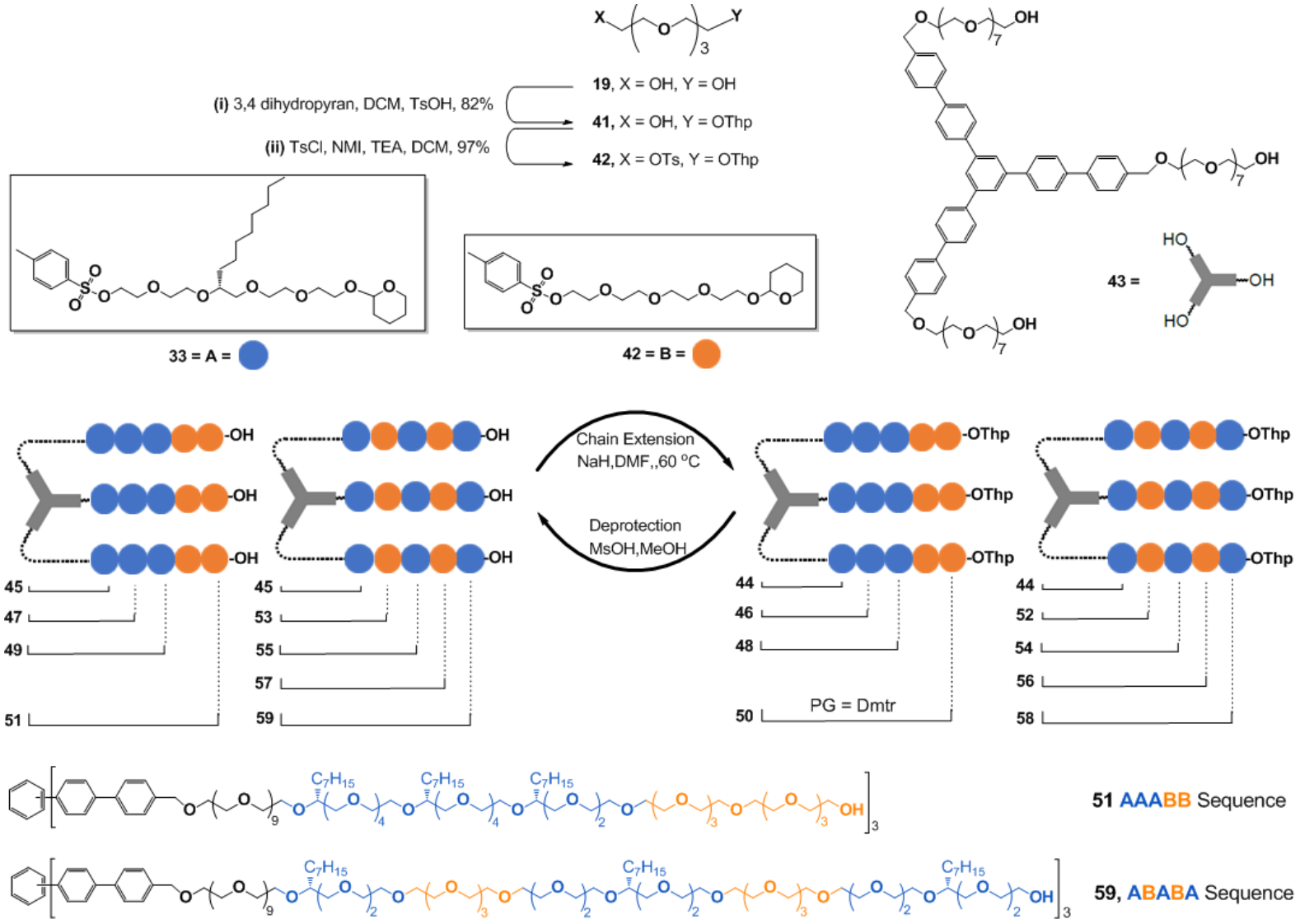


Figure 6.13 The approach to sequence-defined PEG polymers synthesis.

6.4.2.1. Membrane and solvent system selection

Membrane separation appropriate for the ItSyN scheme undertaken was investigated. Membranes with appropriate pore sizes to separate reaction debris from the growing polymer were required. There were two building blocks **33** and **42** that would need to be removed from the membrane. In order to simplify the purification and increase the efficiency of process, the membrane that was installed in the diafiltration rig needed to have the ability to remove both building blocks, so as to avoid changing membranes in between the chain extension cycles. Therefore the building block **33** with an octyl side chain was chosen for membrane screening, because it was branched and had a greater size of building block, so was theoretically harder to remove by membrane separation compared to the smaller linear building block. Here it is assumed that the smaller building block **42** has even lower rejection if building block **33** can be removed. The membrane selectivity would be based on the relative difference in molecular size between the building block **33** and the bulky three-armed star with flexible octagol spacers $Hub(OEG_8OH)_3$ **43**. The decision for the hub structure was discussed in Chapter 5. It showed advantages of tripling the chain growth; it is a good soluble support for polyether unidirectional growth and has a strong UV signal for online monitoring. The membrane rejection of homostar was enhanced by the large rigid central unit with the increasing chain length and side chains from the three arms. Therefore compared to the relatively small building blocks, the separation efficiency is becomes greater with the chain extensions.

The requirements for the membrane to separate the crude reaction mixtures are similar as in Chapter 4. It is required that the membrane has the pore size big enough to permeate organic solvents, acids, bases, and various reactive species; but tight enough to retain the homostar product. A number of commmerically available membranes were assessed on these criteria, alongside the membranes reported in Chapter 4.

The commercial membranes for organic solvent use were first screened for this reaction crude mixture, because they are available in different MWCOs and they are highly reproducible. There were five different types of commercially available membranes that were screened in MeOH; the membrane performances are shown in Figure 6.4. The black and grey bars represented the membrane rejections of octyl building blocks and homostar product respectively, while the red dots show the value of each membrane's permeance for MeOH.

Despite some incredible membrane permeance, the membranes were either too loose or too tight for both solutes. None of the chosen commercial membranes offered a significant separating effect, and therefore could not be used for this synthesis application.

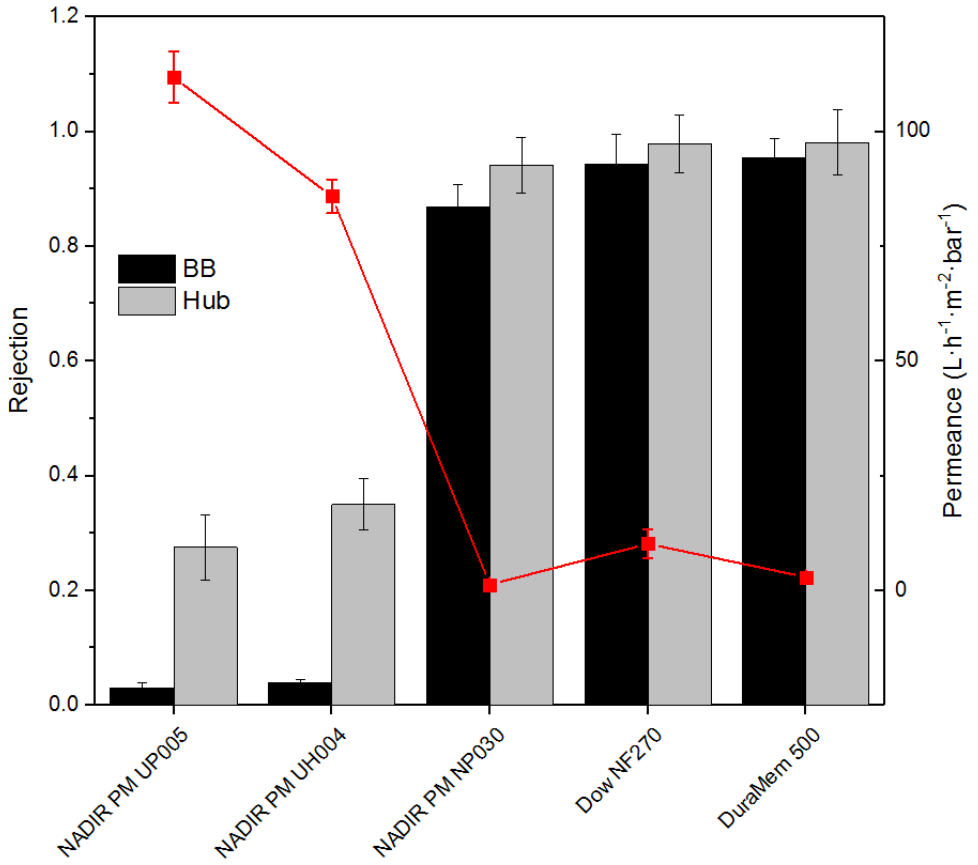


Figure 6.14 Screening membrane performance of five different membranes with Octyl building block and Hub product in MeOH.

In Chapter 4, both the octyl building block **33** and the Hub(OEG$_8$OH)$_3$ **43** were screened as a case study with four robust OSN membranes, including three modified 18 wt% PBI membranes (M-600, M-2005 and RE1-2007) and one 12 wt% PEEK membrane. Based on the membrane performance, characterisations and solute molecular modelling analysis, the 18 wt% PBI-DBX-M2005 membrane showed the second highest permenace of 5.3 L m^{-2} h^{-1} bar^{-1} and excellent selectivity with a hub rejection of 92% and a building block rejection of 42%. It gave the highest separation factor of 7.2 to rapidly and efficiently separate the various reaction debris from the homostar product.

The membranes were initially screened in MeOH due to its wide application in industry. In order to ensure the salvations of both hydrophobic hub homostar and the octyl side chain, the membrane 18 wt% PBI-DBX-M2005 was tested in different solvent combinations to determine its best performance. The relatively apolar solvents - MeCN, toluene, and ethyl acetate - were mixed with MeOH respectively in the ratio of 1:1 and were screened; the results are shown in Figure 6.15. MeOH showed the lowest rejection for the building blocks but rejection of the hub product was also too low to secure a good yield. When another apolar solvent was added, all the membrane rejections increased, especially MeCN-MeOH (1:1) which enhanced the separation factor up to 7.25. The second part of the study of the solvent effect is about the ratio of the solvent combination.

In Figure 6.15, the different ratios between MeCN and MeOH are shown to affect the membrane performance; 30%, 50%, 80% MeOH in MeCN were tested as the diafiltration solvent. The rejection of the building block decreased with increasing MeOH; however the rejection of homostar had the highest value when MeCN-MeOH was (1:1). Therefore, MeCN-MeOH (1:1) was chosen as the diafiltration solvent, being sufficient to ensure rapid and efficient separation of the growing polymer-star from the reaction debris by membrane separation.

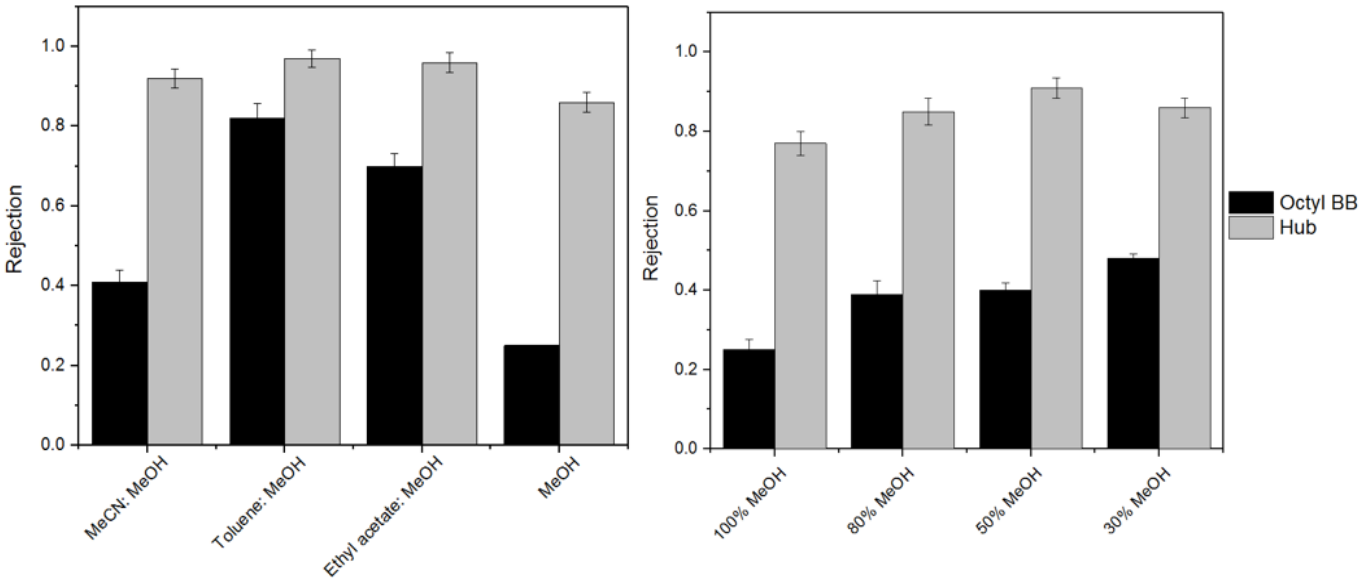


Figure 6.15 Screening membrane performance of 18 wt% PBI-DBX-M2005 with Octyl building block and Hub product in different organic solvents; on the right panel the MeOH was mixed with MeCN in the proportion indicated.

6.4.2.2. Chain extension and membrane diafiltration

The branched building block with an octyl side chain (10 equiv. **33**, letter code **A**) was attached to the Hub(OEG$_8$OH)$_3$ as the first chain extension attempt via Williamson etherification, in the same conditions as Chapter 5; 6 equiv. of NaH in DMF at 60 °C for 12 h. The reaction then was quenched with sat. NH_4Cl and the crude mixture was ready to be loaded in the membrane rig for purification.

The chosen 18 wt% PBI-DBX-M2005 has hub rejection of 92% in MeOH: MeCN (1:1); however for practical membrane purification, it is necessary to isolate the homostar product at a high yield after each chain extension cycle. Again the two-stage membrane diafiltration system was applied to this work. Similar to the experience reported in Chapter 5, it increased the stepwise product recovery from each cycle of diafiltration. The excess building block and other reaction debris were removed while most of the homostar product was retained in the membrane. The purified homostar was then washed from the membrane rig and deprotected with catalytic 0.05 M MsOH in MeOH for 30 min. The resultant Hub(OEG$_8$**A**OH)$_3$ **45,** was

purified by simple extraction to remove protecting group debris and was ready for the next round of chain extension.

After the necessary chain extensions and diafiltrations, two targeted sequence-defined polyether-stars were prepared. A block copolymer was prepared, Hub(OEG$_8$**AAABB**OH)$_3$ **51**, in 61% overall yield, with a good purity of >98% over 8 steps, including 4 chain extension syntheses and 4 deprotections. An alternating copolymer was prepared, Hub(OEG$_8$**ABABA**OH)$_3$ **59**, in 54% overall yield, with a good purity of >98% over 10 synthesis steps. The HPLC online monitoring of the diafiltration of the crude reaction mixture revealed the dynamic migration of solutes to different parts of membrane rig. The diafiltration was stopped when the quantity of building block became undetectable and the required purification yield was also indicated by the change of the homostar product concentrations. The concentration profiles of Hub(OEG$_8$**A**OThp)$_3$ and building block A during diafiltration are showed in Figure 6.16.The decrease of the building block concentration in Stage 1 was like an exponential decay. More than half of the building blocks were removed by the PBI membrane within three diafiltration volumes. The purification was completed in 18 diafiltration volumes; by the ninth diafiltration volume, the building block concentrations in the whole membrane rig including Stage 1 and Stage 2, and permeance reached equilibrium; there was only 10% of building block left in the solution. The rejection of the hub stayed at 90% and there is little hub product being flushed out to the permeance. 4L of diafiltration volume was washed through the system for each purification. The overall yield of each diafiltration cycle was about 85%-98%.

Table 6.3 includes all the diafiltation detail; purity and yield of each homostar intermediates are shown after each cycle. It is shown that over the initial cycles of growing homostar product in length, their rejection increased from around 90% to around 98% due to the building block additions, while the building block rejection remained roughly the same. The rejection of the hub was significantly higher for the two-stage membrane rig and the value roughly held constant after a certain size of the homostar. Homostar yields enhanced while as the chain length grew, which is opposite to the chromatography behaviour of the strong affinity with the polyether chain. The deprotection and extraction procedure remained the same as in Chapter 5, and the deprotection was completed in one hour with the high yield of 93-99%.

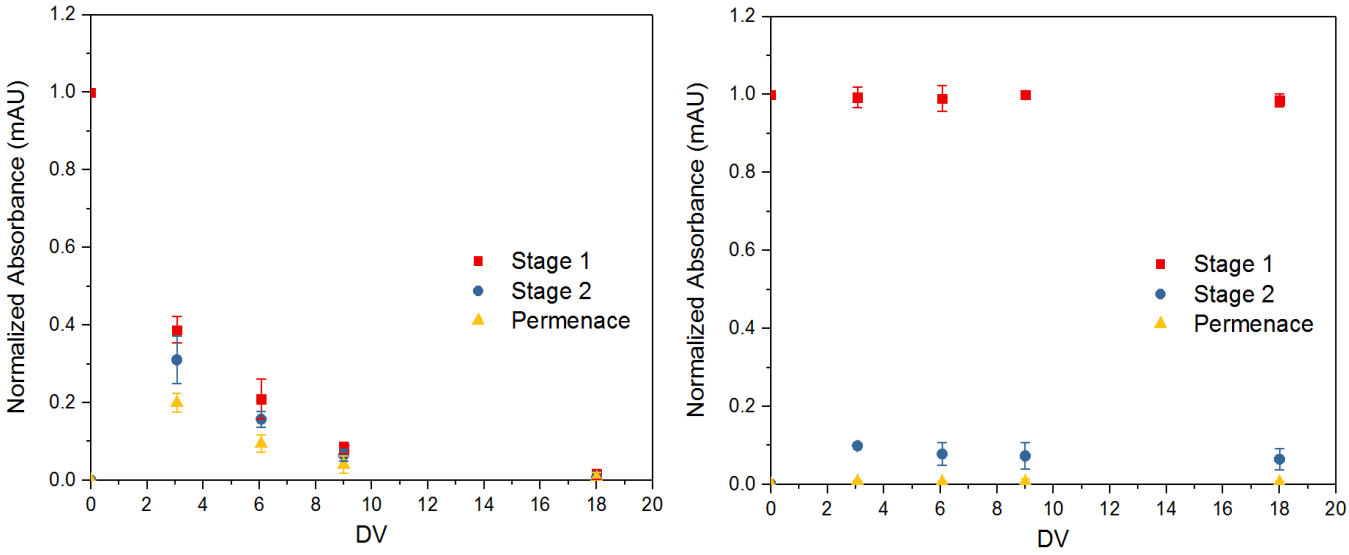


Figure 6.16 Concentration profiles of building block and Hub product in two-stage membrane diafiltration rig.

Online monitoring using HPLC was applied to all the steps including coupling, membrane diafiltration and deprotection during each iterative synthesis cycle. Due to the hydrophobic property of the octyl side chain, every attachment of the building block would shift the homostar product peak to 2-3 minutes later in retention time. During the chain extension progress, the formation of the 1-arm, 2-arm intermediates, and the 3-arm product was seen, together with the disappearance of the starting materials, 1-arm and 2-arm intermediates.

It was also shown that the time of the coupling reaction was getting longer with increasing chain length and number of building blocks. This may have been as the long PEG polymer entangled to embrace the reactive sites on the homostar. Another possible reason might have been the poor solubility of the long hydrophobic octyl chains, as the side chains may have slowed down the contacting rate with building blocks and reduced the coupling rate. Therefore, the chain extensions of the latter sequence took 18-24 h and the equivalents of building blocks (12 equiv. in total) also increased. When the reaction could not be brought to completion, the reaction temperature was elevated to 80 °C while doubling the amount of NaH. However, the change to the reaction conditions may have increased the formations of dimer and other impurities, which made diafiltration more difficult. Therefore there is a trade-off between increasing the reaction rate and eliminating the impurity formation.

During work, the HPLC spectra from online monitoring for synthesizing Hub(OEG$_8$**ABAB**OThp)$_3$ **56** were misinterpreted due to the overlapping peaks of the intermediates and product. The polarity of the Hub(OEG$_8$**ABAB**OThp)$_3$ **56** product was dominated by the long hydrophilic PEG backbone, the hydrophobic central hub support and the octyl chain. Therefore the additions of the small linear building blocks TsOEG$_4$OThp **42** did not change the polarities of the homostar significantly. The resulting intermediates and product did not give obvious peak shifts. Therefore the diafiltration and deprotection were undertaken despite incomplete reaction. The Maldi-Tof analysis after the deprotection showed that 25% of the 2-arm intermediate had not yet converted into product. Due to the similar polarity and molecular size, it was difficult to separate the 2-arm intermediate and the 3-arm product by either chromatography or membrane. It was decided to continue to the next chain extension in which, by using the new addition of octyl building block **A**, it was possible to distinguish the impurities and the final product. It was assumed that the completed arm **ABAB** from the starting homostar was easier to extend building block **A** to form the sequence **ABABA**, compared to the chain extension of the incomplete **ABA** to give **ABAA**. Based on the experience of synthesizing sequence **AAA** for compound **48**; the chain extension between building blocks **A,** especially for a longer sequence, got slower and slower due to the steric hindrance and solubility issues from the long hydrophobic octyl chains. Therefore, the previous 2-arm intermediate could be chain extended with 2 arms of **ABABA** and 1 arm of **ABA**. This impurity now had one octyl building block difference from the final product, 3 arms of **ABABA**, which made it possible to separate them by a reverse phase column chromatography.

Table 6.3 Summary of the diafiltation of each of the homostar intermediates and products after each cycle with purities and yields.

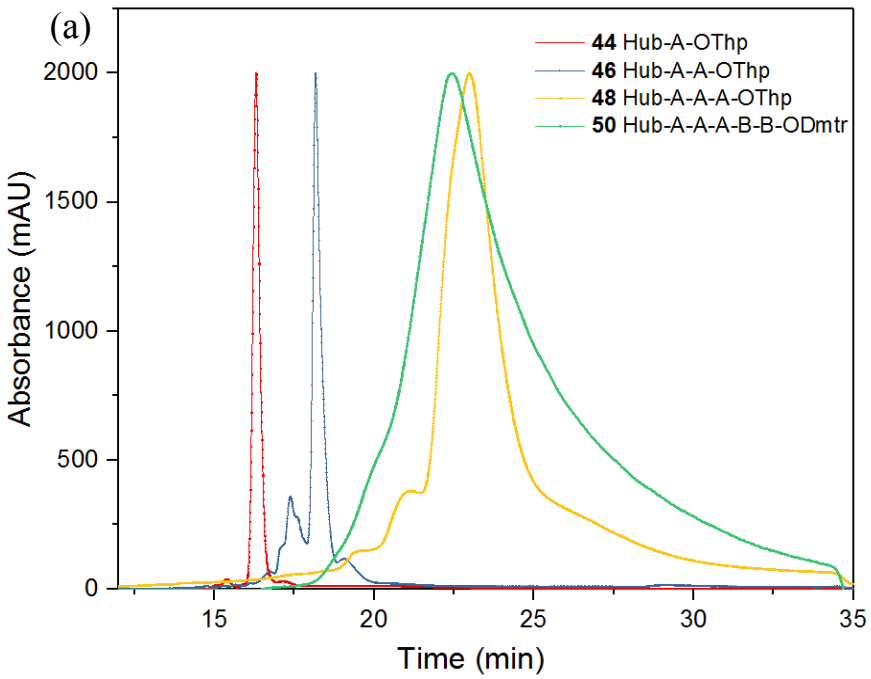
Membrane: PBI18_CC001_DBX/JM2005_003 **Solvent: MeOH : MeCN (1:1); Solute: A is Octyl building block and B is linear building block**										
Hub-A-A-A										
Diafiltration	Solute starting mass (g) (±0.001)	Rejection (±2%)		Permeance ($L \cdot h^{-1} \cdot m^{-2} \cdot bar^{-1}$) (±0.02)	Ending Mass (g) (±0.001)		Yield (±1%)		Purity (±1%)	
		BB	Hub product		Ret	Perm	HPLC	Mass	NMR	HPLC
D1	Hub-A / A (1.013)	21%	90%	3.06	0.337	0.643	84%	85%	≥98%	≥99%
D2	Hub-A-A/A (2.018)	22%	93%	2.99	0.407	1.593	87%	91%	≥99%	≥99%
D3	Hub-A-A-A/ A (1.248)	28%	97%	3.06	0.501	0.730	96%	98%	≥99%	≥99%
Hub-A-B-A-B-A										
D1	Hub-A / A (1.013)	21%	90%	3.06	0.337	0.643	84%	85%	≥98%	≥99%
D4	Hub-A-B/ B (1.317)	24%	94%	3.08	0.505	0.764	88%	93%	≥99%	≥99%
D5	Hub-A-B-A/A (0.982)	25%	97%	3.13	0.487	0.444	95%	94%	≥99%	≥99%
D6	Hub-A-B-A-B/B (0.902)	28%	98%	3.00	0.453	0.405	97%	95%	≥99%	99%

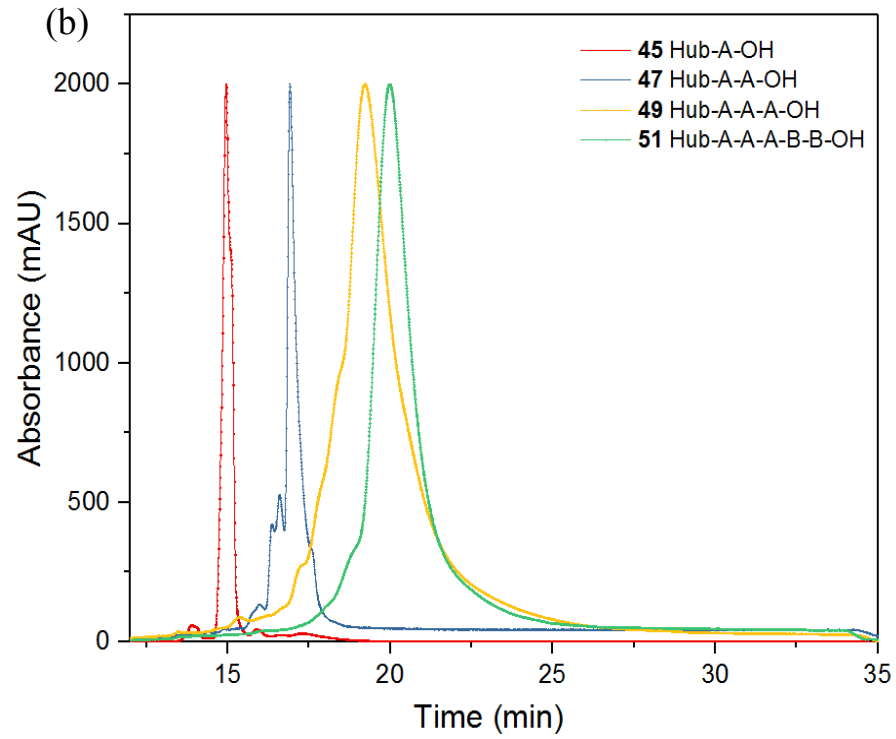
A long 3 cm diameter, porosity 3, glass sinter funnel was used for a reverse phase column chromatography. The crude mixture of Hub(OEG$_8$**ABABA**OThp)$_3$ **58** with incomplete arms was fractionated and eluted with a gradient of acetone-water (1:99 to 90:10, v/v). Every 20 mL was collected as a fraction. Samples were taken from each fraction and analysed by HPLC system. The impurity and the product showed two distinct peaks on the HPLC spectrum due the strong hydrophobicity from one single monomer **A**. The reverse phase column chromatography separated impurity from product in a high purity. The Maldi-Tof of the final product Hub(OEG$_8$**ABABA**OThp)$_3$ **58** confirmed the success of the chromatography.

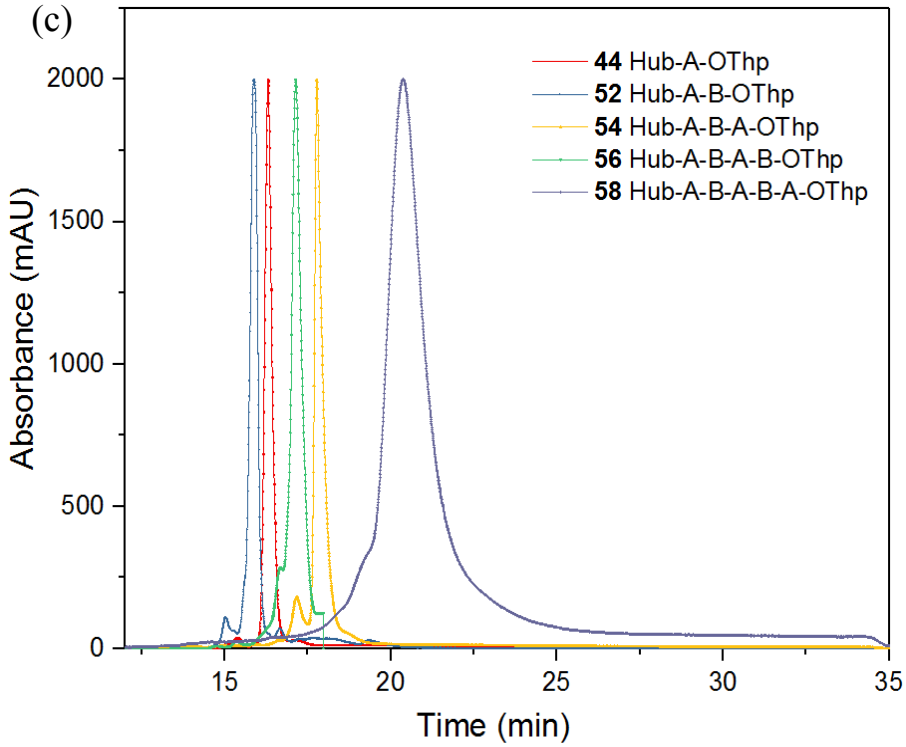
In general, HPLC online monitoring played an important role to determine the reaction progress and quality control. For monitoring the deprotection reaction, the retention times of the protected and deprotected homostar had less significant difference, due to the small Thp protecting group: only one minute difference after the Thp cleavage. All the intermediates up to the Hub(OEG$_8$**AAABB**OH)$_3$ **51** gave HPLC peaks, as shown in Figure 6.17, at both protected and deprotected stages. It was observed that the retention time was significantly lengthened with the growing of octyl building blocks; however the homostar reamined at a similar retention time with the growing of the linear building blocks. The Hub(OEG$_8$**ABABA**OH)$_3$ **59** intermediates exhibited similar patterns in their HPLC profiles, which are shown in Figure 6.17. However, the peaks of all the homostars appeared with neighbouring shoulder like peaks, with the addition of the hydrophobic octyl building block (**33**, A). The shoulders were suspected as being incomplete 2-arm homostar; however, the Maldi-ToF proved the high purity of the 3-arm homostar. Therefore the HPLC sprectrum's roughness is thought to be an HPLC artefact. The final PEG homostar products were purified as pale yellow oils on the scale of 100 mg. The products were readily soluble in most organic solvents such as MeOH, MeCN, THF, CH_2Cl_2, $CHCl_3$, DMF and dimethyl sulfoxide (DMSO). Although the pure polymer backbone HOEG$_{33}$OH is a semi-crystalline solid, the PEG homostar with EG$_{33}$ backbone appeared as oily form. This is possibly due to the effect of the side-arms on the intermolecular packing of the PEG backbone.

The molecular structures of all growing homostar intermediates and products were verified by NMR and Maldi-ToF-MS**.** The Maldi-ToF spectrum showed the observed m/z value of the expected molecular ion $[M+H]^+$ for **50** was 6683, which is consistent with the calculated molar mass of 6682.21 Da. There were also three fragmentation peaks observed with the molecular

ion at m/z 5774-6380 due to loss of Dmtr groups from each arm, which gave $[M\text{-}n(Dmtr)+H]^+$ (n=1-3). For the other synthetic polymer **58**, the Maldi-ToF spectrum showed the observed m/z value of the expected molecular ion $[M+Na]^+$ of 6002.7. Similar fragmentation peaks were observed with the molecular ion, due to loss of Thp groups from each arm, which gave $[M\text{-}n(Thp)+Na]^+$ (*n*=1-3). Despite the shoulder in the later HPLC chromatograms, there was no sign of polyether-star contaminants with deletion sequences and the synthesized polymers were highly pure. The Maldi-ToF results at each synthesis cycle confirmed the accurate sequence order of both polymers.




(b)
45 Hub-A-OH
47 Hub-A-A-OH
49 Hub-A-A-A-OH
51 Hub-A-A-A-B-B-OH
Absorbance (mAU)
2000
1500
1000
500
0
15
20
25
30
35
Time (min)


(c)
44 Hub-A-OThp
52 Hub-A-B-OThp
54 Hub-A-B-A-OThp
56 Hub-A-B-A-B-OThp
58 Hub-A-B-A-B-A-OThp
Absorbance (mAU)
2000
1500
1000
500
0
15
20
25
30
35
Time (min)

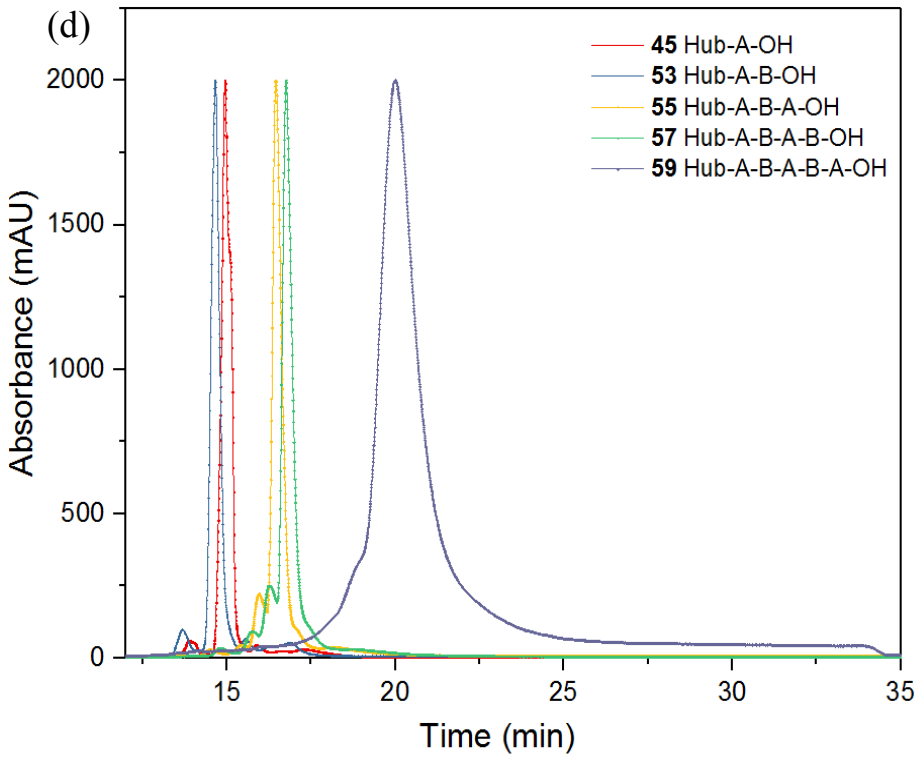


Figure 6.17 HPLC traces of purified sequence-defined intermediates and products after each chain extension and deprotection (a-d).

6.4.2.3. The influences of side chain and its position in coupling reactivity

As discussed in Section 6.4.1, there are two types of octyl branched PEG building blocks with different positions of the incorporated octyl chains, namely compounds **25** and **33**. In the first attempt of the chain extension study, building block **25** with octyl chain in the β position was used to prepare the Hub(OEG$_8$**AAABB**OH)$_3$ **51** sequence. Although the first coupling between Hub(OEG$_8$OH)$_3$ and monomer **A** went to completion within 12 hours, the next reaction to prepare Hub(OEG$_8$**AA**OThp)$_3$ **46** faced a significant challenge to reach completion. Different reaction conditions including reaction solvents, reaction temperatures and drying methods were experimentally tested to improve the coupling efficiency. The methodology referred to the Chapter 5 chemical kinetic study. However there was still 1/3 of incomplete 2-arm products which did not convert after 110 hours. The HPLC spectra monitoring coupling reactions for Hub(OEG$_8$**A**OThp)$_3$ **44** and Hub(OEG$_8$**AA**OThp)$_3$ **46** are shown in Figure 6.18.

The coupling efficiency was significantly improved by altering the building block to **33** with the side chain located in the middle of the PEG building block. The reaction rate to form Hub(OEG$_8$**A**OThp)$_3$ **44** with monomer **33** was exactly the same as monomer **25**. Whereas the reaction rate to obtained Hub(OEG$_8$**AA**OThp)$_3$ **46** went much faster with monomer **33** compared to monomer **25**. The second coupling for Hub(OEG$_8$**AA**OThp)$_3$ **46** was completed in 48 hours. The Maldi-Tof spectrum confirmed the conclusion from HPLC.

The slow coupling rate when preparing Hub(OEG$_8$**AA**OThp)$_3$ from monomer **25** was suspected as being due to steric hindrance caused by the long octyl chains from both starting material Hub(OEG$_8$**A**OH)$_3$ **45** and building block **25**. The long octyl chains may cause repulsions between the bulky homostar and the building block, reducing the contact chance between different chemical species and resulted in low coupling efficiency. In particular, the octyl side chain at the end of the building block from the starting material Homostar may also entangle and embrace the OH reactive site next to the octyl side chain. Therefore the location of the side chain could affect the coupling rate in the reaction.

During the third reaction to prepare Hub(OEG$_8$**AAA**OThp)$_3$ **48**, surprisingly the coupling did not reach completion, although building block **33** was used. The HPLC spectrum showed about 10% of the two-arm Hub(OEG$_8$**AAA**OThp)$_3$ **48** could not proceed further. As was discussed, the accumulation of the tangling hydrophobic octyl side chains may give an adverse effect on the homostar coupling efficiency. In order to continue the synthesis of Hub(OEG$_8$**AAABB**OH)$_3$ **51**, a reverse phase column chromatography with a gradient of acetone-water (1:99 to 90:10, v/v) was used. The chromatography separation relied on the different number of hydrophobic monomers **A** between the completed product and the impurity. The products had 3 arms of **AAA**, while the incomplete impurity contained 2 arms of **AAA** and 1 arm of **AA**. Every 20 mL fraction was collected. Samples were taken from each fraction and analysed by HPLC system. The reverse phase column chromatography separated impurity from product in a high purity. The Maldi-Tof of the final product **48** confirmed the success of the chromatography. The addition of the final sequence **BB** to the Hub(OEG$_8$**AAA**OH)$_3$ **49** to form Hub(OEG$_8$**AAABB**OH)$_3$ **51** went smoothly within 48 hours; probably, because there was no increasing number of monomer **A** the coupling rate was not affected significantly. The influence of the monomer side chain and its position on coupling efficiency needs further investigation. For example, shorter alkyl chains with different side chain positions and hydrophilic side chains could be trialled to prove the hypothetical explanation.

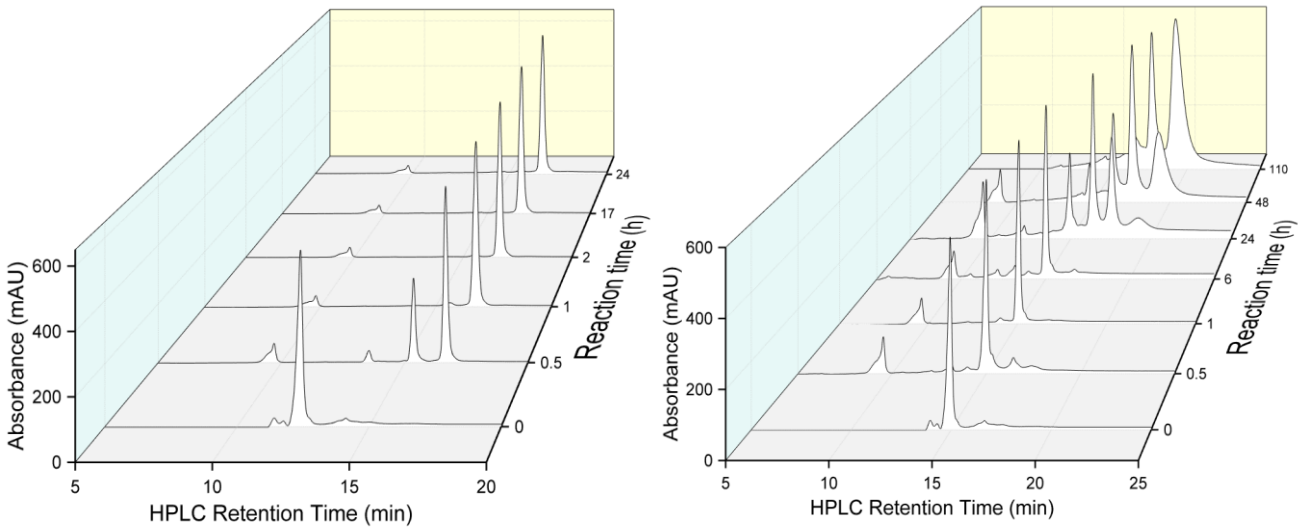


Figure 6.18 The HPLC reaction progression of the 1st and 2nd chain extensions using Hub(OEG$_8$OH)$_3$ and octyl building blocks A **25**.

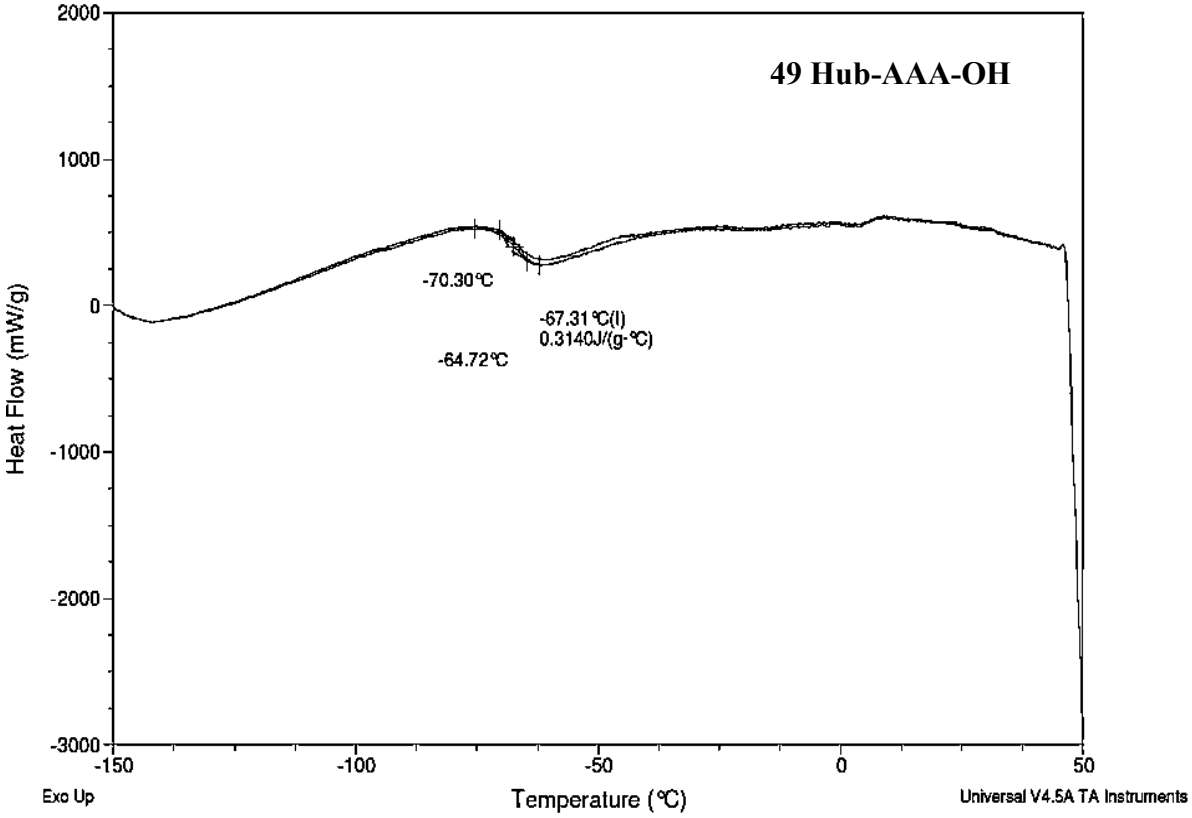
6.4.2.4. Polymer properties characterisation

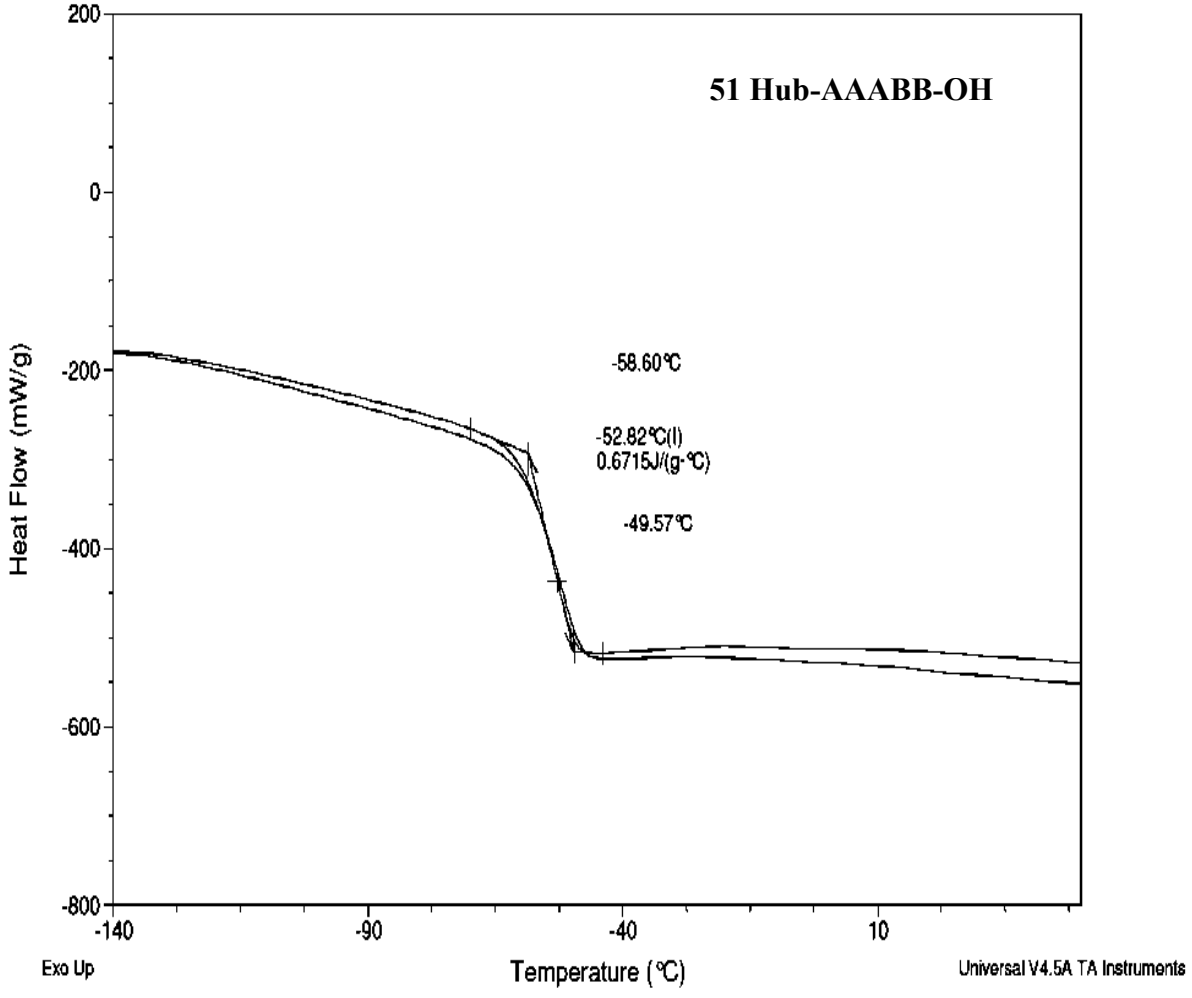
It has been reported in many publications that sequence order in sequence-defined polymers can influence some macroscopic polymers properties. After synthesizing two sequence-defined polymers, the physical properties such as UV-Vis and glass transition temperature of polymers were tested. The observation of different characteristics for the different sequence orders in the polymer would open up opportunities for controlling the structural and macroscopic properties of macromolecular materials.

Two synthetic polymers with the same number of two monomers, but different sequences, Hub(OEG$_8$**AAABB**OH)$_3$ **51** and Hub(OEG$_8$**ABABA**OH)$_3$ **59**, were used here. Also the intermediate Hub(OEG$_8$**AAA**OH)$_3$ **49** was included in the polymer properties characterisation, as it had the same number of hydrophobic monomer **A** but no hydrophilic monomer **B**, which resulted in different hydrophobicity ratios compared to the two final synthetic polymers.

Differential scanning calorimeters (DSC)

Differential scanning calorimetry (DSC) is a technique used to investigate the response of polymers to heating. Here the DSC was used to study the glass transition of the synthesized homostar polymers. The temperature cooling loops, between -150 ℃ to 50 ℃, were run repetitively. In such a cold temperature, the polymers in their molten states were cooled and they would reach their glass transition temperatures (Tg). When polymers are in their glass states their mechanical properties change from those of an elastic material to those of a brittle one, due to changes in chain mobility. The heat flows of the polymers were different before and after the glass transition temperature and steep drops in their cooling profiles were observed. The temperature in the middle of the inclined region was taken as the Tg. The cooling temperature loops of the three polyethers (**49, 51** and **59**) are shown in Figure 6.19 with different scales on each x-axis. The glass transition temperatures are -67℃, -53℃ and -59℃ respectively. This difference in glass transition temperatures shows that the polymer sequence order and the hydrophilic-hydrophobic balance of different monomers influenced the thermal properties of the polymers. The incorporation of more hydrophilic ethylene glycol oligomers increased the glass transition temperatures from the intermediate Hub(OEG$_8$**AAA**OH)$_3$ **49**, which had the lowest Tg of -67℃. Furthermore, the polymer with sequence order of Hub(OEG$_8$**AAABB**OH)$_3$ **51** had a slightly higher Tg than the alternating sequence order of Hub(OEG$_8$**ABABA**OH)$_3$ **59**, indicating differences from sequence order and not just molecular composition.


49 Hub-AAA-OH
2000
1000
0
-1000
-2000
-3000
Heat Flow (mW/g)
-70.30℃
-67.31℃(I)
0.3140J/(g·℃)
-64.72℃
-150
-100
-50
0
50
Exo Up
Temperature (℃)
Universal V4.5A TA Instruments


51 Hub-AAABB-OH
200
0
-200
-400
-600
-800
Heat Flow (mW/g)
-58.60℃
-52.82℃(I)
0.6715J/(g·℃)
-49.57℃
-140
-90
-40
10
Exo Up
Temperature (℃)
Universal V4.5A TA Instruments

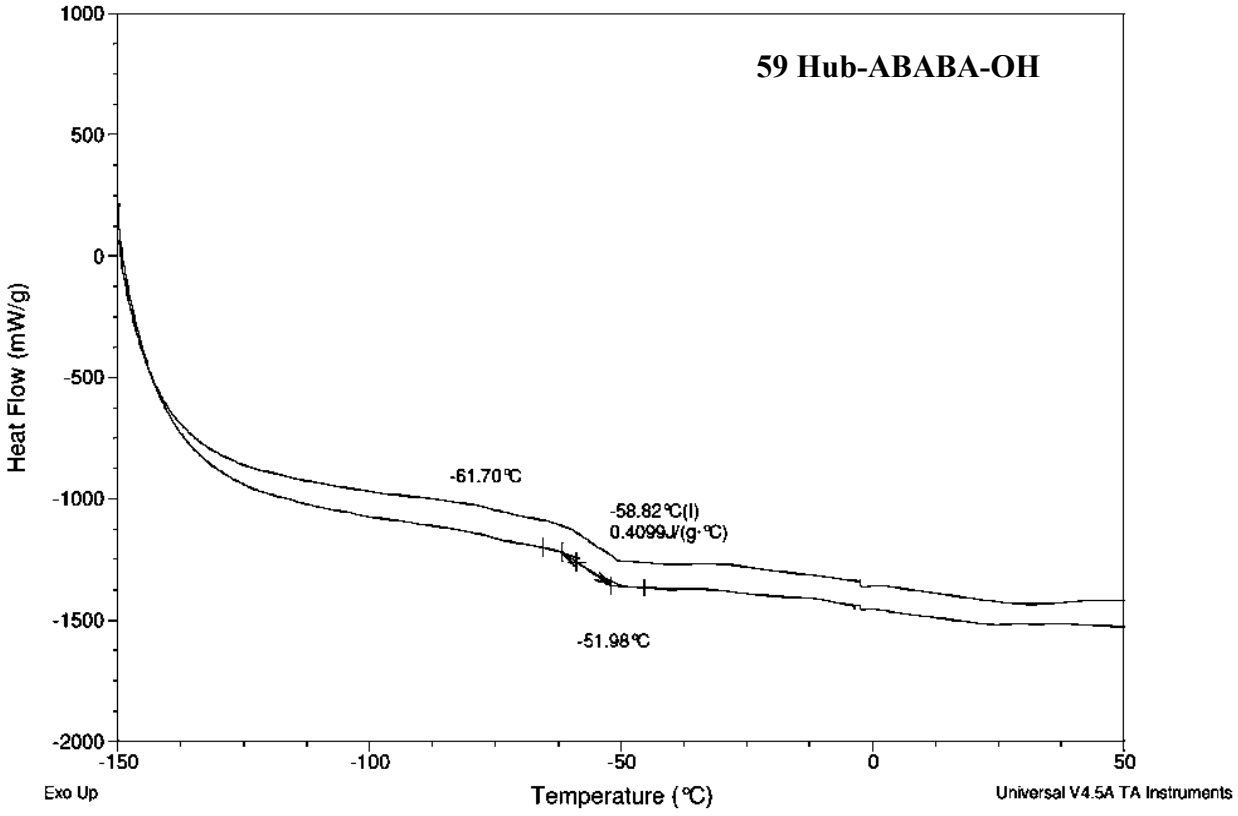


Figure 6.19 DSC temperature cooling profiles of hub-**AAA**, hub-**AAABB** and hub-**ABABA**.

UV-Vis Absorption Spectrometry

The variation in optical behavior with the composition of the pendant side-arms of the two resulting polyethers and Hub(OEG$_8$**AAA**OH)$_3$ **49** was evaluated by UV-Vis. All the polymers were dissolved in DCM in the same concentration, as shown in Figure 6.20. Although the position of the octyl chain and the hydrophobicity distribution were different, all three polyethers (**49, 51** and **59**) showed UV-Vis absorption bands at 295 nm. There was no difference in optical behaviour for all the polyethers in DCM; this may be due to the central homostar dominating the UV absorptions. The effects of the composition of the sequence-defined polyethers on the optical properties cannot be determined without hub cleavage.

The macrostructures of the homostar products gave interesting polymer features; therefore all three polyethers with homostar structures (**49, 51** and **59**) were kept for further polymer property characterisations. In addition the technique of hub cleavage needs further investigation. Both traditional hub cleavage using hydrogennolysis and a new approach using BCl_3 treatment were not successful with chromatography purification. The yields of the PEG polymer sequence were both low and the obtained quantities were even inadequate for property characterisations. Therefore the investigation of a new hub cleavage approach or changes to the reaction conditions needs to be carried out in future work.

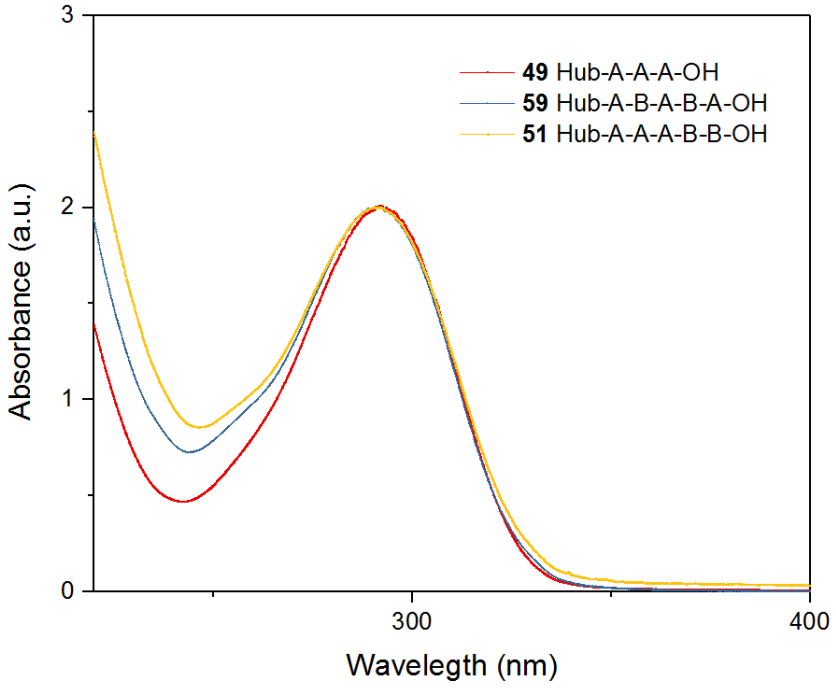


Figure 6.20 UV- Vis spectrums of hub-**AAA**, hub-**AAABB** and hub-**ABABA**.

6.5. Chapter conclusions

A general and versatile PEG building block approach was demonstrated to synthesize PEG building block structures with different side-arm functionalities. The obtained building blocks were used to prove the concept of ItSyN. Two sequence-defined synthetic PEG polymers with octyl side-chain functionalities were precisely assembled via iterative synthesis.

The design of the PEG building blocks was determined by the choice of protecting group, leaving group, types and incorporations of the side chain and polymer chirality.

Tetrahydropyranyl (Thp) was chosen as the final protecting group of the PEG building block chain termini. During the synthesis, it was shown that the Thp group offers good chemical stability. The size of the tetrahydropyranyl acetal is relatively small for membrane purification by removing excess protected building blocks. The choice of the octyl chain as the side chain introduced the hydrophobic property to the building block. This resulted in some interesting physical features for the fabricated polymers. The octyl side chain is compatible for all the reaction conditions in chain extension, deprotection and purification. Therefore, it offers a good opportunity to establish the basic processes of iterative synthesis and diafiltration before exploring site-selective post-polymerization modification of other side chains.

Two chemical synthetic approaches of preparing α, ω-end-functionalised pentagol monomers were reported. They were differentiated by the incorporation position of the side chain using different lengths of assembly units. The flexible side chain insertion showed great potential for more structural diversity using the proposed approaches. A chiral centre has been was designed in the building block to construct chiral macromolecules. Sharpless' catalytic asymmetric dihydroxylation and crystallisation were used in the chemical synthesis to improve the optical purity of the building block. The purities of the intermediates and the final building block were examined by GC, HPLC, NMR and MS. The synthesis process was also scaled up gradually in three rounds with increasing yields. The final purity of the building blocks with functionalised side chain was 99% on multi-gram scales.

Using octyl branched building blocks and linear building blocks, two sequence-defined synthetic polyethers with octyl side-chain functionalities were produced in high purity using the versatile liquid phase ItSyN process. A chiral α, ω-end-functionalised pentagol monomer with an octyl side chain and a linear tetragol with α, ω-end-functionalised were prepared and assigned the coding letters **A** and **B** respectively. Two sequence-defined polymers **AAABB** and **ABABA** were constructed in this chapter by repeated etherification of the monomers growing from a central three-armed macromolecule (hub).

The 18 wt% PBI-DBX-M2005 membrane was used in the diafiltration with MeCN-MeOH (1:1). It gave excellent permenace of 5.3 L m^{-2} h^{-1} bar^{-1} and good selectivity with a rejections hub of 92% and a building block of 42%. It was able to separate the various reaction debris from the homostar product rapidly and efficiently. The overall yield of each diafiltration cycle was about 85%-98%. The online monitoring during each cycle of coupling/deprotection and

membrane purification prevented the accumulation of inaccurate or incomplete polymer sequences.

The two obtained polymers with different sequence orders and one intermediate were subjected to two polymer properties characterisations, both UV-Vis and differential scanning calorimetry. In particular, the different glass transition temperatures from DSC showed that the polymer sequence order and the hydrophilic-hydrophobic balance of different monomers influenced the thermal properties of the polymers. The incorporation of more hydrophilic ethylene glycol oligomers increased their glass transition temperatures and the block sequence order of Hub(OEG$_8$**AAABB**OH)$_3$ had a slightly higher glass transition temperature than the alternating sequence order of Hub(OEG$_8$**ABABA**OH)$_3$.

The chemical synthesis with membrane separation took advantage of fast liquid-phase reaction kinetics to allow reactions to reach completion and membrane separation. This ItSyN process improved the sequence accuracy, purity, yield and potential scalability of target polymers. It opens up opportunities for controlling the structural and macroscopic properties of the macromolecule materials by tuning the polymer construction. Future work with site-selective post-synthetic modification could also provide a versatile pathway to precisely control side-chain structures and functions.

7. Conclusions and recommendations for future work

7.1. Conclusions

It is known that the monodispersity and sequence precision of polymers significantly affect their functionalities and properties, and also offer an important opportunity for more accurate polymer characterisation in research. Such well-characterised polymers with controlled sequence and properties have a wide range of applications, and especially offer high value in drug delivery and therapeutics. Therefore, monodisperse and sequence-defined polymers were the target of this project.

Ultimately, the new concept of iterative synthesis with organic solvent nanofiltration (ItSyN) for synthesizing highly pure monodisperse, sequence-defined polyethylene glycol (PEG) polymers was pioneered. In this method, monomers are added iteratively to the growing polymer chains and all impurities are removed after each cycle with organic solvent membrane separation. This new approach was designed to overcome the problems of conventional solid phase synthesis and other industrial polymerisation methods, such as inaccurate polymer sequence, poor reaction kinetics, difficulty with online purity monitoring to facilitate high purity, and scaling up for high yield. ItSyN provides new benchmarks in the field of sequence-defined polymer synthesis, and represents the most advanced technology for the synthesis of sequence-defined polymers with a polyethylene glycol (PEG) backbone.

A side-chain alphabet designed specifically for PEG ItSyN was developed and characterised; whilst it was small, consisting of only two letters, it nevertheless offered different side-chain functionalities, and was shown to have utility for tuning polymer structure and complexity. Furthermore, manufacture was scaled up to the gram level and a versatile set of building block fabrication reactions were developed. This could open up a wide range of applications - for healthcare, nanotechnology and data storage - and marks a significant milestone in the realisation of mature ItSyN technology.

After preparatory investigation - the design of the building block, the implementation of an appropriate OSN membrane in diafiltration, and the discovery of a number of favourable reaction conditions - two innovative sequence-defined PEG polymers were synthesized by

ItSyN; they achieved high purity and good yield, consisting of two 5-mers with the same sequence composition but different monomer order. The physical properties of the obtained polymers were characterised to prove the diversity of polymer properties achievable using the ItSyN platform.

The development of ItSyN to fabricate monodisperse linear PEG polymers of high molecular weight was also investigated. This was not successful so a series of monodisperse PEG kinetic studies were carried out to resolve the problems of incompletion and incorrect chain extension, as discussed below.

The following sections summarise the main conclusions from the different sections of work that have been reported in this thesis.

7.1.1. Preparation of OSN PBI membranes with enhanced chemical stability and selectivity for ItSyN and harsh chemical environments

In order to operate the process in a fully liquid environment, organic solvent nanofiltration (OSN) membranes were fabricated from polybenzimidazole (PBI) with different surface modifiers. Surface modifications were discovered that enhances membrane stability in harsh chemical environments, which are ideal for chemical synthesis separation. In addition, surface modifiers with different chain lengths and hydrophobicity significantly influenced membrane performance. Longer surface modifiers offered greater resistance inside the pore channels and resulted in tighter membrane structures, whereas the shorter surface modifiers could penetrate further inside the membrane and react more on the interior of the membrane channel. A case study showed that surface modification plays an important role in determining membrane selectivity and permeance. For application to different solvents and solutes, membrane pore size can be tuned by surface modifiers with different hydrophobicity, interactions and functionalities.

7.1.2. The design of the soluble support and building block assembly

The design of the soluble three-armed support enables the ItSyN process to operate in a fully liquid environment. The three unidirectional growing chains triple polymer production and enlarge the size of the homostar product to facilitate retention by the membrane while the

impurities are removed with the solvents. Therefore, it improves the chain extension efficiency and membrane performance.

The design of the monodisperse linear building blocks $TsOEG_{28}ODmtr$ and chiral α, ω-end-functionalised pentagol monomers with an octyl side-arm has been established. The study of their protecting groups has enhanced product stability during the reaction and diafiltration, whilst ensuring they can be cleaved during deprotection without damaging the product. It has been demonstrated that the position and chirality of the side chains can be altered along the PEG chain, showing the usefulness of PEG backbones for sequence controlled polymers. Different functional side chains on the building blocks enrich the diversity of sequence-defined polymers that can be synthesised with site-selective modifications. This approach is general and versatile and showed a great potential to assemble a variety of PEG building block structures with different functionalities. The optical purity of the final building block was over 99% and the production scale can be grams with good yields in each synthetic step.

7.1.3. Kinetic studies of chain extension using long, linear building blocks

A series of chemical kinetic studies of building block coupling was reported using the asymmetric modified monomer EG_{12} and EG_{28}. The completion of each etherification reaction on the three armed support is critical to avoid the accumulation of inaccurate or incomplete polymer sequences after each cycle. In order to increase the coupling rates and minimise the formation of the impurities, the effects of different reaction conditions were investigated. It was found that changes to common reaction factors, such as reaction concentrations, temperatures and base equivalent, all improved coupling efficiency but the rates of the impurities also increased. Therefore other parameters such as reaction solvents, drying methods and the reaction kit were investigated. It was found that surface passivation of the reaction flask is can limit the formation of impurities while increasing other reaction conditions for more efficient coupling. Although the long building blocks are appealing because they require fewer chain extension cycles to reach targeted polymers, the building block $TsOEG_{28}ODmtr$ has low coupling efficiency, probably due to the entangled long polymer chain embracing reactive sites. Therefore, the shorter building block $TsOEG_{12}ODmtr$ was used for monodisperse polymer chain extension, the first chain extension had at least 99.6% coupling completion of the 3-arm in 12 hours.

7.1.4. The development of the ItSyN process with product characterizations

After the establishing the building block assembly and OSN membrane fabrication, two sequence-defined polymers, consisting of the same numbers of chiral octyl building blocks and linear building blocks, but in different sequence orders, were fabricated by the ItSyN process. By considering the size difference between the three-armed hub and building blocks, the 18 wt% PBI-DBX-M2005 membrane showed excellent permeance of 5.3 L m^{-2} h^{-1} bar^{-1} and high selectivity with a hub rejection of 92% and a building block rejection of 42% in MeCN-MeOH (1:1). A cascade membrane system was designed and the chosen membrane was installed for use in purification. The rejection of the growing homostar product increased from approximately 90% to 98% as more building block were added, while the building block rejection remained roughly the same. The two sequence-defined polymers were synthesized in a good yield and purity. The polymer characterisations UV-VIS and DSC were carried out with both sequence-defined polymers, which showed that the sequence order of the polymers influenced the physical properties of the polymers.

The ItSyN process was proved as a versatile platform on which to synthesize a wide diversity of sequence-defined polymers with good purities and yields. It shows the potential to tune polymer structures and physical properties by controlling the polymer sequence order for applications in nanotechnology, healthcare and information storage.

7.2. Recommendations for future work

7.2.1. Investigate the cascade membrane system and its scale up

Although a cascade membrane rig has been established and the concentration profile of the separating components were monitored, the cascade membrane system has not been studied. The solute concentration that worked in the rig so far was dilute, at 5 g L^{-1}, due to the limited product production scale. Therefore, it is important to understand membrane behaviours and performance with different mass loadings and solute concentrations. For example, when in high concentration, factors such as concentration polarisation and surface absorbance effects may become significant to membrane rejection and permeance. In future work, it would be worth investigating the maximum boundary of the solute concentration for the cascade membrane rig in order to maintain stable purification performance. In addition, the membrane fabrication

could be scaled up to industrial scale, especially by studying the process of fabricating the spiral-wound module and the separation performance.

7.2.2. Prepare building blocks with more diversity

The approach to building block assembly that has been proposed should be general and versatile. However, in the study it was only demonstrated in PEG polymers with an inactive octyl side chain and R-chiral centre. Therefore a wider range of side chain functionalities, backbone chemistries, and chirality could be studied. This is the best way to prove the versatility of this synthetic approach. A wider variety of building blocks would enrich the structural and functional diversity of the sequence-defined polymers achievable via iterative synthesis. In addition, site-selective modifications of the side-arms of the building blocks could be also designed. With the precise control over polymer sequence, the attachment of targeting molecules, imaging agents or drugs could be accomplished in precise locations in the macromolecules for healthcare applications and information storage.

7.2.3. Synthesise monodisperse PEG (5000 Da) via ItSyN

One of the original objectives of this work was to prepare monodisperse PEG polymers $HOEG_{112}OH$ (Mw=4952 Da) with an excellent purity via the ItSyN process. The chain extension could be started with $Hub(OEG_{28}OH)_3$, followed by seven couplings with successive additions of building block $TsOEG_{12}ODmtr$. Based on the discoveries from the kinetics study, the optimised reaction conditions could be applied in the chain extensions with a quick UPLC online monitoring system. The purities and the yields of intermediate products after each cycle should be strictly examined and assessed. Once the desired target length is attained, the chain backbone could be functionalized and cleaved from the hub via hydrogenolysis to yield the linear, uniform, heterobifunctional PEG polymers.

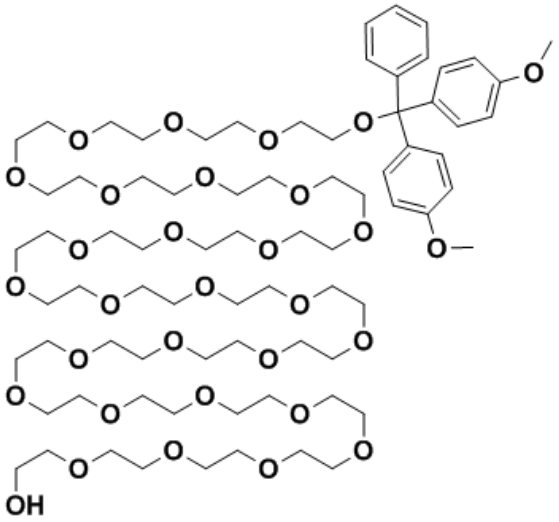
7.2.4. Study site modification and characterise chiral sequence-defined polymers

Only two sequence-defined polymers were synthesised and characterised in this preliminary study. Given an increased variety of building blocks with different chirality and side chains,

more types of sequence-defined polymer could be synthesized to verify the versatility of the ItSyN process. For example, the effect of controlling sequence order, with different side chain functionalities, on polymer properties such as conformational structure and self-assembly in solvents, polymer morphology and other physical properties, could be determined. Furthermore, the chiral structures and crystalline forms of sequence-defined macromolecules, with multiple chiral centres, could be investigated. The study of site modification and physical characterisations would be useful for controlling and tuning polymer properties and functionalities via polymer sequence order.

8. Chemical synthesis experimental procedures

HOEG$_{28}$ODmtr (3)



Monodisperse HOEG$_{28}$OH (**2,** 10.9 g, 8.74 mmol) was co-evaporated from anhydrous MeCN (3 × 50 mL) and dissolved in CH_2Cl_2 (28.6 mL) with Et_3N (2.4 mL, 17.5 mmol, 2 equiv.). To the well stirred solution was slowly added 4, 4'-dimethoxytriphenylmethyl chloride (2.96 g, 8.74 mmol, 1 equiv.) in CH_2Cl_2. The reaction was stirred for 2 hours and partitioned with half-sat. $NaHCO_3$ (3×100 mL). The combined organic layers were dried over Na_2SO_4, and the solvent was stripped off under reduced pressure. The crude (**3**, 14.7 g) was fractionated by a reverse column chromatography, eluting with a gradient of acetone-water (10:90 to 90:10, v/v), all solvents containing 1 vol% sat.$NaHCO_3$ to afford the title compound as a pale yellow oil (**3**, 7.2 g, 53 %).

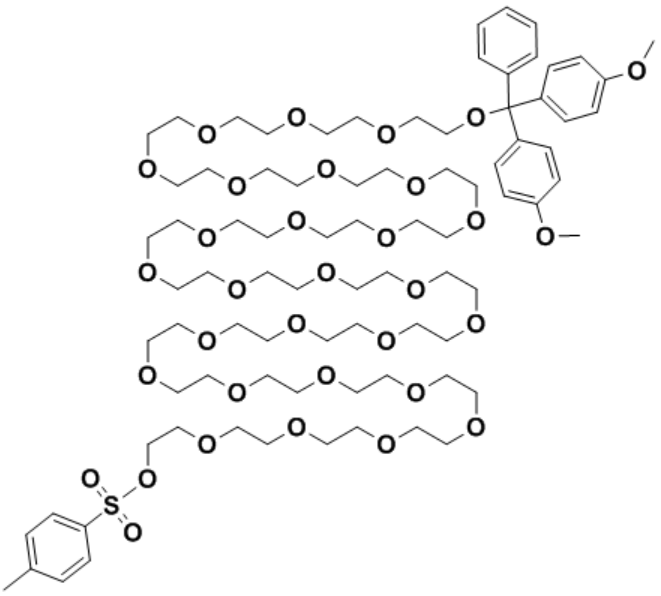
R_f (MeOH-$CHCl_3$ 1:19 + trace Et_3N) = 0.35.

^{1}H NMR (400 MHz, $CDCl_3$) δ = 7.43 (dd, J = 7.8, 1.7 Hz, 2H), 7.33 (d, J = 8.5 Hz, 4H), 7.14 (d, J = 7.5 Hz, 2H), 7.16 (d, J = 7.3 Hz, 1H), 6.79 (d, J = 8.8 Hz, 4H) (13×Dmtr C***H***), 3.76 (s, 7H, 2×ArOC***H$_3$*** + C***H***OH), 3.73 – 3.51 m, 109H, 55×C***H$_2$***O), 3.20 (t, J = 5.2 Hz, 2H, C***H$_2$***ODmtr).

^{13}C NMR (101 MHz, $CDCl_3$) δ = 158.34(2C), 145.06, 136.31, 136.13(5×Ar ***C***), 130.02(4C), 128.17(2C), 127.68(2C), 126.59, 112.99(4C) (13×Ar ***C***H), 85.88(O***C***Ar$_3$), 72.59(***C***HOH), 70.54, 63.12, 61.62(55×***C***H$_2$O), 55.16(2C, O***C***H$_3$),

***m/z* (ESI$^+$)** $[M+Na]^+$ = 1576.8, *calc.* $C_{77}H_{132}O_{31}Na^+$ = 1576.8.

TsOEG$_{28}$ODmtr (4)



HOEG$_{28}$ODmtr (**3,** 9.16 g, 5.9 mmol) was evaporated from anhydrous MeCN (3 × 50 mL) and re-dissolved in CH_2Cl_2 (45 mL). To the solution were added Et_3N (2.5 mL, 17.7 mmol, 3 equiv.), *N*-methyl imidazole (0.47 mL, 5.9 mmol) and toluene sulfonyl chloride (1.46 g, 7.66 mmol, 1.3 equiv.), and the reaction was stirred for 6h at room temperature. The solution appeared orange-brown and the reaction was quenched with $NaHCO_3$ (1.29 g, 15.3 mmol, 2.6 equiv.) with vigorous stirring. Then the mixture was partitioned with the original CH_2Cl_2, the aqueous layer was extracted with further CH_2Cl_2 (2 ×100 mL). The combined organic layers were dried over Na_2SO_4, and the solvent was stripped off under reduced pressure. The crude residue was fractionated by chromatography on flash silica, eluting with a gradient of MeOH-$CHCl_3$ (1:99 to 10:90, v/v), all solvents containing 1 vol% Et_3N, to afford the title compound as a pale yellow oil (**4**, 8.86 g, 88%).

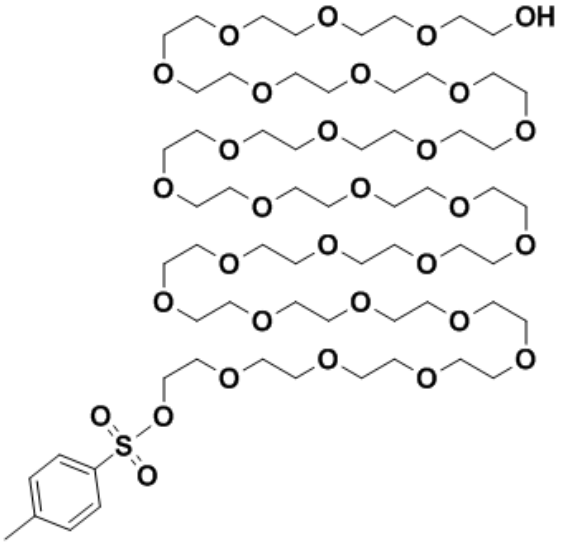
R_f (MeOH-$CHCl_3$ 1: 9 + trace Et_3N) = 0.5

^{1}H NMR (400 MHz, DMSO-*d*$_6$) δ = 7.75 (d, *J* = 8.4 Hz, 2×Ts C***H***), 7.42 (dd, *J* = 8.4, 1.3 Hz, 2×Dmtr C***H***), 7.31 (dd, *J* = 8.8, 1.9 Hz, 6H, 2×Ts C***H*** + 4×Dmtr C***H***), 7.26 – 7.21 (m, 2H, ×Dmtr C***H***), 7.18 – 7.12 (m, 1×Dmtr C***H***), 6.81 – 6.75 (m, 4×Dmtr C***H***), 4.15 – 4.10 (m, 2H, C***H$_2$***OTs), 3.74 (s, 6H, 2×ArOC***H$_3$***), 3.68 – 3.52 (m, 108H,54×C***H$_2$***O), 3.19 (t, *J* = 5.2 Hz, 2H, C***H$_2$***ODmtr), 2.41 (s, 3H, ArC***H$_3$***).

^{13}C NMR (101 MHz, DMSO) δ=158.33(2×Ar ***C***), 145.06(Ar ***C***), 144.71(Ts ***C***), 136.30(Ar ***C***), 136.13 (Ar ***C***), 133.04(Ts ***C***), 130.01(4×Ar ***C***H), 129.78(2×Ts ***C***), 128.16(2×Ar ***C***H), 127.92(2×Ts ***C***), 127.67(2×Ar ***C***H), 126.58(Ar ***C***H), 112.99(4×Ar ***C***H), 85.87(O***C***Ar$_3$), 70.69, 70.53, 69.22, 68.63, 63.11 (56×***C***H$_2$O), 55.14(2C, O***C***H$_3$), 21.60(Ar***C***H$_3$).

***m/z* (ESI$^+$)** [M+Na]$^+$ = 1731.06, *calc.* $C_{84}H_{138}O_{33}SNa^+$ = 1731.06.

TsOEG$_{28}$OH (5)



To a solution of TsOEG$_{28}$ODmtr **(4**, 3.39 g, 2.18 mmol) in CH_2Cl_2 (10mL) was added pyrrole (0.76 mL, 10.9 mmol, 5 equiv.) and dichloroacetic acid (0.18 mL, 2.18 mmol).The reaction was briskly stirred for 45 minutes and quenched with sat. $NaHCO_3$. The resulting mixture was extracted with half-sat. $NaHCO_3$ (30 mL × 3), the combined organic layers were dried over Na_2SO_4, and the solvent was evaporated under reduced pressure. The residue was fractionated through a column of flash silica in a sinter funnel**.** The crude material (**5**, 3.14 g) was fractionated by chromatography on flash silica, eluting with a gradient of MeOH-$CHCl_3$ (1:99 to 5:95, v/v), to afford the title compound as a pale yellow oil (**5**, 2.83 g, 87%).

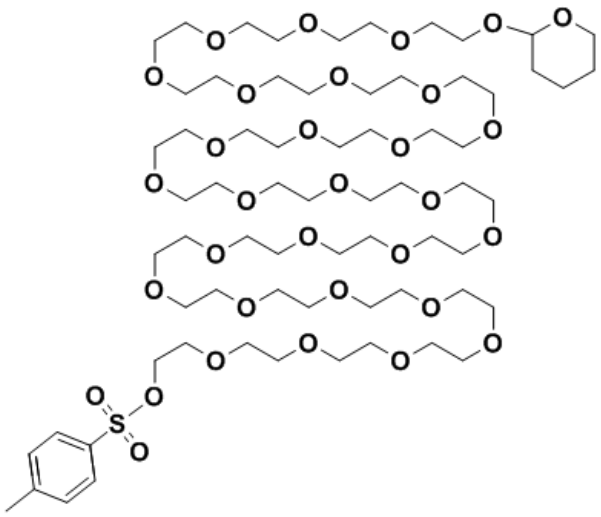
R_f (EtOH-$CHCl_3$ 1:19) = 0.25.

^{1}H NMR (400 MHz, CDCl$_3$) δ = 7.79 (d, J = 8.2 Hz, 2H, 2×Ts C***H***), 7.34 (d, J = 8.0 Hz, 2H, 2×Ts C***H***), 4.17 – 4.13 (m, 2H, C***H$_2$***OTs), 3.78 – 3.51 (m, 110H, 55×C***H$_2$***O), 3.45 (d, J = 4.0 Hz, 1H, CH$_2$O***H***), 2.44 (s, 3H, ArC***H$_3$***).

^{13}C NMR (101 MHz, $CDCl_3$) δ = 144.74, 133.05(2×Ts ***C***), 129.80(2C), 127.95 (2C) (4×Ts ***C***H), 70.55, 69.22, 68.66, 61.68 (56×***C***H_2O), 21.62(Ar***C***H_3).

***m/z* (ESI$^+$)** $[M+NH_4]^+$ = 1428.7, *calc.* $C_{63}H_{120}O_{31}SNa^+$ = 1428.7.

$TsOEG_{28}OThp$ (6)



$TsOEG_{28}OH$ (**5**, 2.73 g, 1.94 mmol) was co-evaporated from anhydrous MeCN (3 × 30 mL) and dissolved in CH2Cl2 (8.4 mL). To this mixture was added 3, 4-dihydro-2H-pyran (0.44 mL, 4.84 mmol, 2.5 equiv.) and making sure it was well stirred. A solution of p-toluenesulfonic acid (19.3 mg, 112 μmol, 0.01 equiv.) in 1 mL THF was slowly added with a drop of 0.1 mL per time. The extent of the reaction was monitored by TLC with every addition. The mixture was left to stir for 2 hours and quenched with sat. NaHCO3. The mixture was extracted with CH2Cl2 (3 ×100 mL), the combined organic layers were dried over Na2SO4, and the solvent was stripped off. The crude residue (**6**, 2.56 g) was fractionated by chromatography on flash silica, with a gradient of MeOH-$CHCl_3$ mixture (0.5:99.5 to 10:90, v/v), all solvents contained 1 vol% Et_3N, to afford the title compound as a yellow oil (**6**, 2.44 g, 85%).

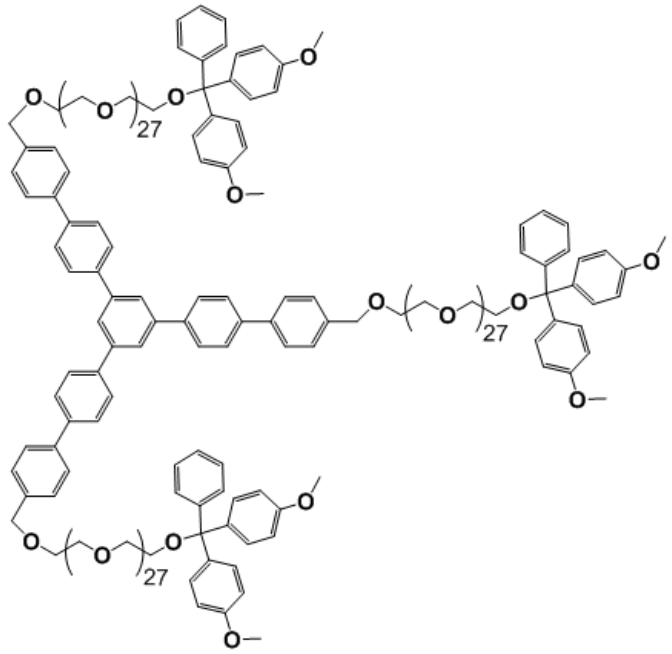
R_f (MeOH-$CHCl_3$ 1: 9 + trace Et_3N) = 0.36.

^{1}H NMR (400 MHz, $CDCl_3$) δ = 7.81 – 7.77 (m, 2H, 2×Ts C***H***), 7.36 – 7.32 (m, 2H, 2×Ts C***H***), 4.63 (dd, *J* = 4.3, 3.0 Hz, 1H, Thp C***H***), 4.19 – 4.09 (m, 2H, C***H$_2$***OTs), 3.73 – 3.35 (m, 110H, 56×C***H$_2$***O), 2.45 (s, 3H, ArC***H$_3$***), 1.90 – 1.37 (m, 6H, Thp C***H$_2$***).

^{13}C NMR (101 MHz, $CDCl_3$) δ = 144.73, 133.04 (2×Ts ***C***), 129.79(2C), 127.96(2C) (4×Ts ***C***H), 98.92(Thp ***C***H), 70.56, 69.22, 68.67, 66.64(56×***C***H_2O), 62.19 (Thp ***C***H_2O), 30.56(Thp ***C***H_2), 25.43(Thp ***C***H_2), 21.62(Ar***C***H_3), 19.47(Thp ***C***H_2).

***m/z* (ESI$^+$)** $[M+NH_4]^+$ = 1507.8, *calc.* $C_{68}H_{132}NO_{32}S^+$ = 1507.8.

Hub(OEG$_{28}$ODmtr)$_3$ (7)



TsOEG$_{28}$OThp (**6**, 1.46 g, 0.94 mmol, 5 equiv.) was co-evaporated from MeCN (50 mL × 3) and re-dissolved in THF (2 mL). To the solution were added KO*t*Bu (0.08 g, 0.63 mmol, 3.35 equiv.) then Hub(CH_2Br)$_3$ (**S1**, 0.15 g, 0.19 mmol) and the reaction was stirred at 35 ºC for 3 h. The reaction was quenched with sat. NH_4Cl (0.2 mL) and the THF was evaporated. The residue was re-dissolved in CH_2Cl_2 (100 mL) containing a trace Et_3N, washed with half-sat. $NaHCO_3$ (30 mL × 3), the organic phase was dried with Na_2SO_4 and concentrated under vacuum. The residue was fractionated through a column of silanised silica, eluting with a gradient of acetone-water (20:80 to 95:5, v/v) containing a trace of sat. $NaHCO_3$. After evaporation of the solvent, the title compound (**7**, 0.88 g, 90%) was obtained as a light yellow waxy solid.

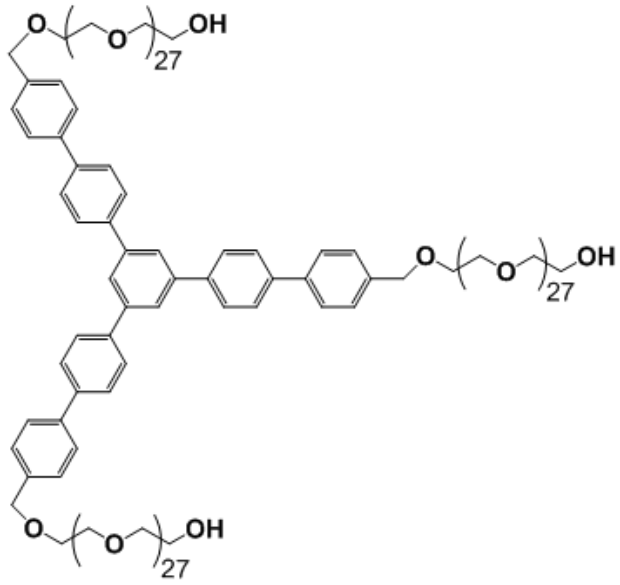
R_f (MeOH-$CHCl_3$ 1:19+ trace Et_3N) = 0.35.

^{1}H NMR (400 MHz, $CDCl_3$) δ = 7.89 (s, 3H, Hub C***H***), 7.83 – 7.79 (m, 6H Hub C***H***), 7.75 – 7.71 (m, 6H, Hub C***H***), 7.68 – 7.62 (m, 6H, Hub C***H***), 7.49 – 7.41 (m, 12H, 6×Dmtr C***H*** + 6×Hub C***H***), 7.37 – 7.31 (m, 12H, 12×Dmtr C***H***), 7.27 – 7.24 (m, 6H, 6×Dmtr C***H***), 7.21 – 7.17 (m, 3H, 3×Dmtr C***H***), 6.83 – 6.78 (m, 12H, 12×Dmtr C***H***), 5.30 (s, 18H, 6×ArOC***H$_3$***), 4.64 (s, 6H, 3×OC***H$_2$***Ar), 3.82 – 3.42 (m, 336H, 168×C***H$_2$***O).

^{13}C NMR (101 MHz, $CDCl_3$) δ = 158.37(6×Ar ***C***), 145.06(3×Ar ***C***), 141.98(3×Hub ***C***),140.20(3×Hub ***C***),140.00(3×Hub ***C***),139.95(3×Hub ***C***), 137.56(3×Hub ***C***),136.34((3×Ar ***C***)), 136.13(3×Ar ***C***), 130.04(12×Ar ***C***H), 128.27(6×Hub ***C***H), 128.20(6×Ar ***C***H),127.75(6×Hub ***C***H), 127.70(6×Ar ***C***H), 127.52(6×Hub ***C***H), 127.04(6×Hub ***C***H), 126.60(3×Ar ***C***H),125.00(3×Hub ***C***H), 113.01(12×Ar ***C***H), 85.88(3×O***C***Ar$_3$), 72.65 (3×O***C***H$_2$Ar), 70.74, 70.56, 69.56(168×***C***H$_2$O), 55.17(6C, O***C***H$_3$).

m/z **(MALDI-ToF$^+$)** $[M+Na]^+$ = 5267.8, *calc.* $C_{276}H_{426}O_{93}Na^+$ = 5267.8.

Hub(OEG$_{28}$OH)$_3$ (8)



To Hub(OEG$_{28}$ODmtr)$_3$ (**7**, 0.8g, 0.15 mmol) in CH_2Cl_2 (5 mL) were added pyrrole (0.05 mL, 2.29 mmol, 15 equiv.) and dichloroacetic acid (0.04 mL, 0.46 mmol, 3 equiv.). The mixture was stirred for 30 min, when an initially strong orange/red colour dissipated to a pale yellow solution, and quenched with sat. $NaHCO_3$. Then the resulting mixture was diluted with CH_2Cl_2 (50 mL), washed with half-sat. $NaHCO_3$ (20 mL × 3), and the aqueous phase was further

extracted with CH_2Cl_2 (50 mL × 3). The combined CH_2Cl_2 phase was dried over Na_2SO_4, and concentrated under reduced pressure. The residue was fractionated through a column of flash silica, eluting with a gradient of MeOH-$CHCl_3$ (1:99 to 30:70, v/v) to afford the title compound as a light yellow waxy solid (**8**, 0.53 g, 81%).

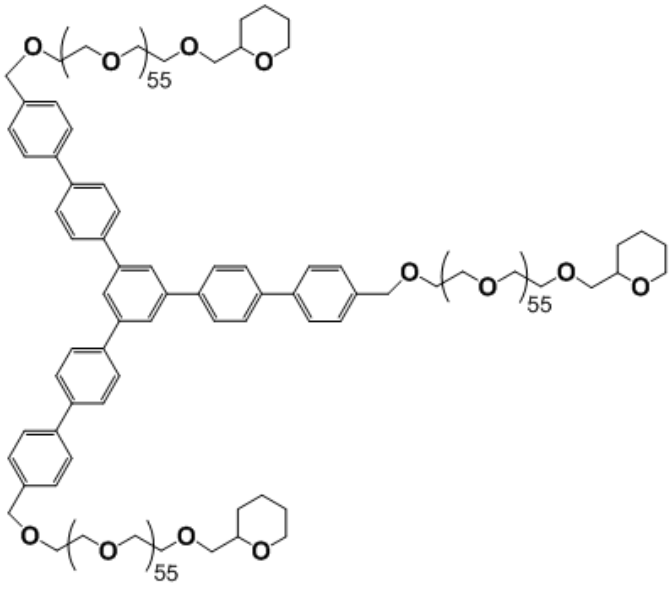
R_f (MeOH-$CHCl_3$ 1:9) = 0.32.

^{1}H NMR (400 MHz, $CDCl_3$) δ = 7.90 (s, 3H, Hub C***H***), 7.82 (d, *J* = 8.2 Hz, 6H, Hub C***H***), 7.74 (d, *J* = 8.3 Hz, 6H Hub C***H***), 7.67 (d, *J* = 8.1 Hz, 6H, Hub C***H***), 7.47 (d, *J* = 8.0 Hz, 6H, Hub C***H***), 4.65 (s, 6H, 3×OC***H₂***Ar), 3.79 – 3.55 m, 336H, 165×C***H₂***O), 3.12 (dq, *J* = 10.9, 6.3 Hz, 6H, 3×C***H₂***OH).

^{13}C NMR (101 MHz, $CDCl_3$) δ = 141.98 (3C), 140.20 (3C), 140.00 (3C), 139.95 (3C), 137.57 (3C) (15×Hub ***C***), 128.29(6C), 127.73(6C), 127.54(6C), 127.05(6C), 125.00 (3C) (27×Hub ***C***H), 72.98(3×O***C***H_2Ar), 72.60, 70.57, 69.57(165×***C***H_2O), 61.72(3C, 3×***C***H_2OH), 45.83, 8.63.

m/z **(MALDI-ToF$^+$)** $[M+Na]^+$ = 4345.4, *calc.* $C_{213}H_{372}O_{87}Na^+$ = 4345.4.

Hub(OEG$_{56}$OThp)$_3$ (9) (*Coupling procedure*)



Hub(OEG$_{28}$OH)$_3$ (**8**, 0.35 g, 0.08 mmol) and TsOEG$_{28}$ODmtr BB (**4**, 1.19 g, 0.8 mmol, 10 equiv.) were co-evaporated from MeCN (50 mL × 3) in a 100 mL round-bottomed flask, and then re-dissolved in DMF (3 mL). To this solution was slowly added NaH (60% dispersion in

mineral oil, 19.3 mg, 0.48 mmol, 6 equiv.). The reaction was stirred for 24 h at 60 °C; complete coupling was confirmed by HPLC before quenching. The reaction was quenched with sat. NH_4Cl (1 mL), and the solution was evaporated to dryness in vacuo. The residue was re-dissolved in CH_2Cl_2 (50 mL), extracted with half-sat. $NaHCO_3$ (20 mL × 3), the combined CH_2Cl_2 phase was dried with $NaSO_4$ and evaporated to dryness.

The crude material was purified using a two-stage 18 wt% PBI-DBX-M2005 membrane apparatus diafiltering with MeOH as solvent. After 4 h, all impurities, including excess monomer and other reaction debris, were removed completely (real-time HPLC monitoring). The retentate was washed from the diafiltration apparatus and evaporated to afford the title compound (**9**, 0.62 g, 94%) as a pale yellow oil. The concentration profiles of building block and Hub product during diafiltration is shown in Figure 8.1.

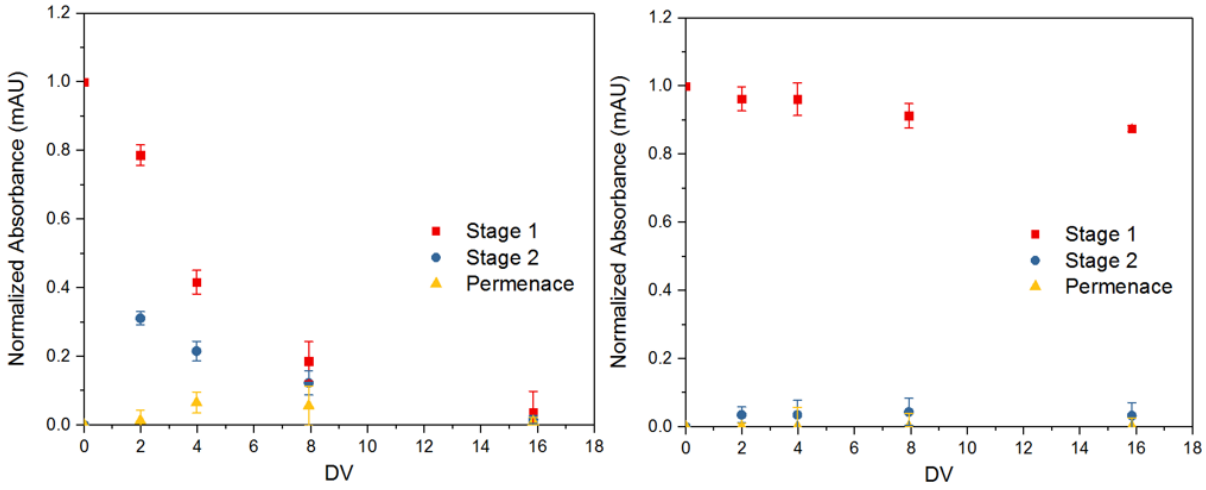


Figure 8.1 Concentration profiles of building block **4** and product **9** in two-stage membrane diafiltration rig.

R_f (MeOH- $CHCl_3$ 1: 19 + trace Et_3N) = 0.55.

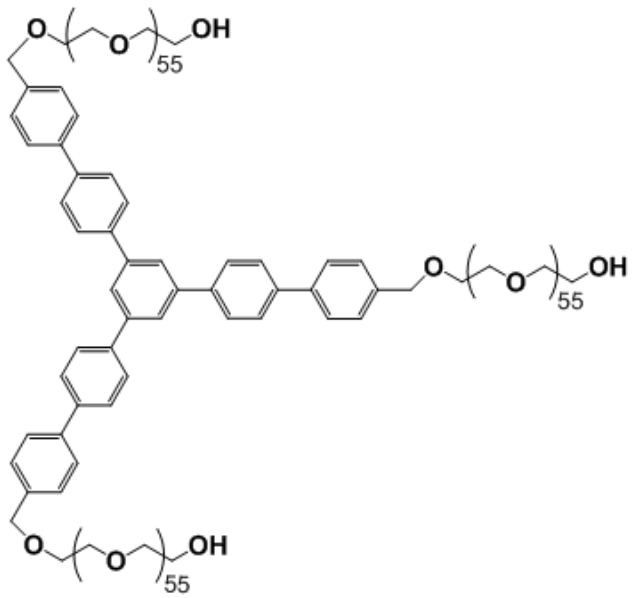
^{1}H NMR (400 MHz, $CDCl_3$) δ=7.89 (s, 3H, Hub C***H***), 7.82 (d, J = 8.0 Hz, 6H, Hub C***H***), 7.74 (d, J = 8.0 Hz, 6H, Hub C***H***), 7.66 (d, J = 7.8 Hz, 6H, Hub C***H***), 7.46 (d, J = 7.9 Hz, 6H, Hub C***H***), 4.64 (d, J = 4.5 Hz, 9H, 3×OC***H$_2$***Ar + 3×Thp C***H***), 3.96 – 3.42 (m, 678H, 339×C***H$_2$***O), 1.92 – 1.46 (m, 18H, 3×Thp C***H$_2$***).

^{13}C NMR (101 MHz, $CDCl_3$) δ = 141.96 (3C), 140.18(3C), 139.98(3C), 139.93(3C), 137.55(3C) (15×Hub ***C***), 128.29(6C), 127.72(6C), 127.53(6C), 127.05(6C), 124.97(3C)

(27×Hub ***C***H), 98.92(3×Thp ***C***H), 72.97(3C, 3×O***C***H_2Ar), 70.55, 69.53, 66.64 (339×***C***H_2O), 62.21(3×Thp ***C***H_2), 30.56, 25.43, 19.48(6×Thp ***C***H_2)

No MALDI-ToF was performed. Purity of **9** was referred to MALDI-ToF of **10** below.

Hub(OEG$_{56}$OH)$_3$ (10) (*Deprotection procedure*)



To Hub(OEG$_{56}$OThp)$_3$ (**9**, 0.23 g, 0.03 mmol) dissolved in MeOH (10 mL) was added MsOH (81 μL). The reaction was stirred for 30 min at room temperature, then quenched with sat. $NaHCO_3$ (2 mL). The solvent was evaporated and the residue re-dissolved in $CHCl_3$ (50 mL) The solution was extracted with half-sat. $NaHCO_3$ (30 mL × 3), the combined organic phase was dried over Na_2SO_4, and the solvent was evaporated under vacuum to afford the title compound (**10**, 0.2 g, 92.2%) as a pale yellow oil.

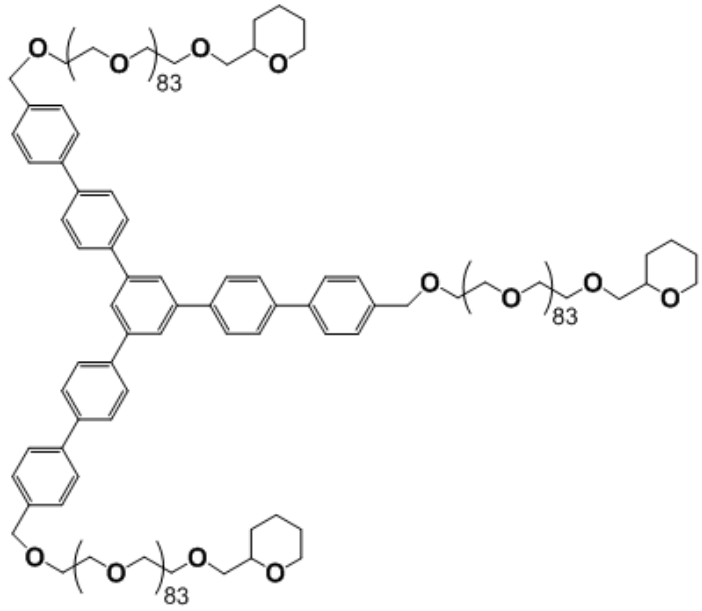
R_f (MeOH- $CHCl_3$ 1: 9) = 0.28.

^{1}H NMR (400 MHz, $CDCl_3$) δ = 7.90 (s, 3H, Hub C***H***), 7.82 (d, J = 8.1 Hz, 6H,Hub C***H***), 7.74 (d, J = 8.0 Hz, 6H, Hub C***H***), 7.66 (d, J = 7.9 Hz, 6H, Hub C***H***), 7.47 (d, J = 7.9 Hz, 6H, Hub C***H***), 4.64 (s, 6H, 3×OC***H$_2$***Ar), 3.81 – 3.59 (m, 672H, 336×C***H$_2$***O).

^{13}C NMR (101 MHz, $CDCl_3$) δ = 141.96(3C), 140.17(3C), 139.97(3C), 139.93(3C), 137.55(3C) (15×Hub ***C***), 128.30(6C), 127.73(6C), 127.54(6C), 127.05(6C), 124.98(3C) (27×Hub ***C***H), 72.98(3C, 3×O***C***H_2Ar), 70.55, 69.53(336×***C***H_2O).

***m*/*z* (MALDI-ToF$^+$)** $[M+Na]^+$ = 8045 (90% 3-arm product), 6813 (5% 2-arm product) and 5580 (5% 1-arm product) , *calc.* $C_{381}H_{708}O_{171}Na^+$ = 8045.

Hub(OEG$_{84}$OThp)$_3$ (11)



The reaction was conducted using the *coupling procedure* described above: To Hub(OEG$_{56}$OH)$_3$ (**10**, 0.21 g, 0.02 mmol) and TsOEG$_{28}$ODmtr BB (**4**, 0.36 g, 0.24 mmol, 10 equiv.) in DMF (2 mL) was added NaH (60%, 5.86 mg, 0.15 mmol, 6 equiv.). After stirring for 24 h at 60 ^{o}C, the reaction was worked up then purified using the two-stage membrane apparatus, diafiltering for 5 h to afford the title compound (**11**, 0.28 g, 95%) as a pale yellow oil. The concentration profiles of building block and Hub product during diafiltration is shown in Figure 8.2.

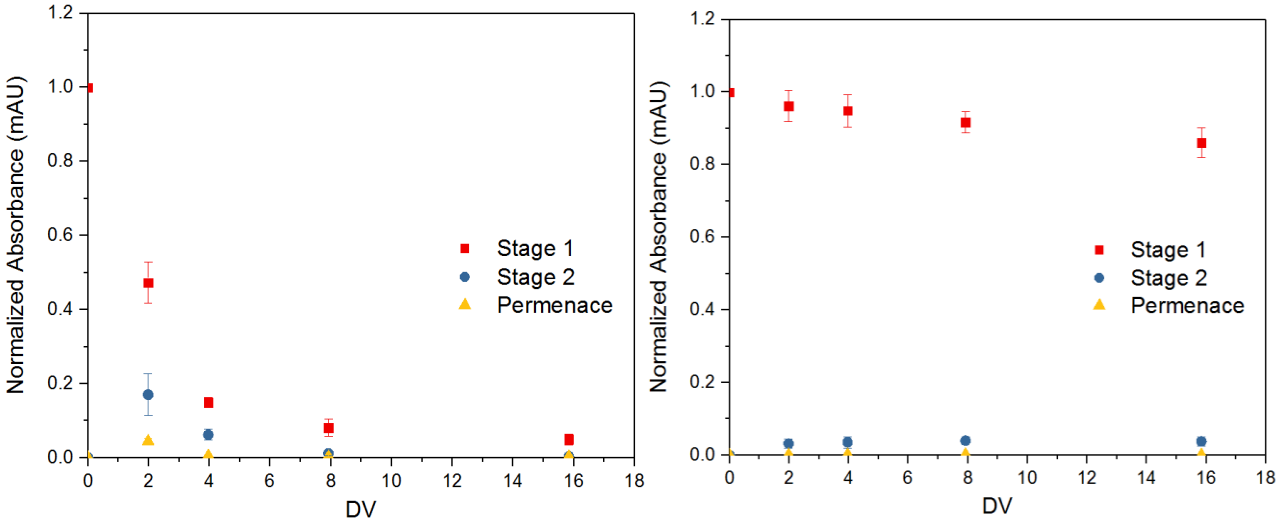


Figure 8.2 Concentration profiles of building block 4 and product 11 in two-stage membrane diafiltration rig.

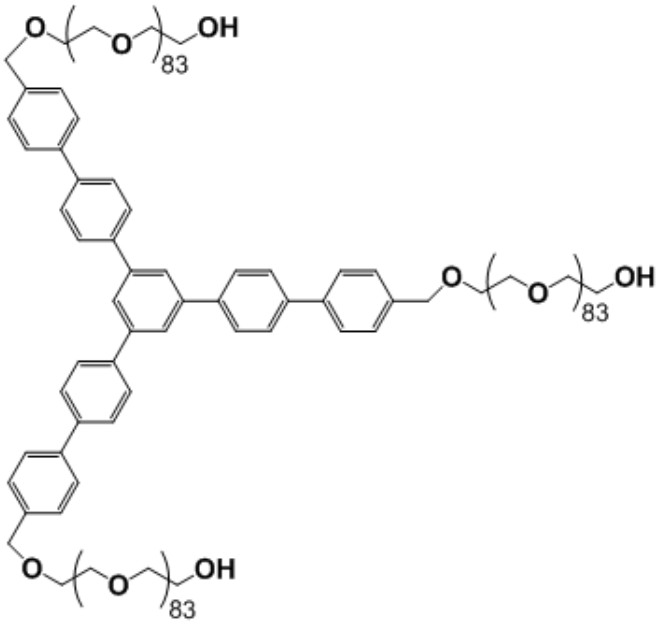
R_f (MeOH- $CHCl_3$ 1: 19+ trace Et_3N) = 0.43.

^{1}H NMR (400 MHz, $CDCl_3$) δ=7.88 (s, 3H, Hub C***H***), 7.81 (d, J = 8.3 Hz, 6H, Hub C***H***), 7.72 (d, J = 8.4 Hz, 6H, Hub C***H***), 7.64 (d, J = 7.8 Hz, 6H, Hub C***H***), 7.45 (d, J = 8.0 Hz, 6H, Hub C***H***), 4.63 (d, J = 2.5 Hz, 9H, 3×OC***H$_2$***Ar + 3×Thp C***H***), 3.91 – 3.38 (m, 1014H, 507×C***H$_2$***O), 1.91 – 1.46 (m, 18H, 3×Thp C***H$_2$***).

^{13}C NMR (101 MHz, $CDCl_3$) δ = 141.96 (3C), 140.18(3C), 139.98(3C), 139.93(3C), 137.55(3C) (15×Hub ***C***), 128.26(6C), 127.71(6C), 127.51(6C), 127.02(6C), 124.97(3C) (27×Hub ***C***H), 98.93(3×Thp ***C***H), 72.95(3C, 3×O***C***H_2Ar), 70.55, 69.55, 66.64(507×***C***H_2O), 62.19(3×Thp ***C***H_2), 30.55, 25.42, 19.47(6×Thp ***C***H_2).

No MALDI-ToF was performed. No MALDI-ToF was performed. Purity of **11** was referred to MALDI-ToF of **12** below.

Hub(OEG$_{84}$OH)$_3$ (12)



The reaction was conducted using the *deprotection procedure* described above: To Hub(OEG$_{84}$OThp)$_3$ (**11**, 0.09 g, 0.007 mmol) dissolved in MeOH (10 mL) was added 0.05 M MsOH (81 µL). After 30 min, the reaction mixture was worked up as above to afford the title compound (**12**, 0.09 g, 98 %) as a pale yellow oil.

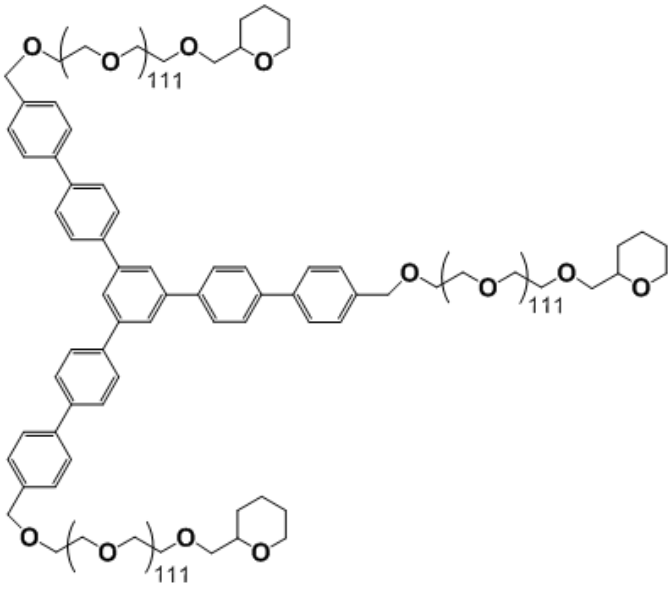
R_f (MeOH- $CHCl_3$ 1: 9) = 0.19.

^{1}H NMR (400 MHz, $CDCl_3$) δ = 7.90 (s, 3H, Hub C***H***), 7.82 (d, J = 8.1 Hz, 6H,Hub C***H***), 7.74 (d, J = 8.0 Hz, 6H, Hub C***H***), 7.66 (d, J = 7.9 Hz, 6H, Hub C***H***), 7.47 (d, J = 7.9 Hz, 6H, Hub C***H***), 4.64 (s, 6H, 3×OC***H$_2$***Ar), 3.81 – 3.59 (m, 1008H, 504×C***H$_2$***O).

^{13}C NMR (101 MHz, $CDCl_3$) δ = 141.96(3C), 140.17(3C), 139.97(3C), 139.93(3C), 137.55(3C) (15×Hub ***C***), 128.30(6C), 127.73(6C), 127.54(6C), 127.05(6C), 124.98(3C) (27×Hub ***C***H), 72.98(3C, 3×O***C***H$_2$Ar), 70.55, 69.53(504×***C***H$_2$O).

***m*/*z* (MALDI-ToF$^+$)** [M+Na]$^+$ = 11745 (60% 3-arm product), 10512 (20% 2-arm product), 9282 (5% 1-arm product) and 8045 (15% starting material **10**), *calc.* $C_{549}H_{1044}O_{255}Na^+$ = 11745.

Hub(OEG$_{112}$OThp)$_3$ (13)



The reaction was conducted using the *coupling procedure* described above: To Hub(OEG$_{84}$OH)$_3$ (**12**, 0.09 g, 0.008 mmol) and TsOEG$_{28}$ODmtr BB (**4**, 0.11 g, 0.08 mmol, 10 equiv.) in DMF (2 mL) was added NaH (60%, 1.83 mg, 0.05 mmol, 6 equiv.). After stirring for 24 h at 60 ^{o}C, the reaction was purified was fractionated by a column chromatography, eluting with a gradient of MeOH- $CHCl_3$ (1:99 to 10:90, v/v), all solvents containing 1 vol% Et_3N, to afford the title compound as a pale yellow oil (**13**, 0.12 g, 97%).

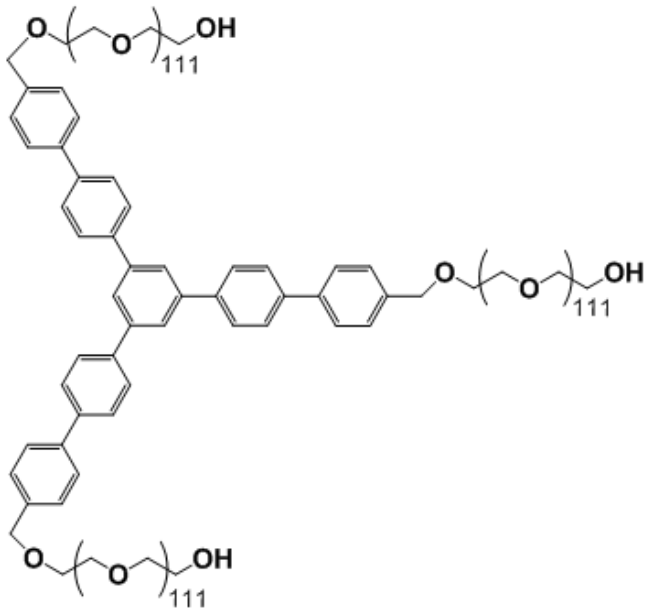
R_f (MeOH- $CHCl_3$ 1: 19+ trace Et_3N) = 0.37.

^{1}H NMR (400 MHz, $CDCl_3$) δ=7.90 (s, 3H, Hub C***H***), 7.82 (d, J = 8.0 Hz, 6H, Hub C***H***), 7.74 (d, J = 8.2 Hz, 6H, Hub C***H***), 7.66 (d, J = 7.7 Hz, 6H, Hub C***H***), 7.47 (d, J = 7.7 Hz, 6H, Hub C***H***), 4.64 (d, J = 4.3 Hz, 9H, 3×OC***H$_2$***Ar + 3×Thp C***H***), 3.91 – 3.31 (m, 1350H, 675×C***H$_2$***O), 1.86 – 1.45 (m, 18H, 3×Thp C***H$_2$***).

^{13}C NMR (101 MHz, $CDCl_3$) δ = 141.96 (3C), 140.18(3C), 139.98(3C), 139.93(3C), 137.55(3C) (15×Hub ***C***), 128.26(6C), 127.71(6C), 127.51(6C), 127.02(6C), 124.97(3C) (27×Hub ***C***H), 98.93(3×Thp ***C***H), 72.95(3C, 3×O***C***H$_2$Ar), 70.55, 69.55, 66.64(675×***C***H$_2$O), 62.19(3×Thp ***C***H$_2$), 30.55, 25.42, 19.47(6×Thp ***C***H$_2$).

No MALDI-ToF was obtained.

Hub(OEG$_{112}$OH)$_3$ (14)



The reaction was conducted using the *deprotection procedure* described above: To Hub(OEG$_{112}$OThp)$_3$ (**13**, 0.04 g, 0.003 mmol) dissolved in MeOH (5 mL) was added 0.05 M MsOH (67 μL). After 30 min, the reaction mixture was worked up as above to afford the title compound (**14**, 0.04 g, 93 %) as a pale yellow oil.

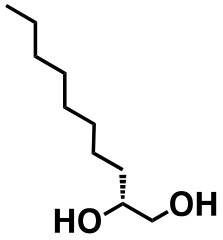
R_f (MeOH- $CHCl_3$ 1: 9) = 0.16.

^{1}H NMR (400 MHz, $CDCl_3$) δ = 7.90 (s, 3H, Hub C***H***), 7.82 (d, *J* = 8.1 Hz, 6H,Hub C***H***), 7.74 (d, *J* = 8.0 Hz, 6H, Hub C***H***), 7.66 (d, *J* = 7.9 Hz, 6H, Hub C***H***), 7.47 (d, *J* = 7.9 Hz, 6H, Hub C***H***), 4.64 (s, 6H, 3×OC***H$_2$***Ar), 3.81 – 3.59 (m, 1344H, 672×C***H$_2$***O).

^{13}C NMR (101 MHz, $CDCl_3$) δ = 141.96(3C), 140.17(3C), 139.97(3C), 139.93(3C), 137.55(3C) (15×Hub ***C***), 128.30(6C), 127.73(6C), 127.54(6C), 127.05(6C), 124.98(3C) (27×Hub ***C***H), 72.98(3C, 3×O***C***H$_2$Ar), 70.55, 69.53(672×***C***H$_2$O).

No MALDI-ToF was obtained.

(*R*)-1, 2-decanediol (17)



Hydroquinidine 1, 4-phthalazinediyl diether [$(DHQD)_2PHAL$, 0.77 g, 0.99 mmol], potassium ferricyanide $K_3[Fe(CN)_6]$ (98.3 g, 300 mmol) and K_2CO_3 (41.5 g, 300 mmol) were dissolved in *tert*-butyl alcohol (510 mL), plus water (510 mL). 4 vol. % OsO_4 in water (2.6 mL) was added to the solution. To the ice-water bath cooled suspension was then slowly added 1-decene (**16**, 19.2 mL, 101.4 mmol), and the mixture was briskly stirred for 3 hours. The reaction was then quenched with Na_2SO_3 (153 g, 1.2 mol) and stirred at room temperature for another 45 minutes. The mixture was partitioned between ethyl acetate (500 mL) and half sat. $NaHCO_3$ (2L). The aqueous layer was re-extracted with further ethyl acetate (2 × 100 mL). The combined organic layers were dried over Na_2SO_4, and the solvent was stripped off to give the crude 1, 2-octanediol (**17**, 16. 6 g) as a pale yellow oil. This material was twice crystallised from MeCN to afford the title compound as white flaky crystals (**17**, 6.18 g, 35%).

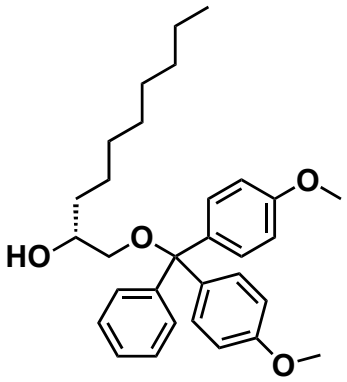
R_f (EtOH-$CHCl_3$ 1:19) = 0.28.

^{1}H NMR (400 MHz, $CDCl_3$) δ = 3.72-3.66 (m, 1H, C***H***OH), 3.64 (dd, *J* = 11.2, 2.9 Hz, 1H, C***H***HOH), 3.42 (dd, *J* = 11.2, 7.8 Hz, 1H, CH***H***OH), 3.15 (b.s, 2H, O***H***), 1.44-1.28 [m, 14H, $(C\boldsymbol{H_2})_7CH_3$], 0.89 [t, *J* = 6.9 Hz, 3H, $(CH_2)_7C\boldsymbol{H_3}$].

^{13}C NMR (101 MHz, $CDCl_3$) δ = 72.38 (***C***HOH), 66.78 (***C***H_2OH), 33.14 [CH***C***$H_2(CH_2)_6CH_3$], 31.88, 29.69, 29.54, 29.28, 25.61, 22.67 (6×***C***H_2), 14.10 (***C***H_3).

***m*/*z* (ESI$^+$)** $[M+H]^+$ = 175.1, *calc.* $C_{10}H_{23}O_2^+$ = 175.2.

(*R*)-1-(4, 4'-Dimethoxytriphenylmethyl)-decan-2-ol (18)



(*R*)-1, 2-Decanediol (**17,** 4.35 g, 24.9 mmol) was co-evaporated from anhydrous MeCN (3 × 30 mL) and dissolved in CH_2Cl_2 (67 mL) with Et_3N (6.9 mL, 50 mmol, 2 equiv.). To the well stirred solution was slowly added 4, 4'-dimethoxytriphenylmethyl chloride (9.28 g, 27.4 mmol, 1.1 equiv.) in CH_2Cl_2 (133 mL) from a dropping funnel. The reaction was stirred for 2 hours and partitioned with half-sat. $NaHCO_3$ (3×100 mL). The combined organic layers were dried over Na_2SO_4, and the solvent was stripped off under reduced pressure. The crude (**18**, 14.1 g) was fractionated by chromatography on flash silica, eluting with a gradient of $CHCl_3$-heptane (20:80 to 100:0, v/v) then MeOH-$CHCl_3$ (1:99 to 5:95, v/v), all solvents containing 1 vol% Et_3N to afford the title compound as a pale yellow oil (**18**, 9.13 g, 72 %).

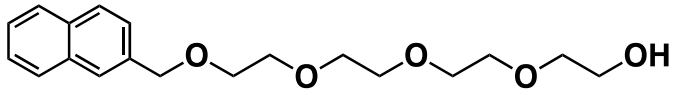
R_f (acetone-CH_2Cl_2 1:49 + trace Et_3N) = 0.54.

^{1}H NMR (400 MHz, $CDCl_3$) δ = 7.50 (dd, J = 7.3, 1.2 Hz, 2H), 7.39 (d, J = 8.5 Hz, 4H), 7.33 (b.t, J = 7.5 Hz, 2H), 7.25 (b.t, J = 7.3 Hz, 1H), 6.88 (d, J = 8.9 Hz, 4H) (13×Dmtr C***H***), 3.81 (s, 7H, 2×ArOC***H*****$_3$** + C***H***OH), 3.22 (dd, J = 9.3, 3.4 Hz, 1H, C***H***HODmtr), 3.09 (dd, J = 9.3, 7.4 Hz, 1H, CH***H***ODmtr), 1.45-1.31 [m, 14H, (C***H*****$_2$)$_7$CH$_3$], 0.93 [t, J = 6.5 Hz, 3H, $(CH_2)_7$C***H*****$_3$**].

^{13}C NMR (101 MHz, $CDCl_3$) δ = 158.51 (2C), 144.99, 136.17, 136.13 (5×Ar ***C***), 130.09 (4C), 128.19 (2C), 127.84 (2C), 126.80, 113.13 (4C) (13×Ar ***C***H), 86.06 (O***C***Ar$_3$), 71.00 (***C***HOH), 67.70 (***C***H$_2$ODmtr), 55.18 (2C, O***C***H$_3$), 33.49, 31.93, 29.70, 29.57, 29.31, 25.56, 22.71 (7×***C***H$_2$), 14.17 (***C***H$_3$).

***m*/*z* (ESI$^+$)** $[M+Na]^+$ = 499.3, *calc.* $C_{31}H_{40}NaO_4^+$ = 499.3.

α-(2-Naphthyl methyl) tetragol (19a)



Tetragol (**19**, 110 g, 565 mmol, 5 equiv.) was diluted with DMF (220 mL). To the briskly stirred, ice-water bath cooled solution was added potassium *tert*-butoxide (19 g, 170 mmol, 1.5 equiv.), then 2-naphthylmethyl chloride (25 g, 113 mmol). After 15 min the ice bath was removed and stirring was continued for 4 h, reaction was then quenched with aq. NH_4Cl to reduce the PH to *ca.* 10 (spotting onto damp indicator strips). The reaction was concentrated at reduced pressure at 70 °C. The residue was partitioned between ethyl acetate (500 mL) and 10% brine (500 mL) and extracted with further 10% brine (2 ×250 mL). The combined organic phases were dried over Na_2SO_4, and the solvent was stripped off. The crude 2-naphthylmethyl tetragol (**19a**, 34.2 g) was fractionated by chromatography on flash silica, eluting with a gradient of $CHCl_3$-heptane (20:80 to 100:0, v/v), then EtOH-$CHCl_3$ (1:99 to 10:90, v/v) to afford the title compound as a dark yellow oil (**19a**, 27.2 g, 72 %).

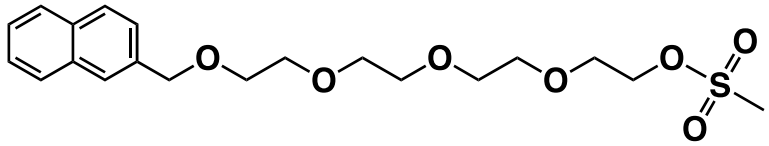
R_f (EtOH-$CHCl_3$ 1:19) = 0.44.

^{1}H NMR (400 MHz, $CDCl_3$) δ = 7.86-7.81 (m, 4H, Npm C***H***), 7.51-7.47 (m, 3H, Npm C***H***), 4.75 (s, 2H, OC***H*****$_2$**Ar), 3.73-3.67 (m, 14H, 7×C***H*****$_2$**O), 3.61-3.59 (m, 2H, C***H*****$_2$**O).

^{13}C NMR (101 MHz, $CDCl_3$) δ = 135.71, 133.26, 132.99 (3×Npm ***C***), 128.16, 127.87, 127.69, 126.52, 126.08, 125.84 (2C) (7×Npm ***C***H), 73.33 (O***C***H_2Ar), 72.59 (***C***H_2CH_2OH), 70.64 -70.57 (4C, m), 70.30, 69.42 (6×***C***H_2O), 61.69 (***C***H_2OH).

***m/z* (ESI$^+$)** $[M+NH_4]^+$ = 352.2, *calc.* $C_{19}H_{30}NO_5^+$ = 352.2.

α-(2-Naphthyl methyl) tetragol-ω-methanesulfonate (20)



α-(2-Naphthyl methyl) tetragol (**19a**, 26.9 g, 81 mmol) was co-evaporated from anhydrous MeCN (3 × 100 mL) and dissolved in CH_2Cl_2 (250 mL). To the well stirred, ice-water bath cooled solution were added Et_3N (22.5 mL, 161 mmol, 2 equiv.), *N*-methyl imidazole (3.2 mL, 40 mmol, 0.5 equiv.), and slowly adding methane sulfonyl chloride (8.13 mL, 105 mmol, 1.3 equiv.) from a syringe. The reaction was stirred for 2 h at room temperature. With vigorous stirring, the resulting orange-brown solution was quenched with $NaHCO_3$ (17.6 g, 210 mmol, 2.6 equiv.), and then washed with half-sat. brine (100 mL × 3). The combined organic phases were dried over Na_2SO_4, and the solvent was stripped off in vacuum, to provide the title compound (**20,** 31.1 g, 93%) as a yellow oil, which was used without further purification.

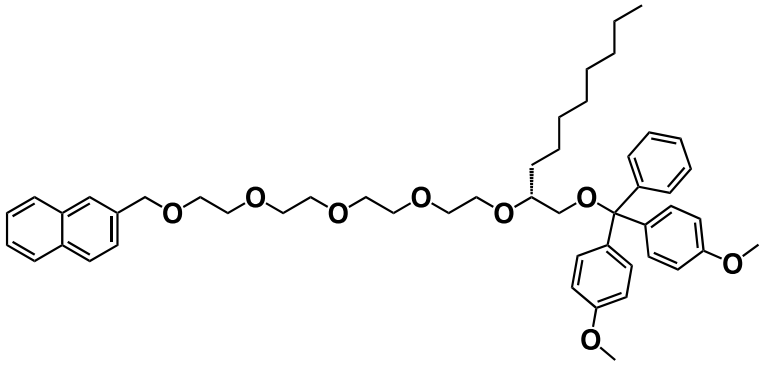
R_f (EtOH-$CHCl_3$ 1:19) = 0.47.

^{1}H NMR (400 MHz, $CDCl_3$) δ = 7.81-7.76 (m, 4H, Npm C***H***), 7.47-7.41 (m, 3H, Npm C***H***), 4.68 (s, 2H, OC***H*****$_2$**Npm), 4.28-4.26 (m, 2H, C***H*****$_2$**OMs), 3.64-3.55 (m, 14H, 7×C***H*****$_2$**O), 2.99 (s, 3H, C***H*****$_3$**).

^{13}C NMR (101 MHz, $CDCl_3$) δ = 135.88, 133.24, 132.93 (3×Npm ***C***), 128.13, 127.87, 127.71, 126.41, 126.13, 125.88, 125.84 (7×Npm ***C***H), 73.18 (O***C***H_2Npm), 70.57 (2C), 70.50 (2C), 70.43, 69.50 (2C) (7×***C***H_2O), 68.88 (***C***H_2OMs), 37.54 (***C***H_3).

***m*/*z* (ESI$^+$)** $[M+NH_4]^+$ = 430.2, *calc.* $C_{20}H_{32}NO_7S^+$ = 430.2.

(*R*)-β-Octyl-α-(4, 4′-dimethoxytriphenylmethyl)-ω-(2-naphthyl methyl) pentagol (21)



(*R*)-1-(4,4'-Dimethoxytriphenylmethyl) decan-2-ol (**18**, 10.1 g, 21.2 mmol) and (2-naphthyl methyl) tetragol methanesulfonate (**20,** 26.2 g, 63.5 mmol, 3 equiv.) were pre-mixed and co-evaporated from MeCN (3 × 100 mL). The mixture was dissolved in DMF (40 mL). To the solution was added a 60% dispersion of NaH in mineral oil (1.7 g, 42.4 mmol, 2 equiv.). The reaction was well stirred and held at 60 °C for 6 h. The reaction was quenched by the dropwise addition of aq. NH_4Cl until a pH to ca. 10 was attained (spotting onto moistened indicator strips). The DMF was evaporated under reduced pressure and the residue was re-dissolved in CH_2Cl_2 (200 mL). The solution was extracted with half-sat. $NaHCO_3$ (3×100 mL), the combined organic layers were dried over Na_2SO_4, and the solvent was stripped off. The crude residue (**21**, 34.3 g) was fractionated by chromatography on flash silica, eluting with a gradient of diethyl ether-heptane, all solvents containing 1 vol% Et_3N to afford the title compound as a dark yellow oil (**21**, 14.3 g, 85 %).

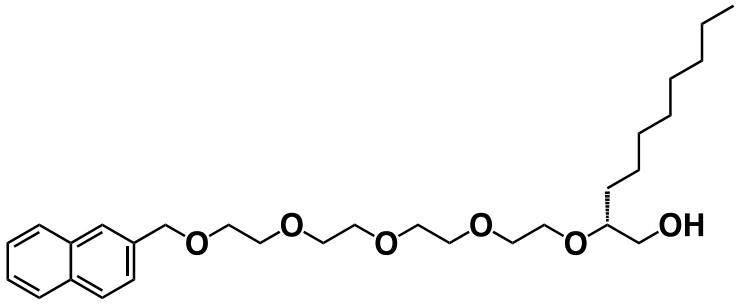
R_f (EtOH-$CHCl_3$ 1:19 + trace Et_3N) = 0.47.

^{1}H NMR (400 MHz, $CDCl_3$) δ = 7.87-7.83 (m, 4H, Npm C***H***), 7.53-7.48 (m, 5H, 2×Dmtr + 3×Npm C***H***), 7.41-7.38 (m, 4H), 7.32 (b.t, J = 7.5 Hz, 2H), 7.24 (b.t, J = 7.3 Hz, 1H), 6.86 (d, J = 8.9 Hz, 4H) (11×Dmtr C***H***), 4.77 (s, 2H, OC***H₂***Ar), 3.81 (s, 6H, 2×ArOC***H₃***), 3.77-3.65 (m, 16H, 8×C***H₂***O), 3.46 (m, 1H, C***H***CH_2ODmtr), 3.20 (dd, J = 9.8, 5.9 Hz, 1H), 3.10 (dd, J = 9.8, 4.2 Hz, 1H, C***H₂***ODmtr), 1.55-1.29 (m, 14×C***H₂***), 0.95-0.91 (t, J = 6.5 Hz, 3H, CH_2C***H₃***).

^{13}C NMR (101 MHz, $CDCl_3$) δ = 158.38 (2C), 145.23, 136.45, 136.41 (2C) (5×Dmtr***C***), 135.83, 133.30, 133.00 (3×Npm ***C***), 130.13 (4C), 128.28 (2C), 128.15, 127.88, 127.74 (2C), 127.70, 126.64, 126.47, 126.07, 125.82 (2C), 113.03 (4C) (20×Dmtr + Npm ***C***H), 85.92 (O***C***Ar_3), 79.84 (***C***HCH_2ODmtr), 73.35 (Npm O***C***H_2Ar), 70.98, 70.68 (5C), 69.69, 69.49 (8C, 8×***C***H_2O), 65.99 (***C***H_2ODmtr), 55.17 (2C, O***C***H_3), 32.23, 31.94, 29.77, 29.62, 29.34, 25.48, 22.74 (7×***C***H_2), 14.18 (CH_2***C***H_3).

***m*/*z* (ESI$^+$)** $[M+NH_4]^+$ = 810.5, *calc.* $C_{50}H_{68}NO_8^+$ = 810.5.

(*R*)-β-Octyl-*ω*-(2-naphthyl methyl) pentagol (22)



To a solution of (*R*)-β-Octyl-*α*-(4, 4′-dimethoxytriphenylmethyl)-*ω*-(2-naphthyl methyl) pentagol **(21**, 12.5 g, 15.8 mmol) in CH_2Cl_2 (120 mL) was added pyrrole (5.5 mL, 79 mmol, 5 equiv.) and dichloroacetic acid (1.3 mL, 15.8 mmol). The reaction was briskly stirred for 45 minutes and quenched with sat. $NaHCO_3$. The resulting mixture was extracted with half-sat. $NaHCO_3$ (60 mL × 3), the combined organic layers were dried over Na_2SO_4, and the solvent was evaporated under reduced pressure. The residue was fractionated through a column of flash silica in a sinter funnel**.** The crude material (**22**, 15.1 g) was dissolved and loaded in 20% CHCl3/ heptane. The silica was then washed with a gradient of $CHCl_3$-heptane (20:80 to 100:0, v/v) then MeOH-$CHCl_3$ (1:99 to 5:95, v/v), to afford the title compound as a pale yellow oil (**22**, 6.8 g, 87%).

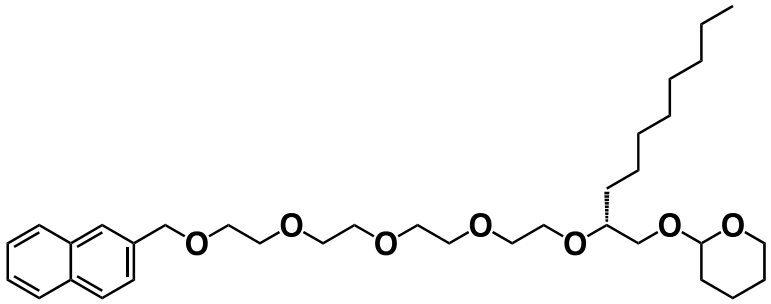
R_f (EtOH-$CHCl_3$ 1:19) = 0.38.

^{1}H NMR (400 MHz, $CDCl_3$) δ = 7.81-7.77 (m, 4H, Npm C***H***), 7.47-7.41 (m, 3H, Npm C***H***), 4.70 (s, 2H, C***H*****$_2$**Npm), 3.76-3.55 (m, 17H, 8×C***H*****$_2$**O + C***H***HCH_2OH), 3.46 (dd, *J* = 11.6, 7.1 Hz, 1H, CH***H***OH), 3.38-3.31 (m, 2H, CH***H***CH_2O***H***), 1.50-1.26 (m, 14H, 7×C***H*****$_2$**), 0.89 (t, *J* = 6.7 Hz, 3H, CH_2C***H*****$_3$**).

^{13}C NMR (101 MHz, $CDCl_3$) δ = 135.82, 133.26, 132.96 (3×Npm ***C***), 128.09, 127.84, 127.66, 126.39, 126.03, 125.77 (2C) (7×Npm ***C***H), 81.55 (***C***HCH_2OH), 73.25 (Npm O***C***H_2Ar), 70.93, 70.62 (3C), 70.49 (2C), 69.46, 69.15 (8×***C***H_2O), 64.78 (***C***H_2OH), 31.88, 31.41, 29.79, 29.55, 29.28, 25.64, 22.68 (7×***C***H_2), 14.17 (CH_2***C***H_3).

***m*/*z* (ESI$^+$)** $[M+NH_4]^+$ = 508.4, *calc.* $C_{29}H_{50}NO_6^+$ = 508.4.

(*R*)-β-Octyl-*α*-tetrahydropyranyl-*ω*-(2-naphthyl methyl) pentagol (23)



(*R*)-β-Octyl-*ω*-(2-naphthyl methyl) pentagol (**22**, 5.48 g, 11.2 mmol) was co-evaporated from anhydrous MeCN (3 × 30 mL) and dissolved in CH_2Cl_2 (85 mL). To this mixture was added 3, 4-dihydro-2H-pyran (2.6 mL, 28 mmol, 2.5 equiv.) and making sure it was well stirred. A solution of *p*-toluenesulfonic acid (19.3 mg, 112 μmol, 0.01 equiv.) in 1 mL THF was slowly added with a drop of 0.1 mL per time. The extent of the reaction was monitored by TLC with every addition. The mixture was left to stir for 2 hours and quenched with sat. $NaHCO_3$. The mixture was extracted with CH_2Cl_2 (3 ×200 mL), the combined organic layers were dried over Na_2SO_4, and the solvent was stripped off. The crude residue (**23**, 6.22 g) was fractionated by chromatography on flash silica, with a gradient of $CHCl_3$-heptane (20:80 to 100:0, v/v) then a MeOH-$CHCl_3$ mixture (1:99 to 5:95, v/v), all solvents contained 1 vol% Et_3N, to afford the title compound as a yellow oil (**23**, 5.98 g, 93%).

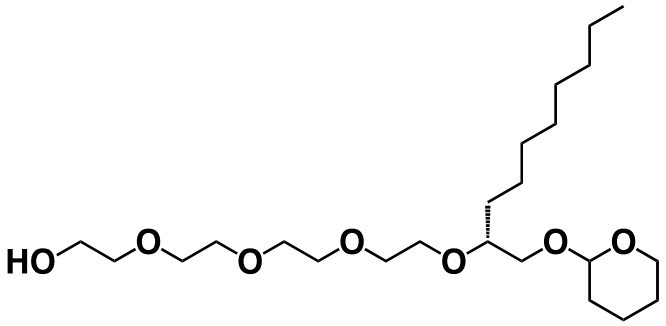
R_f (EtOH-$CHCl_3$ 1:19 + trace Et_3N) = 0.44.

^{1}H NMR (400 MHz, $CDCl_3$) δ = 7.81-7.77 (m, 4H, Npm C***H***), 7.47-7.41 (m, 3H, Npm C***H***), 4.71 (s, 2H, C***H*****$_2$**Npm), 4.61-4.58 (m, 1H, Thp C***H***), 3.86-3.59 (m, 18H, 9×C***H*****$_2$**O), 3.59-3.51 (m, 3H, C***H*****$_2$**O + C***H***CH_2OThp), 1.84-1.25 (m, 20H, 10×C***H*****$_2$**), 0.86 (t, *J* = 6.9 Hz, 3H, CH_2C***H*****$_3$**).

^{13}C NMR (101 MHz, $CDCl_3$) δ = 135.76, 133.24, 132.94 (3×Npm ***C***), 128.09, 127.82, 127.63, 126.40, 126.01, 125.76, 125.74 (7×Npm ***C***H), 99.18 (0.5C), 98.58 (0.5C) (Thp ***C***H), 79.44 (0.5C), 79.17 (0.5C) (***C***HCH_2OThp), 73.29 (Npm O***C***H_2Ar), 70.88, 70.66-70.55 (5C), 70.41 (0.5C), 69.53, 69.43, 69.32 (0.5C), 62.16 (0.5C), 61.81 (0.5C) (10×O***C***H_2), 32.03, 31.87, 30.64 (0.5C), 30.52 (0.5C), 29.74, 29.56, 29.28, 25.57 (0.5C), 25.46 (1.5C), 22.67, 19.49 (0.5C), 19.25 (0.5C) (10×***C***H_2), 14.12 (CH_2***C***H_3).

***m*/*z* (ESI$^+$)** $[M+NH_4]^+$ = 592.4, *calc.* $C_{34}H_{58}NO_7^+$ = 592.4.

(*R*)-β-Octyl-α-tetrahydropyranyl pentagol (24)



(*R*)-β-Octyl-α-tetrahydropyranyl-ω-(2-naphthyl methyl) pentagol (**23**, 5.97 g, 10.4 mmol) was dissolved in MeOH (50 mL), to which were added activated charcoal (1.44 g), and then a freshly prepared solution of palladium diacetate (154 mg, 0.7 mmol, 0.066 equiv.) in THF (10 mL). The suspension was evacuated to the point that bumping commenced, then let down to argon, and this process was repeated five times. After a final evacuation, the argon line was replaced with a hydrogen balloon, and the flask was filled with hydrogen gas. The suspension was stirred vigorously at room temperature for 6h. Then the hydrogen was evacuated, flushing the flask with argon for five times. The solution was filtered through a pad of Celite S in a small sintering funnel, and the charcoal rinsed with MeOH (50 mL); ethyl acetate (50 mL) and $CHCl_3$(50 mL) sequentially. The combined filtrate was evaporated under vacuum, and the residue (5.95 g) was fractionated through a column of flash silica, eluting with a gradient of EtOAc-heptane (5:95 to 100:0) then MeOH-EtOAc (1:99 to 10:90), all solvents containing 1 vol% Et_3N, to afford a pale yellow oil (**24**, 3.32 g, 74%).

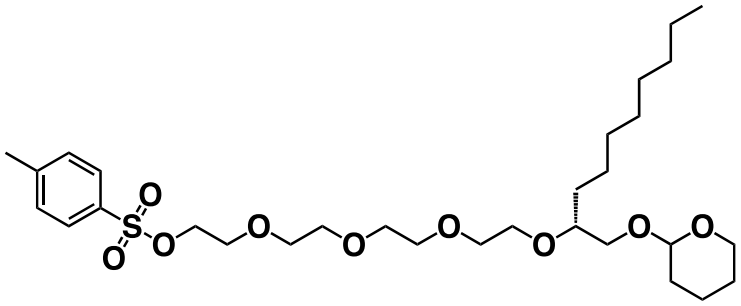
R_f (EtOH-$CHCl_3$ 1:19 + trace Et_3N) = 0.28.

^{1}H NMR (400 MHz, $CDCl_3$) δ = 4.44-4.42 (m, 1H, Thp C***H***), 3.69-3.39 (m, 17H, 8.5×C***H*₂**O), 3.33-3.20 (m, 4H, 1.5×C***H*₂**O + C***H***CH_2OThp), 1.68-1.34 (m, 6H, Thp C***H*₂**), 1.32-1.10 (m, 7×C***H*₂**), 0.70 (t, J = 6.8 Hz, 3H, CH_2C***H*₃**).

^{13}C NMR (101 MHz, $CDCl_3$) δ = 98.89 (0.5C), 98.34 (0.5C) (Thp ***C***H), 79.21 (0.5C), 78.97 (0.5C) (***C***HCH_2OThp), 72.51, 70.70, 70.42, 70.38, 70.34, 70.14 (1.5C), 69.34, 69.17 (0.5C), 61.84 (0.5C), 61.54 (0.5C), 61.29 (10×***C***H_2O), 31.81, 31.69, 30.45 (0.5C), 30.35 (0.5C), 29.55, 29.37, 29.08, 25.36-25.35 (m, 2C), 22.47, 19.26 (0.5C), 19.06 (0.5C) (10×***C***H_2), 13.92 (CH_2***C***H_3).

***m*/*z* (ESI$^+$)** $[M+Na]^+$ = 457.3, *calc.* $C_{23}H_{46}NaO_7^+$ = 457.3.

(*R*)-β-Octyl-α-tetrahydropyranyl pentagol-ω-toluenesulfonate (25)



(*R*)-β-Octyl-α-tetrahydropyranyl pentagol (**24,** 3.12 g, 7.2 mmol) was co-evaporated from anhydrous MeCN (3 × 20 mL) and re-dissolved in CH_2Cl_2 (105 mL). To the solution were added Et_3N (3 mL, 21.6 mmol, 3 equiv.), *N*-methyl imidazole (0.3 mL, 3.6 mmol, 0.5 equiv.) and toluene sulfonyl chloride (2.05 g, 10.8 mmol, 1.5 equiv.), and the reaction was stirred for 2h at room temperature. The solution appeared orange-brown and the reaction was quenched with $NaHCO_3$ (1.57 g, 18.7 mmol, 2.6 equiv.) with vigorous stirring. Then the mixture was partitioned with the original CH_2Cl_2, the aqueous layer was extracted with further CH_2Cl_2 (2 ×200 mL). The combined organic layers were dried over Na_2SO_4, and the solvent was stripped off under reduced pressure. The crude residue (**25**, 4.65 g) was fractionated by chromatography on flash silica, eluting with a gradient of EtOAc-heptane (10:90 to 100:0, v/v) then MeOH-EtOAc (1:99 to 5:95, v/v), all solvents containing 1 vol% Et_3N to afford the title compound as a pale yellow oil (**25**, 4.05 g, 96%).

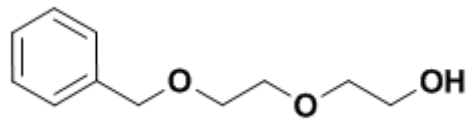
R_f (EtOH-$CHCl_3$ 1:19 + trace Et_3N) = 0.59.

^{1}H NMR (400 MHz, $CDCl_3$) δ = 7.81 (d, J = 8.3 Hz, 2***H***), 7.35 (d, J = 8.0 Hz, 2H) (4×Ts C***H***), 4.63-4.60 (m, 1H, Thp C***H***), 4.18-4.16 (m, 2H, C***H$_2$***OTs), 3.89-3.39 (m, 19H, 9×C***H$_2$***O + C***H***CH_2OThp), 2.46 (s, 3H, ArC***H$_3$***), 1.86-1.27 (m, 20H, 10×C***H$_2$***), 0.89 (t, J = 6.8 Hz, 3H, CH_2C***H$_3$***).

^{13}C NMR (101 MHz, $CDCl_3$) δ = 144.76, 133.03 (2×Ts ***C***), 129.83 (2C), 127.96 (2C) (4×Ts ***C***H), 99.19 (0.5C), 98.62 (0.5C) (Thp ***C***H), 79.44 (0.5C), 79.18 (0.5C) (***C***HCH_2OThp), 70.89, 70.71, 70.63, 70.53 (2C), 70.38 (0.5C), 69.54, 69.34 (0.5C), 69.28, 68.65, 62.18 (0.5C), 61.85 (0.5C) (10×***C***H_2O), 32.03, 31.89, 30.67 (0.5C), 30.56 (0.5C), 29.75, 29.58, 29.29, 25.58 (0.5C), 25.48 (1.5C), 22.68 (9×***C***H_2), 21.62 (Ar***C***H_3), 19.52 (0.5C), 19.30 (0.5C) (***C***H_2), 14.14 (CH_2***C***H_3).

***m/z* (ESI$^+$)** $[M+NH_4]^+$ = 606.4, *calc.* $C_{30}H_{56}NO_9S^+$ = 606.4.

Di(ethylene glycol) benzyl ether (26a)



Di(ethylene glycol) (**26**, 275.9 g, 2.6 mol , 10 equiv.) and potassium *tert*-butoxide (43.8 g, 0.4 mol) was dissolved in DMF (120 mL).To the ice-water bath cooled suspension was then slowly added benzyl bromide (30.9 mL, 0.26 mol). The ice bath was removed after 15mins, and the reaction mixture was left to stir at room temperature for 2.5 h. The reaction was then quenched with aq. NH_4Cl to reduce the PH to *ca.* 10 (spotting onto damp indicator strips). DMF was evaporated at reduced pressure by a rotary evaporator at 70 °C. The residue was partitioned between ethyl acetate (800 mL) and 10% brine (800 mL) and extracted with further 10% brine (2 ×300 mL). The combined organic layers were dried over Na_2SO_4, and the filtrate was evaporated and the crude material (116 g) was fractionated through a column of flash silica, eluting with a gradient of $CHCl_3$-heptane (20:80 to 100:0, v/v) then MeOH-$CHCl_3$ mixture (1:99 to 5:95, v/v), all solvents containing 1 vol% Et_3N, to afford a pale yellow oil (**26a**, 37.2 g, 73%).

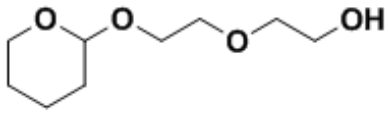
R_f (MeOH-$CHCl_3$ 1:19 + trace Et_3N) = 0.4.

^{1}H NMR (400 MHz, $CDCl_3$) δ = 7.25 – 7.04 (m, 5H, C***H*** on Ar), 4.41 (s, 2H, OC***H*$_2$**Ar), 3.59 – 3.53 (m, 2H, C***H*$_2$**OH), 3.53 – 3.40 (m, 6H, C***H*$_2$**O).

^{13}C NMR (101 MHz, $CDCl_3$) δ = 138.05 (**C** on Ar), 128.25 (2C), 127.63 (2C), 127.51 (5× ***C***H on Ar), 73.03(O***C***H_2Ar), 72.56, 70.23, 69.38 (6×***C***H_2O), 61.35 (***C***H_2OH).

***m*/*z* (ESI$^+$)** $[M+Na]^+$ = 219.1, *calc.* $C_{11}H_{16}NaO_3^+$ = 219.1.

α- Tetrahydropyranyl ethylene glycol (26c)

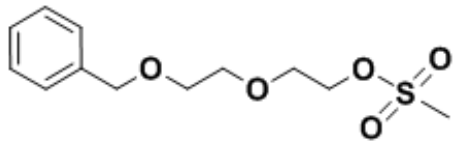


Di(ethylene glycol) (**26**, 244 g, 2.3 mol, 10 equiv.) was dissolved in CH_2Cl_2 (1 L). To this mixture was slowly added 3, 4-dihydro-2H-pyran (21 mL, 0.2 mol) and making sure it was

well stirred. Methanesulfonic acid (0.15 mL, 2.3 mmol, 0.01 equiv.) was prepared and slowly added into solution with a drop of 0.05 mL per time as acid catalysis. The extent of the reaction was monitored by TLC with every addition. The mixture was left to stir for 2 hours and quenched with sat. $NaHCO_3$. The mixture was extracted with CH_2Cl_2 (3 ×800 mL), the combined organic layers were dried over Na_2SO_4, and the solvent was stripped off. The crude residue (**26c**, 42.8 g) was fractionated by chromatography on flash silica, with a gradient of $CHCl_3$-heptane (20:80 to 100:0, v/v) then MeOH-$CHCl_3$ mixture (1:99 to 5:95, v/v), all solvents containing 1 vol% Et_3N, to afford the title compound as a colourless oil (**26c**, 37 g, 85%).

R_f (MeOH-$CHCl_3$ 1:19 + trace Et_3N) = 0.29.
^{1}H NMR (400 MHz, $CDCl_3$) δ= 4.43-4.41 (dd, J = 4.3, 2.9 Hz, 1H Thp C***H***), 3.71 – 3.58 (m, 2H, C***H*****$_2$**OH), 3.51 – 3.23 (m, 8H, C***H*****$_2$**O + Thp C**H**$_2$O), 1.68 – 1.25 (m, 6H, Thp C***H*****$_2$**).
^{13}C NMR (101 MHz, $CDCl_3$) δ = 98.70 (Thp ***C***H), 72.42, 70.16, 66.55 (2×O***C***H$_2$), 61.95 (Thp ***C***H$_2$O), 61.27 (***C***H$_2$OH), 30.31, 25.18, 19.23 (Thp ***C***H$_2$).
***m*/*z* (ESI$^+$)** $[M+Na]^+$ = 213.1, *calc.* $C_9H_{18}NaO_4^+$ = 213.1.

α-benzyloxy ethylene glycol-ω-methanesulfonate (27)



Di(ethylene glycol) benzyl ether (**26a,** 37.2 g, 0.19 mol) was co-evaporated from anhydrous MeCN (3 × 200 mL) and dissolved in CH_2Cl_2 (120 mL). To this ice-water bath cooled solution were added Et_3N (53 mL, 0.38 mol, 2 equiv.), and slowly added methane sulfonyl chloride (19 mL, 0.25 mol, 1.3 equiv.) from a syringe. The reaction was stirred for 2 h at room temperature. With vigorous stirring, the resulting orange-brown solution was quenched with $NaHCO_3$ (41.5 g, 0.5 mol, 2.6 equiv.), then the mixture was extracted with further CH_2Cl_2 (2 ×200 mL). The combined organic layers were dried over Na_2SO_4, and the solvent stripped off under reduced pressure. The product (**27,** 38.7 g, 74%) as a yellow oil, was used without further purification.

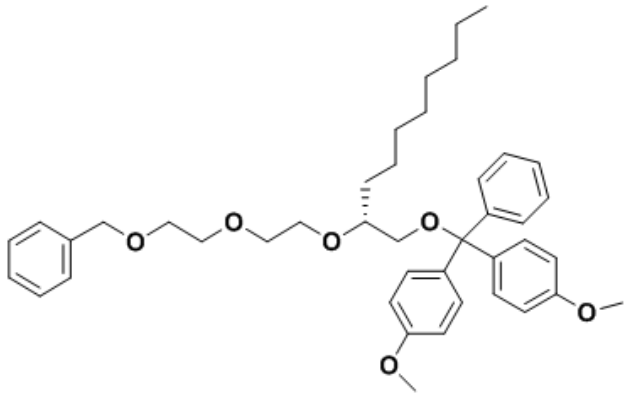
R_f (EtOH-CH_2Cl_2 1:19) = 0.86.

^{1}H NMR (400 MHz, $CDCl_3$) δ = 7.34 – 7.20 (m, 5H, C***H*** on Ar), 4.49 (s, 2H, OC***H*$_2$**Ar), 4.32 – 4.25 (m, 2H, C***H*$_2$**OMs), 3.70 – 3.55 (m, 6H, 3×C***H*$_2$**O), 2.94 (s, 3H, C***H*$_3$**).

^{13}C NMR (101 MHz, $CDCl_3$) δ = 138.21(**C** on Ar), 128.39 (2C), 127.73(2C), 127.66 (5× ***C***H on Ar), 73.06, 70.52, 69.63, 69.39(4×***C***H_2O), 68.89(***C***H_2OMs), 37.43(***C***H_3).

***m/z* (ESI$^+$)** $[M+NH_4]^+$ = 292.1, *calc.* $C_{12}H_{22}NO_5S^+$ = 292.1.

(*R*)-β-Octyl-α-(4, 4′-dimethoxytriphenylmethyl) -ω-benzyloxy trigol (28)



(*R*)-1-(4, 4'-Dimethoxytriphenylmethyl)-decan-2-ol (**18**, 26 g, 54 mmol) and α-benzyloxy ethylene glycol-ω-methanesulfonate (**27**, 37.4 g, 0.14 mol, 2.5 equiv.) were pre-mixed and co-evaporated from anhydrous MeCN (3 × 200 mL). The mixture was dissolved in DMF (60 mL). To the solution was added a 60% dispersion of NaH in mineral oil (4.36 g, 0.11 mmol, 2 equiv.). The reaction was well stirred and held at 50 °C overnight. The reaction was then quenched by the dropwise addition of aq. NH_4Cl until a pH to ca. 10 was attained (spotting onto moistened indicator strips). The DMF was evaporated under reduced pressure and the residue was re-dissolved in CH_2Cl_2 (400 mL). The solution was extracted with half-sat. $NaHCO_3$ (3×200 mL). The combined organic layers were dried over Na_2SO_4, and the solvent was stripped off. The crude residue (**28**, 67.8 g) was fractionated by chromatography on flash silica, eluting with a gradient of $CHCl_3$-heptane (20:80 to 100:0, v/v) then MeOH-$CHCl_3$ mixture (1:99 to 5:95, v/v), all solvents containing 1 vol% Et_3N, to afford the title compound as a dark yellow oil (**28**, 31.5 g, 88 %).

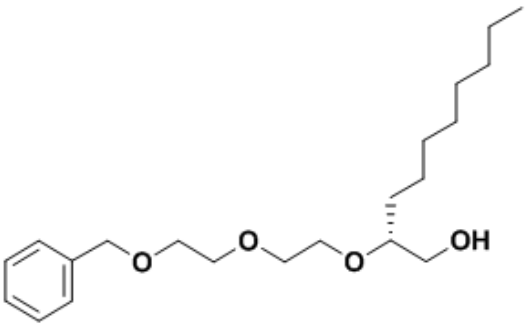
R_f (MeCN-CH_2Cl_2 1:49 + trace Et_3N) = 0.4.

^{1}H NMR (400 MHz, $CDCl_3$) δ = 7.57 – 7.51 (m, 2H, Bn C***H***), 7.46 – 7.20 (m, 12H, 9×Dmtr + 3×Bn C***H***), 6.90 – 6.83 (m, 4H, Dmtr C***H***), 4.60 (s, 2H, OC***H$_2$***Bn), 3.79 (s, 6H, 2×ArOC***H$_3$***), 3.76 – 3.65 (m, 8H, 4×C***H$_2$***O), 3.51 (m, 1H, C***H***CH_2ODmtr), 3.23 (dd, J = 9.8, 5.8 Hz, 1H, C***H***$_2$ODmtr), 3.14 (dd, J = 9.8, 4.2 Hz, 1H, C***H***$_2$ODmtr), 1.66 – 1.22 (m, 14H, 7×C***H$_2$***), 0.95-0.91 (t, J = 6.5 Hz, 3H, CH_2C***H$_3$***).

^{13}C NMR (101 MHz, $CDCl_3$) δ = 158.44 (2C), 145.30 (3×Dmtr***C***), 138.41(Bn ***C***), 136.46, 136.44 (2×Dmtr***C***), 130.15 (4C), 128.36(2C), 128.29, 127.77(2C), 127.73(2C), 127.56, 126.67(2C), 113.07(4C) (18×Dmtr + Bn ***C***H), 85.96 (O***C***Ar_3), 79.84(***C***HCH_2ODmtr), 73.26 (Bn O***C***H_2Ar), 71.08, 70.72, 69.75, 69.57 (4C, 4×***C***H_2O), 66.03(***C***H_2ODmtr), 55.15(2C, O***C***H_3), 32.26, 31.96, 29.78, 29.63, 29.34, 25.49, 22.74(7×***C***H_2), 14.20(CH_2***C***H_3).

***m/z* (ESI$^+$)** $[M+NH_4]^+$ = 672.4, *calc.* $C_{42}H_{58}NO_6^+$ = 672.4.

(*R*)-β-Octyl-*ω*-benzyloxy trigol (29)



To a solution of (*R*)-β-Octyl-*α*-(4, 4′-dimethoxytriphenylmethyl) -*ω*-benzyloxy trigol (**28**, 31.5 g, 48.1 mmol) in CH_2Cl_2 (442 mL) were added pyrrole (18.8 mL, 0.24 mol, 5 equiv.) and dichloroacetic acid (4.5 mL, 48 mmol). The reaction was briskly stirred for 3 h and quenched with sat. $NaHCO_3$. The resulting mixture was diluted with half-sat. $NaHCO_3$ (3 ×200 mL), the combined organic layers were dried over Na_2SO_4, and the solvent was evaporated under reduced pressure. The residue was fractionated through a column of flash silica in a sinter funnel**.** The crude material (**29**, 47.2 g) was dissolved and loaded in 20% CHCl3/ heptane. The silica was then washed with a gradient of EtOAc-heptane (5:95 to 100:0, v/v), to afford the title compound as a yellow oil (**29**, 16.2 g, 95%).

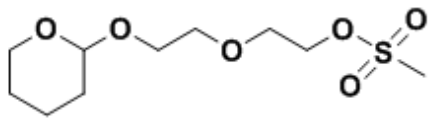
R_f (neat EtOAc) = 0.52.

^{1}H NMR (400 MHz, $CDCl_3$) δ = 7.37 – 7.23 (m, 5H, C***H*** on Ar), 4.56 (s, 2H, OC***H*$_2$**Ar), 3.84 – 3.74 (m, 1H, CH***H***OH), 3.71 – 3.55 (m, 8H, 4×C***H*$_2$**O), 3.47 (dd, *J* = 11.5, 7.2 Hz, 1H, CH***H***OH), 3.44 – 3.36 (m, 1H, C***H***CH_2OH), 1.55 – 1.23 (m, 14H, 7×C***H*$_2$**), 0.89 (t, *J* = 6.7 Hz, 3H, CH_2C***H*$_3$**).

^{13}C NMR (101 MHz, $CDCl_3$) δ = 138.16(**C** on Ar), 128.21(2C), 127.60(2C), 127.44(5× ***C***H on Ar), 73.12(O***C***H_2Ar), 70.93, 70.46, 69.30, 69.11, 64.62, (5C, 5×***C***H_2O), 60.15(***C***H_2OH), 31.82, 31.36, 29.75, 29.50, 29.22, 25.56, 22.60 (7×***C***H_2), 14.03(CH_2***C***H_3).

***m*/*z* (ESI$^+$)** $[M+NH_4]^+$ = 370.3, *calc.* $C_{21}H_{40}NO_4^+$ = 370.3.

α-tetrahydropyranyl ethylene glycol-ω-methanesulfonate (30)



Tetrahydropyranyl ethylene glycol (**26c**, 31.1 g, 0.19 mol) was co-evaporated from anhydrous MeCN (3 × 100 mL) and dissolved in CH_2Cl_2 (120 mL). To this ice-water bath cooled solution were added Et3N (51.5 mL, 0.37 mol, 2 equiv.) and slowly added methane sulfonyl chloride (18.6 mL, 0.24 mol, 1.3 equiv.) from a syringe. The reaction was stirred for 2 h at room temperature. With vigorous stirring, the resulting orange-brown solution was quenched with $NaHCO_3$ (40.3 g, 0.48 mmol, 2.6 equiv.), then the mixture was extracted with further CH_2Cl_2 (2 ×200 mL). The combined organic layers were dried over Na_2SO_4, and the solvent was stripped off under reduced pressure. The crude product (**30,** 45.2 g, 91%) as a pale yellow oil was used without further purification.

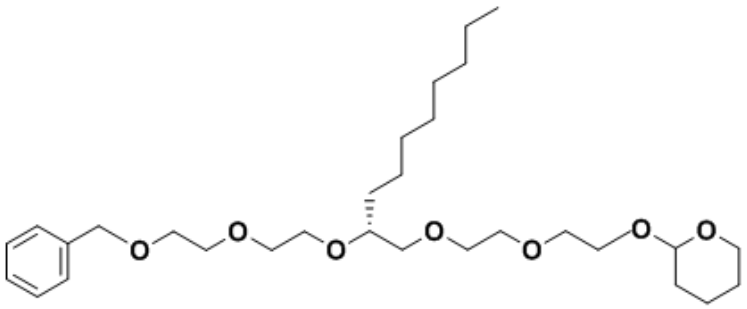
R_f (MeOH-$CHCl_3$ 1:19) = 0.53.

^{1}H NMR (400 MHz, $CDCl_3$) δ = 4.44 (dd, *J* = 4.4, 2.8 Hz, 1H, Thp C***H***), 4.26 – 4.16 (m, 2H, C***H*$_2$**OMs), 3.73 – 3.64 (m, 2H, Thp OC***H*$_2$**), 3.64 – 3.28 (m, 6H, 3×C***H*$_2$**O), 2.92 (s, 3H, C***H*$_3$**), 1.71 – 1.28 (m, 6H, 3×C***H*$_2$**).

^{13}C NMR (101 MHz, $CDCl_3$) δ = 98.78(Thp ***C***H), 70.41, 69.49, 68.81(3×***C***H_2O), 66.42(***C***H_2OMs), 62.06(Thp ***C***H_2O), 37.39 (***C***H_3), 30.44, 25.24, 19.37(Thp 3× ***C***H_2).

***m*/*z* (ESI$^+$)** $[M+NH_4]^+$ = 286.1, *calc.* $C_{10}H_{24}NO_6S^+$ = 286.1.

(*R*)-8-Octyl-α-tetrahydropyranyl-ω-benzyloxy pentagol (31)



(*R*)-β-Octyl-ω-benzyloxy trigol (**29**, 16.2 g, 46 mmol) and α- tetrahydropyranyl ethylene glycol-ω-methanesulfonate (**30**, 30.8 g, 115 mmol, 2.5 equiv.) were pre-mixed and co-evaporated from MeCN (3 × 150 mL). The mixture was dissolved in DMF (71 mL). To the solution was added a 60% dispersion of NaH in mineral oil (3.7 g, 92 mmol, 2 equiv.). The reaction was well stirred and held at 50 °C for overnight. The reaction was quenched by the dropwise addition of aq. NH_4Cl until a pH to ca. 10 was attained (spotting onto moistened indicator strips). The DMF was evaporated under reduced pressure and the residue was re-dissolved in CH_2Cl_2 (300 mL). The solution was extracted with half-sat. $NaHCO_3$ (3×200 mL), the combined organic layers dried over Na_2SO_4, and the solvent was stripped off. The crude residue was fractionated by chromatography on flash silica, eluting with a gradient of ethyl acetate-heptane, all solvents containing 1 vol% Et_3N to afford the title compound as a dark yellow oil (**31**, 21.9 g, 91 %).

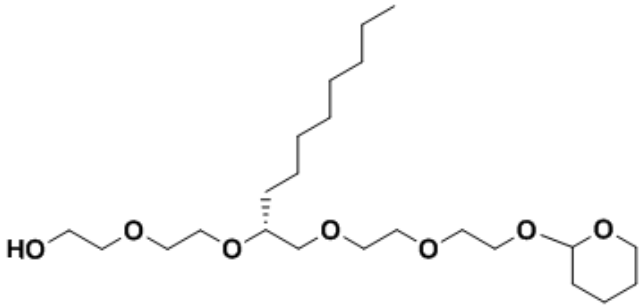
R_f (neat EtOAc + trace Et_3N) = 0.56.

^{1}H NMR (400 MHz, $CDCl_3$) δ = 7.23 – 7.08 (m, 5H, C***H*** on Ar), 4.50 (t, *J* = 3.6 Hz, 1H, Thp C***H***), 4.43 (s, 2H, OC***H*$_2$**Ar), 3.78 – 3.61 (m, 3H, C***H***(Oct)CH_2+ C***H*$_2$**O), 3.58 – 3.30 (m, 18H, 9×C***H*$_2$**O), 1.78 – 1.36 (m, 6H, Thp 3×C***H*$_2$**), 1.36 – 1.07 (m, 14H, 7×C***H*$_2$**), 0.77 (t, *J* = 6.7 Hz, 3H, CH_2C***H*$_3$**).

^{13}C NMR (101 MHz, $CDCl_3$) δ = 138.29 (**C** on Ar), 128.13(2C), 127.45(2C), 127.32 (5× ***C***H on Ar), 98.63(0.5C), 98.57(0.5C) (Thp ***C***H), 79.08 (***C***H(Oct)CH_2), 73.93 (O***C***H_2(Oct)), 73.02 (O***C***H_2Ar), 70.86, 70.70, 70.53, 70.43, 69.40, 69.31 (6C, 6×***C***H_2O), 66.49 (Thp O***C***H_2), 61.74, 31.85, 31.78(0.5C), 30.46(0.5C), 29.67, 29.48, 29.19, 25.39, 25.35, 22.56, 19.29(0.5C), 19.25 (0.5C) (10×***C***H_2), 14.00(CH_2***C***H_3).

***m*/*z* (ESI$^+$)** $[M+NH_4]^+$ = 542.4, *calc.* $C_{30}H_{56}NO_7^+$ = 542.4.

(*R*)-8-Octyl-α-tetrahydropyranyl pentagol (32)



(*R*)-8-Octyl-α-tetrahydropyranyl-ω-benzyloxy pentagol (**31,** 10.1 g/ 11.7 g, 19.4 mmol/ 22.4 mmol) was dissolved in MeOH (270 mL/ 310 mL), to which were added activated charcoal (2.51 g/ 2.91 g), then a freshly prepared solution of palladium diacetate (619 mg, 2.76 mmol, 0.07 equiv.) in THF (30 mL). The suspension was evacuated to the point that bumping commenced, then let down to argon, and this process was repeated five times. After a final evacuation, the argon line was replaced with a hydrogen balloon, and the flask was filled with hydrogen gas. The suspension was stirred vigorously at room temperature for 2.5 h. The hydrogen was evacuated, flushing the flask five times with argon in an ice bath. The solution was filtered through a filter paper and the charcoal rinsed with MeOH (200 mL); ethyl acetate (200 mL) and $CHCl_3$ (200 mL) sequentially. The combined filtrate was evaporated under vacuum and the crude material was fractionated through a column of flash silica, eluting with a gradient of EtOAc-heptane (5:95 to 100:0) then MeOH-EtOAc (1:99 to 10:90), all solvents containing 1 vol% Et_3N, to afford a pale yellow oil (**32**, 14.1 g, 78%).

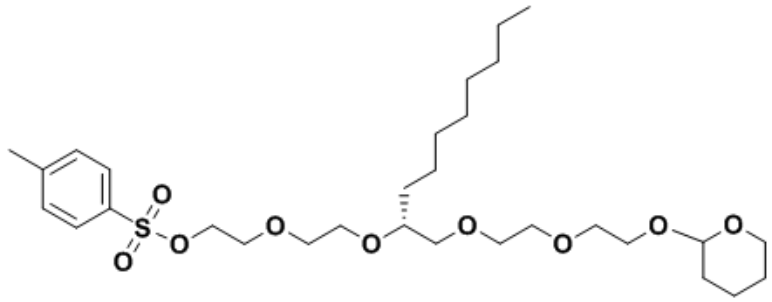
R_f (neat EtOAc + trace Et_3N) = 0.17.

^{1}H NMR (400 MHz, $CDCl_3$) δ = 4.52 – 4.45 (m, 1H, Thp C***H***), 3.76 – 3.40 (m, 17H, 8.5×C***H*₂**O), 3.39 – 3.22 (m, 4H, 1.5×C***H*₂**O + C***H***CH_2OThp), 1.75 – 1.34 (m, 6H, Thp C***H*₂**), 1.36 – 0.99 (m, 14H, 7×C***H*₂**), 0.72 (t, J = 6.8 Hz, 3H, CH_2C***H*₃**).

^{13}C NMR (101 MHz, $CDCl_3$) δ = 98.63(Thp ***C***H), 79.15(***C***HCH_2OThp), 73.88, 72.44, 70.61, 70.46, 70.36, 69.23, 66.47, 61.84, 61.40, 45.96 (10×***C***H_2O), 31.71, 31.63, 30.38, 29.59, 29.38, 29.11, 25.30, 22.49, 19.24, 13.93(10×***C***H_2), 11.24(CH_2***C***H_3).

***m*/*z* (ESI$^+$)** $[M+NH_4]^+$ = 452.3, *calc.* $C_{23}H_{50}NO_7^+$ = 452.3.

(*R*)-8-Octyl-α-tetrahydropyranyl-ω-toluenesulfonyl pentagol (33)



(*R*)-8-Octyl-α-tetrahydropyranyl pentagol (**32,** 3.8 g, 8.7 mmol) was evaporated from anhydrous MeCN (3 × 30 mL) and re-dissolved in CH_2Cl_2 (130 mL). To the solution were added Et_3N (3.6 mL, 26.1 mmol, 3 equiv.), *N*-methyl imidazole (0.35 mL, 4.4 mmol, 0.5 equiv.) and toluene sulfonyl chloride (2.48 g, 13 mmol, 1.5 equiv.), and the reaction was stirred for 2h at room temperature. The solution appeared orange-brown and the reaction was quenched with $NaHCO_3$ (1.9 g, 22.6 mmol, 2.6 equiv.) with vigorous stirring. Then the mixture was partitioned with the original CH_2Cl_2, the aqueous layer was extracted with further CH_2Cl_2 (2 ×200 mL). The combined organic layers were dried over Na_2SO_4, and the solvent was stripped off under reduced pressure. The crude residue was fractionated by chromatography on flash silica, eluting with a gradient of EtOAc-heptane (10:90 to 100:0, v/v) then MeOH-EtOAc (1:99 to 5:95, v/v), all solvents containing 1 vol% Et_3N, to afford the title compound as a pale yellow oil (**33**, 4.94 g, 97%).

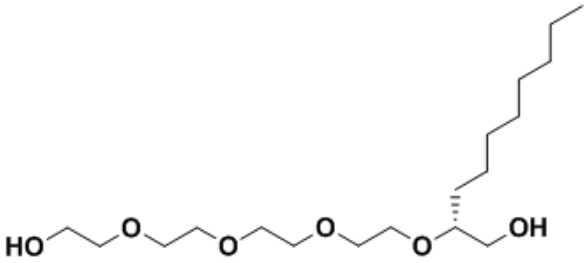
R_f (MeOH-$CHCl_3$ 1:19 + trace Et_3N) = 0.6

^{1}H NMR (400 MHz, $CDCl_3$) δ = 7.64 (d, J = 8.3 Hz, 2***H***), 7.20 (d, J = 8.0 Hz, 2H) (4×Ts C***H***), 4.48 (t, J = 3.6 Hz, 1H, Thp C***H***), 4.01-3.99 (m, 2H, C***H*****$_2$**OTs), 3.77 – 3.22 (m, 19H, 9×C***H*****$_2$**O + C***H*** (Oct)CH_2O), 2.30 (s, 3H, ArC***H*****$_3$**), 1.76 – 1.03 (m, 20H, 10×C***H*****$_2$**), 0.74 (t, J = 6.7 Hz, 3H, CH_2C***H*****$_3$**).

^{13}C NMR (101 MHz, $CDCl_3$) δ =144.51, 133.05(2×Ts ***C***), 129.67(2C), 127.77(2C) (4×Ts ***C***H), 98.65(Thp ***C***H), 79.09(***C***H(Oct)CH_2O), 73.84, 70.84, 70.63, 70.48, 70.37, 69.21, 69.17, 68.42, 66.48, 61.87 (10×***C***H_2O), 31.73, 30.45, 29.61, 29.41, 29.15, 28.88, 25.34, 25.31, 22.53(9×***C***H_2), 21.40(Ar***C***H_3), 19.33(***C***H_2), 13.97(CH_2***C***H_3).

***m*/*z* (ESI$^+$)** $[M+NH_4]^+$ = 606.4, *calc.* $C_{30}H_{56}NO_9S^+$ = 606.4.

(*R*)-2-Octyl pentagol (34)



(*R*)-β-Octyl-α-tetrahydropyranyl-ω-(2-naphthyl methyl) pentagol (**23**, 25 g, 43.5 mmol) was dissolved in MeOH (50 mL), to which were added activated charcoal (6 g), then a freshly prepared solution of palladium diacetate (0.64 g, 2.9 mmol, 0.066 equiv.) in THF (40 mL). The suspension was evacuated to the point that bumping commenced, then let down to argon, and this process was repeated five times. After a final evacuation, the argon line was replaced with a hydrogen balloon, and the flask was filled with hydrogen gas. The suspension was stirred vigorously at room temperature overnight. Then the hydrogen was evacuated, flushing the flask five times with argon. The solution was filtered through a pad of Celite S in a small sintering funnel, and the charcoal rinsed with MeOH (100 mL); ethyl acetate (100 mL) and $CHCl_3$(100 mL) sequentially. The combined filtrate was evaporated under vacuum, and the residue (30.4 g) was fractionated through a column of flash silica, eluting with a gradient of EtOAc-heptane (1:90 to 100:0) then MeOH-EtOAc (1:99 to 10:90), all solvents containing 1 vol% Et_3N, to afford a pale yellow oil (**34**, 14.1 g, 70%).

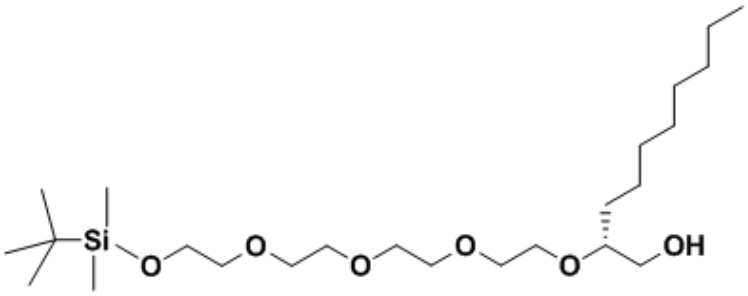
R_f (EtOH-$CHCl_3$ 1:19 + trace Et_3N) = 0.24.

^{1}H NMR (400 MHz, $CDCl_3$) δ = 3.77 – 3.69 (m, 2H, C***H*₂**OH), 3.68 – 3.40 (m, 16H, 8×C***H*₂**O), 3.34 (dd, *J* = 4.9, 2.7 Hz, 1H, C***H***CH_2OH), 1.54 – 1.09 (m, 14H, 7×C***H*₂**), 0.82 (t, *J* = 6.8 Hz, 3H, CH_2C***H*₃**).

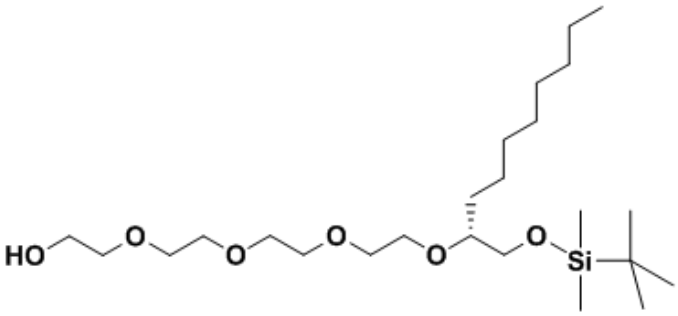
^{13}C NMR (101 MHz, $CDCl_3$) δ = 81.58 (***C***HCH_2OH), 72.67, 70.83, 70.51, 70.34 (2C), 70.12, 69.03, 64.65 (8×***C***H_2O), 61.42 (CH***C***H_2OH), 46.09 (***C***H_2OH), 31.81, 31.25, 29.71, 29.47, 29.20, 25.59, 22.60, (7×***C***H_2), 14.05 (CH_2***C***H_3).

***m*/*z* (ESI$^+$)** $[M+NH_4]^+$ = 368.5, *calc.* $C_{18}H_{42}O_6N^+$ = 368.5.

(*R*)-β-Octyl-*ω*- *tert*-Butyldimethylsilyl pentagol (35)



(*R*)-β-Octyl-*α*- *tert*-Butyldimethylsilyl pentagol (36)



(*R*)-2-Octyl pentagol (**34**, 13.3 g, 37.9 mmol) and imidazole (5.17 g, 75.9 mmol, 2 equiv.) were dissolved in 30 mL dry DMF. Subsequently, 60 mL DMF solution of TbdmsCl (5.72 g, 37.9 mmol) was added dropwise to the above solution via a constant pressure dropping funnel over 30 mins. The resulting reaction mixture was stirred for 3 h under argon atmosphere at room temperature. The reaction was concentrated at reduced pressure at 70 °C. The residue was then diluted in DCM (100 mL) and extracted with 20 % $NaHCO_3$ aqueous solution (3×50 mL). The DCM phase was collected and dried with Na_2SO_4, the solvent was stripped off under reduced pressure. The crude residue was fractionated by chromatography on flash silica, eluting with a gradient of EtOAc-heptane (5:95 to 100:0, v/v) then MeOH-EtOAc (1:99 to 5:95, v/v), all solvents containing 1 vol% Et_3N, to afford the title compound as a pale yellow oil (**35**, 6.24 g, 35 %; **36**, 2.37g, 13 %).

Compound **35**: R_f (neat EtOAc + trace Et_3N) = 0.42.

^{1}H NMR (400 MHz, DMSO-*d*$_6$) δ = 4.46 (t, *J* = 5.6 Hz, 1H, O***H***), 3.68 (t, *J* = 5.1 Hz, 2H, C***H*$_2$**OTbdms), 3.65 – 3.40 (m, 14H, 7×C***H*$_2$**O), 3.25 – 3.18 (m, 1H, C***H***CH_2OTbdms), 2.51 (p, *J* = 1.8 Hz, 2H, C***H*$_2$*OH*), 1.25 (s, 14H, 7×C***H*$_2$**), 0.86 (s, 12H, CH_2C***H*$_3$**+ 3×CC***H*$_3$**), 0.04 (s, 6H, 2×SiC***H*$_3$**).

^{13}C NMR (101 MHz, DMSO) δ=80.77 (***C***HCH$_2$OH), 72.38, 70.68, 70.42, 70.32(2***C***), 70.28, 68.87 (7×***C***H$_2$O), 63.55 (***C***H$_2$OH), 62.78 (***C***H$_2$OTbdms), 31.78 (***C***Si), 31.60, 29.75, 29.52, 29.17(4×***C***H$_2$), 26.26(3×Si***C***H$_3$), 25.33, 22.57, 18.37(3×***C***H$_2$), 14.41(CH$_2$***C***H$_3$), -4.82 (2×Si***C***H$_3$).

***m/z* (ESI$^+$)** [M+NH$_4$]$^+$ = 482.3, *calc.* $C_{24}H_{56}O_6SiN^+$ = 482.3.

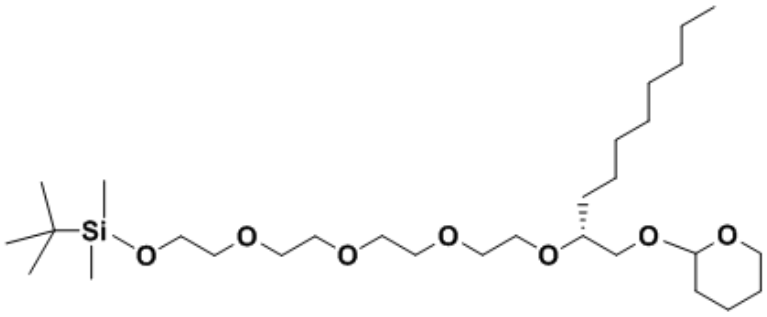
Compound **36**: R_f (neat EtOAc + trace Et_3N) = 0.33.

^{1}H NMR (400 MHz, DMSO-*d*$_6$) δ = 4.58 (t, *J* = 5.4 Hz, 1H, O***H***), 3.67 – 3.46 (m, 14H, 7×C***H$_2$***O), 3.41 (dd, *J* = 5.3, 4.5 Hz, 2H, C***H$_2$***OTbdms), 3.30 – 3.23 (m, 1H, C***H***CH$_2$OTbdms), 2.51 (p, *J* = 1.9 Hz, 2H, C***H$_2$OH***), 1.53 – 1.15 (m, 14H, 7×C***H$_2$***), 0.89 – 0.81 (m, 12H, CH$_2$C***H$_3$***+ 3×CC***H$_3$***), 0.04 (s, 6H, 2×SiC***H$_3$***).

^{13}C NMR (101 MHz, DMSO) δ= 80.28 (***C***H(Oct)), 72.82, 70.67, 70.32, 70.28 (2***C***), 70.24, 69.21 (7×***C***H$_2$O), 65.24(***C***H$_2$OTbdms), 60.67(***C***H$_2$OH), 31.76(***C***Si), 31.40, 29.62, 29.39, 29.10(4×***C***H$_2$), 26.22(3×Si***C***H$_3$), 25.09, 22.56, 18.37(3×***C***H$_2$), 14.40(CH$_2$***C***H$_3$), -4.95, -4.98(2×Si***C***H$_3$).

***m/z* (ESI$^+$)** [M+NH$_4$]$^+$ = 482.3, *calc.* $C_{24}H_{56}O_6SiN^+$ = 482.3.

(*R*)-β-Octyl-*α*-tetrahydropyranyl-*ω*-*tert*-Butyldimethylsilyl pentagol (37)



(*R*)-β-Octyl-*ω*-*tert*-Butyldimethylsilyl pentagol (**35**, 5.13 g, 11 mmol) was dissolved in CH_2Cl_2 (100 mL). To this mixture was slowly added 3, 4-dihydro-2H-pyran (2.5 mL, 28 mmol, 2.5 equiv.) and making sure it was well stirred. A solution of p-toluenesulfonic acid (18.9 mg, 0.11 mmol, 0.01 equiv.) in 1 mL THF was slowly added with a drop of 0.1 mL per time as acid catalysis. The extent of the reaction was monitored by TLC with very addition. The mixture was left stirring for 2 hours and quenched with sat. $NaHCO_3$. The mixture was extracted with CH_2Cl_2 (3 ×100 mL), the combined organic layers were dried over Na_2SO_4, and the solvent

was stripped off. The crude residue (**37**, 5.94 g, 98%) as a pale yellow oil, was used without further purification.

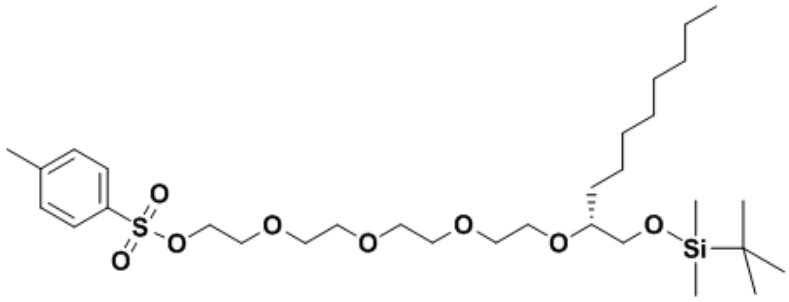
R_f (MeOH-$CHCl_3$ 1:19 + trace Et_3N) = 0.6.

^{1}H NMR (400 MHz, DMSO-*d*$_6$) δ = 4.58 (d, *J* = 3.2 Hz, 1H, Thp C***H***), 3.87 – 3.75 (m, 2H, C***H***$_2$OTbdms), 3.75 – 3.34 (m, 19H, 8.5×C***H***$_2$O+ Thp C***H***$_2$), 1.84 – 1.18 (m, 20H, 10×C***H***$_2$), 0.86 (s, 9H, 3×CC***H***$_3$), 0.83 (d, *J* = 7.0 Hz, 3H, CH_2C***H***$_3$), 0.03 (s, 6H, 2×SiC***H***$_3$).

^{13}C NMR (101 MHz, DMSO) δ= 98.55(Thp ***C***H), 79.43(***C***H(Oct)CH_2O), 72.62, 70.87, 70.70, 70.55, 70.39, 69.52, 69.31, 62.67 (8×***C***H_2O), 62.11(***C***H_2OTbdms), 61.76(Thp ***C***H_2O), 32.02(***C***Si), 31.84, 30.61, 30.50, 29.70, 29.53, 29.24 (6×***C***H_2), 25.88, 25.53, 25.45(3×Si***C***H_3), 22.62, 19.46, 19.22, 18.30 (4×***C***H_2), 14.06 (CH_2***C***H_3), -5.31 (2×Si***C***H_3).

***m*/*z* (ESI$^+$)** $[M+NH_4]^+$ = 566.4, *calc.* $C_{29}H_{64}O_7SiN^+$ = 566.4.

(*R*)-β-Octyl-*α*-*tert*-Butyldimethylsilyl-*ω*-toluenesulfonyl pentagol (38)



(*R*)-β-Octyl-*α*-*tert*-Butyldimethylsilyl pentagol (**36,** 2.02 g, 4.34 mmol) was evaporated from anhydrous MeCN (3 × 15 mL) and re-dissolved in CH_2Cl_2 (65 mL). To the solution were added Et_3N (1.82 mL, 13 mmol, 3 equiv.), *N*-methyl imidazole (0.17 mL, 2.17 mmol, 0.5 equiv.) and toluene sulfonyl chloride (1.24 g, 6.52 mmol, 1.5 equiv.), and the reaction was stirred for 6h at room temperature. The solution appeared orange-brown and the reaction was quenched with $NaHCO_3$ (0.95 g, 11.3 mmol, 2.6 equiv.) with vigorous stirring. Then the mixture was partitioned with the original CH_2Cl_2, the aqueous layer was extracted with further CH_2Cl_2 (2 ×100 mL). The combined organic layers were dried over Na_2SO_4, and the solvent was stripped off under reduced pressure. The crude residue was fractionated by chromatography on flash silica, eluting with a gradient of EtOAc-heptane (20:80 to 100:0, v/v) then MeOH-EtOAc (1:99

to 5:95, v/v), all solvents containing 1 vol% Et_3N, to afford the title compound as a pale yellow oil (**38**, 2.59 g, 96%).

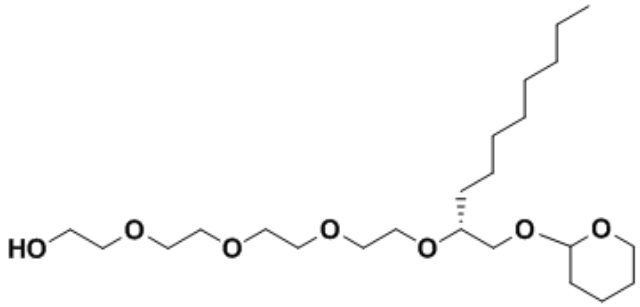
R_f (MeOH-$CHCl_3$ 1:19 + trace Et_3N) = 0.64

^{1}H NMR (400 MHz, DMSO-*d*$_6$) δ = 7.75 (d, *J* = 8.4 Hz, 2***H***), 7.29 (d, *J* = 8.3 Hz, 2***H***) (4×Ts C***H***), 4.14 – 4.07 (m, 2H, C***H*****$_2$**OTbdms), 3.75 – 3.45 (m, 16H, 8×C***H*****$_2$**O), 3.27 (s, 1H, C***H***CH_2OTbdms), 2.40 (s, 3H, ArC***H*****$_3$**), 0.85 (s, 12H, CH_2C***H*****$_3$**+ 3×CC***H*****$_3$**), 0.01 (s, 6H, 2×SiC***H*****$_3$**).

^{13}C NMR (101 MHz, DMSO) δ=144.67, 133.05(2×Ts ***C***), 129.75(2C), 127.90(2C) (4×Ts ***C***H), 80.98(***C***HCH_2OTbdms), 70.87, 70.67, 70.58, 70.49(2***C***), 69.50, 69.20, 68.60(8×***C***H_2O), 65.62(***C***H_2OTbdms), 31.83(***C***Si), 31.54, 29.73, 29.51, 29.23 (4×***C***H_2), 25.87(3×Si***C***H_3), 25.34, 22.61(2×***C***H_2), 21.54(Ar***C***H_3), 18.22(***C***H_2), 14.06(CH_2***C***H_3), -5.38, -5.44(2×Si***C***H_3).

***m*/*z* (ESI$^+$)** $[M+NH_4]^+$ = 636.39, *calc.* $C_{31}H_{62}O_8SSiN^+$ = 636.36.

(*R*)-β-Octyl-α-tetrahydropyranyl pentagol (39)



(*R*)-β-Octyl-α-tetrahydropyranyl-ω-*tert*-Butyldimethylsilyl pentagol (**37**, 6.36 g, 11.6 mmol) was dissolved in 1M of Et_4NF in MeCN (19.3 mL, 1.5 equiv.). After being stirred for 8 hours at room temperature, the mixture was concentrated under reduced pressure. The residue was then diluted in $CHCl_3$ (150 mL) and extracted with 10 % $NaHCO_3$ aqueous solution (3×50 mL). The organic phase was collected and dried with Na_2SO_4, the solvent was stripped off under reduced pressure. The crude residue was fractionated by chromatography on flash silica, eluting with a gradient of $CHCl_3$-heptane (20:80 to 100:0, v/v) then MeOH-$CHCl_3$ (1:99 to 10:90, v/v), all solvents containing 1 vol% Et_3N, to afford the title compound as a pale yellow oil (**39**, 4.62 g, 92%).

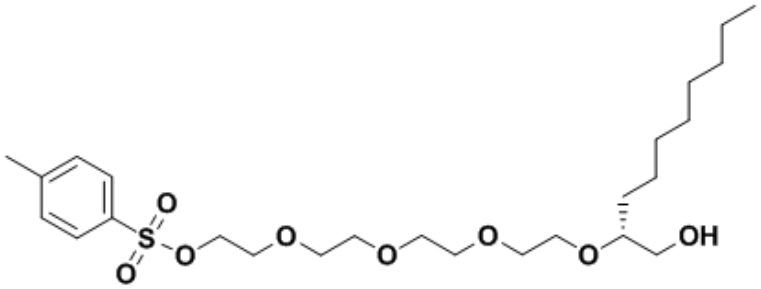
R_f (MeOH-$CHCl_3$ 1:19 + trace Et_3N) = 0.41

^{1}H NMR (400 MHz, DMSO-*d*$_6$) δ = 4.57 (q, *J* = 3.9 Hz, 1H, Thp C***H***), 3.87 – 3.32 (m, 21H, 9.5×C***H***$_2$O+ Thp C***H***$_2$), 1.86 – 1.13 (m, 20H, 10×C***H***$_2$), 0.85 – 0.80 (m, 3H, CH_2C***H***$_3$).

^{13}C NMR (101 MHz, DMSO) δ= 99.11 (0.5C), 98.54(0.5C) (Thp ***C***H), 79.43(0.5C), 79.16(0.5C) (***C***H(Oct)CH_2O), 72.55, 70.85, 70.59, 70.54, 70.50, 70.37(0.5C), 70.30, 69.50, 69.29(0.5C), 62.08 (0.5C), 61.75 (0.5C), 61.59, (9×***C***H_2O+Thp ***C***H_2O), 31.97, 31.82, 30.59 (0.5C), 30.47(0.5C), 29.69, 29.51, 29.22, 25.65, 25.42, 22.61, 19.40(0.5C), 19.18 (0.5C) (10×***C***H_2), 14.05(CH_2***C***H_3).

***m*/*z* (ESI$^+$)** $[M+NH_4]^+$ = 452.3, *calc.* $C_{23}H_{50}O_7N^+$ = 452.3.

(*R*)-β-Octyl-*ω*-toluenesulfonyl pentagol (40)



(*R*)-β-Octyl-*α*-*tert*-Butyldimethylsilyl-*ω*-toluenesulfonyl pentagol (**38**, 2.8 g, 4.51 mmol) was dissolved in MeOH: H_2O mixture (95:5 v/v, 100 mL). To this mixture was added 4M HCl slowly with a drop of 30 μL per time. The extent of the reaction was monitored by TLC with every addition. The resulting reaction mixture was stirred for 3 h under argon atmosphere at room temperature and quenched with sat. $NaHCO_3$. The reaction was concentrated at reduced pressure. The residue was then diluted in $CHCl_3$ (100 mL) and extracted with half sat. $NaHCO_3$ aqueous solution (3×50 mL). The organic phase was collected and dried with Na_2SO_4, the solvent was stripped off under reduced pressure. The crude residue was fractionated by chromatography on flash silica, eluting with a gradient of $CHCl_3$-heptane (20:80 to 100:0, v/v) then MeOH-$CHCl_3$ (1:99 to 10:90, v/v), to afford the title compound as a pale yellow oil (**40**, 2.17 g, 95 %).

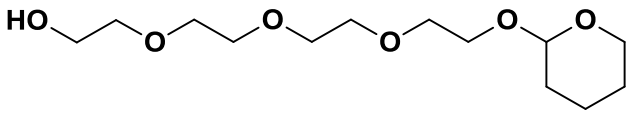
R_f (MeOH-$CHCl_3$ 1:19) = 0.36

^{1}H NMR (400 MHz, DMSO-*d*$_6$) δ =7.77 (d, *J* = 8.4 Hz, 2***H***), 7.32 (d, *J* = 8.1 Hz, 2***H***) (4×Ts C***H***), 4.17 – 4.10 (m, 2H, C***H***$_2$OTs), 3.83 – 3.29 (m, 18H, 9×C***H***$_2$O), 3.15 (s, 1H, C***H***CH$_2$OH), 2.42 (s, 3H, ArC***H***$_3$), 1.25 (m, 14H, 7×C***H***$_2$), 0.85 (t, *J* = 6.8 Hz, 3H, CH$_2$C***H***$_3$).

^{13}C NMR (101 MHz, DMSO) δ=^{13}C NMR (101 MHz, Chloroform-*d*) δ 144.75, 133.00(2×Ts ***C***), 129.80(2C), 127.93(2C) (4×Ts ***C***H), 81.56(***C***HCH$_2$OH), 70.90, 70.67, 70.48(2C), 70.43, 69.25, 69.13, 68.61(8×***C***H$_2$O), 64.81(***C***H$_2$OH), 31.83, 31.36, 29.74, 29.50, 29.22, 25.61, 22.62(7×***C***H$_2$), 21.60(Ar***C***H$_3$), 14.08 (CH$_2$***C***H$_3$).

***m*/*z* (ESI$^+$)** [M+Na]$^+$ = 527.3, *calc.* $C_{25}H_{44}O_8SNa^+$ = 527.3.

α-tetrahydropyranyl tetraethylene glycol (41)



Tetraethylene glycol (**19**, 100 g, 0.51 mol, 10 equiv.) was dissolved in CH_2Cl_2 (500 mL). To this mixture was slowly added 3, 4-dihydro-2H-pyran (4.6 mL, 0.05 mol) and making sure it was well stirred. Methanesulfonic acid (0.03 mL, 0.5 mmol, 0.01 equiv.) was prepared and slowly added into solution with a drop of 0.005 mL per time as acid catalysis. The extent of the reaction was monitored by TLC with every addition. The mixture was left to stir for 2 hours and quenched with sat. NaHCO3. The mixture was extracted with CH2Cl2 (3 ×400 mL), the combined organic layers were dried over Na2SO4, and the solvent was stripped off. The crude residue (**41**, 13.3 g) was fractionated by chromatography on flash silica, with a gradient of $CHCl_3$-heptane (20:80 to 100:0, v/v) then MeOH-$CHCl_3$ mixture (1:99 to 5:95, v/v), all solvents containing 1 vol% Et_3N, to afford the title compound as a colourless oil (**41**, 11.4 g, 82%).

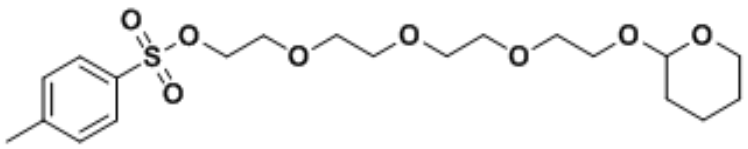
R_f (MeOH-$CHCl_3$ 1:19 + trace Et_3N) = 0.31.

^{1}H NMR (400 MHz, CDCl$_3$) δ= 4.61 (dd, *J* = 4.3, 3.0 Hz, 1H Thp C***H***), 3.87 – 3.8 (m, 2H, C***H***$_2$OH), 3.71 – 3.43 (m, 16H, 7×C***H***$_2$O + Thp C**H**$_2$O), 1.86 – 1.40 (m, 6H, Thp 3×C***H***$_2$).

^{13}C NMR (101 MHz, CDCl$_3$) δ = 98.88(Thp ***C***H), 72.58, 70.59, 70.55, 70.52, 70.49, 70.29, 66.60(7×O***C***H$_2$), 62.16(Thp ***C***H$_2$O), 61.64(***C***H$_2$OH), 30.48, 25.38, 19.40(Thp 3× ***C***H$_2$).

***m*/*z* (ESI$^+$)** [M+Na]$^+$ = 301.2, *calc.* $C_{13}H_{26}NaO_6^+$ = 301.2.

α-tetrahydropyranyl tetraethylene glycol-ω- toluenesulfonate (42)



α-tetrahydropyranyl tetraethylene glycol (**41,** 7.37 g, 26.5 mmol) was co-evaporated from anhydrous MeCN (3 × 40 mL) and re-dissolved in CH_2Cl_2 (200 mL). To the solution were added Et_3N (11.1 mL, 79.4 mmol, 3 equiv.), *N*-methyl imidazole (1.1 mL, 13.2 mmol, 0.5 equiv.) and toluene sulfonyl chloride (7.57 g, 39.7 mmol, 1.5 equiv.), and the reaction was stirred for 2h at room temperature. The solution appeared orange-brown and the reaction was quenched with $NaHCO_3$ (5.78 g, 68.9 mmol, 2.6 equiv.) with vigorous stirring. Then the mixture was partitioned with the original CH_2Cl_2, the aqueous layer was extracted with further CH_2Cl_2 (2 ×400 mL). The combined organic layers were dried over Na_2SO_4, and the solvent was stripped off under reduced pressure. The crude residue (**42**, 13.6 g) was fractionated by chromatography on flash silica, eluting with a gradient of EtOAc-heptane (5:95 to 70:30, v/v), all solvents containing 1 vol% Et_3N to afford the title compound as a pale yellow oil (**42**, 9.36 g, 82%).

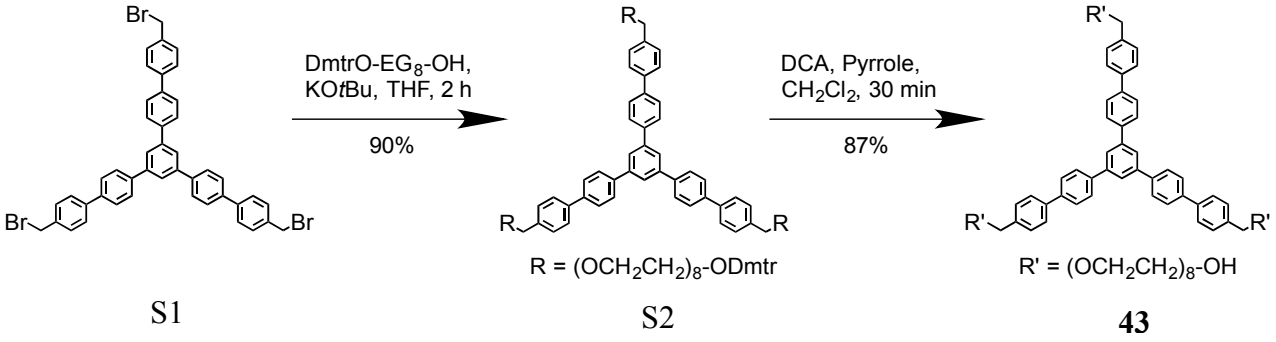
R_f (MeOH-$CHCl_3$ 1:19 + trace Et_3N) = 0.43.

^{1}H NMR (400 MHz, $CDCl_3$) δ = 7.62 (d, J = 8.3 Hz, 2***H***), 7.20 (d, J = 8.1 Hz, 2H) (4×Ts C***H***), 4.46 (dd, J = 4.3, 2.9 Hz, 1H, Thp C***H***), 4.03 – 3.97 (m, 2H, C***H$_2$***OTs), 3.75 – 3.63 (m, 2H, Thp OC***H$_2$***), 3.56 – 3.29 (m, 14H, 7×C***H$_2$***O), 2.28 (s, 3H C***H$_3$***), 1.77 – 1.22 (m, 6H, Thp 3×C***H$_2$***).

^{13}C NMR (101 MHz, $CDCl_3$) δ = 144.65, 132.92(2×Ts ***C***), 129.73(2C), 127.76(2C) (4×Ts ***C***H)), 98.69(Thp ***C***H), 70.51, 70.45, 70.41, 70.35, 69.26, 68.46, 66.46 (7×O***C***H_2), 61.94 (Thp ***C***H_2O), 46.14(***C***H_3), 30.46, 25.32, 19.35(Thp 3× ***C***H_2).

***m/z* (ESI$^+$)** $[M+Na]^+$ = 455.2, *calc.* $C_{20}H_{32}O_8NaS^+$ = 455.2.

Hub(OEG$_8$OH)$_3$ (43)



S1 S2 **43**

Figure 8.3 Synthesis of S2 and compound **43** from S1.

Compounds **S1** and **S2** were synthesized by our group. 4, 4'-Dimethoxytriphenylmethyl octagol (DmtrOEG$_8$OH, 6.50 g, 14.75 mmol, and 4 equiv.) synthesized according to the literature [173], shown in Figure 8.3, was co-evaporated from MeCN (50 mL × 3) and re-dissolved in THF (40 mL). To the solution were added KO*t*Bu (1.07 g, 14.8 mmol, 4 equiv.) then Hub(CH$_2$Br)$_3$ (**S1**, 1.95 g, 3.69 mmol) and the reaction was stirred at 35 ^{o}C for 3 h. The reaction was quenched with sat. NH$_4$Cl (0.3 mL and the THF was evaporated. The residue was re-dissolved in CH$_2$Cl$_2$ (100 mL) containing a trace Et$_3$N, washed with half-sat. NaHCO$_3$ (60 mL × 3), the organic phase was dried with Na$_2$SO$_4$ and concentrated under vacuum. The residue was fractionated through a column of silanised silica, eluting with a gradient of acetone-water (20:80 to 95:5, v/v) containing a trace of ammonium hydroxide. After evaporation of the solvent, the title compound (**S2**, 5.60 g, 90%) was obtained as a light yellow waxy solid.

To Hub(OEG$_8$ODmtr)$_3$ (**S2**, 2.67g, 1.03 mmol) in CH$_2$Cl$_2$ (26 mL) were added pyrrole (1.07 mL, 15.5 mmol, 15 equiv.) and dichloroacetic acid (0.255 mL, 3.09 mmol, 3 equiv.). The mixture was stirred for 30 min, when an initially strong orange/red colour dissipated to a pale yellow solution, and quenched with sat. NaHCO$_3$. Then the resulting mixture was diluted with CH$_2$Cl$_2$ (80 mL), washed with half-sat. NaHCO$_3$ (50 mL × 3), and the aqueous phase was further extracted with CH$_2$Cl$_2$ (100 mL × 3). The combined CH$_2$Cl$_2$ phase was dried over Na$_2$SO$_4$, and concentrated under reduced pressure. The residue was fractionated through a column of flash silica, eluting with a gradient of MeOH-CHCl$_3$ (1:99 to 30:70, v/v) to afford the title compound as a light yellow waxy solid (**43**, 1.51 g, 87%).

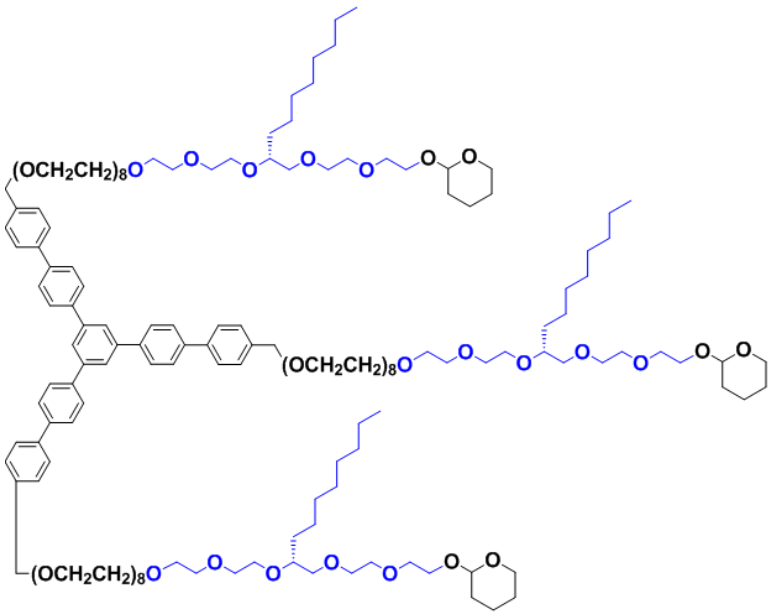
R_f (MeOH-$CHCl_3$ 1:9) = 0.43.

^{1}H NMR (400 MHz, $CDCl_3$) δ = 7.90 (s, 3H, Hub C***H***), 7.83 (d, J = 8.4 Hz, 6H, Hub C***H***), 7.75 (d, J = 8.4 Hz, 6H, Hub C***H***), 7.67 (d, J = 8.2 Hz, 6H, Hub C***H***), 7.47 (d, J = 8.3 Hz, 6H, Hub C***H***), 4.66 (s, 6H, 3×OC***H$_2$***Ar), 3.74-3.65 (m, 90H, 45×C***H$_2$***O), 3.62-3.60 (m, 6H, 3×C***H$_2$***OH), 3.05 (s, 3H, 3×O***H***).

^{13}C NMR (101 MHz, $CDCl_3$) δ = 141.98 (3C), 140.20 (3C), 140.00 (3C), 139.95 (3C), 137.56 (3C) (15×Hub ***C***), 128.32 (6C), 127.75 (6C), 127.56 (6C), 127.07 (6C), 125.00 (3C) (27×Hub ***C***H), 72.98, 72.65 (2C) (3×O***C***H_2Ar), 70.67-70.54 (m, 39C), 70.26 (3C), 69.55 (3C) (45×***C***H_2O), 61.69 (3C, 3×***C***H_2OH).

m/z **(ESI$^+$)** $[M+Na]^+$ = 1704.9, **(MALDI-ToF$^+$)** $[M+Na]^+$ = 1705.7, *calc.* $C_{93}H_{132}NaO_{27}^+$ = 1704.9.

Hub(OEG$_8$A-OThp)$_3$ (44) (*Coupling procedure*)



Hub(OEG$_8$OH)$_3$ (**43**, 0.23 g, 0.13 mmol) and Octyl-BB (**33**, 0.79 g, 1.34 mmol, 10 equiv.) were co-evaporated from MeCN (30 mL × 3) in a 100 mL round-bottomed flask, and then re-dissolved in DMF (2 mL). To this solution was slowly added NaH (60% dispersion in mineral oil, 32.3 mg, 0.81 mmol, 6 equiv.). The reaction was stirred for 24 h at 60 °C; complete coupling was confirmed by HPLC before quenching. The reaction was quenched with sat. NH_4Cl (1 mL), and the solution was evaporated to dryness in vacuo. The residue was re-dissolved in

CH_2Cl_2 (50 mL), extracted with half-sat. $NaHCO_3$ (20 mL × 3), the combined CH_2Cl_2 phase was dried with $NaSO_4$ and evaporated to dryness.

The crude material was purified using a two-stage 18 wt% PBI-DBX-M2005 membrane apparatus diafiltering with MeCN-MeOH (1:1, v/v) as solvent. After 5 h, all impurities, including excess monomer and other reaction debris, were removed completely (real-time HPLC monitoring). The retentate was washed from the diafiltration apparatus and evaporated to afford the title compound (**44**, 0.35 g, 90%) as a pale yellow oil. The concentration profiles of building block and Hub product during diafiltration is shown in Figure 8.4.

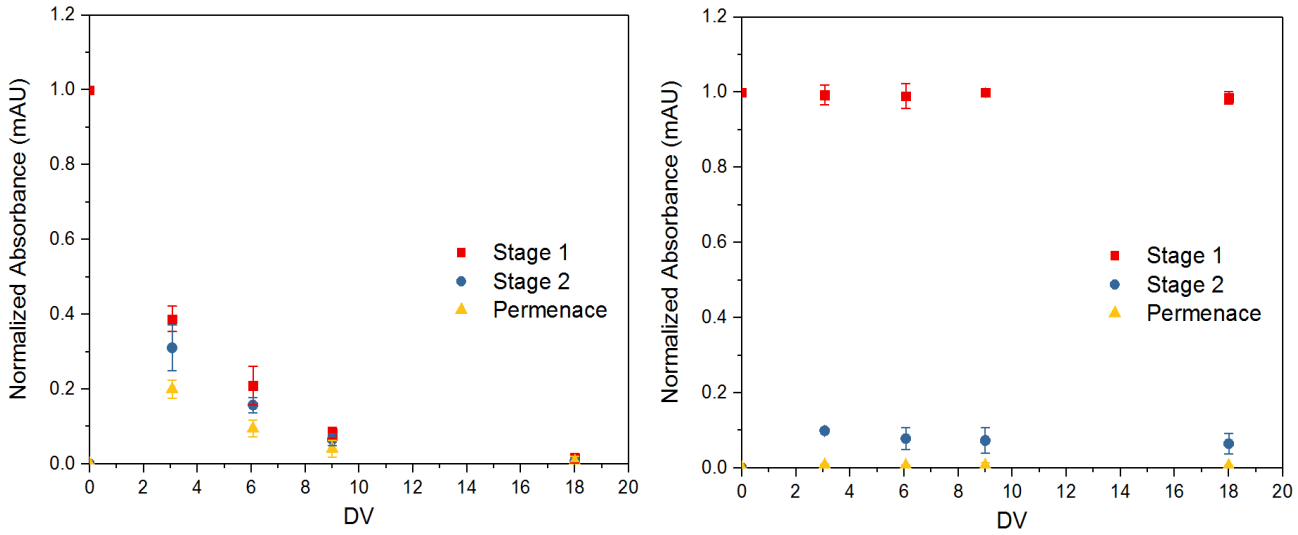


Figure 8.4 Concentration profiles of building block **33** and product **44** in two-stage membrane diafiltration rig.

R_f (MeOH- $CHCl_3$ 1: 19 + trace Et_3N) = 0.54.

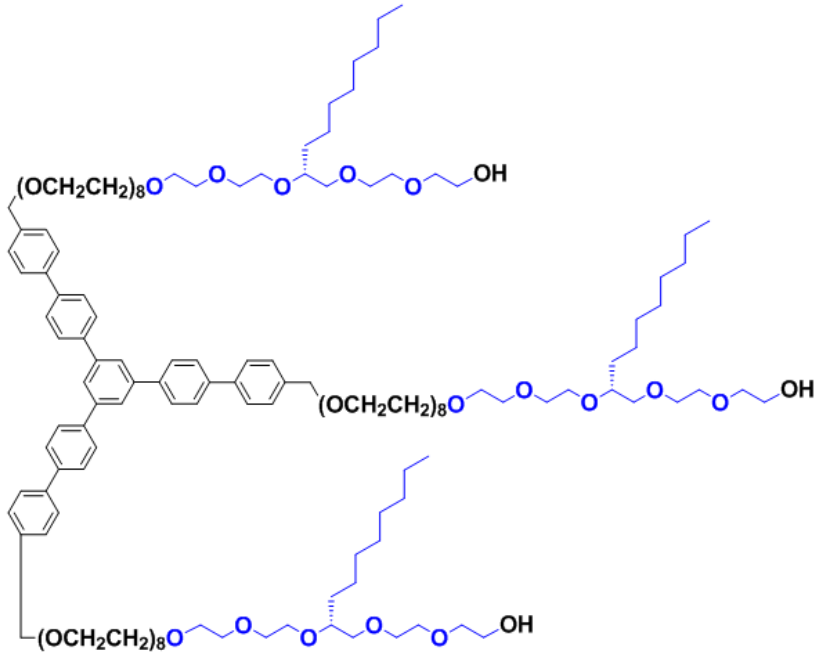
^{1}H NMR (400 MHz, $CDCl_3$) δ=7.89 (s, 3H, Hub C***H***), 7.82 (d, J = 8.3 Hz, 6H, Hub C***H***), 7.75 (J = 8.3 Hz, 6H, Hub C***H***), 7.65 (J = 8.2 Hz, 6H, Hub C***H***), 7.46 (d, J = 8.0 Hz, 6H Hub C***H***), 4.64 (m, 9H, 3×OC***H$_2$***Ar + 3×Thp C***H***), 3.90 – 3.81 (m, 3H, 3× C***H*** (Oct)CH_2O), 3.79 – 3.36 (m, 156H, 78×C***H$_2$***O), 1.91 – 1.36 (m, 18H, Thp C***H$_2$***), 1.35 – 1.17 (m, 42H, 21×C***H$_2$***), 0.88 (t, J = 5.9 Hz, 9H, CH_2C***H$_3$***).

^{13}C NMR (101 MHz, $CDCl_3$) δ = 141.96 (3C), 140.18(3C), 139.98(3C), 139.93(3C), 137.55(3C) (15×Hub ***C***), 128.29(6C), 127.72(6C), 127.53(6C), 127.04(6C), 124.97(3C) (27×Hub ***C***H), 98.92(3×Thp ***C***H), 79.28(3×***C***H(Oct)CH_2), 72.97(3C, 3×O***C***H_2Ar), 70.85-70.57, 69.55, 69.28, 68.84, 66.67 (75×***C***H_2O), 62.44(1.5C), 62.20(1.5C)(3×Thp ***C***H_2), 31.88,

30.57, 29.77, 29.58, 29.29, 25.54, 25.48, 25.44, 22.66(27×***C***H_2), 19.48(3×Thp ***C***H_2), 14.12(3×CH_2***C***H_3)

***m/z* (MALDI-ToF$^+$)** $[M+Na]^+$ = 2954.8, *calc.* $C_{162}H_{264}O_{45}Na^+$ = 2954.8.

Hub(OEG$_8$A-OH)$_3$ (45) (*Deprotection procedure*)



To Hub(OEG$_8$A-OThp)$_3$ (**44**, 0.34 g, 0.12 mmol) dissolved in MeOH (30 mL) was added MsOH (195 μL). The reaction was stirred for 30 min at room temperature, then quenched with sat. $NaHCO_3$ (2 mL). The solvent was evaporated and the residue re-dissolved in $CHCl_3$ (50 mL). The solution was extracted with half-sat. $NaHCO_3$ (30 mL × 3), the combined organic phase was dried over Na_2SO_4, and the solvent was evaporated under vacuum to afford the title compound (**45**, 0.3 g, 97.2%) as a pale yellow oil.

R_f (MeOH- $CHCl_3$ 1: 19) = 0.18.

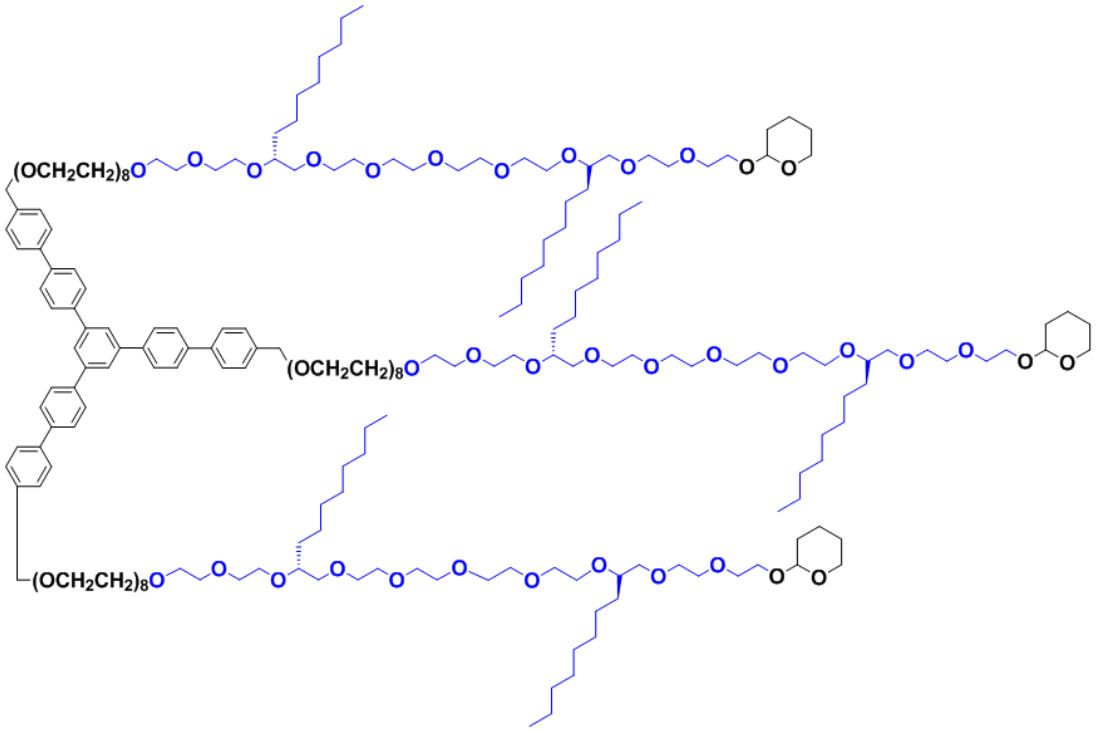
^{1}H NMR (400 MHz, $CDCl_3$) δ = 7.91 (s, 3H, Hub C***H***), 7.83 (d, J = 8.3 Hz, 6H, Hub C***H***), 7.75 (d, J = 8.4 Hz, 6H, Hub C***H***), 7.67 (d, J = 8.3 Hz, 6H, Hub C***H***), 7.48 (d, J = 8.0 Hz, 6H Hub C***H***), 4.66 (s, 6H, 3×OC***H$_2$***Ar), 3.81 – 3.59 (m, 150H, 75×C***H$_2$***O), 3.55 – 3.45 (m, 3H, 3× C***H*** (Oct)CH_2O), 1.56 – 1.17 (m, 42H, 21×C***H$_2$***), 0.89 (t, J = 5.9 Hz, 9H, 3×CH_2C***H$_3$***).

^{13}C NMR (101 MHz, $CDCl_3$) δ = 141.96(3C), 140.17(3C), 139.97(3C), 139.93(3C), 137.55(3C) (15×Hub ***C***), 128.30(6C), 127.73(6C), 127.54(6C), 127.05(6C), 124.98(3C)

(27×Hub ***C***H), 79.28(3×***C***H (Oct) CH2), 72.97(3C, 3×O***C***H_2Ar), 70.86-70.57, 70.41, 69.54, 69.21(75×***C***H_2O), 31.88, 30.52, 29.77, 29.57, 29.29, 25.43, 22.67(21×***C***H_2), 14.14. (3×CH_2***C***H_3).

***m/z* (MALDI-ToF$^+$)** $[M+Na]^+$ = 2702.5, *calc.* $C_{147}H_{240}O_{42}Na^+$ = 2702.5.

Hub(OEG$_8$AA-OThp)$_3$ (46)



The reaction was conducted using the *coupling procedure* described above: To Hub(OEG$_8$A-OH)$_3$ (**45**, 0.28 g, 0.11 mmol) and Octyl-BB (**33**, 0.62 g, 1.05 mmol, 10 equiv.) in DMF (2 mL) was added NaH (60%, 25.3 mg, 0.63 mmol, 6 equiv.). After stirring for 24 h at 60 °C, the reaction was worked up then purified using the two-stage membrane apparatus, diafiltering for 5 h to afford the title compound (**46**, 0.4 g, 93%) as a pale yellow oil. The concentration profiles of building block and Hub product during diafiltration is shown in Figure 8.5.

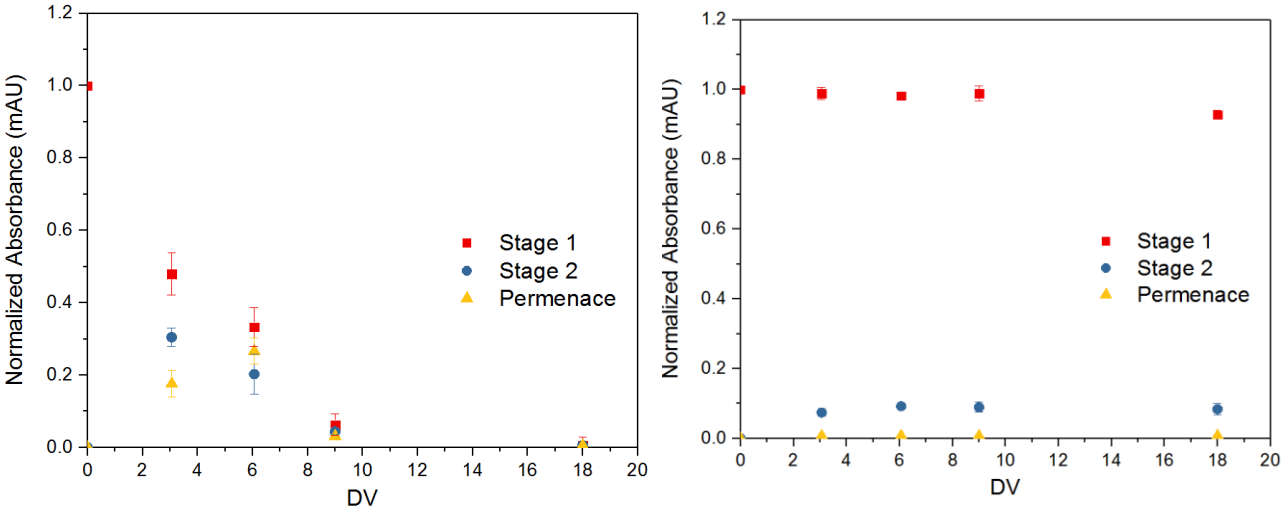


Figure 8.5 Concentration profiles of building block **33** and product **46** in two-stage membrane diafiltration rig.

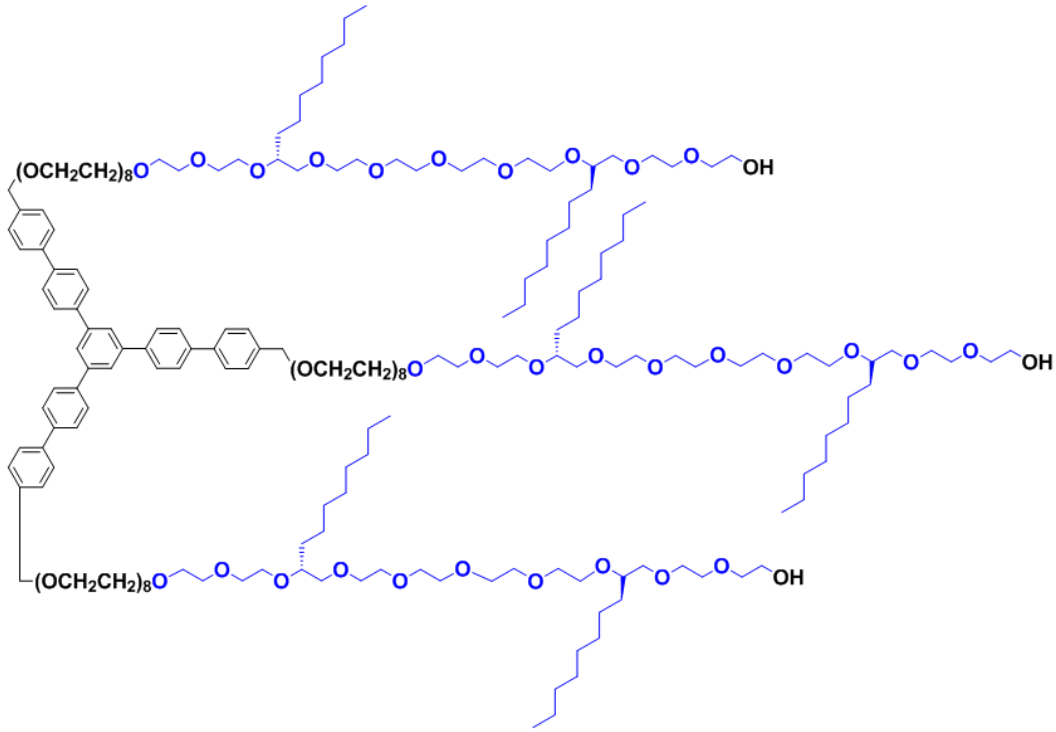
R_f (MeOH- $CHCl_3$ 1: 19+ trace Et_3N) = 0.43.

^{1}H NMR (400 MHz, $CDCl_3$) δ = 7.90 (s, 3H, Hub C***H***), 7.82 (d, *J* = 8.4 Hz, 6H, Hub C***H***), 7.74 (d, *J* = 8.3 Hz, 6H, Hub C***H***), 7.66 (d, *J* = 8.2 Hz, 6H, Hub C***H***), 7.47 (d, *J* = 8.0 Hz, 6H Hub C***H***, 4.64 (m, 9H, 3×OC***H₂***Ar + 3×Thp C***H***), 3.93 – 3.83 (m, 6H, 6× C***H*** (Oct)CH_2O), 3.80 – 3.36 (m, 210H, 105×C***H₂***O), 1.90 – 1.44 (m, 18H, Thp C***H₂***), 1.28 (m, 84H, 42×C***H₂***), 0.89 (t, *J* = 6.7 Hz, 18H, 6×CH_2C***H₃***).

^{13}C NMR (101 MHz, $CDCl_3$) δ = 141.97(3C), 140.19(3C), 139.99(3C), 139.94(3C), 137.55(3C) (15×Hub ***C***), 128.29(6C), 127.73(6C), 127.54(6C), 127.05(6C), 124.97(3C) (27×Hub ***C***H), 98.94(3×Thp ***C***H), 79.30, 73.97(6×***C***H(Oct)CH_2), 72.98(3C, 3×O***C***H_2Ar), 70.86-70.57, 69.55, 69.28, 66.67(96×***C***H_2O), 62.21(3×Thp ***C***H_2), 31.89, 30.57, 29.78, 29.58, 29.30, 25.54, 25.48, 25.44, 22.67(54×***C***H_2), 19.49(3×Thp ***C***H_2), 14.12(6×CH_2***C***H_3).

***m/z* (MALDI-ToF$^+$)** $[M+Na]^+$ = 3952.3, *calc.* $C_{216}H_{372}O_{60}Na^+$ = 3952.3.

Hub(OEG$_8$AA-OH)$_3$ (47)



The reaction was conducted using the *deprotection procedure* described above: To Hub(OEG$_8$AA-OThp)$_3$ (**46**, 0.15 g, 0.03 mmol) in MeOH (10 mL) was added 0.05 M MsOH (290 µL). After 30 min, the reaction mixture was worked up as above to afford the title compound (**47**, 0.13 g, 97.1%) as a pale yellow oil.

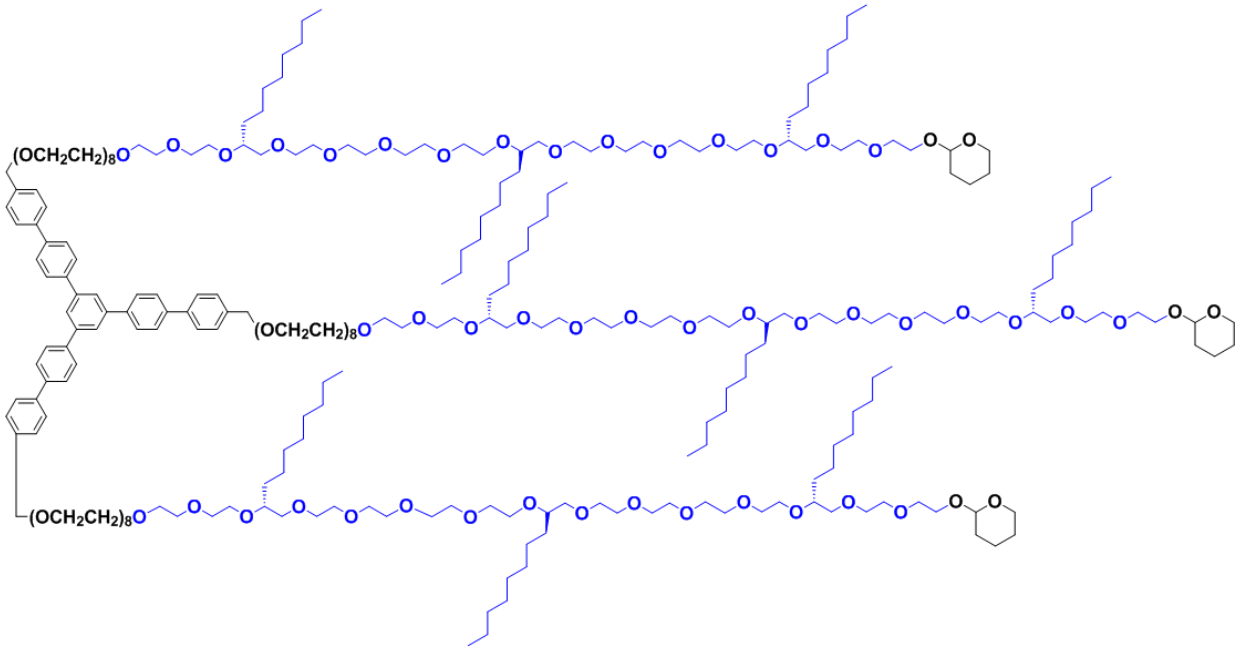
R_f (MeOH- $CHCl_3$ 1: 19) = 0.15

^{1}H NMR (400 MHz, $CDCl_3$) δ = 7.90 (s, 3H, Hub C***H***), 7.84(d, J = 8.3 Hz, 6H, Hub C***H***), 7.75 (d, J = 8.4 Hz, 6H, Hub C***H***), 7.67 (d, J = 8.3 Hz, 6H, Hub C***H***), 7.48 (d, J = 8.0 Hz, 6H Hub C***H***), 4.65 (s, 6H, 3×OC***H$_2$***Ar), 3.80 – 3.57 (m, 204H, 102×C***H$_2$***O), 3.49 – 3.42 (m, 6H, 6× C***H*** (Oct)CH_2O), 1.56 – 1.18 (m, 84H, 42×C***H$_2$***), 0.92 – 0.85 (t, J = 5.9 Hz, 18H, 6×CH_2C***H$_3$***).

^{13}C NMR (101 MHz, $CDCl_3$) δ = 141.95(3C), 140.17(3C), 139.97(3C), 139.93(3C), 137.52(3C) (15×Hub ***C***), 128.29(6C), 127.71(6C), 127.52(6C), 127.04(6C), 124.96(3C) (27×Hub ***C***H), 79.28, 73.96(6×***C***H (Oct) CH2), 72.98(3C, 3×O***C***H_2Ar), 70.86- 70.58, 70.41, 69.55, 69.28, 69.20(102×***C***H_2O), 31.88, 31.70, 29.77, 29.57, 29.29, 25.47, 22.67(42×***C***H_2), 14.12(6×CH_2***C***H_3).

***m/z* (MALDI-ToF$^+$)** $[M+Na]^+$ = 3699.9, *calc.* $C_{201}H_{348}O_{57}Na^+$ = 3699.9.

Hub(OEG$_8$AAA-OThp)$_3$ (48)



The reaction was conducted using the *coupling procedure* described above: To Hub(OEG$_8$AA-OH)$_3$ (**47**, 0.13 g, 0.03 mmol) and Octyl-BB (**33**, 0.18 g, 0.3 mmol, 10 equiv.) in DMF (2 mL) was added NaH (60%, 7.68 mg, 0.19 mmol, 6 equiv.). After stirring for 24 h at 60 °C, the reaction was worked up then purified using the two-stage membrane apparatus, diafiltering for 5 h to afford the title compound (**48**, 0.4 g, 93%) as a pale yellow oil. The concentration profiles of building block and Hub product during diafiltration is shown in Figure 8.6.

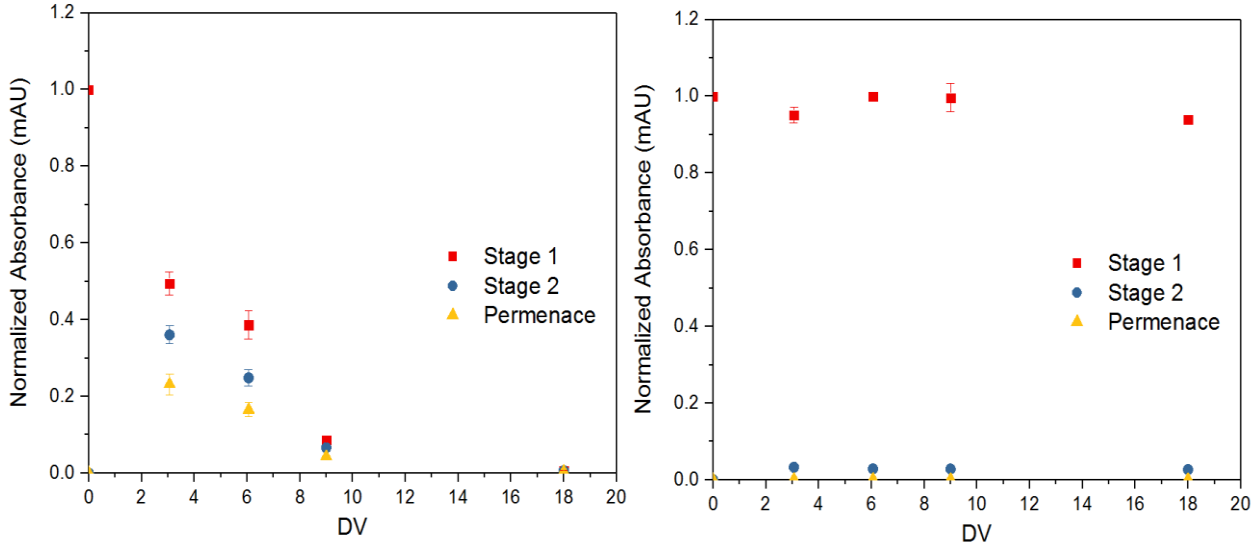


Figure 8.6 Concentration profiles of building block **33** and product **48** in two-stage membrane diafiltration rig.

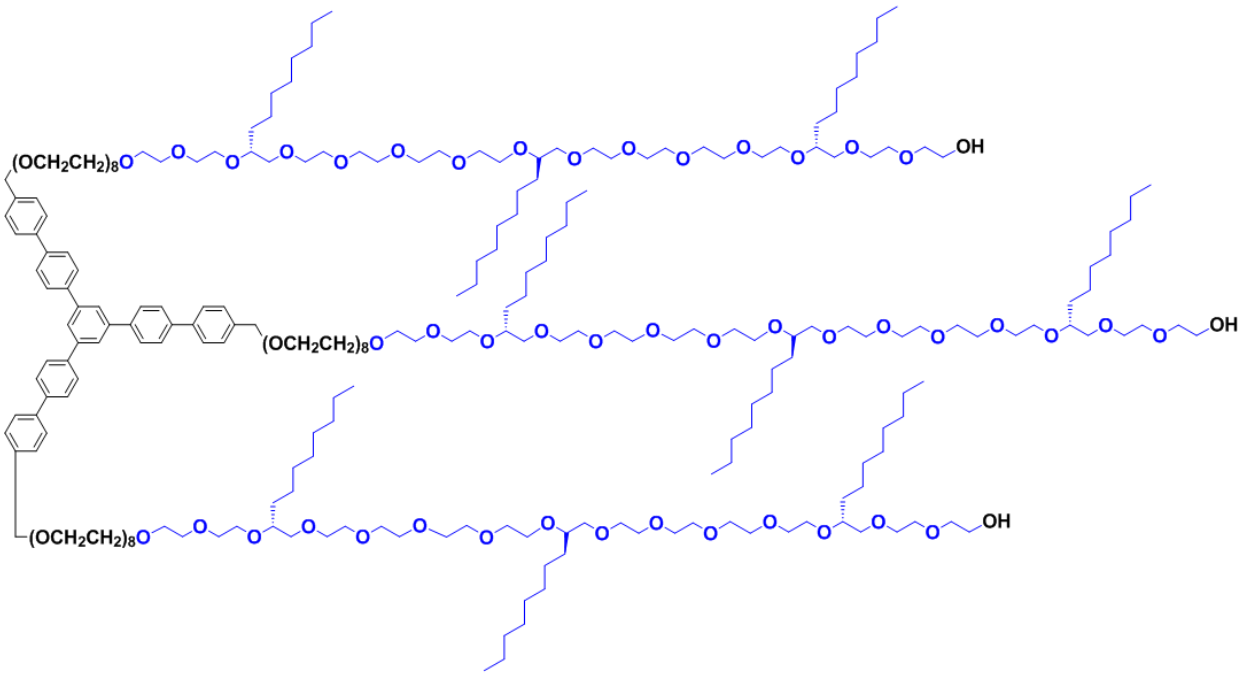
R_f (MeOH- $CHCl_3$ 1: 19+ trace Et_3N) = 0.43.

^{1}H NMR (400 MHz, $CDCl_3$) δ = 7.89 (s, 3H, Hub C***H***), 7.82 (d, J = 8.4 Hz, 6H, Hub C***H***), 7.74 (J = 8.3 Hz, 6H, Hub C***H***), 7.66 (J = 8.2 Hz, 6H, Hub C***H***), 7.46 (d, J = 8.2 Hz, 6H, Hub C***H***), 4.63 (m, 9H, 3×OC***H$_2$***Ar + 3×Thp C***H***), 3.92 – 3.79 (m, 9H, 9× C***H*** (Oct)CH_2O), 3.79 – 3.23 (m, 264H, 132×C***H$_2$***O), 1.90 – 1.44 (m, 18H, Thp C***H$_2$***), 1.35 – 1.12 (m, 126H, 63×C***H$_2$***), 0.88 (t, J = 6.8 Hz, 27H, 9×CH_2C***H$_3$***).

^{13}C NMR (101 MHz, $CDCl_3$) δ = 141.97(3C), 140.19(3C), 139.99(3C), 139.94(3C), 137.55(3C) (15×Hub ***C***),128.27(6C), 127.71(6C), 127.52(6C), 127.04(6C), 124.96(3C) (27×Hub ***C***H), 98.92(3×Thp ***C***H), 79.27, 73.97(9×***C***H(Oct)CH_2), 72.97(3C, 3×O***C***H_2Ar), 70.86-70.58, 69.56, 69.27, 66.67(120×***C***H_2O), 62.18(3×Thp ***C***H_2), 31.89, 30.57, 29.77, 29.68, 29.57, 29.28, 27.07, 25.46, 22.65 (81×***C***H_2), 14.09(9×CH_2***C***H_3).

***m/z* (MALDI-ToF$^+$)** $[M+Na]^+$ = 4949.7, *calc.* $C_{270}H_{480}O_{75}Na^+$ = 4949.7.

Hub(OEG$_8$AAA-OH)$_3$ (49)



The reaction was conducted using the *deprotection procedure* described above: To Hub(OEG$_8$AAA-OThp)$_3$ (**48**, 0.11 g, 0.02 mmol) in MeOH (10 mL) was added 0.05 M MsOH (290 µL). After 30 min, the reaction mixture was worked up as above to afford the title compound (**49**, 0.10 g, 96%) as a pale yellow oil.

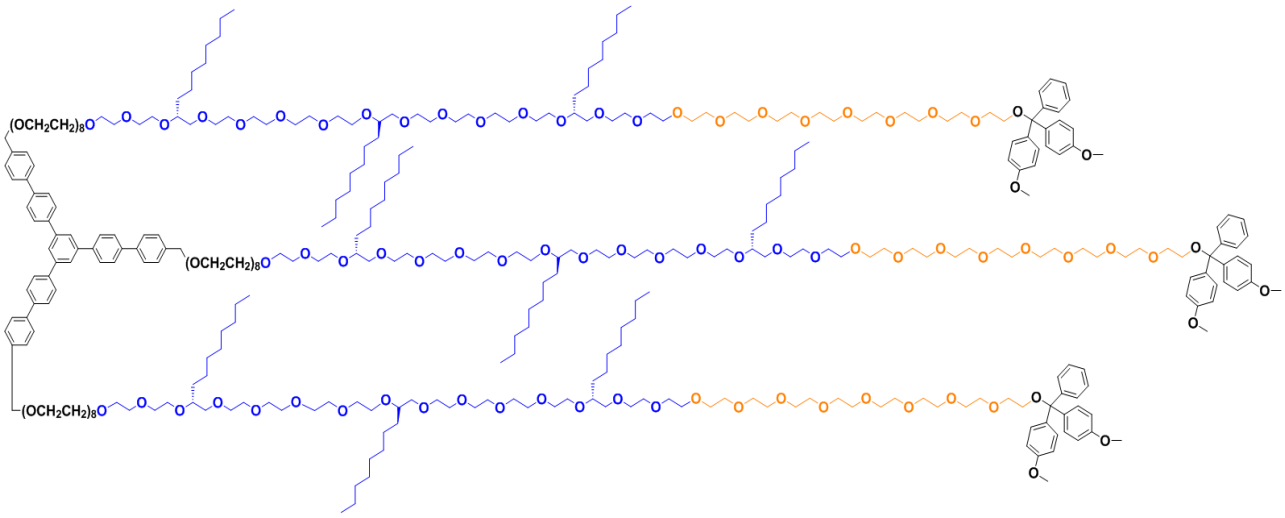
R_f (MeOH- $CHCl_3$ 1: 19) = 0.14

^{1}H NMR (400 MHz, $CDCl_3$) δ = 7.90 (s, 3H, Hub C***H***), 7.82 (d, J = 8.2 Hz, 6H, Hub C***H***), 7.74 (d, J = 8.3 Hz, 6H, Hub C***H***), 7.66 (d, J = 8.1 Hz, 6H, Hub C***H***), 7.47 (d, J = 8.0 Hz, 6H, Hub C***H***), 4.64 (s, 6H, 3×OC***H$_2$***Ar), 3.82 – 3.57 (m, 258H, 129×C***H$_2$***O), 3.49 – 3.44 (m, 9H, 9× C***H*** (Oct)CH_2O), 1.56 – 1.13 (m, 126H, 63×C***H$_2$***), 0.89 (t, J = 6.7 Hz, 27H, 9×CH_2C***H$_3$***).

^{13}C NMR (101 MHz, $CDCl_3$) δ = 141.97(3C), 140.17(3C), 139.97(3C), 139.93(3C), 137.52(3C) (15×Hub ***C***), 128.28(6C), 127.72(6C), 127.53(6C), 127.05(6C), 124.95(3C) (27×Hub ***C***H), 79.27, 73.97 (9×***C***H (Oct) CH2), 72.98(3C, 3×O***C***H_2Ar), 70.86-70.58, 70.42, 69.56, 69.28, 69.22(129×***C***H_2O), 31.88, 31.73, 29.77, 29.57, 29.28, 25.47, 22.66(63×***C***H_2), 14.11(9×CH_2***C***H_3).

***m/z* (MALDI-ToF$^+$)** $[M+Na]^+$ = 4697.4, *calc.* $C_{255}H_{456}O_{72}Na^+$ = 4697.4.

Hub(OEG$_8$AAABB-ODmtr)$_3$ (50)



The reaction was conducted using the *coupling procedure* described above: To Hub(OEG$_8$AAA-OH)$_3$ (**49**, 0.10 g, 0.02 mmol) and linear TsOEG$_8$ODmtr BB was synthesized by our group [173] (**S3**, 0.19 g, 0.23 mmol, 10 equiv.) in DMF (2 mL) was added NaH (60%, 9.16 mg, 0.23 mmol, 6 equiv.). After stirring for 24 h at 60 °C, the reaction was purified was fractionated by a reverse phase column coluchromatography, eluting with a gradient of acetone-water (1:99 to 90:10, v/v), all solvents containing 1 vol% sat. $NaHCO_3$, to afford the title compound (**50**, 0.09 g, 61%) as a pale yellow oil.

R_f (MeOH- $CHCl_3$ 1: 19+ trace Et_3N) = 0.48.

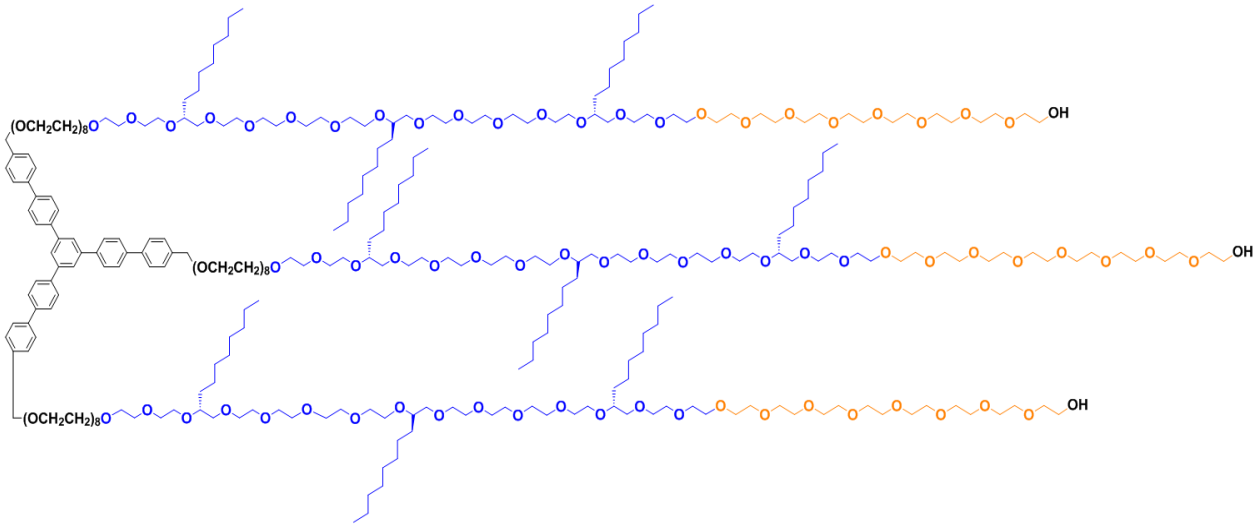
^{1}H NMR (400 MHz, $CDCl_3$) δ = 7.91 (s, 3H, Hub C***H***), 7.83 (d, J = 8.0 Hz, 6H Hub C***H***), 7.75 (d, J = 8.0 Hz, 6H, 6×Hub C***H***), 7.67 (d, J = 7.9 Hz, 6H Hub C***H***), 7.47 (d, J = 7.8 Hz, 12H 6×Hub C***H*** +6×Dmtr C***H***), 7.36 (d, J = 8.8 Hz, 12H, 12×Dmtr C***H***), 7.28 (d, J = 8.0 Hz, 6H, 6×Dmtr C***H***), 7.22 (d, J = 7.2 Hz, 3H, 3×Dmtr C***H***), 6.88 – 6.78 (m, 12H, 12×Dmtr C***H***), (39×Dmtr C***H***), 4.65 (s, 6H, 3×OC***H$_2$***Ar), 3.90 – 3.73 (m, 9H, 9× C***H*** (Oct)CH_2O), 3.88 – 3.35 (m, 372H, 177×C***H$_2$***O + 6×ArOC***H$_3$***), 3.24 (t, J = 5.2 Hz, 6H, 3× C***H$_2$***ODmtr), 1.38 – 1.19 (m, 126H, 63×C***H$_2$***), 0.90 (t, J = 6.7 Hz, 27H, 9×CH_2C***H$_3$***).

^{13}C NMR (101 MHz, $CDCl_3$) δ = 158.36(6 ×Dmtr Ar ***C***), 145.08 (3 ×Dmtr Ar ***C)***, 141.97(3×Hub ***C***), 140.19(3×Hub ***C***), 139.97(3×Hub ***C***), 139.94(3×Hub ***C***), 137.54 (3×Hub ***C***), 136.33(6 ×Dmtr Ar ***C***), 130.05(12×Dmtr Ar ***C***H), 128.30(6×Hub ***C***H), 128.20(6×Dmtr Ar ***C***H), 127.73(6×Dmtr Ar ***C***H), 127.70 (6×Hub ***C***H), 127.55(6×Hub ***C***H), 127.06(6×Hub ***C***H), 126.63(3×Dmtr Ar ***C***H), 124.97(3×Hub ***C***H), 113.02(12×Dmtr Ar ***C***H), 85.91(3×Dmtr O***C***Ar$_3$),

79.26, 73.96(9×***C***H(Oct)CH_2), 72.98(3C, 3×O***C***H_2Ar), 70.86, 70.73, 70.58, 69.55, 69.29, (159×***C***H_2O), 55.20(6C, 6×Dmtr O***C***H_3), 31.91, 30.05, 29.79, 29.71, 29.60, 29.38, 29.31, 25.48, 22.69(81×***C***H_2), 14.14(9×CH_2***C***H_3)

***m/z* (MALDI-ToF$^+$)** $[M+Na]^+$ = 6657.2, *calc.* $C_{366}H_{606}O_{102}Na^+$ = 6657.2.

Hub(OEG$_8$AAABB-OH)$_3$ (51)



The reaction was conducted using the *deprotection procedure* described above: To Hub(OEG$_8$AAABB-ODmtr)$_3$ (**50**, 0.08 g, 0.02 mmol) in MeOH (10 mL) was added 0.05 M MsOH (290 μL). After 30 min, the reaction mixture was worked up. The reaction was purified was fractionated by a reverse phase column coluchromatography, eluting with a gradient of acetone-water (1:99 to 90:10, v/v) to afford the title compound (**51**, 0.06 g, 94%) as a pale yellow oil.

R_f (MeOH- $CHCl_3$ 1: 19) = 0.14

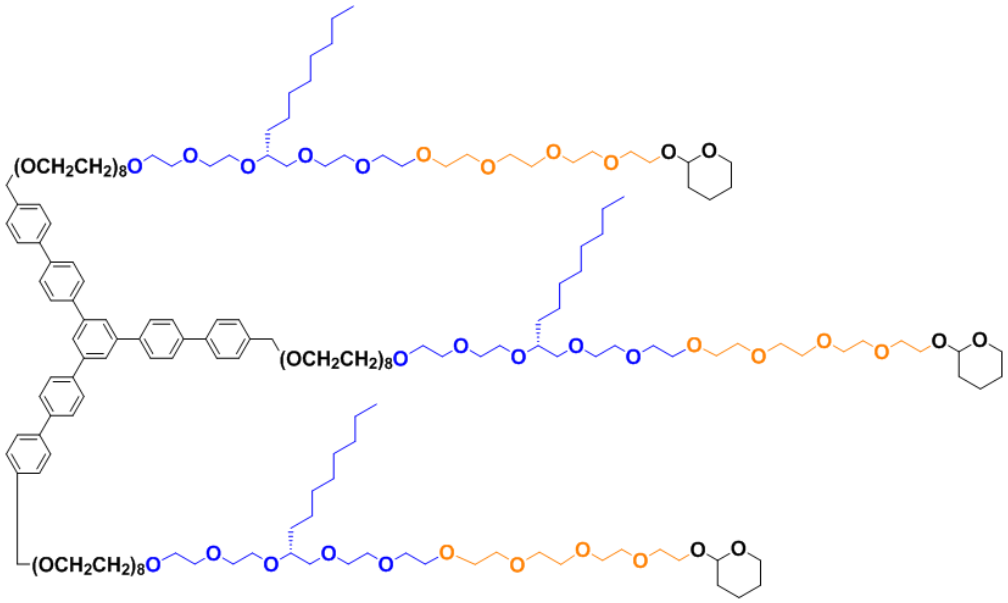
^{1}H NMR (400 MHz, $CDCl_3$) δ = 7.91 (s, 3H, Hub C***H***), 7.83 (d, J = 8.0 Hz, 6H Hub C***H***), 7.75 (d, J = 8.0 Hz, 6H, 6×Hub C***H***), 7.67 (d, J = 7.9 Hz, 6H Hub C***H***), 7.47 (d, J = 7.8 Hz, 6H Hub C***H***), 4.65 (s, 6H, 3×OC***H$_2$***Ar), 3.82 – 3.57 (m, 354H, 177×C***H$_2$***O), 3.49 – 3.44 (m, 9H, 9× C***H*** (Oct)CH_2O),1.38 – 1.19 (m, 126H, 63×C***H$_2$***), 0.90 (t, J = 6.7 Hz, 27H, 9×CH_2C***H$_3$***).

^{13}C NMR (101 MHz, $CDCl_3$) δ = 141.97(3C), 140.19(3C), 139.97(3C), 139.94(3C), 137.54 (3C) (15×Hub ***C***),128.30(6C), 127.73(6C), 127.55(6C), 127.06(6C), 124.97(3C) (27×Hub ***C***H), 79.26, 73.96(9×***C***H(Oct)CH_2), 72.98(3C, 3×O***C***H_2Ar), 70.86, 70.73, 70.58, 69.55, 69.29,

(177×***C***H_2O), 31.91, 30.05, 29.79, 29.71, 29.60, 29.38, 29.31, 25.48, 22.69(63×***C***H_2), 14.14(9×CH_2***C***H_3).

***m/z* (MALDI-ToF$^+$)** $[M+K]^+$ = 5770.7, *calc.* $C_{303}H_{552}O_{96}K^+$ = 5770.7.

Hub(OEG$_8$AB-OThp)$_3$ (52)



The reaction was conducted using the *coupling procedure* described above: To Hub(OEG$_8$A-OH)$_3$ (**45**, 0.4 g, 0.15 mmol) and linear TsOEG$_4$OThp-BB (**42**, 0.65 g, 1.5 mmol, 10 equiv.) in DMF (1.5 mL) was added NaH (60%, 36 mg, 0.9 mmol, 6 equiv.). After stirring for 24 h at 60 °C, the reaction was worked up then purified using the two-stage membrane apparatus, diafiltering for 5 h to afford the title compound (**52**, 0.48 g, 93%) as a pale yellow oil. The concentration profiles of building block and Hub product during diafiltration is shown in Figure 8.7.

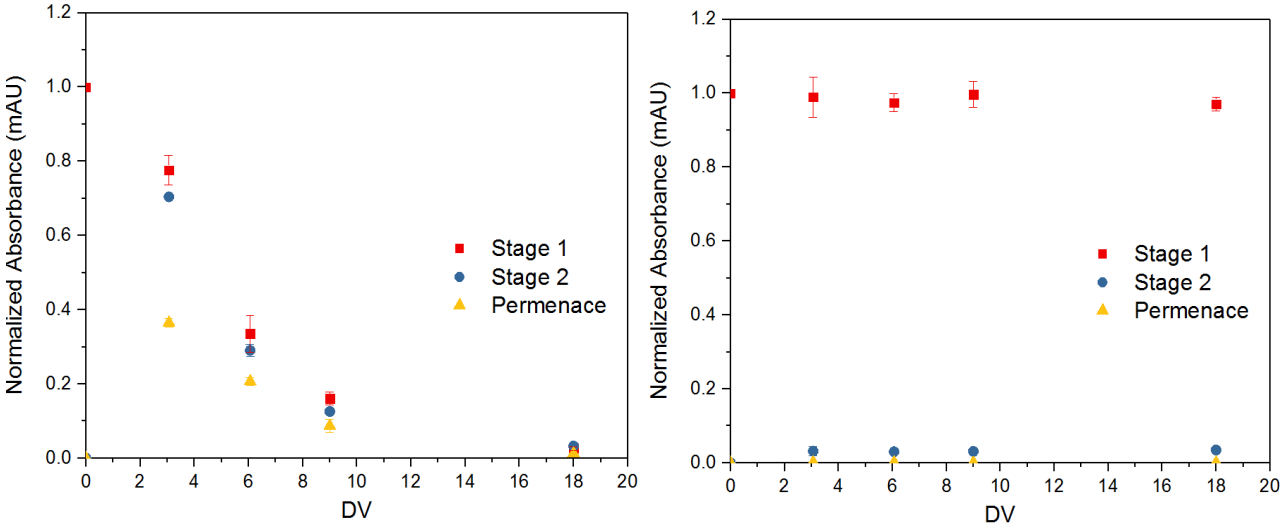


Figure 8.7 Concentration profiles of building block **42** and product **52** in two-stage membrane diafiltration rig.

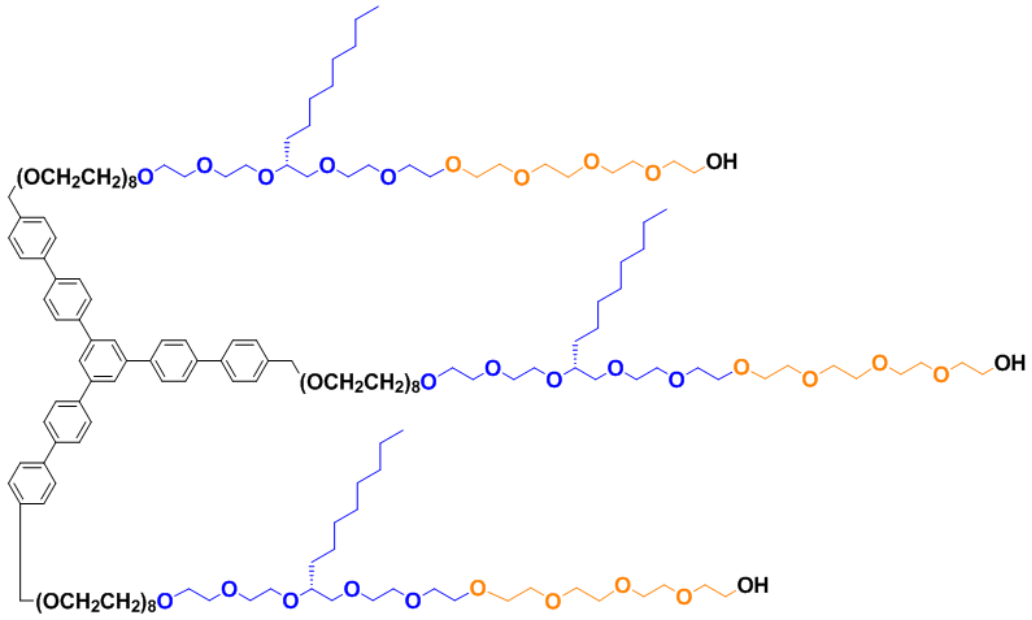
R_f (MeOH- $CHCl_3$ 1: 19+ trace Et_3N) = 0.45.

^{1}H NMR (400 MHz, $CDCl_3$) δ = 7.89 (s, 3H, Hub C***H***), 7.81 (d, J = 8.4 Hz, 6H, Hub C***H***), 7.73 (d, J = 8.4 Hz, 6H Hub C***H***), 7.65 (J = 8.2 Hz, 6H, Hub C***H***), 7.46 (d, J = 8.0 Hz, 6H Hub C***H***), 4.63 (d, J = 2.5 Hz, 9H, 9H, 3×OC***H$_2$***Ar + 3×Thp C***H***), 3.88 – 3.84 (m, 3H, 3× C***H*** (Oct)CH_2O), 3.73 – 3.39 (m, 204H, 102×C***H$_2$***O), 1.91 – 1.33 (m, 18H, Thp C***H$_2$***), 1.35 – 1.17 (m, 42H, 21×C***H$_2$***), 0.88 (t, J = 5.9 Hz, 9H, CH_2C***H$_3$***).

^{13}C NMR (101 MHz, $CDCl_3$) δ = 141.95(3C), 140.16(3C), 139.96(3C), 139.92(3C), 137.53(3C) (15×Hub ***C***), 128.29(6C), 127.72(6C), 127.53(6C), 127.04(6C), 124.97(3C) (27×Hub ***C***H), 98.91(3×Thp ***C***H), 79.25(3×***C***H(Oct)CH_2), 72.96(3C, 3×O***C***H_2Ar), 70.84, 70.57, 69.53, 69.27, 66.63(99×***C***H_2O), 62.19(3×Thp ***C***H_2), 31.88, 30.55, 29.77, 29.57, 29.29, 25.54, 25.47, 25.43, 22.67(27×***C***H_2), 19.47(3×Thp ***C***H_2), 14.12(3×CH_2***C***H_3).

***m/z* (MALDI-ToF$^+$)** $[M+Na]^+$ = 3483.5, *calc.* $C_{186}H_{312}O_{57}Na^+$ = 3483.5.

Hub(OEG$_8$AB-OH)$_3$ (53)



The reaction was conducted using the *deprotection procedure* described above: To Hub(OEG$_8$AB-OThp)$_3$ (**52**, 0.48 g, 0.13 mmol) dissolved in MeOH (30 mL) was added MsOH (195 µL). After 30 min, the reaction mixture was worked up as above to afford the title compound (**53**, 0.4 g, 98%) as a pale yellow oil.

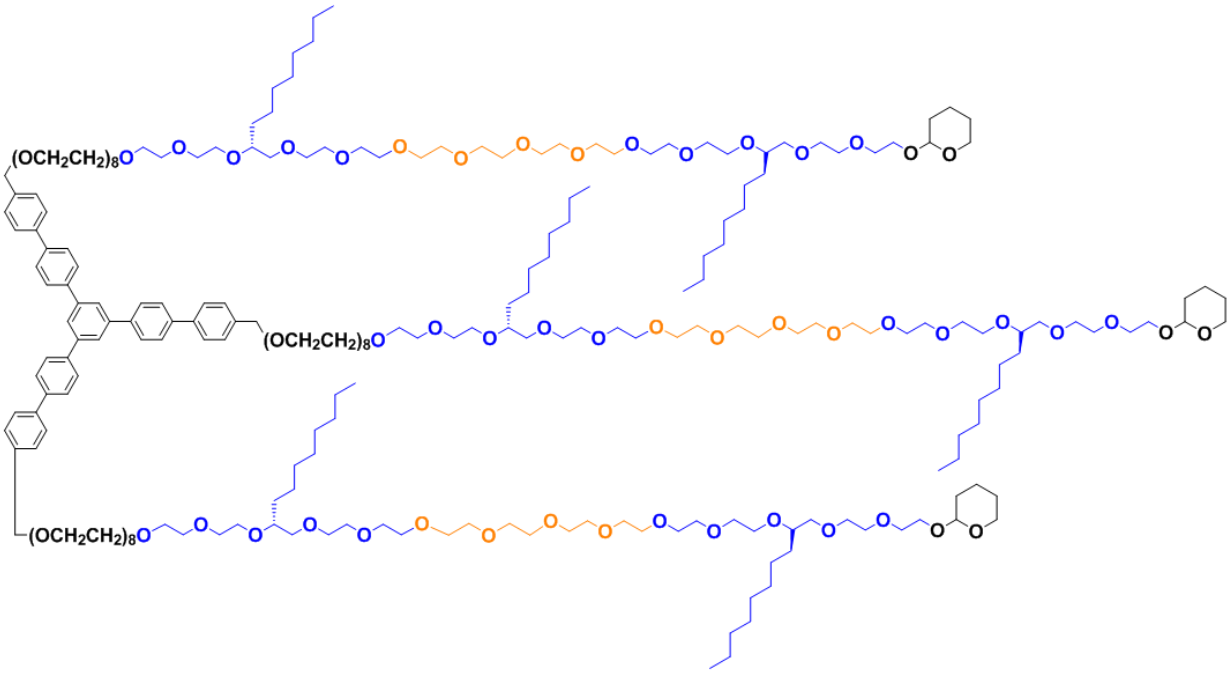
R_f (MeOH- $CHCl_3$ 1: 19) = 0.2.

^{1}H NMR (400 MHz, $CDCl_3$) δ = 7.90 (s, 3H, Hub C***H***), 7.83 (d, J = 8.3 Hz, 6H, Hub C***H***), 7.75 (d, J = 8.4 Hz, 6H, Hub C***H***), 7.67 (d, J = 8.3 Hz, 6H, Hub C***H***), 7.47 (d, J = 8.2 Hz, 6H, Hub C***H***), 4.65 (s, 6H, 3×OC***H$_2$***Ar), 3.79 – 3.58 (m, 198H, 99×C***H$_2$***O), 3.48 – 3.41 (m, 3H, 3× C***H*** (Oct)CH_2O), 1.51 – 1.18 (m, 42H, 21×C***H$_2$***), 0.89 (t, J = 5.9 Hz, 9H, 3×CH_2C***H$_3$***).

^{13}C NMR (101 MHz, $CDCl_3$) δ = 141.96(3C), 140.18(3C), 139.98(3C), 139.94(3C), 137.55(3C) (15×Hub ***C***), 128.29(6C), 127.73(6C), 127.54(6C), 127.05(6C), 124.98(3C) (27×Hub ***C***H), 79.27(3×***C***H (Oct) CH2), 72.97(3C, 3×O***C***H_2Ar), 70.85, 70.68, 70.56, 70.28, 69.55, 69.26, 61.69 (99×***C***H_2O), 31.88, 29.78, 29.69, 29.58, 29.30, 25.48, 22.67(21×***C***H_2),14.13(3×CH_2***C***H_3).

***m/z* (MALDI-ToF$^+$)** $[M+Na]^+$ = 3231.1, *calc.* $C_{171}H_{288}O_{54}Na^+$ = 3231.1.

Hub(OEG$_8$ABA-OThp)$_3$ (54)



The reaction was conducted using the *coupling procedure* described above: To Hub(OEG$_8$AB-OH)$_3$ (**53**, 0.34 g, 0.11 mmol) and Octyl-BB (**33**, 0.65 g, 1.1 mmol, 10 equiv.) in DMF (3 mL) was added NaH (60%, 26 mg, 0.66 mmol, 6 equiv.). After stirring for 24 h at 60 °C, the reaction was worked up then purified using the two-stage membrane apparatus, diafiltering for 5 h to afford the title compound (**54**, 0.43 g, 93%) as a pale yellow oil. The concentration profiles of building block and Hub product during diafiltration is shown in Figure 8.8.

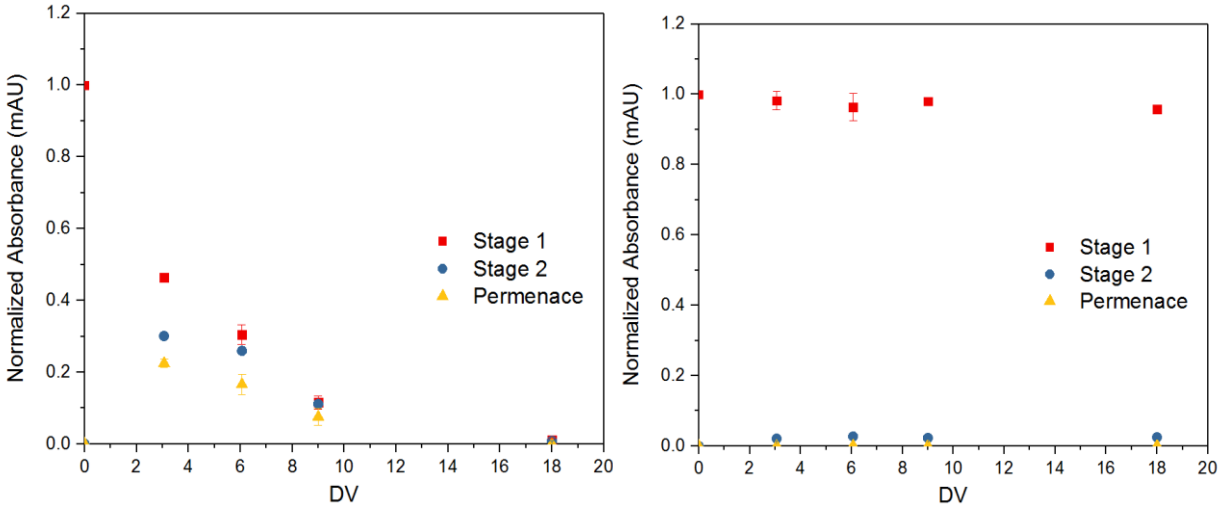


Figure 8.8 Concentration profiles of building block **33** and product **54** in two-stage membrane diafiltration rig.

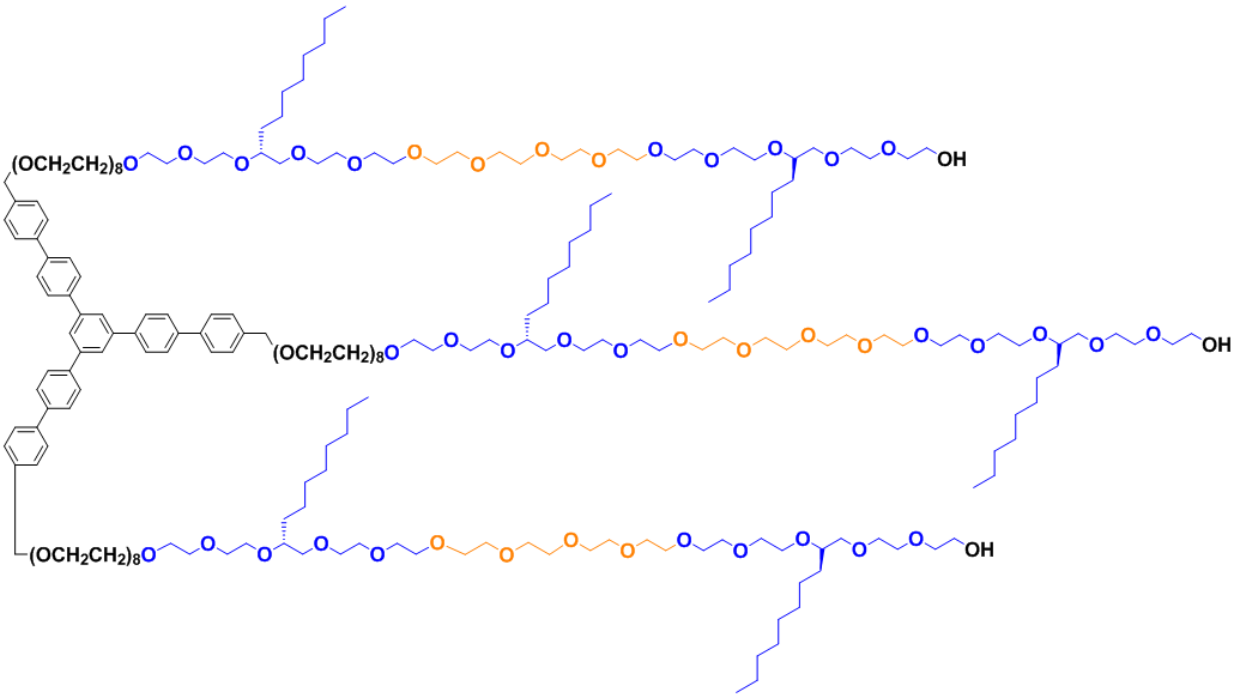
R_f (MeOH- $CHCl_3$ 1: 19+ trace Et_3N) = 0.39.

^{1}H NMR (400 MHz, $CDCl_3$) δ = 7.88 (s, 3H, Hub C***H***), 7.80 (d, *J* = 8.4 Hz, 6H, Hub C***H***), 7.72 (d, *J* = 8.3 Hz, 6H, Hub C***H***), 7.66 (d, *J* = 8.2 Hz, 6H Hub C***H***), 7.45 (d, *J* = 8.0 Hz, 6H Hub C***H***), 4.62 (d, *J* = 5.6 Hz, 9H, 3×OC***H₂***Ar + 3×Thp C***H***), 3.92 – 3.75 (m, 6H, C***H*** (Oct)CH_2O), 3.74 – 3.26 (m, 258H, 129×C***H₂***O), 1.90 – 1.35 (m, 18H, Thp C***H₂***), 1.26 (m, 84H, 42×C***H₂***), 0.87 (t, *J* = 6.8 Hz, 18H, 6×CH_2C***H₃***H).

^{13}C NMR (101 MHz, $CDCl_3$) δ = 141.94(3C), 140.16(3C), 139.96(3C), 139.91(3C), 137.55(3C) (15×Hub ***C***), 128.26(6C), 127.70(6C), 127.51(6C), 127.02(6C), 124.94(3C) (27×Hub ***C***H), 98.90(3×Thp ***C***H), 79.26, 73.98, (6×***C***H(Oct)CH_2), 72.95(3C, 3×O***C***H_2Ar),70.84, 70.78, 70.56, 69.54, 69.28, 66.65(120×***C***H_2O), 62.16(3×Thp ***C***H_2), 31.91, 30.56, 29.75, 29.56, 29.28, 25.54, 25.48, 25.46, 22.65 (54×***C***H_2), 19.47(3×Thp ***C***H_2), 14.10(6×CH_2***C***H_3).

***m/z* (MALDI-ToF$^+$)** $[M+Na]^+$ = 4480.9, *calc.* $C_{240}H_{420}O_{72}Na^+$ = 4480.93.

Hub(OEG$_8$ABA-OH)$_3$ (55)



The reaction was conducted using the *deprotection procedure* described above: To Hub(OEG$_8$ABA-OThp)$_3$ (**54**, 0.45 g, 0.1 mmol) dissolved in MeOH (30 mL) was added MsOH (195 µL). After 30 min, the reaction mixture was worked up as above to afford the title compound (**55**, 0.39 g, 91%) as a pale yellow oil.

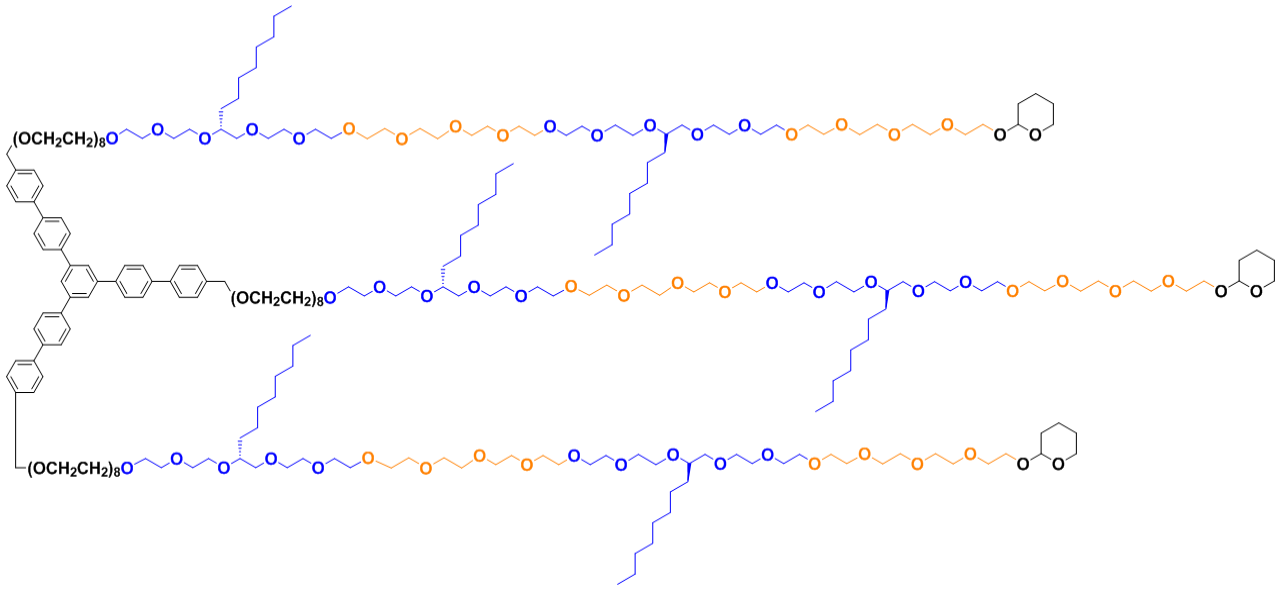
R_f (MeOH- $CHCl_3$ 1: 19) = 0.22.

^{1}H NMR (400 MHz, $CDCl_3$) δ = 7.91 (s, 3H, Hub C***H***), 7.83 (d, J = 8.3 Hz, 6H, Hub C***H***), 7.75 (d, J = 8.4 Hz, 6H, Hub C***H***), 7.67 (d, J = 8.3 Hz, 6H, Hub C***H***), 7.47 (d, J = 8.2 Hz, 6H, Hub C***H***), 4.65 (s, 6H, 3×OC***H$_2$***Ar), 3.88 – 3.50 (m, 252H, 126×C***H$_2$***O), 3.48 – 3.42 (m, 6H, 6× C***H*** (Oct)CH_2O), 1.58 – 1.17 (m, 84H, 42×C***H$_2$***), 0.89 (t, J = 6.7 Hz, 18H, 6×CH_2C***H$_3$***).

^{13}C NMR (101 MHz, $CDCl_3$) δ = δ = 141.95(3C), 140.17(3C), 139.97(3C), 139.93(3C), 137.52(3C) (15×Hub ***C***), 128.30(6C), 127.74(6C), 127.55(6C), 127.06(6C), 124.98(3C) (27×Hub ***C***H), 79.29, 73.97(6×***C***H (Oct) CH2), 72.52(3C, 3×O***C***H_2Ar), 70.86, 70.82, 70.58, 70.43, 69.56, 69.29, 69.22, (126×***C***H_2O), 31.89, 31.73, 29.78, 29.58, 29.30, 25.48, 22.67(42×***C***H_2), 14.13(6×CH_2***C***H_3).

***m/z* (MALDI-ToF$^+$)** $[M+Na]^+$ = 4228.6, *calc.* $C_{225}H_{396}O_{69}Na^+$ = 4228.6.

Hub(OEG$_8$ABAB-OThp)$_3$ (56)



The reaction was conducted using the *coupling procedure* described above: To Hub(OEG$_8$ABA-OH)$_3$ (**55**, 0.4 g, 0.1 mmol) and linear TsOEG$_4$OThp-BB (**42**, 0.4 g, 0.95 mmol, 10 equiv.) in DMF (3 mL) was added NaH (60%, 23 mg, 0.57 mmol, 6 equiv.). After stirring for 24 h at 60 °C, the reaction was worked up then purified using the two-stage membrane apparatus, diafiltering for 5 h to afford the title compound (**56**, 0.45 g, 95%) as a pale yellow oil. The concentration profiles of building block and Hub product during diafiltration is shown in Figure 8.9.

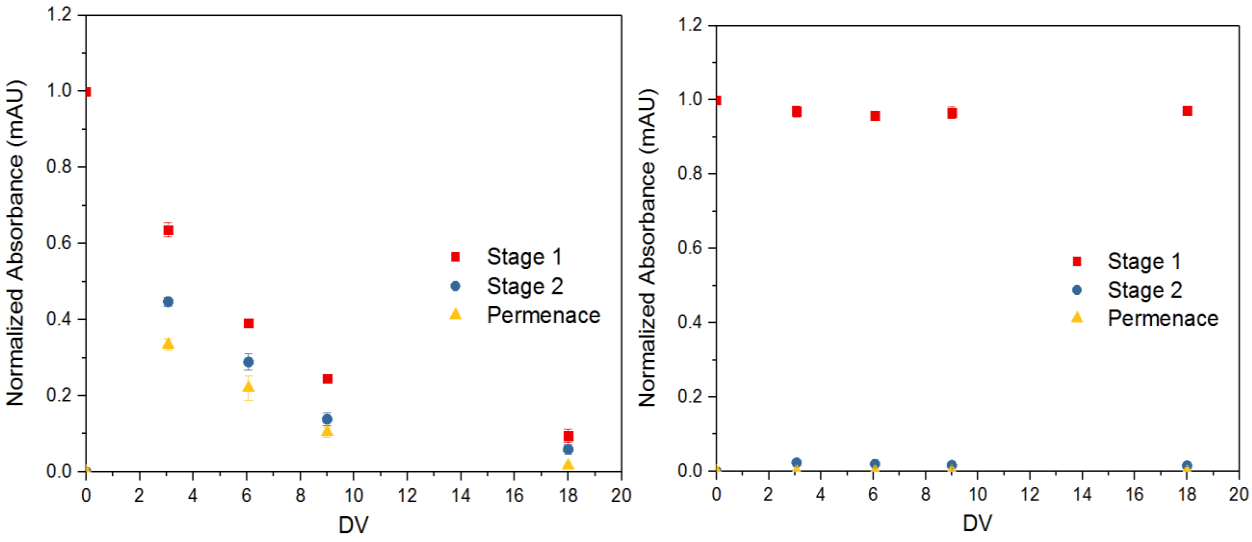


Figure 8.9 Concentration profiles of building block 42 and product 56 in two-stage membrane diafiltration rig.

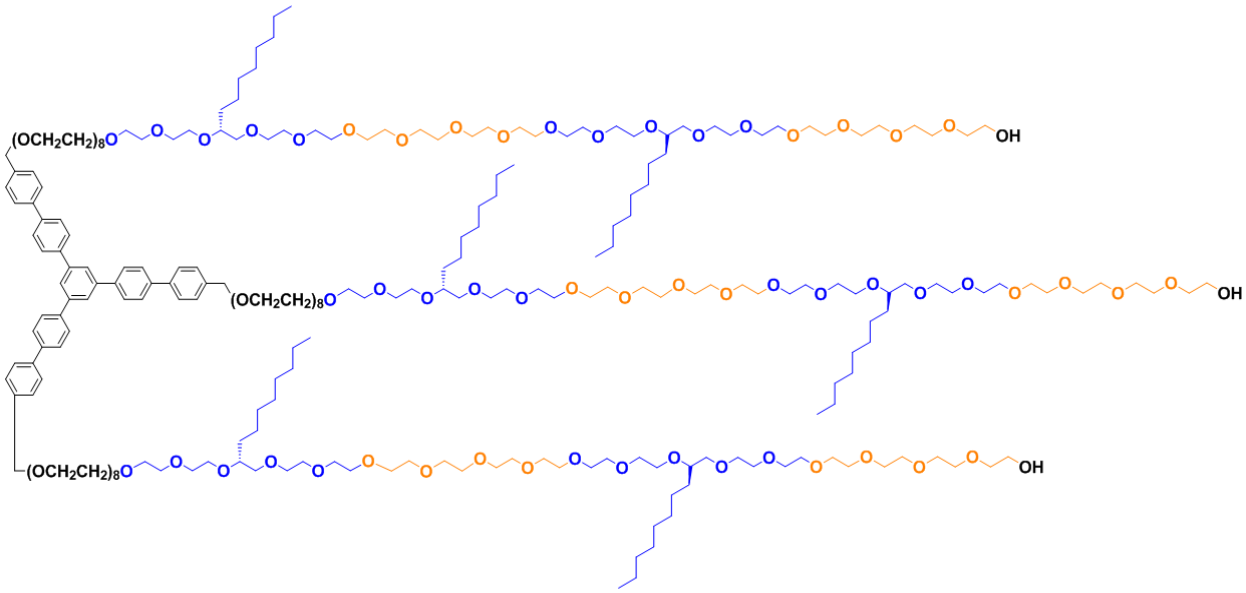
R_f (MeOH- $CHCl_3$ 1: 19+ trace Et_3N) = 0.31.

^{1}H NMR (400 MHz, $CDCl_3$) δ = 7.90 (s, 3H, Hub C***H***), 7.82 (d, *J* = 8.4 Hz, 6H, Hub C***H***), 7.72 (d, *J* = 8.3 Hz, 6H, Hub C***H***), 7.66 (d, *J* = 8.2 Hz, 6H Hub C***H***), 7.47 (d, *J* = 8.2 Hz, 6H, Hub C***H***), 4.64 (d, *J* = 2.2 Hz, 9H, 3×OC***H₂***Ar + 3×Thp C***H***), 3.87 (ddd, *J* = 8.2, 5.9, 4.0 Hz, 6H, C***H*** (Oct)CH_2O), 3.83 – 3.32 (m, 306H, 153×C***H₂***O), 1.93 – 1.38 (m, 18H, Thp C***H₂***), 1.37 – 1.22 (m, 84H, 42×C***H₂***), 0.87 (t, *J* = 6.8 Hz, 18H, 6×CH_2C***H₃***H).

^{13}C NMR (101 MHz, $CDCl_3$) δ = 141.94(3C), 140.16(3C), 139.96(3C), 139.91(3C), 137.55(3C) (15×Hub ***C***), 128.29(6C), 127.73(6C), 127.55(6C), 127.06(6C), 124.94(3C) (27×Hub ***C***H), 98.90(3×Thp ***C***H), 79.27, 73.96(6×***C***H(Oct)CH_2), 72.98(3C, 3×O***C***H_2Ar), 70.86, 70.58, 69.29, 66.65(144×***C***H_2O), 62.21(3×Thp ***C***H_2), 31.89, 30.57, 29.78, 29.59, 29.30, 25.54, 25.48, 25.46, 22.67(54×***C***H_2), 19.48(3×Thp ***C***H_2), 14.12(6×CH_2***C***H_3).

***m/z* (MALDI-ToF$^+$)** $[M+Na]^+$ = 5010.3 (75% 3-arm product) and 4749.1(25% 2-arm product) , *calc.* $C_{264}H_{468}O_{84}Na^+$ = 5010.3.

Hub(OEG$_8$ABAB-OH)$_3$ (57)



The reaction was conducted using the *deprotection procedure* described above: To Hub(OEG$_8$ABAB-OThp)$_3$ (**56**, 0.32 g, 0.065 mmol) dissolved in MeOH (20 mL) was added MsOH (195 µL). After 30 min, the reaction mixture was worked up as above to afford the title compound (**57**, 0.3 g, 98%) as a pale yellow oil.

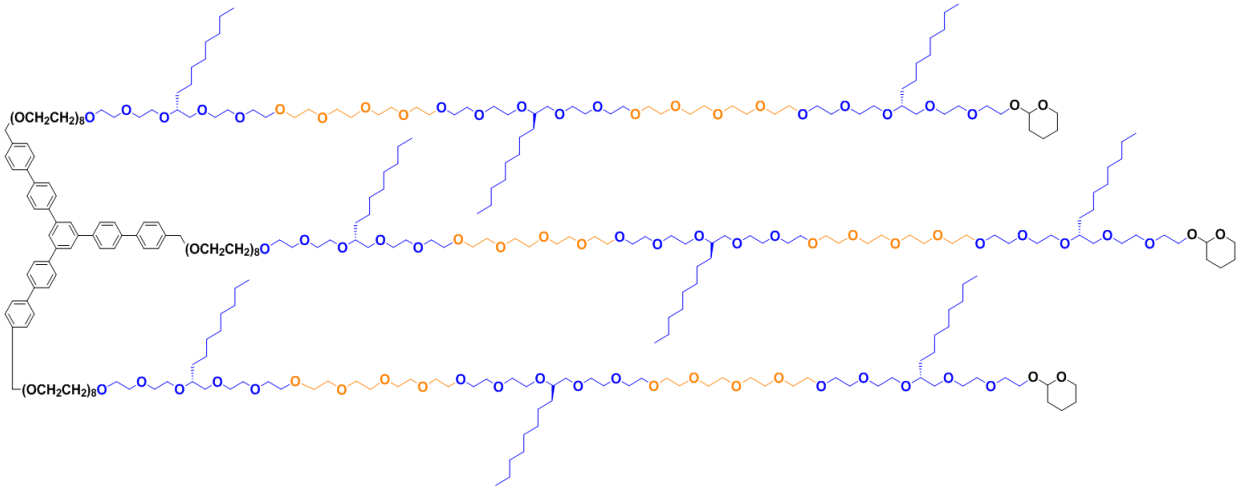
R_f (MeOH- $CHCl_3$ 1: 19) = 0.16.

^{1}H NMR (400 MHz, $CDCl_3$) δ = 7.89 (s, 3H, Hub C***H***), 7.83 (d, J = 8.3 Hz, 6H, Hub C***H***), 7.75 (d, J = 8.4 Hz, 6H, Hub C***H***), 7.67 (d, J = 8.3 Hz, 6H, Hub C***H***), 7.47 (d, J = 8.2 Hz, 6H, Hub C***H***), 4.63 (s, 6H, 3×OC***H$_2$***Ar), 3.79 – 3.46 (m, 300H, 150×C***H$_2$***O), 3.46 – 3.39 (m, 6H, 6× C***H*** (Oct)CH_2O), 1.52 – 1.20 (m, 84H, 42×C***H$_2$***), 0.89 (t, J = 6.7 Hz, 18H, 6×CH_2C***H$_3$***).

^{13}C NMR (101 MHz, $CDCl_3$) δ = 141.95(3C), 140.17(3C), 139.97(3C), 139.93 (3C) 137.55(3C) (15×Hub ***C***), 128.28(6C),, 127.71(6C),, 127.52(6C),, 127.04(6C),124.98(3C) (27×Hub ***C***H), 79.26, 73.95, 72.96(6×***C***H (Oct) CH2), 72.62, (3C, 3×O***C***H_2Ar), 70.85, 70.73, 70.56, 70.32, 69.54, 69.28 (150×***C***H_2O), 31.88, 31.73, 29.77, 29.57, 29.29, 25.46, 22.66(42×***C***H_2), 14.10(6×CH_2***C***H_3).

***m/z* (MALDI-ToF$^+$)** $[M+Na]^+$ = 4757.2 and 4581.2 (2-arm product), *calc.* $C_{249}H_{444}O_{81}Na^+$ = 4757.2.

Hub(OEG$_8$ABABA-OThp)$_3$ (58)



The reaction was conducted using the *coupling procedure* described above: To Hub(OEG$_8$AB AB -OH)$_3$ (**57**, 0.15 g, 0.03 mmol) and Octyl-BB (**33**, 0.18 g, 0.3 mmol, 10 equiv.) in DMF (2 mL) was added NaH (60%, 7.5 mg, 0.18 mmol, 6 equiv.). After stirring for 24 h at 60 °C, the reaction was purified was fractionated by a reverse phase column coluchromatography, eluting with a gradient of acetone-water (1:99 to 90:10, v/v), all solvents containing 1 vol% sat. $NaHCO_3$, to afford the title compound (**58**, 0.16 g, 86%) as a pale yellow oil.

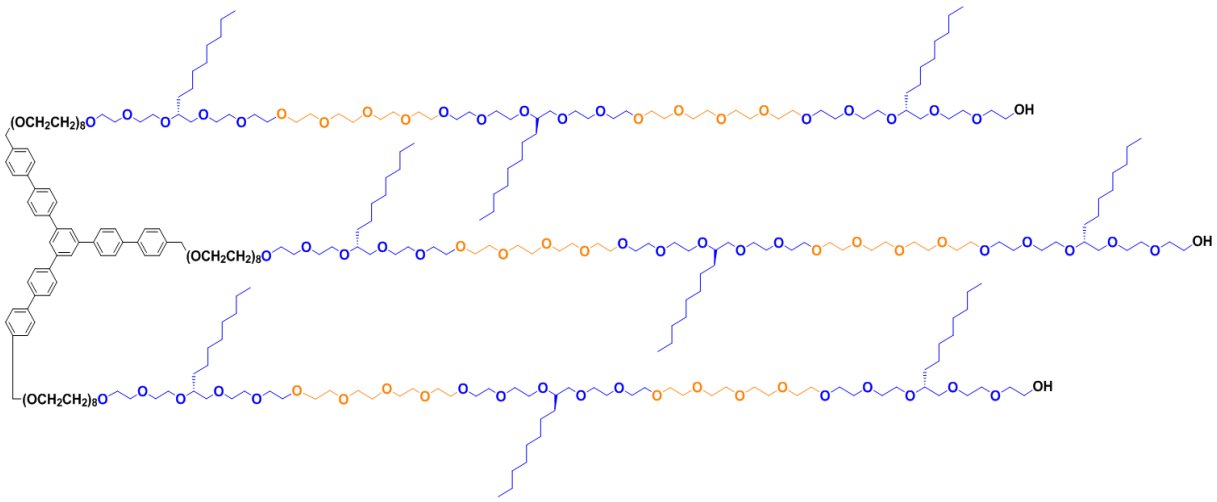
R_f (MeOH- $CHCl_3$ 1: 19+ trace Et_3N) = 0.27.

^{1}H NMR (400 MHz, $CDCl_3$) δ = 7.88 (s, 3H, Hub C***H***), 7.81 (d, *J* = 8.1 Hz, 6H, Hub C***H***), 7.73 (d, *J* = 8.1 Hz, 6H, Hub C***H***), 7.65 (d, *J* = 7.9 Hz, 6H, Hub C***H***), 7.45 (d, *J* = 7.9 Hz, 6H, Hub C***H***), 4.62 (d, *J* = 4.9 Hz, 9H,3×OC***H₂***Ar + 3×Thp C***H***), 3.90 – 3.73 (m, 9H, 9× C***H*** (Oct)CH_2O), 3.73 – 3.21 (m, 360H, 180×C***H₂***O), 1.90 – 1.32 (m, 18H, Thp C***H₂***), 1.26 (m, 126H, 63×C***H₂***), 0.87 (t, *J* = 6.8 Hz, 27H, 9×CH_2C***H₃***).

^{13}C NMR (101 MHz, $CDCl_3$) δ = 141.97(3C), 140.19(3C), 139.97(3C), 139.94(3C), 137.55(3C) (15×Hub ***C***), 128.26(6C), 127.70(6C), 127.51(6C), 127.02(6C), 124.97(3C) (27×Hub ***C***H), 98.90(3×Thp ***C***H), 79.26, 73.95 (9×***C***H(Oct)CH_2), 72.95(3C, 3×O***C***H_2Ar), 70.85, 70.72, 70.56, 69.55, 69.27, 66.65(165×***C***H_2O), 62.16 (3×Thp ***C***H_2), 31.89, 31.86, 30.56, 29.75, 29.66, 29.55, 29.27, 25.45, 22.64(81×***C***H_2), 19.46(3×Thp ***C***H_2), 14.08(9×CH_2***C***H_3).

***m/z* (MALDI-ToF$^+$)** $[M+Na]^+$ = 6002.7, *calc.* $C_{318}H_{576}O_{99}Na^+$ = 6002.7.

Hub(OEG$_8$ABABA-OH)$_3$ (59)



The reaction was conducted using the *deprotection procedure* described above: To Hub(OEG$_8$ABABA-OThp)$_3$ (**58**, 0.1 g, 0.017 mmol) dissolved in MeOH (20 mL) was added MsOH (195 µL). After 30 min, the reaction mixture was worked up as above to afford the title compound (**59**, 0.09 g, 94%) as a pale yellow oil.

R_f (MeOH- $CHCl_3$ 1: 19) = 0.16.

^{1}H NMR (400 MHz, $CDCl_3$) δ = 7.90 (s, 3H, Hub C***H***), 7.82 (d, *J* = 8.2 Hz, 6H, Hub C***H***), 7.74 (d, *J* = 8.3 Hz, 6H, Hub C***H***), 7.66 (d, *J* = 8.1 Hz, 6H, Hub C***H***), 7.47 (d, *J* = 8.0 Hz, 6H, Hub C***H***), 4.64 (s, 6H, 3×OC***H₂***Ar), 3.82 – 3.57 (m, 354H, 177×C***H₂***O), 3.49 – 3.44 (m, 9H, 9× C***H*** (Oct)CH_2O), 1.56 – 1.13 (m, 126H, 63×C***H₂***), 0.89 (t, *J* = 6.7 Hz, 27H, 9×CH_2C***H₃***).

^{13}C NMR (101 MHz, $CDCl_3$) δ = 141.97(3C), 140.17(3C), 139.97(3C), 139.93(3C), 137.52(3C) (15×Hub ***C***), 128.28(6C), 127.72(6C), 127.53(6C), 127.05(6C), 124.95(3C) (27×Hub ***C***H), 79.27, 73.97 (9×***C***H (Oct) CH2), 72.98(3C, 3×O***C***H_2Ar), 70.86-70.58, 70.42, 69.56, 69.28, 69.22(177×***C***H_2O), 31.88, 31.73, 29.77, 29.57, 29.28, 25.47, 22.66(63×***C***H_2), 14.11(9×CH_2***C***H_3).

***m/z* (MALDI-ToF$^+$)** $[M+Na]^+$ = 5754.7, *calc.* $C_{303}H_{552}O_{96}Na^+$ = 5754.7.

References

1. Lutz, J.-F., et al., Sequence-controlled polymers. Science, 2013. 341(6146): p. 1238149.
2. MacEwan, S.R., et al., Phase Behavior and Self-Assembly of Perfectly Sequence-Defined and Monodisperse Multiblock Copolypeptides. Biomacromolecules, 2017. 18(2): p. 599-609.
3. Vroman, I. and L. Tighzert, Biodegradable Polymers. Materials, 2009. 2(2): p. 307.
4. Middleton, J.C. and A.J. Tipton, Synthetic biodegradable polymers as orthopedic devices. Biomaterials, 2000. 21(23): p. 2335-2346.
5. Kurreck, J., RNA Interference: From Basic Research to Therapeutic Applications. Angewandte Chemie, 2009. 48(8): p. 1378-1398.
6. Gaynor, J.W., B.J. Campbell, and R. Cosstick, RNA interference: a chemist's perspective. Chemical Society Reviews, 2010. 39(11): p. 4169-4184.
7. Caruthers, M.H., A brief review of DNA and RNA chemical synthesis. Biochemical Society Transactions, 2011. 39(2): p. 575-580.
8. Kim, B.K., J.W. Seo, and H.M. Jeong, Morphology and properties of waterborne polyurethane/clay nanocomposites. European Polymer Journal, 2003. 39(1): p. 85-91.
9. Gunatillake, P., R. Mayadunne, and R. Adhikari, Recent developments in biodegradable synthetic polymers. Biotechnology annual review, 2006. 12: p. 301-347.
10. Nair, L.S. and C.T. Laurencin, Biodegradable polymers as biomaterials. Progress in polymer science, 2007. 32(8-9): p. 762-798.
11. Lawton, J. and G. Fanta, Glycerol-plasticized films prepared from starch—poly (vinyl alcohol) mixtures: effect of poly (ethylene-co-acrylic acid). Carbohydrate Polymers, 1994. 23(4): p. 275-280.
12. Malafaya, P.B., G.A. Silva, and R.L. Reis, Natural–origin polymers as carriers and scaffolds for biomolecules and cell delivery in tissue engineering applications. Advanced drug delivery reviews, 2007. 59(4-5): p. 207-233.
13. Pachence, J.M.B., M.P.; KohnNewly, J., Biodegradable polymers. In Principles of Tissue Engineering, 2007. 3rd Ed: p. pp. 323-339.
14. Ibim, S.E., et al., Preliminary in vivo report on the osteocompatibility of poly (anhydride-co-imides) evaluated in a tibial model. Journal of biomedical materials research, 1998. 43(4): p. 374-379.
15. Nakajima-Kambe, T., et al., Microbial degradation of polyurethane, polyester polyurethanes and polyether polyurethanes. Applied microbiology and biotechnology, 1999. 51(2): p. 134-140.
16. Guelcher, S.A., et al., Synthesis of biocompatible segmented polyurethanes from aliphatic diisocyanates and diurea diol chain extenders. Acta Biomaterialia, 2005. 1(4): p. 471-484.
17. Hassan, M.K., et al., Biodegradable aliphatic thermoplastic polyurethane based on poly (ε-caprolactone) and l-lysine diisocyanate. Journal of Polymer Science Part A: Polymer Chemistry, 2006. 44(9): p. 2990-3000.
18. Okada, M., Chemical syntheses of biodegradable polymers. Progress in polymer science, 2002. 27(1): p. 87-133.
19. Noble, K.-L., Waterborne polyurethanes. Progress in organic coatings, 1997. 32(1-4): p. 131-136.
20. Wicks Jr, Z.W., D.A. Wicks, and J.W. Rosthauser, Two package waterborne urethane systems. Progress in organic coatings, 2002. 44(2): p. 161-183.

21. Delpech, M.C. and F.M. Coutinho, Waterborne anionic polyurethanes and poly (urethane-urea) s: influence of the chain extender on mechanical and adhesive properties. Polymer testing, 2000. 19(8): p. 939-952.
22. Lapienis, G., Star-shaped polymers having PEO arms. Progress in Polymer Science, 2009. 34(9): p. 852-892.
23. Guo, Y., et al., The PEG-Fluorochrome Shielding Approach for Targeted Probe Design. Journal of the American Chemical Society, 2012. 134(47): p. 19338-19341.
24. Chattopadhyay, J., et al., Synthesis of Water-Soluble PEGylated Single-Walled Carbon Nanotubes. Chemistry of Materials, 2006. 18(25): p. 5864-5868.
25. Li, W., et al., Current drug research on PEGylation with small molecular agents. Progress in Polymer Science, 2013. 38: p. 421-444.
26. Gong, Y., et al., Releasable and traceless PEGylation of arginine-rich antimicrobial peptides. Chemical Science, 2017. 8(5): p. 4082-4086.
27. Gothard, C.M. and B.A. Grzybowski, A Cost-Effective, Column-Free Route to Ethylene Glycol Oligomers EG6, EG10, and EG12. Synthesis, 2012. 44(05): p. 717-722.
28. Tonnesen, H.H. and J. Karlsen, Alginate in Drug Delivery Systems. Drug Development and Industrial Pharmacy, 2002. 28(6): p. 621-630.
29. Gabizon, A., et al., Long-circulating liposomes for drug delivery in cancer therapy: a review of biodistribution studies in tumor-bearing animals. Advanced Drug Delivery Reviews, 1997. 24(2-3): p. 337-344.
30. Lentz, B.R. and J. Lee, Poly (ethylene glycol)(PEG)-mediated fusion between pure lipid bilayers: a mechanism in common with viral fusion and secretory vesicle release? Molecular membrane biology, 1999. 16(4): p. 279-296.
31. French, A.C., A.L. Thompson, and B.G. Davis, High-Purity Discrete PEG-Oligomer Crystals Allow Structural Insight. Angewandte Chemie, 2009. 121(7): p. 1274-1278.
32. Brocchini, S., et al., Disulfide bridge based PEGylation of proteins. Advanced Drug Delivery Reviews, 2008. 60(1): p. 3-12.
33. Kochendoerfer, G.G., Site-specific polymer modification of therapeutic proteins. Current Opinion in Chemical Biology, 2005. 9(6): p. 555-560.
34. J. Whelan, C.P., PCT Application WO 2005-US20469. Bayer Pharmaceuticals Corporation, USA, 2005.
35. Ouchi, T., et al., Synthesis and antitumor activity of poly(ethylene glycol)s linked to 5-fluorouracil via a urethane or urea bond. Drug Design and Discovery, 1992. 9(1): p. 93-105.
36. Ouchi, T., et al., Synthesis of polyether-bound 3-(5-fluorouracil-1-yl)propanoic acid and its hydrolysis reactivity. European Polymer Journal, 1986. 22(7): p. 537-541.
37. Hermanson, G.T., Bioconjugate techniques. 2013: Academic press.
38. Reed, N.N. and K.D. Janda, A One-Step Synthesis of Monoprotected Polyethylene Glycol Ethers. The Journal of Organic Chemistry, 2000. 65(18): p. 5843-5845.
39. Zhang, J., et al., Synthesis of monomethoxy poly(ethylene glycol) without diol poly(ethylene glycol). Journal of Applied Polymer Science, 2007. 105(6): p. 3782-3786.
40. Vicent, M.J., et al., Polymer conjugates as therapeutics: future trends, challenges and opportunities. Expert Opinion on Drug Delivery, 2008. 5(5): p. 593-614.
41. Haag, R. and F. Kratz, Polymer Therapeutics: Concepts and Applications. Angewandte Chemie International Edition, 2006. 45(8): p. 1198-1215.
42. Filpula, D. and H. Zhao, Releasable PEGylation of proteins with customized linkers. Advanced Drug Delivery Reviews, 2008. 60(1): p. 29-49.
43. Matyjaszewski, K. and M. Möller, Polymer science: a comprehensive reference. 2012: Elsevier.

44. Lutz, J.-F., Sequence-controlled polymerizations: the next Holy Grail in polymer science? Polymer Chemistry, 2010. 1(1): p. 55-62.
45. Hill, D.J., et al., A Field Guide to Foldamers. Chemical Reviews, 2001. 101(12): p. 3893-4012.
46. Börner, H.G., Strategies exploiting functions and self-assembly properties of bioconjugates for polymer and materials sciences. Progress in Polymer Science, 2009. 34(9): p. 811-851.
47. Aldaye, F.A., A.L. Palmer, and H.F. Sleiman, Assembling Materials with DNA as the Guide. Science, 2008. 321(5897): p. 1795-1799.
48. Eckhardt, D., et al., Rational design of oligopeptide organizers for the formation of poly(ethylene oxide) nanofibers. Chemical Communications, 2005(22): p. 2814-2816.
49. Frauenrath, H. and E. Jahnke, A General Concept for the Preparation of Hierarchically Structured π-Conjugated Polymers. Chemistry – A European Journal, 2008. 14(10): p. 2942-2955.
50. Hartgerink, J.D., E. Beniash, and S.I. Stupp, Self-Assembly and Mineralization of Peptide-Amphiphile Nanofibers. Science, 2001. 294(5547): p. 1684-1688.
51. Bazzi, H.S., J. Bouffard, and H.F. Sleiman, Self-Complementary ABC Triblock Copolymers via Ring-Opening Metathesis Polymerization. Macromolecules, 2003. 36(21): p. 7899-7902.
52. Ishihara, Y., et al., Molecule-Responsive Block Copolymer Micelles. Chemistry – A European Journal, 2007. 13(16): p. 4560-4570.
53. Petka, W.A., et al., Reversible Hydrogels from Self-Assembling Artificial Proteins. Science, 1998. 281(5375): p. 389-392.
54. Ouchi, M., et al., Single-chain technology using discrete synthetic macromolecules. Nature Chemistry, 2011. 3: p. 917.
55. Terashima, T., et al., Single-Chain Folding of Polymers for Catalytic Systems in Water. Journal of the American Chemical Society, 2011. 133(13): p. 4742-4745.
56. Murnen, H.K., et al., Impact of Hydrophobic Sequence Patterning on the Coil-to-Globule Transition of Protein-like Polymers. Macromolecules, 2012. 45(12): p. 5229-5236.
57. Weiss, J., et al., Water-soluble random and alternating copolymers of styrene monomers with adjustable lower critical solution temperature. Polymer Chemistry, 2012. 3(2): p. 352-361.
58. Hao, Z., et al., Thermoresponsive Synergistic Hydrogen Bonding Switched by Several Guest Units in a Water-Soluble Polymer. Macromolecular Rapid Communications, 2013. 34(5): p. 411-416.
59. Rosales, A.M., et al., Tunable Phase Behavior of Polystyrene–Polypeptoid Block Copolymers. Macromolecules, 2012. 45(15): p. 6027-6035.
60. Smith, J.A., et al., Precisely Controlled Methyl Branching in Polyethylene via Acyclic Diene Metathesis (ADMET) Polymerization. Macromolecules, 2000. 33(10): p. 3781-3794.
61. Aitken, B.S., et al., Precision Ionomers: Synthesis and Thermal/Mechanical Characterization. Macromolecules, 2012. 45(2): p. 681-687.
62. Murnen, H.K., et al., Persistence length of polyelectrolytes with precisely located charges. Soft Matter, 2013. 9(1): p. 90-98.
63. Li, J., R.M. Stayshich, and T.Y. Meyer, Exploiting Sequence To Control the Hydrolysis Behavior of Biodegradable PLGA Copolymers. Journal of the American Chemical Society, 2011. 133(18): p. 6910-6913.

64. Li, J., et al., The Effect of Monomer Order on the Hydrolysis of Biodegradable Poly(lactic-co-glycolic acid) Repeating Sequence Copolymers. Journal of the American Chemical Society, 2012. 134(39): p. 16352-16359.
65. Hartmann, L., et al., Tailor-Made Poly(amidoamine)s for Controlled Complexation and Condensation of DNA. Chemistry – A European Journal, 2008. 14(7): p. 2025-2033.
66. Chen, C.-L., et al., Engineered Biomimetic Polymers as Tunable Agents for Controlling CaCO3 Mineralization. Journal of the American Chemical Society, 2011. 133(14): p. 5214-5217.
67. Lee, D.H., et al., A self-replicating peptide. Nature, 1996. 382: p. 525.
68. Pinheiro, V.B., et al., Synthetic Genetic Polymers Capable of Heredity and Evolution. Science, 2012. 336(6079): p. 341-344.
69. Church, G.M., Y. Gao, and S. Kosuri, Next-Generation Digital Information Storage in DNA. Science, 2012. 337(6102): p. 1628-1628.
70. Bancroft, C., et al., Long-Term Storage of Information in DNA. Science, 2001. 293(5536): p. 1763-1765.
71. Bonnet, J., P. Subsoontorn, and D. Endy, Rewritable digital data storage in live cells via engineered control of recombination directionality. Proceedings of the National Academy of Sciences, 2012. 109(23): p. 8884-8889.
72. Saiki, R.K., et al., Primer-directed enzymatic amplification of DNA with a thermostable DNA polymerase. Science, 1988. 239(4839): p. 487-491.
73. McGrath, K.P., et al., Genetically directed syntheses of new polymeric materials. Expression of artificial genes encoding proteins with repeating -(AlaGly)3ProGluGly- elements. Journal of the American Chemical Society, 1992. 114(2): p. 727-733.
74. Li, T. and K.C. Nicolaou, Chemical self-replication of palindromic duplex DNA. Nature, 1994. 369: p. 218.
75. Sievers, D. and G. von Kiedrowski, Self-replication of complementary nucleotide-based oligomers. Nature, 1994. 369: p. 221.
76. Brudno, Y. and D.R. Liu, Recent Progress Toward the Templated Synthesis and Directed Evolution of Sequence-Defined Synthetic Polymers. Chemistry & Biology, 2009. 16(3): p. 265-276.
77. Inaki, Y., K. Ebisutani, and K. Takemoto, Functional monomers and polymers. CXXXII. Template polymerization of methacrylamide derivatives containing nucleic acid bases. Journal of Polymer Science Part A: Polymer Chemistry, 1986. 24(12): p. 3249-3262.
78. Spijker, H.J., F.L. van Delft, and J.C.M. van Hest, Atom Transfer Radical Polymerization of Adenine, Thymine, Cytosine, and Guanine Nucleobase Monomers. Macromolecules, 2007. 40(1): p. 12-18.
79. Rojas, G., et al., Precision Polyethylene: Changes in Morphology as a Function of Alkyl Branch Size. Journal of the American Chemical Society, 2009. 131(47): p. 17376-17386.
80. Atallah, P., K.B. Wagener, and M.D. Schulz, ADMET: The Future Revealed. Macromolecules, 2013. 46(12): p. 4735-4741.
81. Zhang, J., M.E. Matta, and M.A. Hillmyer, Synthesis of Sequence-Specific Vinyl Copolymers by Regioselective ROMP of Multiply Substituted Cyclooctenes. ACS Macro Letters, 2012. 1(12): p. 1383-1387.
82. Böhler, C., P.E. Nielsen, and L.E. Orgel, Template switching between PNA and RNA oligonucleotides. Nature, 1995. 376: p. 578.
83. Rosenbaum, D.M. and D.R. Liu, Efficient and Sequence-Specific DNA-Templated Polymerization of Peptide Nucleic Acid Aldehydes. Journal of the American Chemical Society, 2003. 125(46): p. 13924-13925.

84. Kleiner, R.E., et al., DNA-Templated Polymerization of Side-Chain-Functionalized Peptide Nucleic Acid Aldehydes. Journal of the American Chemical Society, 2008. 130(14): p. 4646-4659.
85. Niu, J., R. Hili, and D.R. Liu, Enzyme-free translation of DNA into sequence-defined synthetic polymers structurally unrelated to nucleic acids. Nature chemistry, 2013. 5(4): p. 282-292.
86. Orgel, L.E., Molecular replication. Nature, 1992. 358: p. 203.
87. Lo, P.K. and H.F. Sleiman, Nucleobase-Templated Polymerization: Copying the Chain Length and Polydispersity of Living Polymers into Conjugated Polymers. Journal of the American Chemical Society, 2009. 131(12): p. 4182-4183.
88. Mchale, R., et al., Biomimetic radical polymerization via cooperative assembly of segregating templates. Nature Chemistry, 2012. 4(6): p. 491-497.
89. McKee, M.L., et al., Multistep DNA-Templated Reactions for the Synthesis of Functional Sequence Controlled Oligomers. Angewandte Chemie International Edition, 2010. 49(43): p. 7948-7951.
90. Milnes, P.J., et al., Sequence-specific synthesis of macromolecules using DNA-templated chemistry. Chemical Communications, 2012. 48(45): p. 5614-5616.
91. Chen, W. and G.B. Schuster, Precise Sequence Control in Linear and Cyclic Copolymers of 2,5-Bis(2-thienyl)pyrrole and Aniline by DNA-Programmed Assembly. Journal of the American Chemical Society, 2013. 135(11): p. 4438-4449.
92. Ida, S., et al., Selective Radical Addition with a Designed Heterobifunctional Halide: A Primary Study toward Sequence-Controlled Polymerization upon Template Effect. Journal of the American Chemical Society, 2009. 131(31): p. 10808-10809.
93. Ida, S., M. Ouchi, and M. Sawamoto, Template-assisted selective radical addition toward sequence-regulated polymerization: lariat capture of target monomer by template initiator. Journal of the American Chemical Society, 2010. 132(42): p. 14748-14750.
94. Hibi, Y., M. Ouchi, and M. Sawamoto, Sequence-Regulated Radical Polymerization with a Metal- Templated Monomer: Repetitive ABA Sequence by Double Cyclopolymerization. Angewandte Chemie International Edition, 2011. 50(32): p. 7434-7437.
95. Hibi, Y., et al., Design of AB divinyl “template monomers” toward alternating sequence control in metal-catalyzed living radical polymerization. Polymer Chemistry, 2011. 2(2): p. 341-347.
96. Piccirilli, J.A., et al., Enzymatic incorporation of a new base pair into DNA and RNA extends the genetic alphabet. Nature, 1990. 343: p. 33.
97. Kool, E.T., Replacing the Nucleobases in DNA with Designer Molecules. Accounts of Chemical Research, 2002. 35(11): p. 936-943.
98. Malyshev, D.A., et al., Efficient and sequence-independent replication of DNA containing a third base pair establishes a functional six-letter genetic alphabet. Proceedings of the National Academy of Sciences, 2012. 109(30): p. 12005-12010.
99. Lewandowski, B., et al., Sequence-specific peptide synthesis by an artificial small-molecule machine. Science, 2013. 339(6116): p. 189-193.
100. Kramer, J.W., et al., Polymerization of Enantiopure Monomers Using Syndiospecific Catalysts: A New Approach To Sequence Control in Polymer Synthesis. Journal of the American Chemical Society, 2009. 131(44): p. 16042-16044.
101. van Hest, J.C. and D.A. Tirrell, Protein-based materials, toward a new level of structural control. Chemical communications (Cambridge, England), 2001(19): p. 1897.
102. Wang, L. and P.G. Schultz, Expanding the Genetic Code. Angewandte Chemie International Edition, 2005. 44(1): p. 34-66.

103. Kiick, K.L., J.C.M. van Hest, and D.A. Tirrell, Expanding the Scope of Protein Biosynthesis by Altering the Methionyl-tRNA Synthetase Activity of a Bacterial Expression Host. Angewandte Chemie International Edition, 2000. 39(12): p. 2148-2152.
104. Noren, C., et al., A general method for site-specific incorporation of unnatural amino acids into proteins. Science, 1989. 244(4901): p. 182-188.
105. Szwarc, M., 'Living' Polymers. Nature, 1956. 178: p. 1168.
106. Patten, T.E., et al., Polymers with Very Low Polydispersities from Atom Transfer Radical Polymerization. Science, 1996. 272(5263): p. 866-868.
107. Ouchi, M., T. Terashima, and M. Sawamoto, Transition Metal-Catalyzed Living Radical Polymerization: Toward Perfection in Catalysis and Precision Polymer Synthesis. Chemical Reviews, 2009. 109(11): p. 4963-5050.
108. Bielawski, C.W. and R.H. Grubbs, Living ring-opening metathesis polymerization. Progress in Polymer Science, 2007. 32(1): p. 1-29.
109. Bates, F.S., et al., Multiblock Polymers: Panacea or Pandora's Box? Science, 2012. 336(6080): p. 434-440.
110. Leibfarth, F.A., et al., External Regulation of Controlled Polymerizations. Angewandte Chemie International Edition, 2013. 52(1): p. 199-210.
111. Matyjaszewski, K. and J. Xia, Atom transfer radical polymerization. Chemical reviews, 2001. 101(9): p. 2921-2990.
112. Kamigaito, M., T. Ando, and M. Sawamoto, Metal-catalyzed living radical polymerization. Chemical Reviews, 2001. 101(12): p. 3689-3746.
113. Hawker, C.J., A.W. Bosman, and E. Harth, New polymer synthesis by nitroxide mediated living radical polymerizations. Chemical reviews, 2001. 101(12): p. 3661-3688.
114. Moad, G., E. Rizzardo, and S.H. Thang, Radical addition–fragmentation chemistry in polymer synthesis. Polymer, 2008. 49(5): p. 1079-1131.
115. Chan-Seng, D., M. Zamfir, and J.-F. Lutz, Polymer-Chain Encoding: Synthesis of Highly Complex Monomer Sequence Patterns by Using Automated Protocols. Angewandte Chemie International Edition, 2012. 51(49): p. 12254-12257.
116. Schmidt, B.V.K.J., et al., Controlled folding of synthetic polymer chains through the formation of positionable covalent bridges. Nature Chemistry, 2011. 3: p. 234.
117. Natalello, A., et al., Kinetic Control of Monomer Sequence Distribution in Living Anionic Copolymerisation. Macromolecular Rapid Communications, 2011. 32(2): p. 233-237.
118. Saegusa, T., Monomer-monomer interaction in spontaneous initiation and sequence regulation in copolymerization. Die Makromolekulare Chemie: Macromolecular Chemistry and Physics, 1979. 3(S19791): p. 157-176.
119. Rzaev, Z., Complex-radical alternating copolymerization. Progress in Polymer Science, 2000. 25(2): p. 163-217.
120. Kırcı, B., J.-F. Lutz, and K. Matyjaszewski, Synthesis of Well-Defined Alternating Copolymers Poly (methyl methacrylate-a lt-styrene) by RAFT Polymerization in the Presence of Lewis Acid. Macromolecules, 2002. 35(7): p. 2448-2451.
121. Rzaev, Z.M.O., Complex-radical alternating copolymerization. Progress in Polymer Science, 2000. 25(2): p. 163-217.
122. Pfeifer, S. and J.F. Lutz, Development of a library of N-substituted maleimides for the local functionalization of linear polymer chains. Chemistry–A European Journal, 2008. 14(35): p. 10949-10957.

123. Satoh, K., et al., AAB-Sequence Living Radical Chain Copolymerization of Naturally Occurring Limonene with Maleimide: An End-to-End Sequence-Regulated Copolymer. Journal of the American Chemical Society, 2010. 132(29): p. 10003-10005.
124. Lutz, J.-F., T. Pakula, and K. Matyjaszewski. Synthesis and properties of copolymers with tailored sequence distribution by controlled/living radical polymerization. in ACS Symposium Series, Advances in Controlled/Living Radical Polymerization. 2003.
125. Pfeifer, S. and J.-F. Lutz, A Facile Procedure for Controlling Monomer Sequence Distribution in Radical Chain Polymerizations. Journal of the American Chemical Society, 2007. 129(31): p. 9542-9543.
126. Berthet, M.-A., et al., Facile Synthesis of Functional Periodic Copolymers: A Step toward Polymer-Based Molecular Arrays. Macromolecules, 2010. 43(1): p. 44-50.
127. Zamfir, M. and J.-F. Lutz, Ultra-precise insertion of functional monomers in chain-growth polymerizations. Nature Communications, 2012. 3: p. 1138.
128. Berthet, M.-A., et al., Facile Synthesis of Functional Periodic Copolymers: A Step toward Polymer-Based Molecular Arrays. Macromolecules, 2009. 43(1): p. 44-50.
129. Minoda, M., M. Sawamoto, and T. Higashimura, Sequence-regulated oligomers and polymers by living cationic polymerization. 2. Principle of sequence regulation and synthesis of sequence-regulated oligomers of functional vinyl ethers and styrene derivatives. Macromolecules, 1990. 23(23): p. 4889-4895.
130. Houshyar, S., et al., The scope for synthesis of macro-RAFT agents by sequential insertion of single monomer units. Polymer Chemistry, 2012. 3(7): p. 1879-1889.
131. Tong, X., B.-h. Guo, and Y. Huang, Toward the synthesis of sequence-controlled vinyl copolymers. Chemical Communications, 2011. 47(5): p. 1455-1457.
132. Norris, B.N., T. Pan, and T.Y. Meyer, Iterative Synthesis of Heterotelechelic Oligo(phenylene-vinylene)s by Olefin Cross-Metathesis. Organic Letters, 2010. 12(23): p. 5514-5517.
133. Norris, B.N., et al., Sequence Matters: Modulating Electronic and Optical Properties of Conjugated Oligomers via Tailored Sequence. Macromolecules, 2013. 46(4): p. 1384-1392.
134. Ueda, M., Sequence control in one-step condensation polymerization. Progress in polymer science, 1999. 24(5): p. 699-730.
135. Yu, T.-B., J.Z. Bai, and Z. Guan, Cycloaddition-Promoted Self-Assembly of a Polymer into Well-Defined β Sheets and Hierarchical Nanofibrils. Angewandte Chemie International Edition, 2009. 48(6): p. 1097-1101.
136. Satoh, K., M. Mizutani, and M. Kamigaito, Metal-catalyzed radical polyaddition as a novel polymer synthetic route. Chemical Communications, 2007(12): p. 1260-1262.
137. Satoh, K., et al., Sequence-regulated vinyl copolymers by metal-catalysed step-growth radical polymerization. Nature Communications, 2010. 1: p. 6.
138. Takizawa, K., et al., Molecularly defined (L)-lactic acid oligomers and polymers: Synthesis and characterization. Journal of Polymer Science Part A: Polymer Chemistry, 2008. 46(18): p. 5977-5990.
139. Takizawa, K., C. Tang, and C.J. Hawker, Molecularly defined caprolactone oligomers and polymers: synthesis and characterization. Journal of the American Chemical Society, 2008. 130(5): p. 1718-1726.
140. Hackenberger, C.P. and D. Schwarzer, Chemoselective ligation and modification strategies for peptides and proteins. Angewandte Chemie International Edition, 2008. 47(52): p. 10030-10074.
141. Kent, S.B., Total chemical synthesis of proteins. Chemical Society Reviews, 2009. 38(2): p. 338-351.

142. Becer, C.R., R. Hoogenboom, and U.S. Schubert, Click chemistry beyond metal-catalyzed cycloaddition. Angewandte Chemie International Edition, 2009. 48(27): p. 4900-4908.
143. Singh, I., et al., Metal-free "click" chemistry: efficient polymer modification via 1, 3-dipolar cycloaddition of nitrile oxides and alkynes. Macromolecules, 2009. 42(15): p. 5411-5413.
144. Theato, P., Synthesis of well-defined polymeric activated esters. Journal of Polymer Science Part A: Polymer Chemistry, 2008. 46(20): p. 6677-6687.
145. Yokota, K., Periodic copolymers. Progress in polymer science, 1999. 24(4): p. 517-563.
146. Cho, I., New ring-opening polymerizations for copolymers having controlled microstructures. Progress in polymer science, 2000. 25(8): p. 1043-1087.
147. Yu, T.B., J.Z. Bai, and Z. Guan, Cycloaddition-Promoted Self-Assembly of a Polymer into Well-Defined β Sheets and Hierarchical Nanofibrils. Angewandte Chemie, 2009. 121(6): p. 1117-1121.
148. Urry, D.W., T. Trapane, and K. Prasad, Phase-structure transitions of the elastin polypentapeptide–water system within the framework of composition–temperature studies. Biopolymers: Original Research on Biomolecules, 1985. 24(12): p. 2345-2356.
149. Urry, D.W., Physical chemistry of biological free energy transduction as demonstrated by elastic protein-based polymers. 1997, ACS Publications.
150. Tachibana, Y., et al., Efficient and versatile synthesis of mucin-like glycoprotein mimics. Tetrahedron, 2002. 58(51): p. 10213-10224.
151. Chandrudu, S., P. Simerska, and I. Toth, Chemical methods for peptide and protein production. Molecules, 2013. 18(4): p. 4373-4388.
152. Solleder, S.C., et al., Recent Progress in the Design of Monodisperse, Sequence-Defined Macromolecules. Macromolecular rapid communications, 2017. 38(9): p. 1600711.
153. Merrifield, R.B., Solid phase synthesis. Science, 1986. 232(4748): p. 341-347.
154. Lutz, J.-F. and H.G. Börner, Modern trends in polymer bioconjugates design. Progress in Polymer Science, 2008. 33(1): p. 1-39.
155. Plante, O.J., E.R. Palmacci, and P.H. Seeberger, Automated Solid-Phase Synthesis of Oligosaccharides. Science, 2001. 291(5508): p. 1523-1527.
156. Svec, F. and J.M. Frechet, New designs of macroporous polymers and supports: from separation to biocatalysis. Science, 1996. 273(5272): p. 205-211.
157. Engelis, N.G., et al., Sequence-controlled methacrylic multiblock copolymers via sulfur-free RAFT emulsion polymerization. Nature chemistry, 2017. 9(2): p. 171.
158. Vesa, V.S., Progress in the Synthesis of Peptides on Polymers. Russian Chemical Reviews, 1968. 37(2): p. 114-119.
159. Hayatsu, H. and H.G. Khorana, Deoxyribooligonucleotide Synthesis on a Polymer Support1. Journal of the American Chemical Society, 1966. 88(13): p. 3182-3183.
160. Pfeifer, S., et al., Liquid-phase synthesis of block copolymers containing sequence-ordered segments. Journal of the American Chemical Society, 2009. 131(26): p. 9195-9197.
161. Schott, H., Polyvinyl Alcohol Substituted by Nucleotides as Carrier for Liquid Phase Oligonucleotide Synthesis. Angewandte Chemie, 1973. 12(3): p. 246-246.
162. Kamaike, K., Y. Hasegawa, and Y. Ishido, Efficient syntheses of an oligonucleotide on a cellulose acetate derivative as a novel polymer-support using phosphotriester approach. Tetrahedron Letters, 1988. 29(6): p. 647-650.
163. Fischer, P. and D. Zheleva, Liquid-phase peptide synthesis on polyethylene glycol (PEG) supports using strategies based on the 9-fluorenylmethoxycarbonyl amino

protecting group: application of PEGylated peptides in biochemical assays. Journal of Peptide Science, 2002. 8(9): p. 529-542.
164. Zhang, W., Fluorous tagging strategy for solution-phase synthesis of small molecules, peptides and oligosaccharides. ChemInform, 2005. 7(6): p. 784-797.
165. Miao, W. and T. Chan, Ionic-Liquid-Supported Peptide Synthesis Demonstrated by the Synthesis of Leu5-Enkephalin. Journal of Organic Chemistry, 2005. 70(8): p. 3251-3255.
166. Bonora, G.M., et al., A Liquid-Phase Process Suitable for Large-Scale Synthesis of Phosphorothioate Oligonucleotides. Organic Process Research & Development, 2000. 4(3): p. 225-231.
167. Kungurtsev, V., et al., Solution-Phase Synthesis of Short Oligo-2′-deoxyribonucleotides by Using Clustered Nucleosides as a Soluble Support. European Journal of Organic Chemistry, 2013. 2013(29): p. 6687-6693.
168. Matyjaszewski, K., Macromolecular engineering: From rational design through precise macromolecular synthesis and processing to targeted macroscopic material properties. Progress in Polymer Science, 2005. 30(8-9): p. 858-875.
169. Bernaerts, K.V. and F.E. Du Prez, Dual/heterofunctional initiators for the combination of mechanistically distinct polymerization techniques. Progress in polymer science, 2006. 31(8): p. 671-722.
170. Barner-Kowollik, C. and S. Perrier, The future of reversible addition fragmentation chain transfer polymerization. Journal of Polymer Science Part A: Polymer Chemistry, 2008. 46(17): p. 5715-5723.
171. McCormick, C.L., et al., RAFT-synthesized diblock and triblock copolymers: thermally-induced supramolecular assembly in aqueous media. Soft Matter, 2008. 4(9): p. 1760-1773.
172. Gravert, D.J., et al., Soluble supports tailored for organic synthesis: parallel polymer synthesis via sequential normal/living free radical processes. Journal of the American Chemical Society, 1998. 120(37): p. 9481-9495.
173. Székely, G., et al., Beyond PEG2000: Synthesis and functionalisation of monodisperse PEGylated homostars and clickable bivalent polyethyleneglycols. Chemistry-A European Journal, 2014. 20(32): p. 10038-10051.
174. J., G.P.R., et al., Liquid-Phase Synthesis of 2′-Methyl-RNA on a Homostar Support through Organic-Solvent Nanofiltration. Chemistry – A European Journal, 2015. 21(26): p. 9535-9543.
175. Gaffney, P.R.J., et al., Liquid-Phase Synthesis of 2-Methyl-RNA on a Homostar Support through Organic-Solvent Nanofiltration. Chemistry-a European Journal, 2015. 21(26): p. 9535-9543.
176. Barnes, J.C., et al., Iterative exponential growth of stereo- and sequence-controlled polymers. Nature Chemistry, 2015. 7: p. 810.
177. Porel, M. and C.A. Alabi, Sequence-defined polymers via orthogonal allyl acrylamide building blocks. Journal of the American Chemical Society, 2014. 136(38): p. 13162-13165.
178. Hartmann, L. and H.G. Borner, Precision Polymers: Monodisperse, Monomer-Sequence-Defined Segments to Target Future Demands of Polymers in Medicine. Advanced Materials, 2009. 21: p. 3425-3431.
179. Hartmann, L., Polymers for Control Freaks: Sequence-Defined Poly(amidoamine)s and Their Biomedical Applications. Macromolecular Chemistry and Physics, 2011. 212(1): p. 8-13.

180. Zuckermann, R.N., et al., Efficient method for the preparation of peptoids [oligo(N-substituted glycines)] by submonomer solid-phase synthesis. Journal of the American Chemical Society, 1992. 114(26): p. 10646-10647.
181. Paynter, O.I., D.J. Simmonds, and M.C. Whiting, The synthesis of long-chain unbranched aliphatic compounds by molecular doubling. Journal of The Chemical Society, Chemical Communications, 1982(20): p. 1165-1166.
182. Bidd, I. and M.C. Whiting, The synthesis of pure n-paraffins with chain-lengths between one and four hundred. Journal of the Chemical Society, Chemical Communications, 1985(9): p. 543-544.
183. Amir, F., Z. Jia, and M.J. Monteiro, Sequence control of macromers via iterative sequential and exponential growth. Journal of the American Chemical Society, 2016. 138(51): p. 16600-16603.
184. Bootwicha, T., et al., Iterative assembly line synthesis of polypropionates with full stereocontrol. Nature Chemistry, 2017. 9(9): p. 896.
185. Oh, D., et al., Iterative radical addition with a special monomer carrying bulky and convertible pendant: a new concept toward controlling the sequence for vinyl polymers. ACS Macro Letters, 2016. 5(6): p. 745-749.
186. Gravert, D.J. and K.D. Janda, Organic synthesis on soluble polymer supports: liquid-phase methodologies. Chemical reviews, 1997. 97(2): p. 489-510.
187. Wentworth Jr, P. and K.D. Janda, Liquid-phase chemistry: recent advances in soluble polymer-supported catalysts, reagents and synthesis. Chemical Communications, 1999(19): p. 1917-1924.
188. Dickerson, T.J., N.N. Reed, and K.D. Janda, Soluble polymers as scaffolds for recoverable catalysts and reagents. Chemical Reviews, 2002. 102(10): p. 3325-3344.
189. Choi, M.K.W. and P.H. Toy, Soluble polystyrene-based sulfoxide reagents for Swern oxidation reactions. Tetrahedron, 2003. 59(36): p. 7171-7176.
190. Hayatsu, H. and H. Khorana, Deoxyribooligonucleotide Synthesis on a Polymer Support1. Journal of the American Chemical Society, 1966. 88(13): p. 3182-3183.
191. Bayer, E. and M. Mutter, Liquid phase synthesis of peptides. Nature, 1972. 237(5357): p. 512.
192. Burkett, B.A. and T.H. Chan, An expedient synthesis of monodispersed oligo (ethylene glycols). Synthesis, 2004. 2004(07): p. 1007-1010.
193. Polypure. Technology. 2018 [cited 2018 21 July]; Available from: https://polypure.com/technology.
194. Loiseau, F.A., K.K. Hii, and A.M. Hill, Multigram synthesis of well-defined extended bifunctional polyethylene glycol (PEG) chains. The Journal of organic chemistry, 2004. 69(3): p. 639-647.
195. Wawro, A.M., T. Muraoka, and K. Kinbara, Chromatography-free synthesis of monodisperse oligo(ethylene glycol) mono-p-toluenesulfonates and quantitative analysis of oligomer purity. Polymer Chemistry, 2016. 7(13): p. 2389-2394.
196. Zhang, H., et al., Highly Efficient Synthesis of Monodisperse Poly(ethylene glycols) and Derivatives through Macrocyclization of Oligo(ethylene glycols). Angewandte Chemie International Edition, 2015. 54(12): p. 3763-3767.
197. Fishburn, C.S., The pharmacology of PEGylation: balancing PD with PK to generate novel therapeutics. Journal of pharmaceutical sciences, 2008. 97(10): p. 4167-4183.
198. Knop, K., et al., Poly (ethylene glycol) in drug delivery: pros and cons as well as potential alternatives. Angewandte chemie international edition, 2010. 49(36): p. 6288-6308.
199. Szekely, G., et al., Iterative synthesis of monodisperse PEG homostars and linear heterobifunctional PEG. Polymer Chemistry, 2014. 5(3): p. 694-697.

200. Ahmed, S.A. and M. Tanaka, Synthesis of Oligo(ethylene glycol) toward 44-mer. The Journal of Organic Chemistry, 2006. 71(26): p. 9884-9886.
201. Ltd, Q.B. Product. 2018 [cited 2018 25 July]; Available from: https://www.quantabiodesign.com/.
202. Adler, S., et al., Vision 2020: 2000 separations roadmap. New York, NY: AIChE, 2000.
203. Geens, J., B. De Witte, and B. Van der Bruggen, Removal of API's (active pharmaceutical ingredients) from organic solvents by nanofiltration. Separation Science and Technology, 2007. 42(11): p. 2435-2449.
204. Szekely, G., et al., Sustainability assessment of organic solvent nanofiltration: from fabrication to application. Green Chemistry, 2014. 16(10): p. 4440-4473.
205. Vandezande, P., L.E. Gevers, and I.F. Vankelecom, Solvent resistant nanofiltration: separating on a molecular level. Chemical Society Reviews, 2008. 37(2): p. 365-405.
206. Kedem, O. and A. Katchalsky, A physical interpretation of the phenomenological coefficients of membrane permeability. The Journal of general physiology, 1961. 45(1): p. 143-179.
207. Li, K., Ceramic membranes for separation and reaction. 2007: John Wiley & Sons.
208. Van der Bruggen, B., et al., A review of pressure-driven membrane processes in wastewater treatment and drinking water production. Environmental progress, 2003. 22(1): p. 46-56.
209. Strathmann, H., Membrane separation processes. Journal of membrane science, 1981. 9(1-2): p. 121-189.
210. Petersen, R.J., Composite reverse osmosis and nanofiltration membranes. Journal of membrane science, 1993. 83(1): p. 81-150.
211. Solomon, M.F.J., Y. Bhole, and A.G. Livingston, High flux membranes for organic solvent nanofiltration (OSN)—Interfacial polymerization with solvent activation. Journal of membrane science, 2012. 423: p. 371-382.
212. Mayes, A.M. and C.E. Scott, Regenerative Polymer Membranes for Water Treatment Applications. 2002, MASSACHUSETTS INST OF TECH CAMBRIDGE.
213. Escobar, I.C., et al., Committee report: recent advances and research needs in membrane fouling. American Water Works Association. Journal, 2005. 97(8): p. 79.
214. Baker, R.W. and U.b. Staff, Membrane technology. Kirk-Othmer Encyclopedia of Chemical Technology, 2000.
215. Park, Y.-J., et al., UV-and thermal-curing behaviors of dual-curable adhesives based on epoxy acrylate oligomers. International Journal of Adhesion and Adhesives, 2009. 29(7): p. 710-717.
216. Schäfer, A.I., A.G. Fane, and T.D. Waite, Nanofiltration: principles and applications. 2005: Elsevier.
217. Marchetti, P., et al., Molecular separation with organic solvent nanofiltration: a critical review. Chemical reviews, 2014. 114(21): p. 10735-10806.
218. Vanherck, K., G. Koeckelberghs, and I.F. Vankelecom, Crosslinking polyimides for membrane applications: a review. Progress in polymer science, 2013. 38(6): p. 874-896.
219. Toh, Y.S., F. Lim, and A. Livingston, Polymeric membranes for nanofiltration in polar aprotic solvents. Journal of Membrane Science, 2007. 301(1-2): p. 3-10.
220. Vanherck, K., et al., A simplified diamine crosslinking method for PI nanofiltration membranes. Journal of membrane science, 2010. 353(1-2): p. 135-143.
221. Dutczak, S., et al., New Membranes for Organic Solvent Nanofiltration. Vol. 44. 2012. 247–250.
222. Valtcheva, I.B., et al., Beyond polyimide: crosslinked polybenzimidazole membranes for organic solvent nanofiltration (OSN) in harsh environments. Journal of Membrane Science, 2014. 457: p. 62-72.

223. See-Toh, Y.H., F.C. Ferreira, and A.G. Livingston, The influence of membrane formation parameters on the functional performance of organic solvent nanofiltration membranes. Journal of membrane science, 2007. 299(1-2): p. 236-250.
224. Toh, Y.S., et al., In search of a standard method for the characterisation of organic solvent nanofiltration membranes. Journal of membrane science, 2007. 291(1-2): p. 120-125.
225. Strużyńska-Piron, I., et al., Parameter Study on the Preparation of UV Depth-Cured Chemically Resistant Polysulfone-Based Membranes. Macromolecular Chemistry and Physics, 2014. 215(7): p. 614-623.
226. Siddique, H., et al., Mixed matrix membranes for organic solvent nanofiltration. Journal of Membrane Science, 2014. 452: p. 354-366.
227. Gassara, S., et al., Pore size tailoring of poly (ether imide) membrane from UF to NF range by chemical post-treatment using aminated oligomers. Journal of membrane science, 2013. 436: p. 36-46.
228. Tsuru, T., et al., Inorganic porous membranes for nanofiltration of nonaqueous solutions. Separation and purification technology, 2003. 32(1-3): p. 105-109.
229. Tsuru, T., et al., Permeation of nonaqueous solution through organic/inorganic hybrid nanoporous membranes. AIChE journal, 2004. 50(5): p. 1080-1087.
230. Van Gestel, T., et al., Surface modification of γ-Al2O3/TiO2 multilayer membranes for applications in non-polar organic solvents. Journal of membrane science, 2003. 224(1-2): p. 3-10.
231. Tsuru, T., et al., Preparation of hydrophobic nanoporous methylated SiO2 membranes and application to nanofiltration of hexane solutions. Journal of membrane science, 2011. 384(1-2): p. 149-156.
232. Chang, Y., et al., Surface grafting control of PEGylated poly (vinylidene fluoride) antifouling membrane via surface-initiated radical graft copolymerization. Journal of Membrane Science, 2009. 345(1-2): p. 160-169.
233. Sairam, M., et al., Spiral-wound polyaniline membrane modules for organic solvent nanofiltration (OSN). Journal of Membrane Science, 2010. 349(1-2): p. 123-129.
234. Sereewatthanawut, I., et al., Demonstration of molecular purification in polar aprotic solvents by organic solvent nanofiltration. Organic Process Research & Development, 2010. 14(3): p. 600-611.
235. Silva, P., L.G. Peeva, and A.G. Livingston, Organic solvent nanofiltration (OSN) with spiral-wound membrane elements—Highly rejected solute system. Journal of Membrane Science, 2010. 349(1-2): p. 167-174.
236. Székely, G., et al., Removal of potentially genotoxic acetamide and arylsulfonate impurities from crude drugs by molecular imprinting. Journal of Chromatography A, 2012. 1240: p. 52-58.
237. Székely, G., et al., Design of experiments as a tool for LC–MS/MS method development for the trace analysis of the potentially genotoxic 4-dimethylaminopyridine impurity in glucocorticoids. Journal of pharmaceutical and biomedical analysis, 2012. 70: p. 251-258.
238. Kecili, R., et al., Selective scavenging of the genotoxic impurity methyl p-toluenesulfonate from pharmaceutical formulations. Separation and Purification Technology, 2013. 103: p. 173-179.
239. Székely, G., et al., Environmental and economic analysis for selection and engineering sustainable API degenotoxification processes. Green Chemistry, 2013. 15(1): p. 210-225.

240. Darvishmanesh, S., et al., Performance of solvent resistant nanofiltration membranes for purification of residual solvent in the pharmaceutical industry: experiments and simulation. Green Chemistry, 2011. 13(12): p. 3476-3483.
241. Rundquist, E.M., C.J. Pink, and A.G. Livingston, Organic solvent nanofiltration: a potential alternative to distillation for solvent recovery from crystallisation mother liquors. Green Chemistry, 2012. 14(8): p. 2197-2205.
242. Micovic, J., K. Werth, and P. Lutze, Hybrid separations combining distillation and organic solvent nanofiltration for separation of wide boiling mixtures. Chemical Engineering Research and Design, 2014. 92(11): p. 2131-2147.
243. Nimmig, S. and M. Kaspereit, Continuous production of single enantiomers at high yields by coupling single column chromatography, racemization, and nanofiltration. Chemical Engineering and Processing: Process Intensification, 2013. 67: p. 89-98.
244. Székely, G., et al., A hybrid approach to reach stringent low genotoxic impurity contents in active pharmaceutical ingredients: Combining molecularly imprinted polymers and organic solvent nanofiltration for removal of 1,3-diisopropylurea. Separation and Purification Technology, 2012. 86: p. 79-87.
245. Pink, C.J., et al., Organic Solvent Nanofiltration and Adsorbents; A Hybrid Approach to Achieve Ultra Low Palladium Contamination of Post Coupling Reaction Products. Organic Process Research & Development, 2008. 12(4): p. 589-595.
246. So, S., et al., Membrane enhanced peptide synthesis. Chemical Communications, 2010. 46(16): p. 2808-2810.
247. Kilduff, J.E., et al., Photochemical modification of poly (ether sulfone) and sulfonated poly (sulfone) nanofiltration membranes for control of fouling by natural organic matter. Desalination, 2000. 132(1-3): p. 133-142.
248. See-Toh, Y.H., M. Silva, and A. Livingston, Controlling molecular weight cut-off curves for highly solvent stable organic solvent nanofiltration (OSN) membranes. Journal of Membrane Science, 2008. 324(1-2): p. 220-232.
249. Grodowska, K. and A. Parczewski, Organic solvents in the pharmaceutical industry. Acta Pol Pharm, 2010. 67(1): p. 3-12.
250. Tjoeng, F.S., et al., Liquid-phase method for peptide synthesis utilizing photolytic cleavage from a new o-nitrobenzoyl polyethylene glycol support. Biochimica et Biophysica Acta, 1977. 490(2): p. 489-496.
251. So, S., et al., Organic Solvent Nanofiltration: A New Paradigm in Peptide Synthesis. Organic Process Research & Development, 2010. 14(6): p. 1313-1325.
252. Schwartz, L., Diafiltration: A fast, efficient method for desalting, or buffer exchange of biological samples. Pall Scientific & Technical Report, 2003.
253. Martínez, M.B., et al., Effect of impurities in the recovery of 1-(5-bromo-fur-2-il)-2-bromo-2-nitroethane using nanofiltration. Chemical Engineering and Processing: Process Intensification, 2013. 70: p. 241-249.
254. Ormerod, D., et al., Demonstration of purification of a pharmaceutical intermediate via organic solvent nanofiltration in the presence of acid. Separation and Purification Technology, 2013. 115: p. 158-162.
255. Caus, A., et al., The use of integrated countercurrent nanofiltration cascades for advanced separations. Journal of Chemical Technology & Biotechnology: International Research in Process, Environmental & Clean Technology, 2009. 84(3): p. 391-398.
256. Kim, J.F., et al., Increasing the sustainability of membrane processes through cascade approach and solvent recovery—pharmaceutical purification case study. Green Chemistry, 2014. 16(1): p. 133-145.

257. Martínez, M.B., et al., Separation of a high-value pharmaceutical compound from waste ethanol by nanofiltration. Journal of Industrial and Engineering Chemistry, 2012. 18(5): p. 1635-1641.
258. Vanneste, J., et al., Towards high resolution membrane-based pharmaceutical separations. Journal of Chemical Technology & Biotechnology, 2013. 88(1): p. 98-108.
259. Peeva, L., et al., Continuous purification of active pharmaceutical ingredients using multistage organic solvent nanofiltration membrane cascade. Chemical Engineering Science, 2014. 116: p. 183-194.
260. Ghosh, R., Novel cascade ultrafiltration configuration for continuous, high-resolution protein–protein fractionation: a simulation study. Journal of Membrane Science, 2003. 226(1-2): p. 85-99.
261. Lightfoot, E.N., T.W. Root, and J. L. O'Dell, Emergence of ideal membrane cascades for downstream processing. Biotechnology progress, 2008. 24(3): p. 599-605.
262. Kim, J.F., et al., When the membrane is not enough: A simplified membrane cascade using Organic Solvent Nanofiltration (OSN). Separation and Purification Technology, 2013. 116: p. 277-286.
263. Siew, W.E., et al., Molecular separation with an organic solvent nanofiltration cascade–augmenting membrane selectivity with process engineering. Chemical Engineering Science, 2013. 90: p. 299-310.
264. Siew, W.E., et al., Continuous solute fractionation with membrane cascades–a high productivity alternative to diafiltration. Separation and Purification Technology, 2013. 102: p. 1-14.
265. Solleder, S.C. and M.A. Meier, Sequence Control in Polymer Chemistry through the Passerini Three-Component Reaction. Angewandte Chemie International Edition, 2014. 53(3): p. 711-714.
266. Konig, N.F., et al., A Simple Post-Polymerization Modification Method for Controlling Side-Chain Information in Digital Polymers. Angewandte Chemie, 2017. 56(25): p. 7297-7301.
267. Koros, W.J. and C. Zhang, Materials for next-generation molecularly selective synthetic membranes. Nature Materials, 2017. 16(3): p. 289-297.
268. Marchetti, P., L. Peeva, and A. Livingston, The Selectivity Challenge in Organic Solvent Nanofiltration: Membrane and Process Solutions. Annual review of chemical and biomolecular engineering, 2017. 8: p. 473-497.
269. Schaefer, A.I., A.G. Fane, and T.D. Waite, Nanofiltration : principles and applications. 2003, New York: Elsevier Advanced Technology. 560 p.
270. Vanherck, K., G. Koeckelberghs, and I.F.J. Vankelecom, Crosslinking polyimides for membrane applications: A review. Progress in Polymer Science, 2013. 38(6): p. 874-896.
271. Valtcheva, I.B., P. Marchetti, and A.G. Livingston, Crosslinked polybenzimidazole membranes for organic solvent nanofiltration (OSN): Analysis of crosslinking reaction mechanism and effects of reaction parameters. Journal of Membrane Science, 2015. 493: p. 568-579.
272. Gassara, S., et al., Pore size tailoring of poly(ether imide) membrane from UF to NF range by chemical post-treatment using aminated oligomers. Journal of Membrane Science, 2013. 436: p. 36-46.
273. Amirilargani, M., et al., Surface modification methods of organic solvent nanofiltration membranes. Chemical Engineering Journal, 2016. 289: p. 562-582.
274. L.G. Peeva, S.M., A. Livingston, Nanofiltration operations in nonaqueous systems. Comprehensive Membrane Science and Engineering, 2010(Elsevier, Oxford).

275. Zhang, H., et al., Mineralization-inspired preparation of composite membranes with polyethyleneimine–nanoparticle hybrid active layer for solvent resistant nanofiltration. Journal of Membrane Science, 2014. 470: p. 70-79.
276. R. Tanardi, C., et al., PDMS grafting of mesoporous γ-alumina membranes for nanofiltration of organic solvents. Vol. 469. 2014. 471-477.
277. Park, J.Y., et al., Polysulfone-graft-poly (ethylene glycol) graft copolymers for surface modification of polysulfone membranes. Biomaterials, 2006. 27(6): p. 856-865.
278. Verrecht, B.L., R.; Buekenhoudt, A.; Vandecasteele, C.; Vander Bruggen, B., Chemical surface modification of γ-Al2O3 and TiO2 toplayer membranes for increased hydrophobicity. Desalination 2006. 200: p. 385–386.
279. Tsuru, T., et al., Inorganic porous membranes for nanofiltration of nonaqueous solutions. Separation and Purification Technology, 2003. 32(1): p. 105-109.
280. Hosseinabadi, S.R., et al., Organic solvent nanofiltration with Grignard functionalised ceramic nanofiltration membranes. Journal of Membrane Science, 2014. 454: p. 496-504.
281. Valtcheva, I.B.K., S. C.; Kim, J. F.; Bhole, Y.; Livingston, A. G, Beyond polyimide: Crosslinked Polybenzimidazole Membranes for Organic Solvent Nanofiltration (OSN) in Harsh Environments. Journal of Membrane Science, 2014. 457: p. 62–72.
282. LIU, A.G.L.P.M.P.G.R., Process for the production of solvent stable polymeric membranes. PCT/GB2017/051633, 2016.
283. Franklin, S.D.J., Spiral wound module with integrated permeate flow controller. US20170050149A1, 2014.
284. da Silva Burgal, J., L. Peeva, and A. Livingston, Towards improved membrane production: using low-toxicity solvents for the preparation of PEEK nanofiltration membranes. Green Chemistry, 2016. 18(8): p. 2374-2384.
285. da Silva Burgal, J., et al., Controlling molecular weight cut-off of PEEK nanofiltration membranes using a drying method. Journal of Membrane Science, 2015. 493: p. 524-538.
286. Knop, K., et al., Poly(ethylene glycol) in Drug Delivery: Pros and Cons as Well as Potential Alternatives. Angewandte Chemie, 2010. 49(36): p. 6288-6308.
287. Caliceti, P. and F.M. Veronese, Pharmacokinetic and biodistribution properties of poly(ethylene glycol)–protein conjugates. Advanced Drug Delivery Reviews, 2003. 55(10): p. 1261-1277.
288. Abuchowski, A., et al., Alteration of immunological properties of bovine serum albumin by covalent attachment of polyethylene glycol. Journal of Biological Chemistry, 1977. 252(11): p. 3578-3581.
289. Maranski, K., Y.G. Andreev, and P.G. Bruce, Synthesis of Poly(ethylene oxide) Approaching Monodispersity. Angewandte Chemie, 2014. 53(25): p. 6411-6413.
290. Keegstra, E.M.D., et al., A highly selective synthesis of monodisperse oligo(ethylene glycols). The Journal of Organic Chemistry, 1992. 57(24): p. 6678-6680.
291. Zada, A., Y. Avny, and A. Zilkha, Simplified synthesis of oligoethylene glycols. Journal of Surfactants and Detergents, 2001. 4(2): p. 163-166.
292. Niculescuduvaz, D., J. Getaz, and C.J. Springer, Long Functionalized Poly(ethylene glycol)s of Defined Molecular Weight: Synthesis and Application in Solid-Phase Synthesis of Conjugates. Bioconjugate Chemistry, 2008. 19(4): p. 973-981.
293. Thompson, M., et al., Synthesis and applications of heterobifunctional poly (ethylene oxide) oligomers. Polymer, 2008. 49(2): p. 345-373.
294. Fordyce, R., E.L. Lovell, and H. Hibbert, Studies on Reactions Relating to Carbohydrates and Polysaccharides. LVI. The Synthesis of the Higher Polyoxyethylene Glycols. Journal of the American Chemical Society, 1939. 61(7): p. 1905-1910.

295. Bouzide, A. and G. Sauvé, Silver(I) Oxide Mediated Highly Selective Monotosylation of Symmetrical Diols. Application to the Synthesis of Polysubstituted Cyclic Ethers. Organic Letters, 2002. 4(14): p. 2329-2332.
296. La Ferla, B., C. Zona, and F. Nicotra, Easy silica gel supported desymmetrization of PEG. Synlett, 2009. 2009(14): p. 2325-2327.
297. R. G. Gilbert, M.H., A. D. Jenkins, R. G. Jones, P. Kratochvíl, R. F. T. Stepto, Pure Appl. Chem., 2009. 81: p. 351-353.
298. Soni, A., et al., Efficient and Selective Demethylation of Heteroaryl Methyl Ethers in the Presence of Aryl Methyl Ethers. Synthetic Communications, 2011. 41(12): p. 1852-1857.
299. Okaya, S., Okuyama, K., Okano, K. & Tokuyama, H., Trichloroboron-promoted deprotection of phenolic benzyl ether using pentamethylbenzene as a non-Lewis basic cation scavenger. Org. Synth., (2016. 92: p. 63–74.
300. Colgan, A.C., H. Mullerbunz, and E.M. Mcgarrigle, Benzylation Reactions in DMF Lead to an Impurity Which Acts as an Organocatalyst Poison in Thiourea-Catalyzed Glycosylations. Journal of Organic Chemistry, 2016. 81(22): p. 11394-11396.
301. Seeman, N.C., DNA in a material world. Nature, 2003. 421: p. 427.
302. Van Hest, J.C.M. and D.A. Tirrell, Protein-based materials, toward a new level of structural control. Chemical Communications, 2001. 2001(19): p. 1897-1904.
303. Lutz, J., Sequence-controlled polymerizations: the next Holy Grail in polymer science? Polymer Chemistry, 2010. 1(1): p. 55-62.
304. Engelis, N.G., et al., Sequence-controlled methacrylic multiblock copolymers via sulfur-free RAFT emulsion polymerization. Nature Chemistry, 2017. 9(2): p. 171-178.
305. Nakatani, K., et al., Sequence-Regulated Copolymers via Tandem Catalysis of Living Radical Polymerization and In Situ Transesterification. Journal of the American Chemical Society, 2012. 134(9): p. 4373-4383.
306. Palomo, J.M., Solid-phase peptide synthesis: an overview focused on the preparation of biologically relevant peptides. RSC Advances, 2014. 4(62): p. 32658-32672.
307. Thieriet, N., F. Guibe, and F. Albericio, Solid-phase peptide synthesis in the reverse (N --> C) direction. Organic Letters, 2000. 2(13): p. 1815-1817.
308. Svec, F. and J.M.J. Frechet, New designs of macroporous polymers and supports : From separation to biocatalysis. Science, 1996. 273(5272): p. 205-211.
309. Bootwicha, T., et al., Iterative assembly line synthesis of polypropionates with full stereocontrol. Nature Chemistry, 2017. 9(9): p. 896-902.
310. Lewis, J.E.M., et al., Iterative Synthesis of Oligo[n]Rotaxanes in Excellent Yield. Journal of the American Chemical Society, 2016. 138(50): p. 16329-16336.
311. Smith, M., et al., Studies on Polynucleotides. XIV.1 Specific Synthesis of the C3"-C5" Interribonucleotide Linkage. Syntheses of Uridylyl-(3"5")-Uridine and Uridylyl-(3"5")-Adenosine2. Journal of the American Chemical Society, 1962. 84(3): p. 430-440.
312. Patschinski, P., C. Zhang, and H. Zipse, The Lewis Base-Catalyzed Silylation of Alcohols—A Mechanistic Analysis. The Journal of Organic Chemistry, 2014. 79(17): p. 8348-8357.
313. Corey, E.J. and A. Venkateswarlu, Protection of hydroxyl groups as tert-butyldimethylsilyl derivatives. Journal of the American Chemical Society, 1972. 94(17): p. 6190-6191.
314. Gaunt, M.J., J. Yu, and J.B. Spencer, Rational Design of Benzyl-Type Protecting Groups Allows Sequential Deprotection of Hydroxyl Groups by Catalytic Hydrogenolysis. The Journal of Organic Chemistry, 1998. 63(13): p. 4172-4173.

315. Felpin, F.X. and E. Fouquet, A Useful, Reliable and Safer Protocol for Hydrogenation and the Hydrogenolysis of O-Benzyl Groups: The In Situ Preparation of an Active Pd0/C Catalyst with Well-Defined Properties. Chemistry-A European Journal, 2010. 16(41): p. 12440-12445.
316. Song, C.E., Alkaloids as chirality transmitters in asymmetric catalysis, in The Alkaloids: Chemistry and Biology. 1999, Academic Press. p. 1-56.
317. Kolb, H.C., M.S. VanNieuwenhze, and K.B. Sharpless, Catalytic Asymmetric Dihydroxylation. Chemical Reviews, 1994. 94(8): p. 2483-2547.
318. Busch, K.W., M.A. Busch, and C. Calleja-Amador, Instrumental aspects of chiroptical detection, in Chiral Analysis. 2006, Elsevier. p. 299-341.
319. Licea-Perez, H., et al., Camphanic acid chloride: a powerful derivatization reagent for stereoisomeric separation and its DMPK applications. Bioanalysis, 2015. 7(23): p. 3005-3017.
320. Wang, Y. and A.M. Chen, Enantioenrichment by Crystallization. Organic Process Research & Development, 2008. 12(2): p. 282-290.
321. Asao, N., et al., Pd(II) Acts Simultaneously as a Lewis Acid and as a Transition-Metal Catalyst: Synthesis of Cyclic Alkenyl Ethers from Acetylenic Aldehydes. Journal of the American Chemical Society, 2002. 124(5): p. 764-765.

List of publications

Journal papers

Dong R*, Liu R* et al., Sequence-defined multifunctional polyethers via liquid-phase synthesis with molecular sieving, 2018; accepted by Nature Chemistry, in press

Marchetti P, Gaffney P, Liu R et al., Polybenzimidazole-based membranes for applications in organic synthesis (Working title); to be submitted

Patents

Gaffney P, Marchetti P, Dong R, Liu R, Andrew Livingston et al., Defined monomer sequence polymers, PCT/GB2016/052801

Gaffney P, Marchetti P, Liu R, Andrew Livingston et al., Asymmetric membranes for use in nanofiltration, PCT/GB2017/051633

Conference oral presentations

R. Liu et al., Polybenzimidazole Based Membranes for Organic Solvent Nanofiltration, 2017 AIChE Annual Meeting, Minneapolis, United States

R. Liu et al., Iterative Synthesis of Heteropolymers Using Organic Solvent Nanofiltration, 2017 AIChE Annual Meeting, Minneapolis, United States

Conference poster presentation

R. Liu et al., Iterative Synthesis of High Value Polymers Using Organic Solvent Nanofiltration, 2015 Chem Eng Day, UK

Appendix

Permissions summary table for third party copyright works

Page No.	Type of Work	Name of Work	Source of Work	Copyright holder and contact	Permission requested on	I have permission: Y/N
26	Figure	Figure 2.1 Synthesis of sequence-defined artificial macromolecules…	Lutz, J.-F., et al., Sequence controlled polymers. Science, 2013. 341(6146): p. 1238149.	© 2013 AAAS	18/09/2018	Y
31	Figure	Figure 2.2 Chemical synthetic polymerization processes…	Lutz, J.-F., Sequence-controlled polymerizations: the next Holy Grail in polymer science? Polymer Chemistry, 2010. 1(1): p. 55-62	© 2010 The Royal Society of Chemistry	18/09/2018	Y
33	Figure	Figure 2.3 Controlling sequences in a chain-growth polymerization...	Pfeifer, S. and J.F. Lutz, Development of a library of N-substituted maleimides for the local functionalization of linear polymer chains. Chemistry–A European Journal, 2008. 14(35): p. 10949-10957	© 2008 WILEY-VCH	18/09/2018	Y
35	Figure	Figure 2.4 Chemical schemes of metal-catalyzed radical…	Lutz, J.-F., et al., Sequence controlled polymers. Science, 2013. 341(6146): p. 1238149.	© 2013 AAAS	18/09/2018	Y
37	Figure	Figure 2.5 The concept of chemical iterative synthesis…	Lutz, J.-F., et al., Sequence controlled polymers. Science, 2013. 341(6146): p. 1238149.	© 2013 AAAS	18/09/2018	Y
40	Figure	Figure 2.6 Liquid phase synthesis of 2'-Me-RNA…	J., G.P.R., et al., Liquid-Phase Synthesis of 2 Methyl-RNA on a Homostar Support through Organic-Solvent Nanofiltration. Chemistry – A European Journal, 2015. 21(26): p. 9535-9543.	© 2015 WILEY-VCH	18/09/2018	Y

42	Figure	Figure 2.7 Liquid-phase synthesis of sequence ordered…	Pfeifer, S., et al., Liquid-phase synthesis of block copolymers containing sequence-ordered segments. Journal of the American Chemical Society, 2009. 131(26): p. 9195-9197	© 2009 American Chemical Society	18/09/2018	Y
45	Figure	Figure 2.8 Schematic of approaches for the synthesis…	Szekely, G., et al., Iterative synthesis of monodisperse PEG homostars and linear heterobifunctional PEG. Polymer Chemistry, 2014. 5(3): p. 694-697.	© 2014 The Royal Society of Chemistry	18/09/2018	Y
51	Figure	Figure 2.9 ISA membrane formation process by phase inversion…	Marchetti, P., et al., Molecular separation with organic solvent nanofiltration: a critical review. Chemical reviews, 2014. 114(21): p. 10735-10806.	© 2014 American Chemical Society	18/09/2018	Y
58	Figure	Figure 2.10 Iterative synthesis of peptide with membrane purification…	So, S., et al., Organic solvent nanofiltration: a new paradigm in peptide synthesis. Organic Process Research & Development, 2010. 14(6): p. 1313-1325.	© 2010 American Chemical Society	18/09/2018	Y
60	Figure	Figure 2.11 Case studies of purification via constant…	Marchetti, P., et al., Molecular separation with organic solvent nanofiltration: a critical review. Chemical reviews, 2014. 114(21): p. 10735-10806.	© 2014 American Chemical Society	18/09/2018	Y
61	Figure	Figure 2.12 System diagrams of single-stage diafiltration…	Kim, J.F., et al., Increasing the sustainability of membrane processes through cascade approach and solvent recovery—pharmaceutical purification case study. Green Chemistry, 2014. 16(1): p. 133-145.	© The Royal Society of Chemistry 2014	18/09/2018	Y
62	Figure	Figure 2.13 Predicted yield improvement after 10 diavolumes…	Kim, J.F., et al., Increasing the sustainability of membrane processes through cascade approach and solvent recovery—pharmaceutical purification case study. Green Chemistry, 2014. 16(1): p. 133-145.	© The Royal Society of Chemistry 2014	01/10/2018	Y